Late Quaternary climate variability in Southern Ocean Atlantic Sector

Kumulative Dissertation
zur Erlangung des akademischen Grades eines
Doktors der Naturwissenschaften
– Dr. rer. nat. –

Am Fachbereich Geowissenschaften
Der Universität Bremen

vorgelegt von

Wenshen Xiao

Bremen, 2011

This PhD thesis was conducted within the Marine Geology Group of the *Alfred-Wegener-Institut für Polar- und Meeresforchung* (AWI), Columbus Strasse, 27568 Bremerhaven, Germany, between February 2007 and March 2011. The study was embedded in the topic *Past polar climate and inter-hemispheric coupling* at the AWI. This study was supported by *Deutscher Akademischer Austausch Dienst* (DAAD) for 3 years, and further supported by AWI.

Gutachter der Dissertation:

Prof. Dr. Helmut Willems

Prof. Dr. Bernhard Diekmann

Weitere Mitglieder des Prüfungsausschusses:

Prof. Dr. Ruediger Henrich

Dr. Rainer Gersonde

Dr. Mariem Saavedra-Pellitero

Caroline Clotten

Tag des öffentlichen Kolloquiums:

23. May 2011

Geo-Hörsaal, 16 Uhr c.t.

Abstract

Climate variability of the late Quaternary, especially the Last Glacial (LG) to the Holocene, has become the most heated topic for the recent decades, which helps to better understand the shape of current and future climate on our planet. The long term glacial/interglacial changes have been associated to insolation changes controlled by earth's orbit, whereas the millennial scale variations are mostly accepted to be modulated by the "bipolar seesaw" mechanism which redistributes heat between the northern and southern hemispheres through the Atlantic Meridional Overturning Circulation (AMOC). The validation of such hypothesis is hampered by the very limited high resolution records from the high latitudes Southern Ocean.

Situated at the southern end of the AMOC, Southern Ocean Atlantic sector represents one of the key regions for understanding the global climate change. The warm and cold water routes (WWR, south of Africa and CWR, Drake Passage/Scotia Sea) connect the South Atlantic to South Indian and Pacific Oceans, respectively; and the Weddell Gyre connects the open ocean South Atlantic to the Western Antarctic Shelf Ice (WASI), where nowadays the cold surface water and Antarctic Bottom Water (AABW) are generated beneath. These water masses represent the most important constituents of the AMOC in the Southern Hemisphere. This PhD project generated a series of new diatom based high resolution marine records covering wide area of the high latitudes South Atlantic, including from the Bouvet Island area and the Scotia Sea, aimed to provide new insights of the response and drive in Southern Ocean in the context of late Quaternary global climate change.

With focusing on the LG to Holocene time period, by integration of our new generated and other existing records from the Southern Ocean Atlantic and Western Indian sectors, a detailed regional age model for the past 30 kyrs is established by AMS ^{14}C dating and regional core correlation, which can be a template for further paleoenvironment reconstructions in this area. Our reconstructions suggest 2-3˚C cooling in the LG south of the modern Polar Front compared to modern conditions. Winter sea ice in the Bouvet Island area expanded by 5˚ latitude, the more expanded sea ice field resulted in the stronger tropical Atlantic cooling than other tropical oceans by the reduction of warm water to the South Atlantic via the WWR, and intensive export of carbon to the deep Southern Ocean. The two steps of deglacial warming are mainly concurrent with the Heinrich stadial 1 and Younger Dryas cooling in the northern hemisphere which support the bipolar seesaw from the marine archives. The North Atlantic Deep Water (NADW) provided the second source of warming from below to the high latitudes South Atlantic which extended the first step warming till 14 cal. ka (kyr BP). The temporal cooling at ca. 14-12 cal. ka is possibly caused by the melt water input from the Antarctica. Our records support the Southern Ocean control of the deglacial atmospheric CO_2 rise. The early Holocene optimum marks the warmest period and the strongest cold water reduction and confined at ca. 11-10 cal. ka in the southern cores in the study area. Sea ice probably retreated south of modern conditions and maximum opal deposition southward expanded to at least 55˚S. The mid-late Holocene cooling in the study area may be related to the cold water expansion from the Weddell Gyre with the developing cavity under the WASI. The Holocene climate development may have also interplayed with the NADW which represents a rapid resumption at the early Holocene and slight decline during the mid-late Holocene.

The high resolution Holocene record from the central Scotia Sea suggests a stable climate at the core site. The early Holocene high productivity is maintained by the enhanced upwelling at that time. The Holocene reservoir change at the core site is evidenced, which is in agreement with the Southern

Ocean ventilation history. The pre-Holocene release of CO_2 from the Southern Ocean strongly lowered the $\Delta^{14}C_{atm}$ which caused the low surface ocean reservoir at the early Holocene at the core site. The centennial scale climate variability may be mainly linked to solar activity and also influenced by the sea ice induced freshwater variability.

Stratigraphis of long term records from the Scotia Sea covering the past 300 kyrs were established by a combination of radiocarbon chronology, correlation of magnetic susceptibility (MS) to Antarctic ice core dust/climate records, diatom biofluctuation stratigraphy, and geomagnetic chronology. Good consistency of the age models by these proxies improves the reliability of our stratigraphies and indicates the applicability of these approaches. However, detailed investigation show that, the radiocarbon chronology can be affected by the changes in carbon reservoir and fossil carbon contamination in the study area; the abundance pattern of diatom species *Eucampia antarctica* can be used to identify the past 6 marine isotope stages (MIS) while the fluctuation weakens during MIS 7 and 8; the reliability of geomagnetic chronology weakens at low sedimentation rates conditions. The MS-Antarctic ice core correlations represent high efficiency and the best reliability due to the high sensitivity to the changes of surrounding source regions and current systems, which is closely related to the climate changes in the Southern Ocean. In addition, a possible correlation between the ash layers found in our Scotia Sea cores and the Antarctic ice cores is established, which can be used as additional age markers for further studies in this area.

Zusammenfassung

Die Klimavariabilität im Spätquartär, speziell während des letzten Glazials (LG) und des Holozäns, ist eines der heißesten Themenfelder der letzten Jahrzehnte, welche zum Verständnis der Ausprägung des momentanen und zukünftigen Klimas unseres Planeten beitragen. Langzeitige Glazial/Interglazial-Änderungen wurden in Verbindung gebracht zu Änderungen in der Einstrahlung, kontrolliert durch den Erdorbit, wobei Variationen auf der Jahrtausendskala weitestgehend akzeptiert durch den Mechanismus der "bipolaren Wippe" moduliert werden, welcher für einen Wärmeaustausch zwischen Nord- und Südhemisphäre über die "Atlantische Meridionale Umwälz-Zirkulation" (AMOC) sorgt. Die Bestätigung solch einer Hypothese wird behindert durch sehr beschränkt zur Verfügung stehende hochauflösende Archive der hohen Breiten des Südozeans.

Am südlichen Ende der AMOC gelegen repräsentiert der Südatlantiksektor eine der Schlüsselregionen zum Verständnis globaler Klimaänderungen. Die Warm- und Kaltwasserrouten (WWR, südlich Afrika und CWR, Drake Passage/Scotia Meer) verbinden den Südatlantik mit dem Indischen und Pazifischen Ozean; die Weddellgyre verbindet den offenen Ozean des Südatlantiks mit Westantarktischen Eisschelf (WAIS), der Bildungsregion kalten Oberflächenwassers sowie Antarktisches Bodenwasser (AABW). Diese Wassermassen stellen die wichtigsten Komponenten der AMOC auf der Südhemisphäre dar. Dieses Promotionsarbeit generierte eine Serie neuer, hochauflösender mariner Aufzeichnungen basierend auf Diatomeen, welche ein weites Gebiet der hohen Breiten des Südatlantiks abdecken, inklusive des Gebietes um Bouvet Island und dem Scotia Meer, und zielt darauf ab, neue Einblicke in Reaktion und Antrieb des Südozeans im Kontext spätquartärer globaler Klimaänderungen zu liefern.

Mit Fokus auf die LG bis Holozän-Periode wurde ein detailliertes regionales Altersmodell für die letzten 30 ka durch Integration unserer neu generierten und existierenden Aufzeichnungen der atlantischen und westindischen Sektoren des Südozeans mittels AMS ^{14}C Datierung und regionaler Kernkorrelationen errichtet, welches als Grundlage für weitere Paläoumweltrekonstruktionen in dieser Region dienen kann.

Unsere Rekonstruktionen deuten auf eine Abkühlung von 2-3°C für das LG südlich der modernen Polarfront im Vergleich zu heutigen Bedingungen hin. Das Wintermeereis im Gebiet von Bouvet Island dehnte sich um 5° Breite aus, wobei das weiter ausgedehnte Meereisfeld, bedingt durch reduzierten Transport warmen Wassers zum Südatlantik über die WWR und den intensiv Export von Kohlenstoff zum tiefen Südozean, zu einer stärkeren Abkühlung des tropischen Atlantiks im Vergleich zu anderen tropischen Ozeanen führte. Die zwei Schritte deglazialer Erwärmung stehen hautsächlich in Konkurrenz zum Heinrich Stadial 1 und der Jüngeren Dryas Abkühlung der Nordhemisphäre, welche die bipolare Wippe aus marinen Archiven stützen. Das Nordatlantik Tiefenwasser (NADW) liefert die zweite Quelle der Erwärmung aus der Tiefe zu den hohen Breiten des Südatlantiks, welche den ersten Schritt der Erwärmung bis 14 cal. ka (kilo jahre BP) ausdehnte. Die temporäre Abkühlung bei ca. 14-12 cal. ka wurde vermutlich durch Schmelzwassereinfluß aus Antarktika ausgelöst. Unsere Datensätze stützen eine Kontrolle des Südozeans über den deglazialen atmosphärischen CO_2-Anstieg. Das früh-Holozäne Maximum markiert die wärmste Periode und die stärkste Kaltwasserreduktion, begrenzt auf ca. 11-10 cal. ka in den südlichen Kernen im Untersuchungsgebiet. Meereis zog sich wahrscheinlich südlich der heutigen Ausdehnung zurück, die maximale Opalablagerung dehnte sich südwärts bis mindestens 55°S aus. Die mittel- bis spät-Holozäne Abkühlung im Untersuchungsgebiet steht möglicherweise in Verbindung zu einer Kaltwasserausdehnung der Weddellgyre und der

Entwicklung von Aushöhlungen unter dem WAIS. Die holozäne Klimaentwicklung steht möglicherweise auch im Zusammenspiel mit NADW, welches eine schnelle Wiederaufnahme im frühen Holozän und leichten Rückgang während des mittleren Holozäns repräsentiert.

Das hochauflösende holozäne Archiv des zentralen Scotiameeres deutet auf stabiles Klima an der Kernstation hin. Die früh-Holozäne Hochproduktion wird zu dieser Zeit durch erhöhten Auftrieb aufrecht erhalten. Die holozänen Reservoir-Änderung an der Kernposition ist bewiesen, welche in Übereinstimmung mit der Ventilationsgeschichte des Südozeans steht. Die vor-Holozäne Freisetzung von CO_2 aus dem Südozean senkte verstärkt das $\Delta^{14}C_{atm}$, welches zu einem niedrigen Oberflächenreservoir im frühen Holozän führte. Klimavariabilität im Jahrhundertmaßstab mag in der Hauptsache in Verbindung stehen mit Sonnenaktivität und mag ebenso durch Meereis-induzierte Frischwasservariabilität beeinflusst sein.

Stratigraphische Modelle für Langzeitarchive aus dem Scotiameer, welche die letzten 300 ky umfassen, wurden durch die Kombination von Radiokarbon-Chronologie, Korrelation zwischen magnetischer Suszeptibilität (MS) und antarktischen Eiskern-Staub/Klimaaufzeichnungen, Diatomeenbiofluktuationsstratigraphie und geomagnetischer Chronologie errichtet. Eine gute Beständigkeit der Altersmodelle durch diese Proxies verbessert die Zuverlässigkeit unserer Stratigraphien und zeigt die Anwendbarkeit dieser Ansätze an. Allerdings zeigen detaillierte Untersuchungen das die Radiokarbon-Chronologie durch Änderungen im Kohlenstoffreservoir und Kontamination des fossilen Kohlenstoffs im Untersuchungsgebiet beeinflusst werden können; das Verbreitungsmuster der Diatomeen-Art *Eucampia antarctica* kann zur Identifikation der letzten 6 marinen Isotopenstadien (MIS) genutzt werden, wohingegen die Schwankungen während MIS 7 und 8 abgeschwächt waren; die Zuverlässigkeit der geomagnetischen Chronologie ist geschwächt bei Bedingungen niedriger Sedimentationsrate. Die MS-antarktische-Eiskern-Korrelationen repräsentieren hohe Effizienz und die beste Zuverlässigkeit durch hohe Sensibilität gegenüber Änderungen in den umgebenden Quellregionen und Stromsystemen, welches in enger Beziehung zu den Klimaänderungen im Südozean steht. Zusätzlich wurde eine mögliche Korrelation zwischen Aschelagen in unseren Scotiameer-Kernen und antarktischen Eiskernen etabliert, welche zusätzliche Altersmarken für weitere Studien in der Region bieten.

Acknowledgement

First of all, I would like to thank DAAD (*Deutscher Akadenischer Austausch Dienst*), for giving me the opportunity to study in Germany, and the financial support for 3 years.

I would like to express my deepest gratitude to my supervisor Dr. Rainer Gersonde. My work wouldn't be like it is without your support and inspiring advices. From you what I learned is not only the knowledge but also the critical view towards science. I would like to thank Prof. Dr. Helmut Willems and Prof. Dr. Bernhard Diekmann for the review of my thesis. I am also grateful to Prof. Dr. Ralf Tiedemann, Dr. Andrea Abelmann and Dr. Frank Lamy who gave me advices and support in many ways.

Sincere acknowledgement goes to Dr. Oliver Esper, who brought me into the diatom world; Dr. Thomas Frederichs, for the very helpful discussion about the geomagnetic interpretation; Dr. Gerhard Kuhn, for the support of data processing and nice discussion about the Scotia Sea issues; Prof. Thomasz Goslar, for the discussion about the ^{14}C problems. Also acknowledged are Daniela Pittauerova and Dr. Helmut Fischer for the advices in interpreting the $^{210}Pb_{ex}$ data. Thanks to Ute Bock, Rita Fröhlking, Michael Seebeck for the lab assistance. Also thanked are the hard working cruise members of the Polarstern expeditions who brought back the excellent material for the study.

I also would like to thank Bartosz Kotrys, my officemate for 3 years. We had so much discussion not only about science but various topics. We had wonderful time together that will be part of my memory forever. Many many thanks to Ren Jian, who helped me so much especially at the final stage of my PhD. Thanks also go to my colleagues in the Geo department, they are Edith Maier, Ines Borrione, Evgenia Bazhenova, Sze-Ling Ho, David Naafs, Michael Schreck, Michelle Zarrieß, Yao Xiaoping, Zou Hao, Verena Benz, Hartmut Kühn, Johannes Ullermann and all the other AWI colleagues that lightened my life here in Bremerhaven. Thanks also go to the Chinese community at the AWI, they are Ma Haiyan, Gao Shuang, Wei Wei, Xu Xu, Gong Xun, Zhang Xu, Wang Qiang, Wang Tingting, Sun Tingting, Wang Chen, Zhang Qun and so on, I could always have nice dishes with you which reminded me home. Sincere gratitude to my friend Cui Haiyang from TU Delft, Wang Li, Li Xin and Chen Wenwen from Uni. Bremen that share the nice papers which helped me a lot.

Special thanks to Prof. Wang Pinxian and Prof. Wang Rujian at Tongji University in Shanghai, for the great support of my study.

Deepest love to my parents and my girlfriend, without your understanding and support, I would not be able to focus on my study far far away from you.

Contents

Tables and Figures

Chapter 1. Introduction

Chapter 2. Materials and Methods

Chapter 3. Last glacial to Holocene climate variability in the Atlantic Southern Ocean

Chapter 4. Centennial-scale climate variability of the Holocene Scotia Sea

Chapter 5. Scotia stratigraphy and environmental changes of the past 300 kyrs

Chapter 6. Conclusions and future perspectives

Chapter 1. Introduction

1.1. Motivation

The earth's climate during late Quaternary is characterized by cyclicity of glacial and interglacial periods. The pacing of the glacial/interglacial changes has been associated to insolation changes controlled by variations of earth's orbit (Hays et al., 1976; Epica members, 2004; Lisiecki and Raymo, 2005). However, comparison between methane synchronized ice core records from both polar regions (Epica members, 2006) indicates that, millennial scale climate variability in both hemispheres does not follow the same rhythm. The last glacial experienced frequent and abrupt climate changes in both hemispheres that the Antarctic warming phase corresponds to a cold stadial in Greenland (Epica members, 2006). And recent studies extend such asynchronous climate development between both hemispheres to the past two glacial periods (Margari et al., 2010). The "north cooling, south warming", known as "bipolar seesaw", also persists during the postglacial warming (Stocker, 2003; Bianchi and Gersonde, 2004; Epica members, 2006).

The interpretation of the bipolar seesaw involves changes in Atlantic Meridional Overturning Circulation (AMOC) which redistributes heat between the two hemispheres (Seidov and Maslin, 2001; Rahmstorf, 2002; Stocker, 2003; Knorr and Lohmann, 2003; 2004). Other mechanisms have been also proposed such as a sea ice induced climate instability in both North Atlantic (Kaspi et al., 2004; Denton et al., 2005; Wunsch, 2006) and Southern Ocean (Keeling and Stephens, 2001); and the latitudinal migration of Southern Westerlies (Denton et al., 2010). This "bipolar seesaw" mechanism is developed mainly based on comparisons of ice cores from both polar regions and validated by model studies (Knorr and Lohmann, 2003; 2004; Stocker, 2003; Clement and Peterson, 2008), other field observations are sparse.

To better understand the late Quaternary climate variability, the Last Glacial (LG) to Holocene time interval is of great interest, and has been most intensively studied for the past decades. During this time interval, the earth experienced the transition from an extreme cold status (Last Glacial Maximum: LGM) to the current warm period. The mechanisms driving the climate variability during this time interval may serve as analogues for the longer past earth history.

The sea level at the LGM was ca. 120-130m lower than present (Yokoyama et al., 2000; Jansen et al., 2007), and the global temperatures were significantly lower than today (Margo members, 2009). Continental ice covered large areas of high latitude northern hemisphere and lower latitude at high elevations; the East and West Antarctica, South America also housed much larger ice volume than today (Anderson et al., 2002; Clark et al., 2009; Hein et al., 2010). The LGM sea ice cover was much more expanded both in northern and southern hemispheres (Gersonde et al., 2005; de Vernal et al., 2006). It was also a time with much dustier conditions that may have enhanced marine bioproductivity (Maher et al., 2010). The termination from the LGM to the Holocene was characterized by different timing of postglacial warming between northern and southern hemispheres, which may be related to discharge of freshwater to the ocean or shift in Southern Westerlies, and resulted changes in ocean circulation (Bianchi and Gersonde, 2004; McManus et al., 2004; Epica members, 2006; Denton et al., 2010). Holocene is generally considered as a stable interglacial period, yet high temporal and spatial climate variations are widely documented (Mayewski et al., 2004; Jansen et al., 2007).

Although the Last Glacial to Holocene climate development has been intensively studied during the recent decades, the information from the southern high latitudes is still very limited. Compared to

abundant records from northern hemisphere and tropical regions, high resolution records from the southern hemisphere are mainly from Antarctic ice cores, marine records are sparse, especially the high latitudes Southern Ocean, which prevent the validation of the marine processes in response and driving the climate changes.

Another difficulty in interpreting the climate records from Southern Ocean marine sediments lies in the establishment of core stratigraphy. Little carbonate is preserved south of the Antarctic Polar Front, which hampers the application of oxygen isotope records or radiocarbon dating on carbonate microfossils as widely applied in other oceans. Instead, radiocarbon dating has been applied on organic matters in the sediments (Domack et al., 2001; Bianchi and Gersonde, 2004; Denis et al., 2009; Hillenbrand et al., 2009). However, the large uncertainty in carbon reservoir effect in the Southern Ocean further complicates the reliability of the core age model (Sikes et al., 2000; van Beek et al., 2002) and may be related to the Southern Ocean ventilation history (Skinner et al., 2010). Thus, alternative proxies such as diatom (Burckle and Burak, 1988; Kaczmarska et al., 1993; Zielinski et al., 2002; Zielinski and Gersonde, 2002) and radiolarian (Abelmann and Gersonde, 1988; Brathauer et al., 2001) biostratigraphy, magnetic susceptibility record (Schmieder, 2004; Pugh et al., 2009), and geomagnetic paleointensity (Stoner et al., 2002; Lund et al., 2006; Macri et al., 2006; Channell et al., 2009) are used to establish the core age model. However, all these proxies have weaknesses either in accuracy or limited by location or sedimentary environment. The validation of these proxies and the relationship in a bigger context of Southern Ocean climate change are yet not clear.

1.2. Background information

1.2.1. The Southern Ocean

The Southern Ocean was eventually formed during the Eocene-Oligocene Boundary along with the opening of Tasmania-Antarctic and Drake Passages (Lawver and Gahagan, 2003; Scher and Martin, 2006). The opening of the deep water pass ways initiated the formation of the Antarctic Circumpolar Current (ACC) and isolated Antarctica, reducing north-south heat transport, inducing the significant glaciation since Eocene-Oligocene boundary (Zachos et al., 2001; Barker and Thomas, 2004; Mackensen, 2004; Barker et al., 2007). The Southern Ocean is the only water territory that connects the Atlantic, Pacific and Indian Oceans, acting for the mass and heat exchanges for the global oceans, thus it plays a significant role in the global thermohaline circulation. Antarctic Bottom water as the densest water mass in the ocean is formed along the Antarctic coastal regions, which makes up the important end member for the deep water circulation from the south (Foldvik et al., 2004).

The ACC represents the largest ocean current on earth and is a critical component of the global ocean circulation. It averages ~130 Sv (10^6 m^3/s) transport through Drake Passage (Whitworth and Perterson, 1985; Cunningham et al., 2003), extending around the globe with a length of about 24,000 km (Olbers, et al., 2004). The ACC is generally considered as Southern Westerly winds driven and in most places flow to depth to the sea bed (Orsi et al., 1995; Barker and Thomas, 2004). The ACC consists of a series of oceanic fronts, defined by signatures of water properties such as temperature, salinity and density, from north to south the major ones are Subtropical Front (STF), Subantarctic Front (SAF), Polar Front (PF) and Southern ACC Front (Orsi et al., 1995). Bounded by the oceanic fronts, the Southern Ocean is divided to several zones: Subantarctic Zone (SAZ) bounded by STF and

SAF; Polar Frontal Zone (PFZ) by SAF and PF; and Antarctic Zone (AZ) by PF and the Antarctic continent (Belkin and Gordon, 1996).

Among the ACC fronts, the PF represents the most important frontal system in the ACC, it marks the location where Antarctic surface waters moving to the north sink rapidly below Subantarctic waters, also known as the Antarctic Convergence (Orsi et al., 1995). Across the PF, the sea surface temperature (SST) changes ~1.35˚C over a distance less than 60 km (Moore et al., 1997). Today the core of the ACC occurs near the summer SST 4˚C isotherm at the PF (Olbers et al., 2004). The PF is a strong jet within the ACC (Nowlin and Klinck, 1986). At Drake Passage, 12 years observation data show that the strongest surface currents are found in the SAF and PF with average speed of 50 cm/s and 35 cm/s respectively and inversely correlated (Cunningham and Pavic, 2007). Estimation by Gille (1994) shows that 40-70% of ACC transport occurred within the SAF and PF, and the mean pass of SAF and PF are substantially steered by topography (Gille, 1994; Moore et al., 1997; Moore et al., 1999; Dong et al., 2006). The mean position of the PF varies spatially, located roughly at 45-50˚S in the Southern Ocean Atlantic and Indian sectors, it is much more to the north relative to the Pacific sector (roughly 60-65˚S) (Orsi et al., 1995). The mean position of the PF also fluctuates seasonally and varies during glacial-interglacial times, associated with the wind field and sea ice expansion, the meridional shifts of the PF pass correspond to the meridional shifts of the wind field (Moore et al., 1997; 1999; Bryden and Cunningham, 2003; Barker and Thomas, 2004; Dong et al., 2006).

The PF also serves as the northern boundary of Southern Ocean circumpolar opal belt, which is situated between the PF and the seasonal sea ice limit to the south, as a result of intensive biosiliceous productivity in this region, mainly composed of diatoms (Diekmann, 2007). More to the south, lithogenic component inputed by wind, current or ice transport take over the main component due to the opal dissolution and lowered bioproductivity by longer duration of sea ice cover; north of the Polar Front, biogenic carbonate gradually increase towards low latitudes, in response of the influx of North Atlantic Deep Water (Diekmann, 2007). In consequence, the sedimentary pattern shifts northward/southward according to changes in climate and ocean circulation.

The Southern Ocean is a key region in driving and amplifying the global climate. It is actively involved in the global carbon cycle by physical climate system and the marine ecosystem. Ice core studies show that, variations in atmospheric CO_2 content broadly followed Antarctic temperature (Mudelsee, 2001; Sigman et al., 2010), typically by several centuries to a millennium. The marine carbon cycles are assumed to be primarily responsible for the glacial/interglacial variations of atmospheric CO_2 content, and the processes in the Southern Ocean played a significant role in regulating atmospheric CO_2 changes in terms of biological pump and surface/deep water circulation/structure (Sigman and Boyle, 2000; Kohfeld et al., 2005). Southern Ocean waters are high nutrient low chlorophyll (HNLC) waters that favor the growing of phytoplankton and sequestrate CO_2 to the deep ocean. High efficient export of carbon to the deep Southern Ocean by biological pump during the glacial times (Kohfeld et al., 2005; Abelmann et al., 2006) would lower the atmospheric CO_2 and kept in the deep waters resulting from heavy stratification of the surface and deep waters during glacial times, which prevents the ventilation of deep waters (Stephens and Keeling, 2000; Sigman et al., 2004; Hillenbrand and Cortese, 2006; Bouttes et al., 2009). In contrast, during times of post glacial warming, intensive upwelling in the Southern Ocean would have released the stored CO_2 back to the atmosphere and amplified the warming process (Anderson et al., 2009; 2010).

One significant feature of the Southern Ocean is the expansive and seasonally varied sea ice distribution. Satellite observation shows that, in the Antarctic region, large seasonal changes of sea ice

cover occur (Comiso, 2003; 2010). Maximum sea ice cover occurs in austral winter, with an area of ca. 18.3×10^6 km^2 during September, shown as a continuous ring covering a significant part of the southern Atlantic, Indian and Pacific oceans; minimum sea ice cover occurs in austral summer in February covering an area of ca. 3×10^6 km^2 mainly in the western Weddell Sea, Bellingshausen Sea, Amundsen Sea and parts of the Ross Sea and the Indian Ocean (Comiso, 2010). Sea ice acts as an amplifier to the climate through high albedo and modulating the gas and heat exchange between atmosphere and ocean (Stephens and Keeling, 2000). In addition, the growth and decay of sea ice causes redistribution of salt in the ocean and modulate ocean circulation. During sea ice formation, brine rejection can initiate vertical convection and/or bottom water formation. In contrast, the sea ice melting introduces low salinity surface water lens that resulting in stratified upper water column, and favors the phytoplankton growth in terms of surface water stability, as well as iron fertilization by releasing the sea ice loaded dust to the water, and in consequence enhances the carbon export to the deep ocean by "biological pump" (Abelmann et al., 2006).

The Southern Westerlies are the most dominant atmospheric circulation in the Southern Ocean and they are considered as the main driven force of the Antarctic Circumpolar Current (ACC). The wind driven upwelling brings nutrient from deep water to the ocean surface and builds up the phytoplankton biomass. Westerlies carry moisture that has great impact of glacier fluctuation (Douglass et al., 2005; 2006) and controls the precipitation and in turn vegetation distribution on the adjacent land, e.g. South America (Lamy et al., 2010). The Westerlies also regulate heat distribution in the Southern Hemisphere (Schulmeister et al., 2004; McGlone et al., 2010). Moreover, the Westerlies are the carrier of eolian dust transported to the open ocean which fertilizes the water column by iron. The Westerlies are also related to the changes in atmospheric CO_2 content in respect of relative positions of the Westerlies and the ACC. For example, during the warming process, the southward shifted Westerlies induce strong upwelling at the southern high latitudes and release the CO_2 from the deep ocean stored in glacial times and increases the atmospheric CO_2 content (Toggweiler et al., 2006; Anderson et al., 2009; 2010; Skinner et al., 2010). Thus, the changes in intensity and shift in latitudes of the Westerlies have great impact in the wind driven upwelling and associated nutrient supply, dust transport, and CO_2 variability in the atmosphere (Denton et al., 2010).

1.2.2. The South Atlantic

The South Atlantic (Fig. 1; Fig. 2) represents a key region in the Southern Ocean and global ocean circulation system, and it is a crucial area for the global climate change. Warm water from Indian Ocean enters South Atlantic south of Africa, and further delivered to North Atlantic by cross-equatorial transport. The upper and intermediate layers of warm water reach high latitudes North Atlantic and cools and sinks down to form North Atlantic Deep Water (NADW) and returns to the south at depth; to the west, cold water from Pacific Ocean imported into South Atlantic through Drake Passage close the loop of the global oceanic circulation. In such basis, the "warm water route" and "cold water route" were defined in the South Atlantic (Seidov and Maslin, 2001). Acting as a "flywheel", the processes in the South Atlantic may trigger the resumption of NADW formation (Knorr and Lohmann, 2003; 2004).

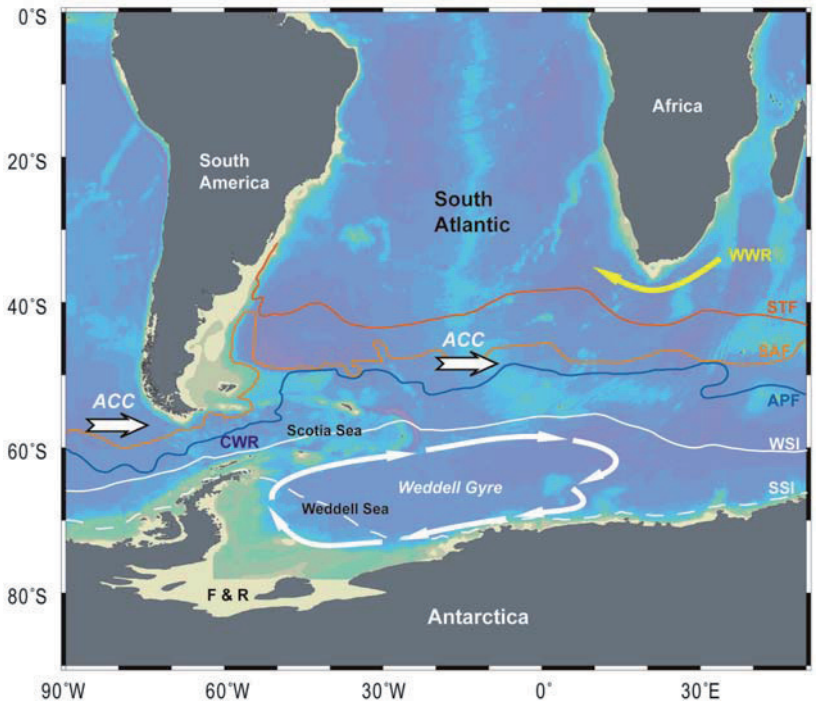

Fig. 1. Surface water circulation and frontal system in the South Atlantic Ocean. ACC: Antarctic Circumpolar Current; APF: Antarctic Polar Front; SAF: Subantarctic Front; STF: Subtropical Front; WSI: modern Winter Sea Ice; SSI: modern Summer Sea Ice. CWR: Cold Water Route; WWR: Warm Water Route (Seidov and Maslin, 2001); F & R: Filchner and Ronne Ice Shelf. Locations of oceanic fronts according to Orsi et al. (1995); sea ice distribution data from Comiso (2003).

Located in the southernmost Atlantic sector of the Southern Ocean, Weddell Sea is embraced by the Antarctic Peninsula in the west and the Antarctic continent in the south, characterized by the large density driven cyclonic circulating Weddell Gyre extending northeastward, the geostrophic shear and a southward return of the ACC mark its northeastern end near 30˚E, to the north it extends over the southern Scotia Sea and loops northward around the South Sandwich Arc (Orsi et al., 1993). Weddell Gyre is one of the biggest gyre on earth, representing the coldest water system in the global ocean.

More than 60% of Antarctic Bottom Water (AABW) is formed in the Weddell Sea (Meredith et al., 2000; Foldvik et al., 2004; Orsi et al., 1993; 1999), thus represents a key region for the global oceanic circulation. The key processes producing these bottom waters are the formation of sea ice over the broad continental shelf of the southwestern Weddell Sea, and more importantly for nowadays, the generation under the shelf ice, in the south the largest as Filchner-Ronne Shelf Ice and other smaller ice shelves such as Larsen Ice Shelf in the western Weddell Sea (Huhn et al., 2008; Nicholls et al., 2009). The AABW from the Weddell Sea spreads towards north and mixes with North Atlantic Deep Water (NADW). In contrast, during the LGM, the WAIS is grounded on the shelf (Bentley and Anderson, 1998; Anderson et al., 2002; Molosa and Anderson, 2006), denser deep water formation in the Southern Ocean mainly results from intensive sea ice formation, causing more stratified deep ocean structure (Watson and Naveira Garabato, 2006). Thus, changes in surface water conditions (and related sea ice conditions) have direct impact on deep water formation. Cold waters are transported to the open ocean by the Weddell Gyre, and closely related to the sea ice formation and thus have great impact on the climate changes of the South Atlantic Ocean. However, the history of the Weddell Gyre

and related cold water expansion is poorly understood, because very little marine sediments in the Weddell Sea have been recovered, and the sedimentation rate in the Weddell Sea is extremely low due to the low bioproductivity caused by sea ice cover (Fischer et al., 1988; Abelmann and Gersonde, 1991; Bianchi et al., 1992).

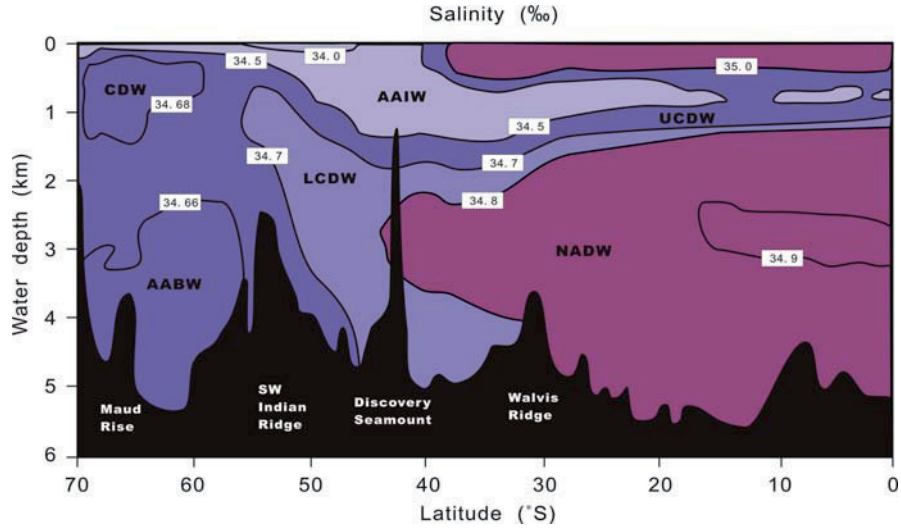

Fig. 2. Deep water structure of the South Atlantic Ocean along the Greenwich Meridian (after Reid, 1989). AABW: Antarctic Bottom Water; AAIW: Antarctic Intermediate Water; CDW: Circumpolar Deep Water; LCDW: Lower Circumpolar Deep Water; UCDW: Upper Circumpolar Deep Water; WSBW: Weddell Sea Bottom Water.

1.2.3. Scotia Sea

Located at the southwest Atlantic, the Scotia Sea is bounded to the south by the South Scotia Ridge, to the north by the North Scotia Ridge, and to the east by the South Sandwich Islands Arc. Scotia Sea was formed with the opening of the Drake Passage, when the Antarctic Peninsula separated from South America (Barker et al., 1991; Lawver et al., 1992; Livermore et al., 1994).

The circulation in the Scotia Sea is characterized by the eastward flowing ACC and the Weddell Sea Deep Water (WSDW) flowing northward from the Weddell Gyre. The ACC transports Pacific waters into the South Atlantic, mostly across the northern part of Drake Passage (Orsi et al., 1995; Moore et al., 1997), It is proposed that much of the flow occurs within narrow jets associated the Polar Front and the Subantarctic Front (Peterson and Whitworth, 1989; Gille, 1994). The WSDW in the Scotia Sea is derived from the Weddell Sea Bottom Water, which clockwise flows in the Weddell Sea following the Weddell Gyre southward of the ACC (Fahrbach et al., 1994; Schröder and Fahrbach, 1999). The WSBW flows through the morphologic gaps along the Powell and Jane Basins, and along the South Sandwich Trench towards South Atlantic (Foster and Middleton, 1980; Locarnini et al., 1993; Howe et al., 1998). The passways of the oceanic currents are strongly geographically confined.

The Scotia Sea receives terrigenous sediments mainly from the nearby terrestrial sources or introduced through interbasinal sediment transfer from adjacent seas (Diekmann et al., 2000). Ice rafting supplies glaciogenic debris to the open ocean from southern Patagonia, Antarctic Peninsula and adjacent islands; current transport disperses sediments to the pelagic Scotia Sea (Pudsey and Howe, 1998; Diekmann et al., 2000).

Besides these two main sources, frequent volcanic activities around Scotia Sea from the Antarctic Peninsula, Patagonia and surrounded islands distribute volcanic ashes to the Scotia Sea in geological time (Moreton and Smellie, 1998; Smellie, 1999). Several recently active volcanoes are located in the Antarctic Peninsula region, which distribute the tephra within the Bransfield Strait and across the South Shetland Islands and dispersed across the Scotia Sea by prevailing eastward oceanic and atmospheric circulation (Björck et al., 1991). Although the volcanic ashes are insignificant as terrigenous supply, they would serve as important age marker in regional scale according to the distributed area, and potentially be correlated to the volcanic activities recorded in the Antarctic ice cores.

1.2.4. Diatoms

Diatoms exist in almost all kinds of aquatic environment including fresh and marine waters. They are photosynthesizing and autotrophic algae thus live in the photic zone in the upper water column. Diatom cells are contained in a silicate cell wall comprising two separate valves (frustules). Based on the structure of their siliceous frustules, they are divided into two orders: the Centrales, which appear radially symmetrical; and the Pennales, which is bilaterally symmetrical (Round et al., 1990).

In cold marine waters, diatoms are especially abundant. In the Southern Ocean, diatoms contribute up to 75% of the primary productivity (Tréguer et al., 1995). The siliceous remains of diatoms constitute the circum Antarctic opal belt, which is the most remarkable sedimentological feature of the Southern Ocean (Diekmann et al., 2007).

Different diatom species adapt to specific environment conditions, such as salinity, temperature and nutrient availability. These environmental indications make it possible to monitor palaeo environmental conditions based on diatoms (e.g. Crosta et al., 1997; Zielinski and Gersonde, 1997; Zielinski et al., 1998; Kemp et al., 2000). In areas of cold water environment such as Southern Ocean, calcareous microfossils are sparse for detailed investigation, and in turn diatom becomes one of the most promising proxies for paleo environment reconstructions. The diatom in marine sediment may only represent 1-5% of the living assemblage in surface plankton. Zooplankton grazing destructs the diatom frustules; more importantly, dissolution during the transfer to the sea floor alters the assemblage by preferentially dissolving lightly silicified frustules, and enriched in more robust forms and resting spores (Gersonde and Wefer, 1987), and thus represents the biggest challenge of using diatoms as paleoenvironmental proxy.

1.3. Objectives

The main objectives of this dissertation are to use diatom based climatic records to provide additional information in understanding the late Quaternary climate variability in the key region Southern Ocean Atlantic sector. This dissertation aims to

1. provide a series of new high resolution marine records covering wide area of the high latitudes South Atlantic by reconstructing summer sea surface temperatures and sea ice changes during the past 30 kyr (Last Glacial to Holocene), in order to give new insights in the processes of the South Atlantic in the context of global climate development;
2. reconstruct the detailed climate history of the Holocene Scotia Sea, including sea surface conditions, bioproductivity and ventilation etc.;

3. establish detailed late Quaternary stratigraphy of Scotia Sea sediment core based on multi-proxy approach, and validate the consistency of different proxies.

1.4. Synopsis

In ***Chapter 2***, the studied cores and investigations are summarized, in order to give an overview of the materials and methods conducted in this study.

The results of this study are discussed in three manuscripts (***Chapter 3-5***), which will be submitted to peer-reviewed international scientific journals.

Chapter 3:
Xiao, W., Esper, O., Gersonde, R., 2011. Last Glacial - Holocene Climate Variability in the Atlantic Southern Ocean. (To be submitted to *Quaternary Science Reviews*)

In this study, 7 new generated diatom based records south of the modern Polar Front, including 4 records from my investigation, are integrated with existing records from the South Atlantic Ocean, which cover a wide area from the Scotia Sea to the Southern Ocean Western Indian sector. With a time span of the past 30 kyrs, we aim to provide new insights in the processes of the South Atlantic in response and driving the climate development of the Last Glacial to Holocene time period. Various components such as sea ice and related cold water expansion, surface water circulation, deep water ventilation, Westerlies, opal deposition, and bioproductivity are discussed.

Chapter 4:
Xiao, W., Gersonde, R., Frederichs, T., 2011. Centennial-scale climate variability of the Holocene Scotia Sea (Atlantic Southern Ocean). (To be submitted to *Paleoceanography*)

We provide the first high resolution Holocene record from the Scotia Sea, which enables detailed investigation of Holocene climate development in this area. We focus on the possible mechanism driving the climate variability in this area. We also discover the reservoir changes, which may be related to the ventilation, in the Holocene Scotia Sea. Bioproductivity and nutrient supply are also discussed.

Chapter 5:
Xiao, W., Gersonde, R., Frederichs, T., Kuhn, G., 2011. Scotia Sea stratigraphy and environmental changes of the past 300 kyrs. (To be submitted to *Earth and Planetary Science Letters*)

Detailed stratigraphies are established by multi-proxy approaches for the high resolution records from the Scotia Sea. Radiocarbon chronology, correlation between magnetic susceptibility and Antarctic ice core dust and climate records, diatom biofluctuation stratigraphy, and geomagnetic chronology are applied. We also discuss the coherency and complexity of the individual proxies applied in this area. The changes in proxy values are related to environmental and further connected to climate changes in this area. We establish a possible correlation between the Scotia Sea ash layers and the Antarctic ice core ash layers, which provide additional age markers in this region.

In the end, conclusions and future perspectives are summarized in ***Chapter 6***.

Chapter 2. Materials and Methods

2.1. Materials

This study focuses on sediments from 3 core sites from the Bouvet Island area in open ocean South Atlantic and 3 core sites from the Scotia Sea, which cover a wide area in the Southern Ocean Atlantic sector (Table 1). All the cores are located south of the modern Polar Front and north of the modern winter sea ice edge, corresponding to the modern circum-Antarctic opal belt, with the maximum opal deposition to the sea floor (Diekmann et al., 2007). The sediments are consist of olive to olive gray diatom ooze and olive gray to gray diatomaceous mud/diatom bearing mud corresponding to warm interglacial intervals and cold glacial intervals, respectively. The core locations are in an area sensitive to the cold water expansion in the Southern Ocean Atlantic sector. Ash layers were identified in the Scotia Sea cores during the visual core description and observed under the microscope on smear slides and diatom slides. These ash layers are normally also presented as spikes in the magnetic susceptibility records, indicating frequent volcanic activities in the surrounding area of the Scotia Sea.

Table 1. Locations of the studied cores.

Core	Latitude	Longitude	Water depth(m)	Coring device	Recovery (m)	Studied section (m)	Cruise
PS1649-1	54° 54.88' S	3° 17.18' E	2446	BC	0.36	0-0.36	ANT VI/3 (1988)
PS1649-2	54° 54.63' S	3° 18.46' E	2427	GC	7.26	0.36-1.57	ANT VI/3 (1988)
PS1652-1	53° 40.21' S	5° 5.03' E	1960	BC	0.45	0-0.45	ANT VI/3 (1988)
PS1652-2	53° 39.84' S	5° 5.97' E	1963	GC	12.8	0-8.02	ANT VI/3 (1988)
PS2102-2	53° 4.38' S	4° 59.14' W	2390	GC	7.29	0-4.09	ANT IX/4 (1991)
PS67/197-1	55° 8.24' S	44° 6.28' W	3837	KOL & TC	23.31	0-23.31	ANT XXII/4 (2005)
PS67/206-1	57° 24.67' S	43° 27.5' W	3206	KOL & TC	23.62	0-23.62	ANT XXII/4 (2005)
PS67/219-1	57° 13.22'S	42° 28.02'W	3619	KOL & TC	20.71	0-20.71	ANT XXII/4 (2005)

Coring device: BC-box core; GC-gravity core; KOL-piston core; TC-trigger core

The studied intervals of the cores from the Bouvet Island area are focused on the past 30 kyr, which documents the last glacial to Holocene climate variability of the open ocean area of Southern Ocean Atlantic Sector (***Chapter 3***). Core PS67/206-1 represents the first centennial resolution Holocene record from the Scotia Sea (***Chapter 4***). Core PS67/197-1 extends back to ca. 86 ka, which documents the first high resolution diatom based climate variability of the last glacial in this area; and core PS67/219-1 covers the past ca. 300 ka, presenting the glacial-interglacial climate variability of the Late Pleistocene high latitudes Southern Ocean (***Chapter 5***).

2.2. Methods

2.2.1. Diatom slides preparation and microscopic estimation

In order to obtain high resolution records, for diatom analysis, the Bouvet Island area southern most cores PS1649-1/PS1649-2 were sampled at 5 cm intervals due to the low sedimentation rates; core PS1652-1 was sampled at 3 cm intervals from the top 15 cm and 5 cm from 15 to 45 cm to obtain the most recent climate change; PS1652-2 was sampled at 10 cm intervals; core PS2102-2 was sampled at 5 cm intervals for the Holocene section and 2.5 cm intervals for the last glacial to termination 1 section. The Scotia Sea cores PS67/197-1, PS67/206-1 and PS67/219-1 were sampled at 10 cm intervals. A total number of 947 samples were taken for diatom analysis.

The cleaning of the sediment samples and the preparation of permanent mounts for microscopy followed a routine method established at the Alfred-Wegener Institute for Polar and Marine Research (AWI) (Gersonde and Zielinski, 2000). 0.5 g freeze dried sediment sample were treated in a 400 ml beaker with ca. 15 ml of hydrogen peroxide (H_2O_2, 35%) and ca. 15 ml of concentrated hydrochloric acid (HCl) and heated to enhance the reaction and evaporate the peroxide. Distilled water was added up to 400 ml after the completion of the reaction. The water was gently removed using a water jet pump after a settling time of 24 h. This washing process was repeated 10 times until all acid and a portion of the clay fraction were removed. The acid cleaned residue was transferred to a 50 ml Nalgene bottle and diluted to exactly 50 ml for storage. For preservation, 2 or 3 drops of neutralized formaldehyde were added.

For diatom estimation, microscopic slides with randomly distributed diatom frustules were made. 3 grease-free circular cover glasses in 1.8 cm diameter were placed in a petri dish (diameter: 4.8 cm, wall height: 1 cm). The petri dish was filled with gelatine solution of 0.085 g/l concentration, in order to mount the suspended diatom frustules to the cover glass later. After the residue sample stored in the Nalgene bottle was resuspended carefully, a defined aliquot (depends on the concentration of diatom frustules) was taken from the center of the homogenized suspension using an automatic pipette. The aliquot was evenly and randomly suspended in the petri dish. After a settling time of 2 h, the water was removed from the petri dish using a strip of absorptive paper slice. From the dry cover glasses, 2 were selected for permanent mounting using the mounting resin Mountex (n^{20}_D~1.67, solvent: toluene). The gelatine covering the cover glasses prevented the particles on the cover glass shifting during the mounting process.

The counting procedure and definition of counting units follow those of Schrader and Gersonde (1978). Light microscopy investigations were carried out at 1000× magnification with a Zeiss Laborlux microscope with apochromatic optics. To ensure the statistical confidence, more than 400 specimens were counted for each sample in a defined area (traverse across the slide).

According to Schrader and Gersonde (1978) and Zielinski (1993) the following diatom valve fragments were counted as one valve (Fig. 1):

A. Centric diatoms with/without pseudonodulus (e.g. *Thalassiosira*, *Actinocyclus*), when more than half of the valve was present;
B. *Chaetoceros sp.*, when more than half of the valve was present;
C. Centric diatoms with horns (e.g. *Eucampia*), when more than half of the valve with horn was present;

D. Araphid diatoms (e.g. *Thalassiothrix*, *Thalassionema*), two ends of the valve were counted as one valve;
E. Diatoms with canal raphe (e.g. *Fragilariopsis*), more than half of the valve was counted as one, or when only central parts without apices were present;
F. Mono- or biraphid diatoms (e.g. *Navicula*), parts with central nodule or more than half of the valve were counted as one;
G. *Rhizosolenia sp.*, when valve with process and ending were present.

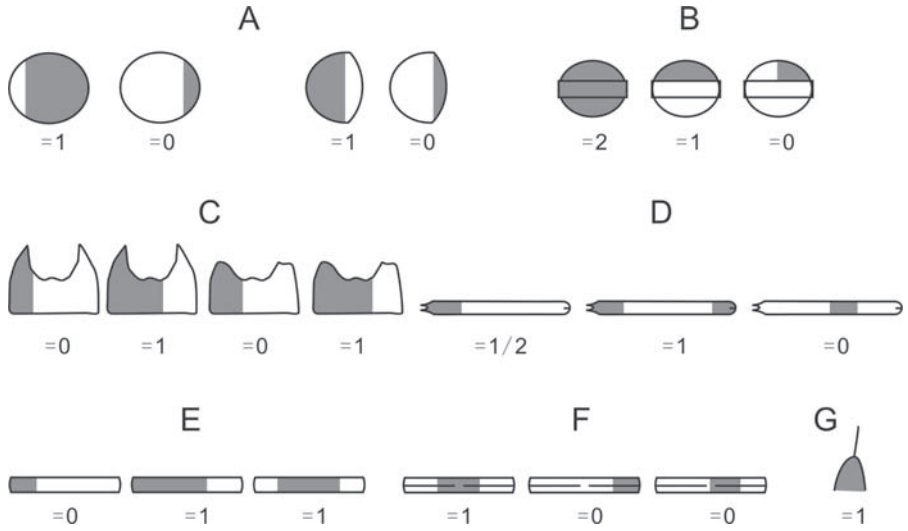

Fig. 1. Schematic illustration of criteria in counting diatom valves (after Zielinski, 1993).

2.2.2. Summer Sea Surface Temperature (SSST) reconstruction

The transfer function Imbrie and Kipp Method (IKM, Imbrie and Kipp, 1971) has been widely applied in reconstructions of paleoceanographic conditions based on microfossils. The main assumption of the IKM is that, the composition of faunal or floral assemblages dwelling in surface waters, which are preserved in the sediment record, mirrors the environmental conditions (e.g. temperature, salinity) in the surface waters. And the relationship can be applied on downcore assemblages and allows the quantitative estimation of physical parameters of the past surface water conditions.

Diatoms are the most widely distributed microorganism in the Southern Ocean, they live in the euphotic zone and thus representing the surface water conditions, and their biogeographic distribution is closely related to the surface water temperature (Zielinski and Gersonde, 1997). Zielinski et al. (1998) have developed a diatom based IKM that allowing the paleo-SSST reconstruction of Southern Ocean based on diatom assemblages, and further improved by Esper and Gersonde (2011, in prep.) recently. The diatom flux to the seafloor in the southern part of the Southern Ocean drops greatly during autumn and winter even in areas not affected by ice cover (Abelmann and Gersonde, 1991; Fischer et al., 2002), the SSSTs of the hydrographic reference data set represent average summer values (December-March) measured at 10 m below sea surface (Olbers et al., 1992). The new reference data set includes 162 sites from Atlantic, Pacific and Indian sector of Southern Ocean, 28 diatom taxa or taxa groups are included for the SSSTs estimation (Esper and Gersonde, 2011, in prep.). Due to the different diatom assemblages in different Southern Ocean sectors, the reference data set we

use for SSST reconstruction exclude the samples from Pacific and Indian Sectors, remaining 133 sites from Atlantic sector. Log transformation of the diatom abundance data was applied in order to reduce the dominance of *Fragilariopsis kerguelensis* and enhance the weight of less abundant taxa (Zielinski et al., 1998; Esper and Gersonde, in prep.). A standard error of the estimates regression with the reference data set is 0.5 ˚C. A related software package (Sieger et al. 1999) was used for calculations.

Note that the biggest challenge for the diatom based IKM reconstruction is the selective dissolution (Zielinski et al., 1998; Esper and Gersonde, in prep.). The selective dissolution will lead to an overall dominance of the robust silicified species in the surface and downcore sediments, and in contrast the lightly silicified species are dissolved that little signal can be preserved. This is particularly the case for the glacial SSST estimations in the high latitude Southern Ocean, where the diatom assemblage is mainly consist of robust species *Eucampia antarctica* and *Fragilariopsis kerguelensis*, whereas the lightly silicified cold water species, e.g. *Fragilariopsis curta* and *Fragilariopsis cylindrus*, are dissolved, and in consequence it may lead to an overestimation of glacial SSSTs (***Chapter 3***).

2.2.3. Sea Ice reconstruction

Prior to the times of satellite observation, Antarctic sea ice extent has been reconstructed by diatom assemblages which adapt to sea ice conditions. Based on combined study of annual diatom transfer from the surface water to the sea floor and mapping the diatom assemblages preserved in the surface sediments, Gersonde and Zielinski (2000) proposed over 3% of *Fragilariopsis cylindrus* and *Fragilariopsis curta*, combined as *F. curta/F. cylindrus* group, as an indicator of winter sea ice presence, whereas the summer sea ice is signaled by the presence of more than 3% of the deep-temperature species *Fragilariopsis obliquecostata*, which restricted to waters colder than -1˚C (Zielinski et al., 1997), together with a distinct drop in biogenic sedimentation rates. Similarly, Crosta et al. (1998) applied the statistical method Modern Analog Technique (MAT) based on diatom assemblages to reconstruct the time duration of sea ice presence in the year. However, the dissolution effect may bias the estimation leading to a relatively lowering of lightly silicified cold water species, and misinterpreting less sea ice occurrence at the locations more to the south (Gersonde and Zielinski, 2000). Alternatively, the sea ice extent is also reconstructed by ice core proxies. Wolff et al. (2003; 2006) interpreted the sea salt Na^+ in the ice core as a proxy for the sea ice production, based on the assumption that the sea ice formation produces most of the sea salt signal. The limitation of such proxy is that, the response of the sea salt flux to increasing sea ice extent diminished during peak glacial conditions, and only minimal variability was recorded in the ice core record (Röthlisberger et al., 2010). Moreover, the sea salt signal is also influenced by uplift, transport and deposition of the aerosol. Thus, it may only serve as overall sea ice area over a long time period when meteorological variability has been averaged out (Röthlisberger et al., 2010). In contrast, the marine proxy by diatom assemblages can trace the sea ice seasonality and the extent in a certain area. In this study, diatom proxies proposed by Gersonde and Zielinski (2000) were used to trace the sea ice variability.

2.2.4. Magnetic susceptibility

High-resolution magnetic susceptibility (MS; volume-specific), was measured at 1-cm intervals on the split half core PS67/206-1 and PS67/219-1 using a GEOTEK multisensory core logger at the

AWI-Bremerhaven. The other cores were measured on board by cruise members prior to core splitting. MS is presented as dimensionless SI units of volume-specific magnetic susceptibility of the bulk sediment.

2.2.5. Geomagnetic paleointensity

Discrete samples were taken at 5 cm intervals from the Scotia Sea cores PS67/197-1 and PS67/219-1, and 10 cm intervals from core PS67/206-1, with 2.2 cm×2.2 cm×1.8 cm plastic cubes. The samples were analyzed by colleagues in the palaeomagnetic laboratory at the *Department of Geosciences*, University of Bremen. Palaeomagnetic directions and magnetization intensities of natural remanent magnetization (NRM), anhysteretic remanent magnetization (ARM) generated in a peak alternating field of 100 mT and a biasing DC field of 40 μT as well as isothermal remanent magnetization (IRM) generated in a DC field of 100 mT were measured on a cryogenic magnetometer (model 2G Enterprises 755 HR). NRM was measured on each sample before these were subjected to a systematic demagnetization treatment involving 16 steps for each sample with a maximum alternating field (AF) intensity of 100 mT. A detailed vector analysis was applied to the results (Kirschvink, 1980) in order to determine the characteristic remanent magnetisation (ChRM). Samples showing no systematic demagnetisation pattern were rejected. Relative paleointensity (RPI) was calculated as ratios NRM_{20mT} / ARM_{20mT}, NRM_{20mT} / IRM_{20mT} using an AF demagnetization level of 20 mT for each type of remanence.

2.3. Stratigraphy

2.3.1. ^{210}Pb excess chronology

In order to determine the modern deposition, core top sediments from core PS1652-1, PS67/197-1 (KOL & TC) and PS67/206-1 (KOL & TC) have been sampled for ^{210}Pb excess analysis (Table 2). Approximately 10 g of freeze-dried sediment were packed into a plastic lid, pressed and sealed in radon proof foil for 3 weeks to establish radioactive equilibrium between ^{226}Ra and ^{222}Rn before measurement. Then the samples were analyzed by low-level low-background gamma spectroscopy using a coaxial HPGe detector (Canberra Industries). Activity concentrations of ^{210}Pb were determined. The determination was performed at the *Institute of Environmental Physics*, University of Bremen.

Table 2. Number of samples for ^{210}Pb excess analysis.

Core	number of $^{210}Pb_{ex}$ analysis
PS1652-1	6
PS67/197-1 TC	6
PS67/197-1 KOL	6
PS67/206-1 TC	6
PS67/206-1 KOL	6

2.3.2. AMS ^{14}C chronology

Southern Ocean is characterized by low carbonate deposition south of the Antarctic Polar Front, which makes it difficult to establish the core stratigraphy based on accelerator mass stectrometry (AMS) ^{14}C dating and δ^{18}O on calcareous microfossils as widely applied in other oceans. Alternatively in this study, AMS ^{14}C dating was performed on humic acid and residue fractions of organic carbon in bulk sediments. A total number of 62 new samples from studied cores have been dated in *Leibniz Labor für Altersbestimmung und Isotopenforschung*, Kiel, Germany and *Poznan Radiocarbon Laboratory*, Poznan, Poland (Table 3). The measured ^{14}C ages have been converted to calendar ages using the calibration program CALIB 6.0.1 with updated calibration curves (Stuiver and Reimer, 1993; Reimer et al., 2009).

Table 3. Number of samples for AMS ^{14}C dating.

Core	number of ^{14}C dating	Institute
PS1649-1	2	a
PS1649-2	5	a
PS1652-2	9	a
PS67/197-1 TC	2	b
PS67/197-1 KOL	10	b
PS67/206-1 TC	2	b
PS67/206-1 KOL	16	b
PS67/219-1 TC	2	b
PS67/219-1 KOL	14	b

a. *Leibniz Labor für Altersbestimmung und Isotopenforschung;*
b. *Poznan Radiocarbon Laboratory.*

2.3.3. Geomagnetic paleointensity chronology

The earth's magnetic field varies substantially in orientation (inclination and declination) and intensity through time, which is recorded in the magnetic minerals in the sediments and rocks. Dating of geological archives based on geomagnetic paleointensity has been proven a useful technique because its independent time series from other dating methods such as radiometric ^{14}C dating which is affected by various carbon reservoir effects in different regions. The geomagnetic paleointensity dating method is based on tuning to a well-dated high resolution reference curve (e.g. Stoner et al., 2002; Laj et al., 2004; Channell et al., 2009). In the Antarctic and sub Antarctic regions, the geomagnetic paleointensity chronology is especially attractive because of the lack of calcite for oxygen isotope stratigraphy and lack of appropriate materials for radiocarbon dating. In the South Atlantic, the late Pleistocene geomagnetic paleointensity has been intensively studied, and a standard curve has been well-established (Channell et al., 2000; Channell and Stoner, 2002; Stoner et al., 2002; 2003). The variation of the geomagnetic paleointensity and some globally correlated sharp excursions provide a good age control of studied cores (Channell et al., 2000; Stoner et al., 2002; 2003; Guillou et al., 2004; Channell, 2006; Lund et al., 2006). In the Antarctic Peninsula region, the geomagnetic paleointensity chronology is also well applied (Macri et al., 2006; Willmott et al., 2006).

In this study, according to the time span, geomagnetic paleointensity chronology of core PS67/206-1 was established by correlating the RPI record to the reference curves by Willmott et al. (2006) from the Antarctic Peninsula area and global reference curve by Knudsen et al. (2008) (***Chapter 4***); for cores PS67/197-1 and PS67/219-1, the RPI records were correlated to global

reference curves of GLOPIS-75 (Laj et al., 2004), SINT-800 (Guyodo and Valet, 1999), PISO-1500 (Channell et al., 2009), and well dated South Atlantic reference curve ODP 1089 (Stoner et al., 2003) (***Chapter 5***).

2.3.4. Correlation to the Antarctic ice cores

Assuming that the signals documented in the Antarctic ice cores are closely related to the climate variability in the surrounding Southern Ocean, the in phase relationship is expected between the ice core records and the marine records. Therefore, additional age models based on correlation between marine signals and ice core records were established.

The estimated SSST records were correlated to the Antarctic ice core temperature proxies $\delta^{18}O$ and δD records (Epica members, 2006; Jouzel et al., 2007); as an indicator of terrigeneous input, the magnetic susceptibility records were correlated to the ice core dust proxies non sea salt Ca^{2+} ($nssCa^{2+}$) (Fischer et al., 2007) and dust concentration record (Lambert et al., 2008) (***Chapter 4*** and ***Chapter 5***).

Chapter 3. Last Glacial - Holocene Climate Variability in the Atlantic Southern Ocean

Wenshen Xiao, Oliver Esper, Rainer Gersonde

Stiftung Alfred-Wegener-Institut für Polar- und Meeresforschung in der Helmholtz-Gemeinschaft, 27568 Bremerhaven, Germany

To be submitted to *Quaternary Science Reviews*

Abstract

The Southern Ocean climate variability is little studied due to the lack of high resolution records and difficulties of a reliable stratigraphy. New high resolution diatom based records spanning the past 30 kyrs from the Southern Ocean Atlantic and western Indian sectors were integrated with existing records from the same region, which provide comprehensive information on mapping the ocean surface conditions and related ocean circulation/ventilation, atmospheric circulation (Westerlies), and opal deposition. A detailed regional age model is established by AMS ^{14}C datings in individual cores and regional core correlations of magnetic susceptibility, stable isotopes and biofluctuations of diatom species. The age model can be a template for further paleoenvironment studies in this area.

Our reconstructions indicate that, the Last Glacial (LG) SSSTs in the area south of the modern Polar Front is 2-3˚C colder than modern conditions, winter sea ice expanded and related opal deposition shifted northward by 5˚ in Bouvet Island area. The more expanded sea ice area reduced the warm surface water imported to the South Atlantic that resulted in stronger tropical Atlantic cooling than other tropical oceans. Our data support that, during the LG, the Southern Ocean became a carbon sink due to the intensive carbon export to the stratified deep ocean. The deglacial warming started at ca. 18 cal. ka. Two steps of warming are concurrent with the Heinrich stadial 1 (18-15 ka) and Younger Dryas (12.8-11.5 ka) cooling in the northern hemisphere, supporting the bipolar seesaw mechanism which modulates the distribution of heat between the two hemispheres. In addition, we show evidences that the North Atlantic Deep Water (NADW) served as the second source of warming to the southern high latitudes ocean which extended the first step warming till ca. 14 cal. ka. The warming was interrupted by a temporal cooling at ca. 14-12 cal. ka, possibly originated from melt water input from the Antarctica and prevented the ocean ventilation. The deglacial warming in our records supports the Southern Ocean control of the deglacial atmospheric CO_2 rise. The early Holocene optimum between 11 and 9 cal. ka, and confined at ca. 11-10 cal. ka in the southern cores, marks the warmest period with the strongest sea ice reduction during the past 30 kyrs. The maximum opal deposition southward expanded to at least 55˚S. The mid-late Holocene is characterized by the cooling in the south and re-expansion of winter sea ice to the Bouvet Island area started at ca. 9-8 cal. ka. This may be related to the cold water expansion from the Weddell Gyre along with the developing cavity under the Western Antarctic Shelf Ice, and may be interplayed with the slight reduction of NADW production. Our data suggest the recent warming and retreat of sea ice may occur after 1990s in the study area.

3.1. Introduction

In their contribution to the Fourth Assessment Report of the Intergovernmental Panel on Climate Change (IPCC), Jansen et al. (2007) highlighted the need to generate well-dated paleoclimate records that document Earth climate development and variability at a large range of time scales and broad geographical coverage. Such knowledge provides insights in a) past climate dynamics including forcing, amplifying and propagating physical and/or biological mechanisms, b) climate stability and C) the range of climate variability at different states of climate conditions. Such knowledge provides the background to test the ability of numerical models to simulate realistic climate development beyond conditions described by instrumental data. Of specific interest is the accurate knowledge of the past ca. 30,000 years including a) the present interglacial (PIG), which since at least 100 y is increasingly modified by anthropogenic activities, b) the preceding Last Glacial Maximum (LGM), a cold climate end member marked by a sea level ca 120-140 below present (Jansen et al., 2007), and c) the LGM-PIG transition (Termination I), which documents a dramatic shift in climate conditions triggered by orbital forcing and punctuated by warm and/or cold on both hemispheres that display a non-synchronous pattern (EPICA, 2006; Denton et al. 2010). This period includes a large range of climate conditions, which can be reconstructed from a broad number of terrestrial (lake sediments, tree ring records) and marine sediment but also from polar and low latitude ice core records at centennial to annual resolution. Land and marine records can be dated with the radiocarbon method allowing within a certain range of limitation for accurate dating and correlation of climate records independent of proxies that are related to regional climate variability.

The substantial progress in the acquisition of LGM-PIG records obtained during the past three decades is primarily reflected by marine and land records from the Northern Hemisphere, specifically from the North Atlantic, North America, Europe and Russia. This is ideally complemented by a series of ice cores recovered from Greenland, Antarctica and low latitude glaciers. LGM-PIG ice core records can be dated by means of annual layer counting (e.g. Svensson et al., 2008) and inverse modeling techniques (e.g. Parrenin et al., 2007; Lemieux-Dudon et al., 2010) and allow for accurate inter-hemispheric correlation of climate records based on the methane records (EPICA Community Members, 2006; Lemieux-Dudon et al., 2010). Our knowledge on LGM-PIG climate development in the southern high-latitudes relies on a) Antarctic ice core records documenting the development and variability of a large scale of climate parameters such as temperature, atmospheric gas composition, dust and aerosols flux (e.g. Masson et al., 2000; Masson-Delmotte et al., 2004; EPICA Community Members, 2004, 2006; Jouzel et al., 2007, Schilt et al., 2010, Sowers, 2010, Wolff et al., 2010), b) geomorphological and lacustrine records providing insights in local glacier history and precipitation conditions (e.g. Markgraf et al., 1992; Anderson et al., 2002; McGlone, 2002; Wagner et al., 2004; Wagner and Melles, 2007; Sugden et al., 2005; Hall, 2009; Schaefer et al., 2009, Putnam et al., 2010), and c) Southern Ocean sediments. Most of the well-dated and high resolution marine records come from the Atlantic sector of the Southern Ocean and many clusters around a latitudinal transect across the eastern Atlantic Southern Ocean drilled during ODP Leg 177 between the Subtropical Front (ODP1089) and north of the winter sea ice (WSI) edge (ODP1094) (Gersonde et al., 1999). The records provide information on the variability of sea surface temperature (SST), sea ice, melt water deposition, export of biogenic components (opal) and nutrient consumption (e.g. Labeyrie et al., 1986; De La Rocha et al., 1998; Frank et al., 2000; Hodell et al., 2001; Shemesh et al., 2002; van Beek et al., 2002; Gersonde et al., 2003a; 2003b; Sachs and Anderson, 2003; Bianchi and Gersonde, 2004; Nielsen

et al., 2004; Allen et al., 2005; Pahnke and Sachs, 2006; Robinson and Sigman, 2008; Anderson et al., 2009). Examples of other Southern high-latitude records include the documentation of the sea surface development southwest of Africa (Stuut et al., 2004), off southern Chile (Lamy et al., 2002; 2007; Kaiser et al., 2005), around and south of New Zealand (Crosta et al., 2004; Pahnke and Sachs, 2006; McGlone et al., 2010), and close to the Antarctic continent: the Antarctic Peninsula (Domack et al., 2001; Shevenell et al., 2011) and off Adelié Land (Crosta et al., 2007; Denis et al., 2009).

In this paper we augment the knowledge on Southern Ocean climate development during the past 30 kyrs using diatom-based paleoceanographic reconstructions from seven sediment cores recovered in the present Permanently Open Ocean Zone (POOZ) between the Polar Front and the WSI edge between 40°48´E (western Indian sector) and 44°06´W (Scotia Sea, western Atlantic sector) (Fig. 1, Table 1). This is compared with published records from the Atlantic sector to generate a spatial picture across the Atlantic Southern Ocean, but also with climate records obtained from other Southern Ocean basins, continental ice cores and land information (Table 1) to provide a broader picture of southern high-latitude LGM-Holocene climate variability in the global context. The new information may support the proper establishment and testing of numerical simulations of past climate conditions and related modulation and forcing mechanisms, e.g. for the present interglacial (e.g. Renssen et al., 2005; 2006; Brovkin et al., 2008; Elsig et al., 2009) and the past glacial/interglacial transition (Termination I).

Our new records are aligned North of the present WSI edge and the northern boundary of the cold Weddell Gyre (Fig. 1) and provide new data on the development of the sea ice field in the Atlantic sector and of the northern Weddell Gyre extent since the last glacial. Sea ice represents an important element in the global climate system as it affects the surface albedo, influences the ocean/atmosphere exchange of heat and gas, impacts thermohaline circulation and affects primary production (Thomas and Dieckmann, 2010). The Weddell Gyre is one of the coldest water circulation systems in the global ocean and can be viewed as an interface between the Antarctic ice sheets and the open ocean. The generation of water masses linked with the presence of caverns beneath and sea ice in front of the Filchner-Ronne ice shelf which controls the production of cold deep and surface waters (Orsi et al., 1999; Hellmer, 2004; Nicholls et al., 2009). These processes are crucial for the production of cold Antarctic Bottom Water (AABW) as well as for the extent of the cold Weddell Gyre and the related sea ice field (Comiso, 2003). The reconstruction of the Weddell Gyre history helps understanding the ice-ocean interaction during colder and warmer than present climate conditions. However, most of the sediment beneath the modern Weddell Gyre is deposited at low sedimentation rates and bears only minor biosiliceous components due to the sea ice cover, thus broadly lacks siliceous microfossil assemblages required for paleoceanographic reconstructions (Fischer et al., 1988; Abelmann and Gersonde, 1991; Zielinski and Gersonde, 1997; Geibert et al., 2005).

The new records will also add information on the Southern Ocean's control on and response to external and internal climate forcing processes related to the variability of insolation and ocean circulation patterns. The last deglaciation is generally considered to be triggered by summer insolation in the Northern Hemisphere. However, the postglacial warming is not synchronous between the northern and southern hemispheres (e.g. Stocker, 2003; EPICA Community Members, 2006). The explanation of the anti-phase relationship between the northern and southern hemispheres involves changes in Atlantic Meridional Overturning Circulation (AMOC) that redistribute heat between the two hemispheres ("bipolar seesaw") as well as the latitudinal shift of Southern Westerlies (Denton et al., 2010). Climate Instability also occurs during the Holocene, but at lower amplitudes than during the

glacial and the glacial/interglacial transition, and Holocene climate evolution is not globally uniform (Jansen et al., 2007).

3.2. Materials and Methods

3.2.1. Materials and Study Area

The high-resolution last glacial-Holocene records investigated during this study (Table 1, Fig. 1) are located at seven sites in the POOZ of the Atlantic and western Indian sectors of the Southern Ocean, between 44°06´W and 40°48´E (Fig. 1, Table 1). This includes cores PS67/197-1 and PS1786-1 recovered during R/V *Polarstern* cruises ANT-XXII/4 (2005) and ANT-VIII/3 (1989) from the northern and northeastern Scotia Sea; sediment sequences combined from gravity and box corer deployments at sites PS1649 and PS1652, and gravity cores PS1651-1 (ANT-VI/3, 1988) and PS2102-2 (ANT IX/4, 1991) gathered west and close to Bouvet Island; and one piston core collected at Conrad Rise in the western Indian Ocean (PS2606-6; ANT-XI/4, 1994). Cores were generally sampled and analyzed for their diatom content at a spacing of 10 cm. Exceptions are gravity core

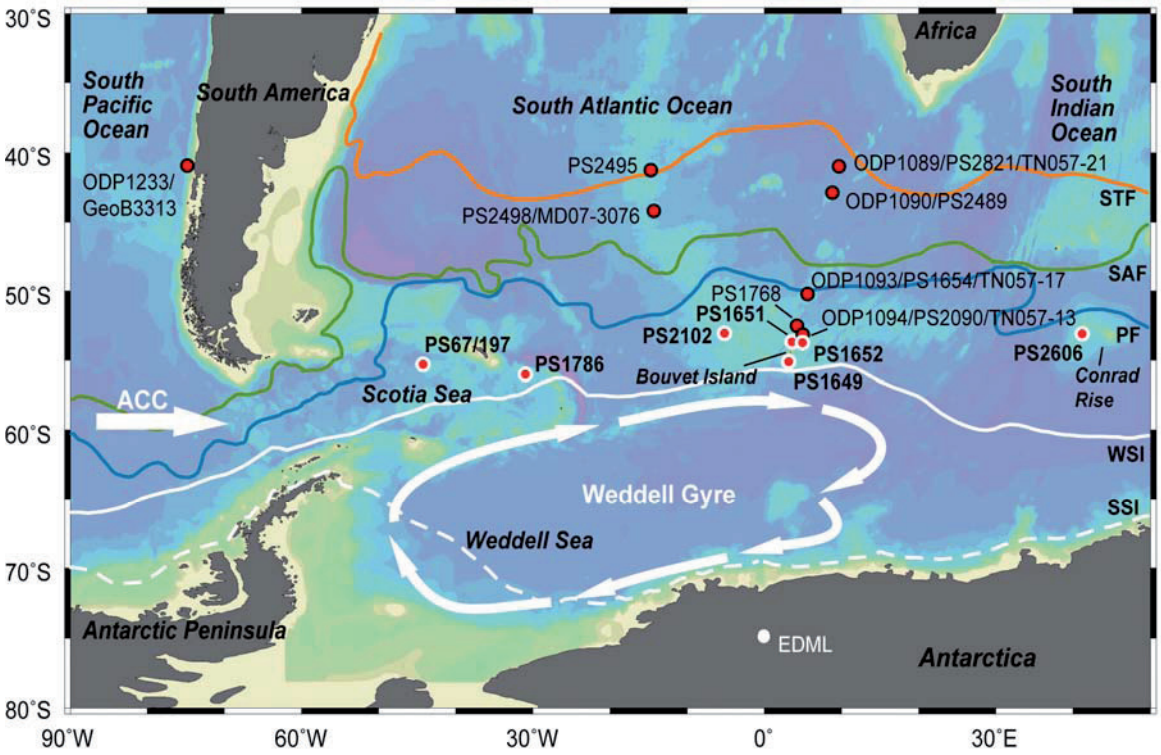

Fig. 1. Locations of studied and discussed core sites (red dots, Table 1). Sites with new records are marked with white circles and bold numbers. WSI/SSI: modern average winter/summer sea ice edge (Comiso, 2003); locations of oceanic fronts according to Orsi et al. (1995). PF: Polar Front; SAF: Subantarctic Front; STF: Subtropical Front.

PS1649-2 and box core PS1649-1, studied at 5 cm spacing and the surface sediment records from box core PS1652-1, studied at 3 cm intervals in the upper 15 cm of the core and at 5cm intervals to the core base at 45 cm. For core PS2102-2, previously investigated by van Beek et al. (2002), we have

increased the resolution of studied samples to 5 cm in the Holocene section and to 2.5 cm in the last glacial to Termination I sediments. Data on the down-core diatom assemblage variation in cores PS1786-1 and PS2606-6, partly presented by Jacot Des Combes et al. (2008), were enhanced and used to establish records of temperature and sea ice variability.

Table 1. Location and water depths, coring devices and data source of studied and discussed cores.

Station	Latitude	Longitude	Water depth/ Elevation (m)	Coring device	Data Source
Marine cores					
PS1649-1	54° 54.88' S	3° 17.18' E	2446	BC	this study
PS1649-2	54° 54.63' S	3° 18.46' E	2427	GC	this study
PS1651-1	53° 37.85' S	3° 51.37' E	2075	GC	this study
PS1652-1	53° 40.21' S	5° 5.03' E	1960	BC	this study
PS1652-2	53° 39.84' S	5° 5.97' E	1963	GC	this study
PS2102-2	53° 4.38' S	4° 59.14' W	2390	GC	this study, van Beek et al., 2002
PS67/197-1	55° 8.24' S	44° 6.28' W	3837	PC	this study
PS1786-1	55° 55.4' S	31° 43.2' W	5826	GC	this study, Jacot des Combes et al., 2008
PS2606-6	53° 13.9' S	40° 48.1' E	2545	PC	this study, Jacot des Combes et al., 2008
ODP1093	49° 58.58' S	5° 51.92' E	3624	OD	Bianchi & Gersonde, 2004
PS1654-2	50° 9.5'S	5° 43.3' E	3744	PC	Bianchi & Gersonde, 2004
TN057-17PC1	50° S	6° E	3700	PC	Nielsen et al., 2004; Divine et al., 2010
ODP1094	53° 10.8' S	5° 7.8' E	2807	OD	Bianchi & Gersonde, 2004
PS2090-1	53° 10.7'S	5° 7.98' E	2819	PC	Bianchi & Gersonde, 2004
TN057-13PC4	53° 12' S	5° 6' E	2800	PC	Anderson et al., 2009; Divine et al., 2010
PS1768-8	52° 35.58' S	4° 28.56' E	3299	GC	Zielinski et al., 1998; Gersonde et al., 2003a
ODP1089	40° 56.18' S	9° 53.64' E	4620	OD	Cortese et al., 2002; Cortese et al., 2007
PS2821-1	40° 56.58' S	9° 53.28' E	4575	PC	Cortese et al., 2002; Cortese et al., 2007
TN057-21	41° 8' S	7° 49' E	4981	PC	Barker et al., 2009; 2010
ODP1090	42° 52.4' S	8° 55.1' E	3699	OD	Martinez-Garcia et al., 2009
PS2489-2	42° 52.4' S	8° 58.4' E	3794	PC	Martinez-Garcia et al., 2009
PS2495-3	41° 16.5' S	14° 29.4' W	3134	GC	Gersonde et al., 2003a
PS2498-1	44° 9.2' S	14° 13.7' W	3783	GC	Gersonde et al., 2003a
MD07-3076	44° 4.46' S	14° 12.47' W	3770	PC	Skinner et al., 2010
ODP1233	41° 0.01' S	74° 26.99' W	838	OD	Lamy et al., 2004; 2007; Kaiser et al., 2005
GeoB3313-1	41° S	74° 27' W	852	GC	Lamy et al., 2002
GGC5	33° 42' N	57° 35' W	4550	PC	McManus et al., 2004
Ice cores					
EDC	75° 6' S	123° 21' E	3233		Jouzel et al., 2007
EDML	75° S	0°	2891		Epica members, 2006
NGRIP	75° 6' N	42° 19.2' W	2917		NGICP members, 2004

Coring device: BC-box core; GC-gravity core; PC-piston core; OD-ocean drilling

3.2.2. Sample Preparation and Diatom Census

The sample treatment and the preparation of permanent mounts for light microscopy followed the standard procedure established at AWI-Bremerhaven (Gersonde and Zielinski, 2000). Counts on diatom species were carried out on the permanent mounted slides of acid-cleaned materials. Following the taxonomy described by Zielinski and Gersonde (1997), the diatom taxa were counted at the magnification of 1000× with a Zeiss Laborlux microscope with apochromatic optics. The counting procedure and definition of counting units followed those of Schrader and Gersonde (1978). A minimum of 400 specimens were counted in each sample.

3.2.3. Summer Sea Surface Temperature and Sea Ice Estimation

To estimate past surface ocean temperature variability we applied a diatom reference data set previously established by Zielinski et al. (1998) and further improved by Esper and Gersonde (2011, in prep.) using the Imbrie and Kipp transfer function method (IKM, Imbrie and Kipp, 1971). The reference data set includes diatom assemblage data obtained from 133 sites in the Atlantic sector of the Southern Ocean, considering the abundance pattern of 28 diatom taxa or taxa groups (Zielinski et al., 1998; Esper and Gersonde, 2011, in prep.). The used hydrographic data set represents values measured at10 m below sea surface as presented by Olbers et al. (1992). We follow the suggestion of Zielinski et al. (1998) and restrict the estimation of past surface ocean temperature to summer sea surface temperature (SSST) considering the results from sediment trap experiments, which show that in the Southern Ocean significant diatom flux to the sea floor is restricted to austral summer (e.g. Abelmann and Gersonde, 1991; Fischer et al., 2002). Log transformation of the diatom abundance data was applied in order to reduce the dominance of *Fragilariopsis kerguelensis* and enhance the weight of less abundant taxa. The standard error of the estimates regression with the reference data set is 0.5 ˚C. A software package prepared by Sieger et al. (1999) was used for the calculations. The diatom based IKM SSST estimation has been previously successfully used e.g. by Kunz-Pirrung et al. (2002), Bianchi and Gersonde (2002, 2004) and, Gersonde et al. (2003a; 2003b; 2005). The calculated communalities for the estimates generally range between 0.8 and 0.9.

Estimation of the WSI extent was preferred to follow the method proposed by Gersonde and Zielinski (2000): relative abundance >3% of the two diatom sea-ice indicator species, *Fragilariopsis curta* and *Fragilariopsis cylindrus*, combined as *F. curta* group, indicates the presence of WSI; and >3% of *Fragilariopsis obliquecostata*, a species restricted to waters colder than -1˚C (Zielinski et al., 1997), along with a distinct drop in biogenic sedimentation rate, are interpreted as the proximity of the summer sea ice edge. The sea ice estimation method proposed by Crosta et al. (1998a), by which the duration of sea ice at the core site (month/year) estimated with the modern analogue technique (MAT), was not used in this study. This statistical method does not consider dissolution of the diatom assemblage, which may strongly affect the preservation and abundance of more weakly silicified sea ice indicators such as *F. curta* and *F. cylindrus*. The dissolution of these taxa may result from decreased biogenic opal export and burial in areas affected by stronger annual sea ice occurrence and thus may lead to an underestimation of the annual duration of sea ice. Such effect has been found especially in the glacial assemblages preserved at the sites located closest to the modern sea ice edge, PS1786 and PS1649 (Fig. 5; Fig. 7).

3.3. Stratigraphy

A major challenge represents the accurate dating of Southern Ocean sediment records needed to put them into a detailed time frame together with other records obtained from marine, ice and land archives. For the dating of Holocene and last glacial records the radiocarbon method calibrated for the past 50,000 years, thus back to the limits of radiocarbon dating, proved to be of greatest utility. However, evidences show that besides differences in regional reservoir ages, reservoir shifts have occurred in the past (Hughen et al., 2004, 2006; Fairbanks et al. 2005), which mirror the impact of ocean circulation and ventilation. This accounts especially for the Southern Ocean where strong reservoir effects that may exceed 1000 yrs (Bard, 1988) and reservoir shifts in surface and deep waters

that may by as large as 1500-5000 yrs in the last glacial and the last glacial-interglacial transition (Termination I), and may also occurred during the Holocene (Sikes et al., 2000; van Beek et al., 2002; Barker et al., 2010; Skinner et al., 2010). Additionally, in Southern Ocean sediments dating based on AMS ^{14}C and oxygen isotope measurements of calcareous hard-parts of foraminifers is hampered by the widespread scarcity or lack of biogenic carbonate.

To generate age models of highest possible accuracy and consistency we combine 129 available and new AMS ^{14}C data from nine core sites derived from planktic foraminifers and organic carbon in bulk samples (Table 2) together with available oxygen and carbon isotope records also considering the regional pattern of magnetic susceptibility, diatom species abundance and transfer function derived summer sea surface temperature (SSST) records.

3.3.1. AMS ^{14}C chronology

New AMS ^{14}C ages dated on organic carbon from both humic acid and residue fractions were obtained from the bulk sediment samples of PS1649-1/PS1649-2, PS1652-2 at the *Leibniz Labor für Altersbestimmung und Isotopenforschung* in Kiel, Germany, and PS67/197-1 at *Poznan Radiocarbon Laboratory* in Poland. The AMS ^{14}C datings of other cores are summarized from previous studies (van Beek et al., 2002; Gersonde et al., 2003a; Bianchi and Gersonde, 2004; Jacot Des Combes et al., 2008) (Table 2). The datings on organic carbon humic acid fraction for cores PS1786-1 and PS2606-6 were previously partly presented in Jacot Des Combes et al. (2008), other datings are first time presented here.

The measured residue ages represent less than 100 to more than 2000 years older than the humic ages (Table 2). Generally, in Bouvet Island area, the residue ages are comparable to the humic ages during the Holocene but diverse largely during the last glacial and termination 1, suggesting the residue fraction is contaminated by re-deposition of old stable organic carbon, and the contamination is less in Holocene than in last glacial and the following deglaciation. This is in agreement with the diatom ooze deposition in the Holocene section and more terrigenous material in the older sections of the cores.

Table 2. Determination of AMS ^{14}C ages of studied cores, together with other datings from previous studies in the area. Values used to establish the age models are marked bold. The conversion to calendar age are obtained using the calibration program CALIB 6.0.1 with updated calibration curves (Stuiver and Reimer, 1993; Reimer et al., 2009), According to previous studies, we use a reservoir age of 1100 years (ΔR=700 years) in the Bouvet Island area and western Indian Sector, and 1300 years (ΔR=900 years) in the Scotia Sea. C sources for dating are: R - residue fraction; H - humic acid fraction; F - foraminifera *N. pachyderma*$_{sin}$.

Core	Depth (cm)	Lab ID	C source	^{14}C age (yrs BP)	Error (yrs)	Calib. Age (cal. yr BP)	^{226}Ra age (yrs BP)	Ref.
PS1649-1	2-5	KIA 36296	R	4495	±40	3741		1
	2-5	**KIA 36296**	**H**	**2500**	**+30/-25**	**1337**		1
	31-34	KIA 36297	R	8775	±50	8532		1
	31-34	**KIA 36297**	**H**	**7445**	**±40**	**7276**		1
PS1649-2	37-40	KIA 36298	R	9735	±50	9730		1
	37-40	**KIA 36298**	**H**	**10100**	**±55**	**10247**		1
	56-59	KIA 36299	R	10560	±60	10761		1
	56-59	**KIA 36299**	**H**	**10415**	**+55/-50**	**10572**		1
	84-87	KIA 36300	R	13940	±80	15316		1
	84-87	**KIA 36300**	**H**	**13350**	**±55**	**14109**		1
	121-124	KIA 36301	R	19320	+210/-200	21786		1
	121-124	**KIA 36301**	**H**	**17900**	**±200**	**19946**		1

Core	Depth (cm)	Lab ID	C source	^{14}C age (yrs BP)	Error (yrs)	Calib. Age (cal. yr BP)	^{226}Ra age (yrs BP)	Ref.
	151-154	KIA 36302	R	19070	+280/-270	21448		1
	151-154	**KIA 36302**	**H**	**19690**	**+310/-300**	**22135**		1
PS1652-2	6.5-10	KIA 36303	R	1855	±30	699		1
	6.5-10	**KIA 36303**	**H**	**1815**	**±30**	**670**		1
	198-202	KIA 36304	R	4640	±25	3924		1
	198-202	**KIA 36304**	**H**	**4415**	**±35**	**3635**		1
	315-319	KIA 36305	R	6335	±35	6036		1
	315-319	**KIA 36305**	**H**	**6255**	**±35**	**5940**		1
	406.5-410.5	KIA 36306	R	8285	±35	8043		1
	406.5-410.5	KIA 36306a	H	7955	**±35**	7717		1
	406.5-410.5	KIA 36306b	H	8265	±40	8815		1
	406.5-410.5	**KIA 36306***	**H**	**8110**	**±40**	**7870**		1
	486.5-490	KIA 36307	R	8875	±45	8668		1
	486.5-490	**KIA 36307**	**H**	**8835**	**±45**	**8609**		1
	627-630	KIA 36308	R	10215	+55/-50	10371		1
	627-630	KIA 36308	H	10055	±55	10201		1
	711-715	KIA 36309	R	22260	+390/-370	25304		1
	711-715	KIA 36309	H	20120	±140	22677		1
	762-766	KIA 36310	R	20360	+280/-270	22962		1
	762-766	KIA 36310	H	18310	±80	20411		1
	801-805	KIA 36311	R	26310	+1410/-1200	29799		1
	801-805	KIA 36311	H	17850	±130	19900		1
PS2102-2	**20-23**	**KIA29590**	**F**	**1890**	**±30**	**727**		1
	26.5-27.5	**KIA9300**	**F**	**2095**	**±40**	**943**	855±35	2
	70.5-71.5	**KIA9299**	**F**	**3345**	**±60**	**2335**	2255±75	2
	72-75	AAR-1530	F	3050	±75	1975	2335±75	2
	207.5-210	AAR-1532	F	6650	±70	6366	6630±220	2
	210.5-211.5	**KIA10019**	**F**	**7110**	**±90**	**6894**	6700±220	2
	266.5	**KIA9298**	**F**	**10150**	**±60**	**10305**		1
	300-302.5	**AAR-1533**	**F**	**10440**	**±140**	**10641**	9560±320	2
PS1654-2	**22-27**	**KIA14938**	**F**	**3930**	**±30**	**3049**		3
	95-100	KIA15510	R	8120	±50	7883		3
	95-100	**KIA15510**	**H**	**7320**	**±50**	**7151**		3
	316-321	KIA15511	R	9525	+60/-55	9488		3
	316-321	**KIA15511**	**H**	**8930**	**±60**	**8758**		3
	441-445	KIA15512	R	10200	±70	10355		3
	441-445	KIA15512	H	9820	±70	9881		3
	460-464	**KIA15514**	**F**	**10270**	**±60**	**10432**		3
	533-538	**KIA15515**	**F**	**10530**	**±55**	**10706**		3
	538-542	KIA14941	R	10460	±70	10628		3
	538-542	KIA14941	H	10450	±70	10616		3
	621-626	KIA14945	R	12730	±60	13468		3
	621-626	KIA14945	H	10410	±80	10573		3
	627-632	**KIA14939**	**F**	**10920**	**±50**	**11205**		3
	748-752	KIA14946	R	11790	±70	12609		3
	748-752	**KIA14946**	**H**	**11670**	**+80/-70**	**12464**		3
	905-909	KIA14942	R	12970	±80	13712		3
	905-909	**KIA14942**	**H**	**13070**	**±90**	**13823**		3
	1009-1013	KIA14943	R	13440	±80	14370		3
	1009-1013	**KIA14943**	**H**	**13700**	**+120/-110**	**14781**		3
	1068-1072	**KIA14944**	**R**	**15860**	**±120**	**17960**		3
	1068-1072	KIA14944	H	17320	±230	19333		3
PS1768-8	**8 - 9.5**	**AAR-1535**	**F**	**2850**	**±75**	**1739**		1
	53 - 55	**AAR-1536**	**F**	**9540**	**±110**	**9513**		4
	77 - 79	**AAR-1537**	**F**	**10510**	**±140**	**10738**		4
	141.5-143.5	**AAR-1538**	**F**	**12850**	**±150**	**13594**		4
PS2090-1	0-4	KIA14947	R	2580	±30	1425		3
	0-4	**KIA14947**	**H**	**1890**	**±35**	**729**		3
	48-52	KIA14948	R	3955	±45	3086		3
	48-52	**KIA14948**	**H**	**3355**	**±50**	**2347**		3

Core	Depth (cm)	Lab ID	C source	^{14}C age (yrs BP)	Error (yrs)	Calib. Age (cal. yr BP)	^{226}Ra age (yrs BP)	Ref.
	249-253	KIA14949	R	7660	±45	7465		3
	249-253	**KIA14949**	**H**	**7240**	**±50**	**7057**		3
	460-464	KIA14950	R	13110	±70	13863		3
	460-464	**KIA14950**	**H**	**9040**	**±80**	**8901**		3
	550-554	KIA14955	R	10755	±60	11063		3
	550-554	**KIA14955**	**H**	**9960**	**±80**	**10070**		3
	675-679	KIA14951	R	11890	±80	12677		3
	675-679	**KIA14951**	**H**	**11130**	**±120**	**11555**		3
	720-724	KIA14956	R	15355	±55	17332		3
	720-724	**KIA14956**	**H**	**11700**	**±100**	**12481**		3
	766-770	KIA14952	R	13740	±70	14927		3
	766-770	**KIA14952**	**H**	**12660**	**±110**	**13409**		3
	826-830	KIA14953	R	19890	+120/-110	22389		3
	826-830	KIA14953a	H	15750	+190/-180	17818		3
	826-830	KIA14953b	H	16050	±110	18241		3
	826-830	**KIA14953***	**H**	**15900**	**+190/-180**	**18025**		3
PS1786-1	2-3.5+6-7.5	KIA 16766	R	4630	±30	3653		1
	2-3.5+6-7.5	**KIA 16766**	**H**	**2725**	**±25**	**1359**		5
	71.5-75	KIA 16767	R	7180	±55	6737		1
	71.5-75	**KIA 16767**	**H**	**5655**	**±40**	**5001**		5
	121.5-124.5	KIA 16768	R	11895	±50	12525		1
	121.5-124.5	KIA 16768a	H	9460	±60	9204		1
	121.5-124.5	KIA 16768b	H	9310	±80	9016		1
	121.5-124.5	**KIA 16768***	**H**	**9385**	**±80**	**9116**		5
	151-154	KIA 16769	R	12970	±100	13525		1
	151-154	**KIA 16769**	**H**	**11470**	**+80/-70**	**11803**		1
	181-184	KIA 16770a	R	19770	±150	22012		1
	181-184	KIA 16770b	R	17960	+100/-90	19792		1
	181-184	KIA 16770*	R	18865	±150	20904		1
	181-184	KIA 16770a	H	15750	+510/-480	17601		1
	181-184	KIA 16770b	H	16800	±100	18708		1
	181-184	**KIA 16770***	**H**	**16275**	**+510/-480**	**18131**		5
PS67/197-1	0-4	Poz-32738	R	7260	±40	6829		1
	0-4	**Poz-32667**	**H**	**4470**	**±40**	**3460**		1
	270-273	Poz-32739	R	16720	±80	18654		1
	270-273	**Poz-32668**	**H**	**13350**	**±110**	**13903**		1
	470-473	Poz-32849	R	17700	±140	19544		1
	470-473	**Poz-32671**	**H**	**16020**	**±160**	**17914**		1
	542-545	Poz-32743	R	20580	±120	22971		1
	542-545	**Poz-32693**	**H**	**17370**	**±130**	**19182**		1
PS2606-6	12-16	KIA 16758a	R	2920	±45	1821		1
	12-16	KIA 16758b	R	3100	±25	2033		1
	12-16	**KIA 16758***	**R**	**3010**	**±45**	**1924**		1
	126-130	KIA 16759a	R	8090	±90	7850		1
	126-130	KIA 16759b	R	8535	±50	8304		1
	126-130	**KIA 16759***	**R**	**8315**	**±70**	**8076**		1
	126-130	KIA 16759	H	6210	±130	5895		5
	197-200	**KIA 23807**	**F**	**9975**	**±130**	**10118**		1
	226-230	KIA 16760a	R	10180	±110	10339		1
	226-230	KIA 16760b	R	10270	±50	10436		1
	226-230	**KIA 16760***	**R**	**10225**	**±110**	**10380**		1
	226-230	KIA 16760	H	7110	±110	6896		5
	273-277	**KIA 16761**	**R**	**11410**	**±70**	**12096**		1
	273-277	KIA 16761	H	7700	+170/-160	7496		5
	304-308	KIA 16762a	R	12460	±70	13233		1
	304-308	KIA 16762b	R	12175	±55	12964		1
	304-308	KIA 16762*	R	12320	±70	13118		1
	316-320	**KIA 23790**	**R**	**12970**	**±90**	**13710**		1
	316-320	KIA 23790	H	9860	±60	9956		5
	355-359	KIA 16763a	R	13715	+69/-55	14873		1

Core	Depth (cm)	Lab ID	C source	^{14}C age (yrs BP)	Error (yrs)	Calib. Age (cal. yr BP)	^{226}Ra age (yrs BP)	Ref.
	355-359	KIA 16763b	R	13330	±60	14084		1
	355-359	**KIA 16763***	**R**	**13525**	**+69/-60**	**14492**		1
	355-359	KIA 16763	H	12960	±130	13695		1
	425-429	**KIA 16764**	**R**	**17400**	**+90/-80**	**19453**		1
	425-429	KIA 16764	H	16650	±100	18736		5
	516-520	**KIA 16765**	**R**	**21860**	**+130/-120**	**24742**		1
	516-520	KIA 16765	H	20340	±210	22932		5

* samples where the ^{14}C ages were obtained by averaging values from two measurements

Reference: 1. this study; 2. van Beek et al., 2002; 3. Bianchi and Gersonde, 2004; 4. Gersonde et al., 2003a; 5. Jacot Des Combes et al., 2008

At certain intervals with same SSST and diatom species biofluctuation pattern, the radiocarbon dates show very close ages in cores both in the western part (PS2102-2) with foraminifera ^{14}C ages and eastern part (PS1652-2, PS1649-1/PS1649-2 and PS2090-2/ODP1094) with humic ^{14}C ages (Fig. 5; Table 2). This indicates that ages dated on both materials are reliable, and the same reservoir effect can be applied. Therefore, the age models of cores from Bouvet Island area are based on the foraminifera and humic ages, and preferentially foraminifera ages. In one sample (PS1654-2; 1068-1072cm), the humic age is significantly older than the residue age, the younger age is conservatively taken for calculation (Bianchi and Gersonde, 2004).

The AMS ^{14}C dates of core PS2102-2 were obtained from two institutes (van Beek et al., 2002) (Table 2). We note that the AAR (*Laboratory Department of Physics and Astronomy University of Aarhus*) ages are systematically ca. 300 years younger than the KIA ages (*Leibniz Laboratory of the University of Kiel*). The AAR age at 300-302.5 cm constrains the start of early Holocene optimum at the core site (Fig. 5), and results in extremely elevated sedimentation rate at this interval (Fig. 4). This age could be also affected by the systematical error, and subsequently the calibrated calendar age could be biased towards younger value by ca. 300 years. However, by comparing with other datings in the adjacent cores (PS1649-2, PS1654-2), this age is still reasonable, thus we kept it for the age model. One dating at the start of early Holocene optimum in core PS1652-2 (627-630 cm) is slightly younger than in other cores. Here we conservatively transfer 2 datings mark the early Holocene optimum in core PS2102-2 into the correspondent interval in core PS1652-2 by diatom species and SSST correlation.

For core PS2606-6, the humic ages are generally 2 to 3 kyr younger than the residue ages in the Holocene and 1 to 2 kyr younger in the last glacial. However, different from the cores in Bouvet Island area, the residue ages fit better to the foraminifera age (197-200cm) of the core and the humic ages in the Atlantic sector cores. Based on the fact that the diatom biofluctuations and SSST variations of core PS2606-6 in the western Indian sector fit well to those from Atlantic sector cores, especially similar to those of core PS2090-1/ODP1094, situated at similar latitude and relative location to the Polar Front. The reason for the significantly young humic ages in core PS2606-6 is yet unclear. We tentatively use the residue and foraminifera ages for the core age model.

Conventional ^{14}C ages were converted to calendar ages using a calibration program CALIB 6.0.1 with updated calibration curves (Stuiver and Reimer, 1993; Reimer et al., 2009) (Table 2). In previous studies, the carbon reservoir effects applied in the calibration were according to Bard (1988) based on latitudinal variations (Gersonde et al., 2003a; Bianchi and Gersonde, 2004; Jacot Des Combes et al., 2008). In van Beek et al. (2002), a regional reservoir for mid-late Holocene of ca. 1100 yrs has been derived at site PS2102 by comparison between AMS ^{14}C dating on planktonic forams (*N.*

pachyderma$_{sin}$) and ^{226}Ra-in-barite dating, and a significantly higher reservoir (ca. 1900 yrs) during the early Holocene. However, a well established uranium-series chronology of deep sea corals in the Southeast Pacific and Southeast Indian Ocean (Goldstein et al., 2001) shows 20-40% greater last glacial reservoir than the Holocene, and the early Holocene improved Southern Ocean ventilation (Skinner et al., 2010) suggests the reservoir effect may decrease during that time. The early Holocene significantly higher sedimentation rate in that core may have biased the early Holocene reservoir estimation (van Beek et al., 2002). Due to the lack of detailed knowledge of changes in last glacial and early Holocene reservoir in the region, a constant reservoir effect of 1100 years (ΔR=700 years) has been applied in cores from Bouvet Island area and western Indian sector core PS2606 due to the similar latitude and relative position to the Polar Front; for cores from the Scotia Sea, we applied a reservoir age of 1300 years (ΔR=900 years) in the calculation, according to previous studies on living organisms in this area (Gordon and Harkness, 1992; Berkman and Forman 1996) (Table 2).

3.3.2. ^{210}Pb excess (^{210}Pb$_{ex}$) determination

Bulk ^{210}Pb$_{ex}$ activities were measured on freeze-dried core top sediments at 2-3 cm intervals from core PS1652-1 to determine the modern deposition. The ^{210}Pb$_{ex}$ measurement was performed at the Institute of Environmental Physics, University of Bremen.

The ^{210}Pb$_{ex}$ activity of PS1652-1 shows stable decay of the upper 15 cm, only except a possibly slightly disturbed surface of the top 3 cm (Fig. 2). With a half-life of 22.3 years, the ^{210}Pb chronology is generally valid for the recent 150 years (~7 half-life, only 0.8% of the original activity left), and most reliable the recent 100 years (~5 half-life, 3% of the original activity left) (Appleby, 2001). The downcore profile suggests that the top 15 cm sediments are from modern deposition.

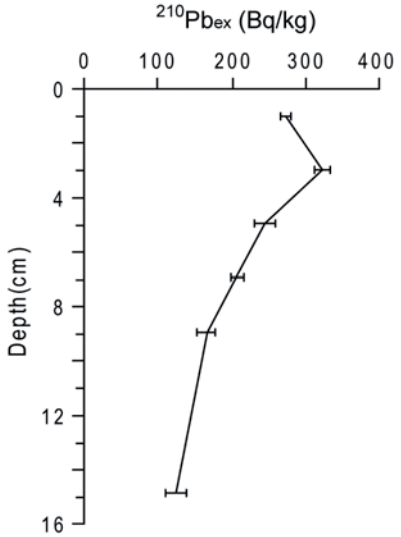

Fig. 2. ^{210}Pb$_{ex}$ activity of PS1652-1 core top sediments. Bars show the errors of the measurements.

3.3.3. Regional core correlation

The individual AMS ^{14}C core chronologies mark the basic time frame of each core. More detailed core stratigraphies were established by regional core correlation. Based on the assumption that the

climate evolution of areas with similar oceanographic conditions (frontal system, sea ice condition, etc.), the climate signals are preserved in the geological records presenting the similar changes; magnetic susceptibility (MS), stable isotopes $\delta^{18}O$ and $\delta^{13}C$ of planktonic foraminifera *Neogloboquadrina pachyderma*$_{sin}$, diatom species composition and estimated SSSTs, were used for regional core correlation (Fig. 5) in terms of general evolution pattern and detailed fluctuations of climate change. The MS and stable isotope records of certain cores presented in this study are available in PANGAEA database (http://www.pangaea.de). For regional correlation, diatom species composition and stable isotope records of Bouvet Island area cores PS1654-2/ODP1093 and

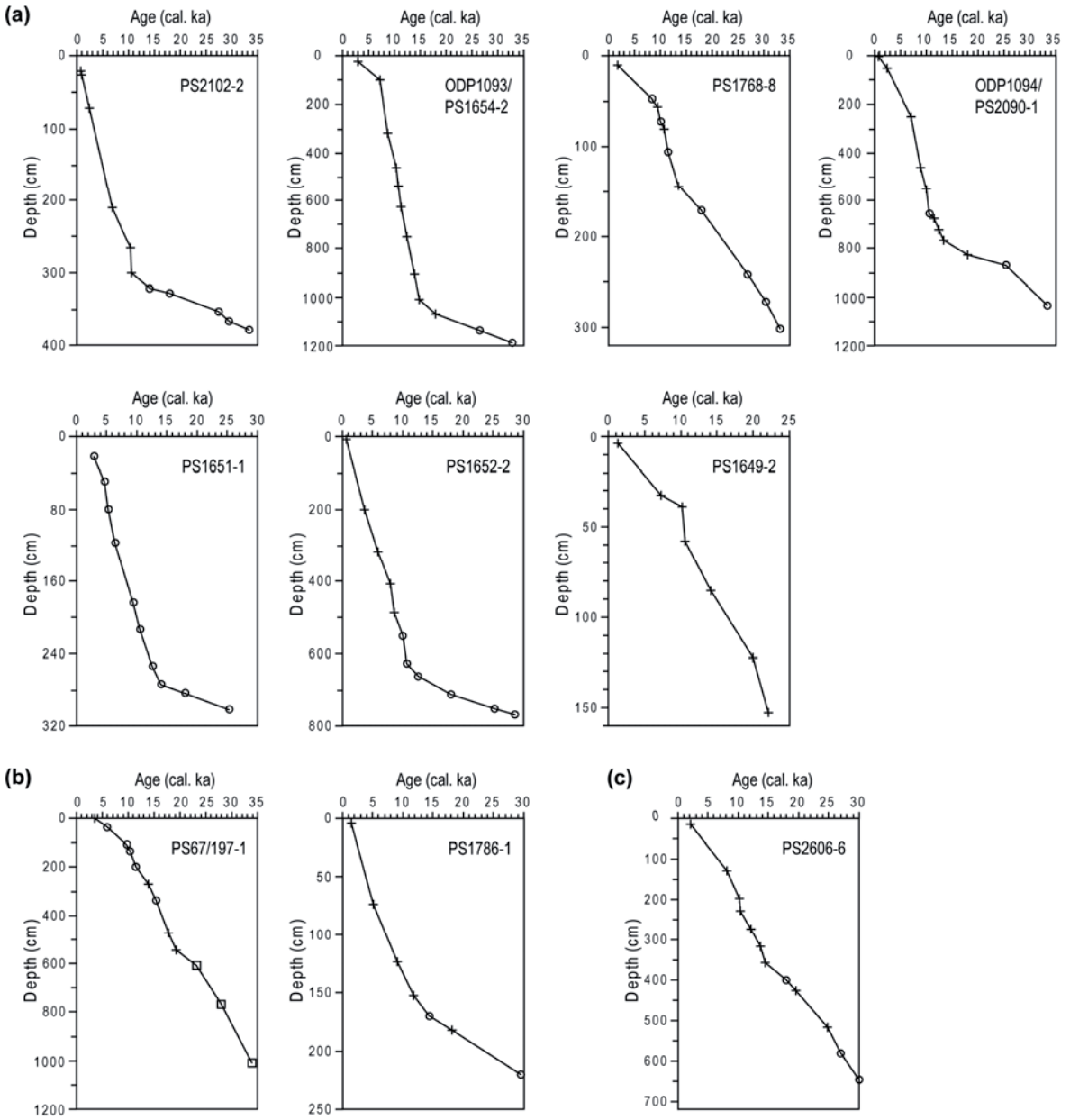

Fig. 3. Age models of studied cores from (a). Bouvet Island area; (b) Scotia Sea; (c). western Indian sector. Pluses: calibrated ^{14}C ages; circles: regional core correlation; squares in core PS67/197-1: correlation between MS signal and Antarctic ice core dust proxies (***Chapter 5***).

PS2090-1/ODP1094 are from Bianchi and Gersonde (2004), and core PS1768-8 from Zielinski et al. (1998). Besides the AMS ^{14}C chronology, the age model of PS67/197-1 is also based on a combination of magnetic susceptibility correlating to Antarctic ice cores, diatom biostratigraphy and paleomagnetic chronology (***Chapter 5***). This core represents the highest time resolution and coefficiency to Antarctic ice cores for the last glacial interval. Due to the lack of glacial ^{14}C dates, the detailed last glacial stratigraphies of the other cores were made by correlation to core PS67/197-1 diatom biofluctuations and SSST variability. By regional core correlation, we were able to transfer the age control points within cores and construct a detailed regional age model with best accuracy and consistency (Fig. 3).

3.4. Results

3.4.1. Sedimentation rate

Low last glacial sedimentation rates occurred in all cores from the Bouvet Island area, with lowest input of biogenic deposition (Fig. 4). The initial rise of sedimentation rates occurred at 14-15 cal. ka (kyr BP) in northern cores of Bouvet Island area and western Indian sector. While the high glacial to Termination 1 sedimentation rates in northern Scotia Sea (PS67/197) is attributed to the high terrigenous input at glacial times in that region (Diekmann, 2007).

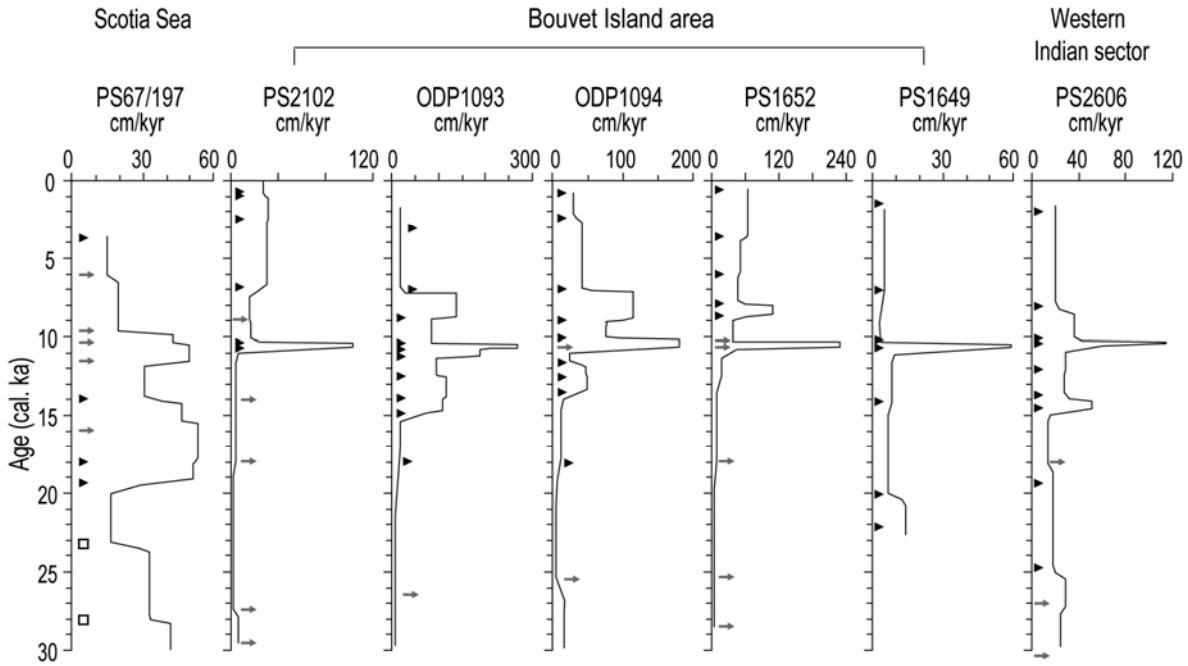

Fig. 4. Sedimentation rates of studied cores from Bouvet Island area, Scotia Sea and western Indian sector with generalized age model, ploted against age. Solid triangles: intervals of AMS ^{14}C dates; arrows: correlation intervals by diatom biofluctuation and SSST variability; open squares in core PS67/197-1: correlation between MS signal to Antarctic ice core dust proxies (***Chapter 5***).

The striking feature is the distinct elevated sedimentation rate presented in all cores at ca. 11-10 cal. ka in Bouvet Island area and western Indian sector (Fig. 4). This interval corresponds to the pure

diatom ooze sediments, maximum estimated SSSTs, almost absence of sea ice diatoms and maximum occurrence of warm/open ocean species in the cores (Fig. 5). This early Holocene high sedimentation rate is also recorded in other cores from southern Scotia Sea close to Antarctic Peninsula (Yoon et al., 2007). The AMS ^{14}C datings from Yoon et al. (2007) clearly show an elevated sedimentation rates at the early Holocene, if taken a ^{14}C correction of reservoir effect by 1300 years as normally applied in this region (Berkman and Forman 1996). However, the authors ignored the ^{14}C ages and just correlate to the inaccurate interval of MS record of ODP1098 from the Palmer Deep.

The remarkable early Holocene high sedimentation rates in Bouvet Island area and western Indian sector are constrained by AMS ^{14}C dating in different cores (Table 2, Fig. 4). The raw ^{14}C ages for this interval are dated at around 10 ka, which is close to the ^{14}C plateau at around 10.3-10.4 ka and spans about 300 years for calibrated age (Reimer et al., 2009). Considering the possible change in Holocene reservoir effect (Skinner et al., 2010), this distinct high sedimentation rate may partly biased by the ^{14}C plateau and changes in reservoir effect.

The sedimentation rates drop distinctly after the optimum, together with the increase of cold water/sea ice diatoms. A second Holocene high sedimentation plateau occurs between 7 and 9 cal. ka in the northern sites of Bouvet Island area (ODP1093 and ODP1094), and maintains at lower than early Holocene level during the mid-late Holocene in the southern cores.

The constant regression of $^{210}Pb_{ex}$ of PS1652-1 core top sediments (Fig. 2) suggests that at least the upper 15 cm sediments are little disturbed within the range of last 100 years. Considering the half life of 22.3 years of ^{210}Pb, a sedimentation rate of ca. 2 m/kyr is calculated for the surface sediment. Such high sedimentation rate is comparable to the situation at the early Holocene (Fig. 4). However, this modern high sedimentation rate at the core site is ambiguous. It may due to the different coring system. The box core PS1652-1 recovers the most undisturbed sediment, whereas the gravity core PS1652-2 may be compacted. In addition, the high porosity of opal, and less condensed surface sediments, which mainly consist of diatom frustules, may also allow the migration of $^{210}Pb_{ex}$ signal to deeper layers through porewater (Appleby, 2001), this is unknown yet.

Despite of local sedimentary conditions, in eastern Bouvet Island area, the sedimentation rates generally decrease from north to south, indicating an influence of sea ice distribution and the favor of open ocean conditions.

3.4.2. Diatom composition

The diatom compositions of the studied cores show a similar evolution pattern through the last glacial to the Holocene (Fig. 5). *Eucampia antarctica*, *Chaetoceros* resting spores (RS) and cold water related species (e.g. *F. curta* group; *Actinocyclus actinochilus*; *F. obliquecostata*) dominated the glacial diatom assemblage, they reduced to low numbers and were replaced by open ocean (e.g. *Fragilariopsis kerguelensis* and *Thalassiothrix antarctica*) and warm water (e.g. *Azpeitia tabularis* and *Thalassiosira oestrupii*) species at the early Holocene. During the mid-late Holocene, *F. kerguelensis* still dominated the diatom assemblage but except the northern most site ODP1093; *F. curta* group strongly increased in the Bouvet Island area (Fig. 7), particularly in the southern sites close to last glacial values, whereas remained at low percentage in the northern Scotia Sea and western Indian sector. Although with the increase of *F. curta* group, the diatom assemblage in the mid-late Holocene differs from the last glacial conditions by very low abundance of *E. antarctica* at all sites and *Chaetoceros* RS in Bouvet Island area and western Indian sector.

All sites show much better preservation during the Holocene than the last glacial, as indicated by the higher presence of lightly silicified species during the Holocene and much greater occurrence of robust species (e.g. *E. antarctica*) during the last glacial, also reflected by changes in sedimentation rates (Fig. 4). Selective dissolution effect plays an important role in the preservation of the diatom valves, especially in the southernmost site PS1649 and northeastern Scotia Sea site PS1786, which displays less sea ice species (*F. curta* group) than the northern site and/or lower last glacial occurrence than Holocene.

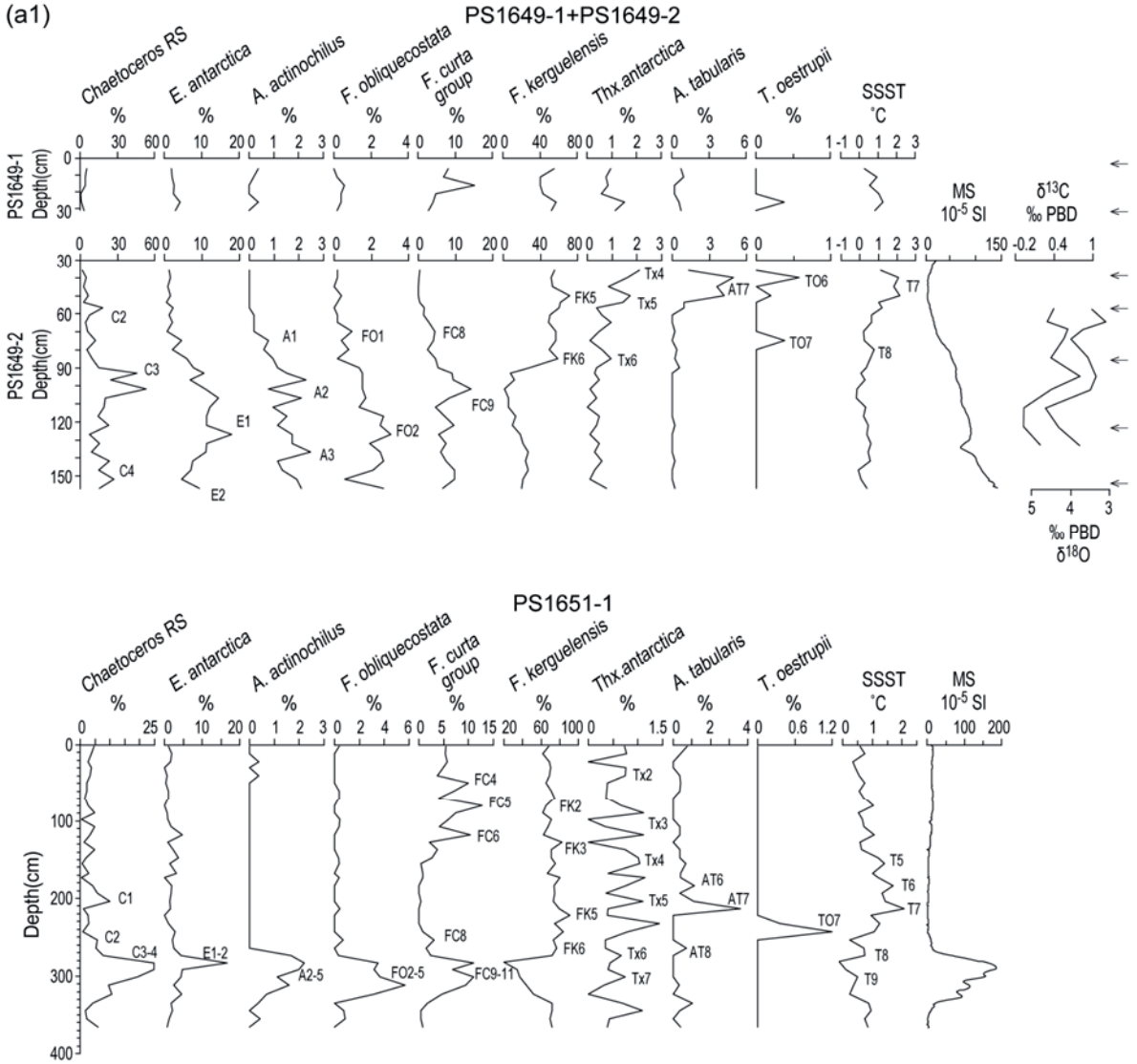

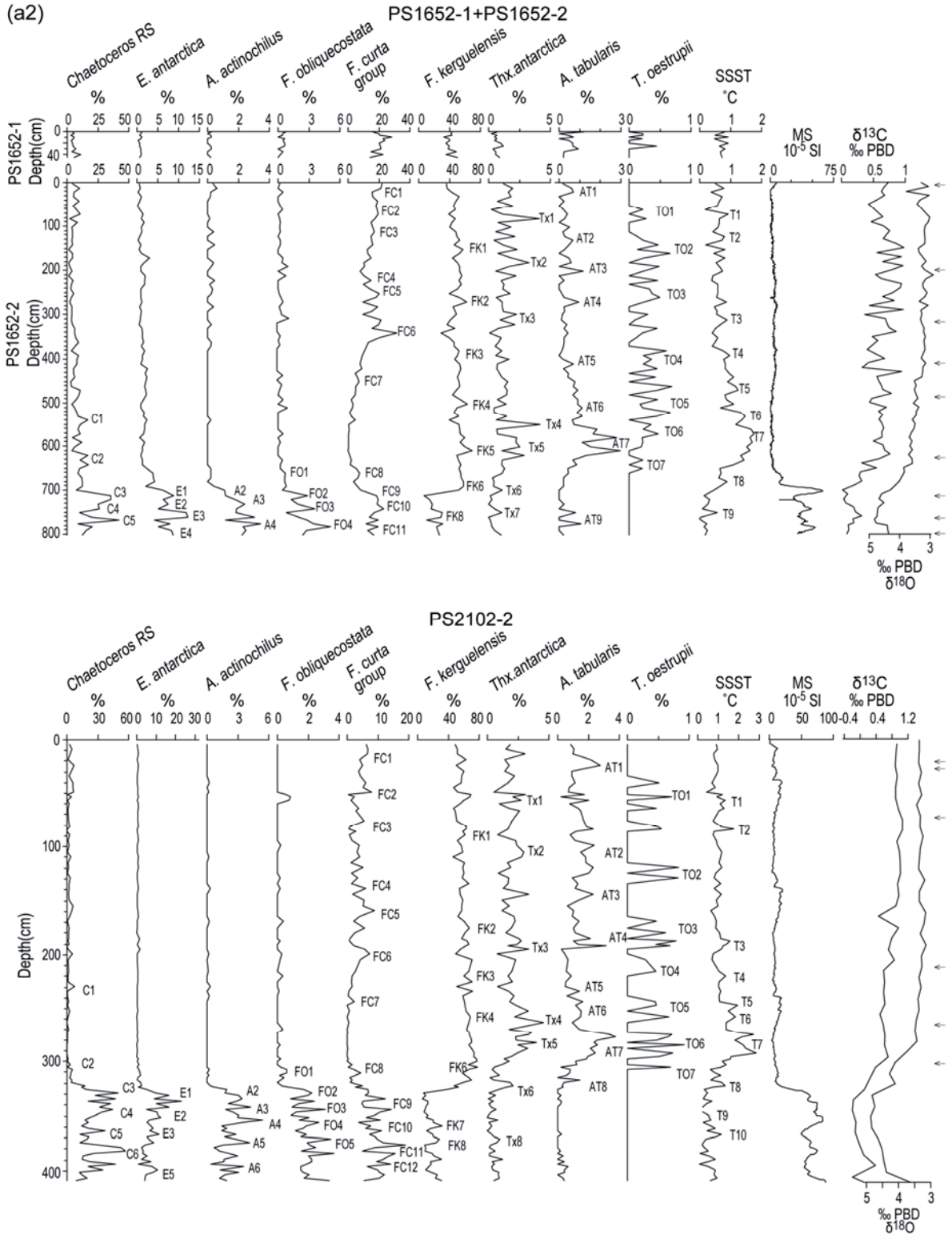
(a2)
PS1652-1+PS1652-2
Chaetoceros RS
E. antarctica
A. actinochilus
F. obliquecostata
F. curta group
F. kerguelensis
Thx.antarctica
A. tabularis
T. oestrupii
SSST
MS
δ13C
PS1652-1 Depth(cm)
PS1652-2 Depth(cm)
‰ PBD δ18O
PS2102-2
Depth(cm)

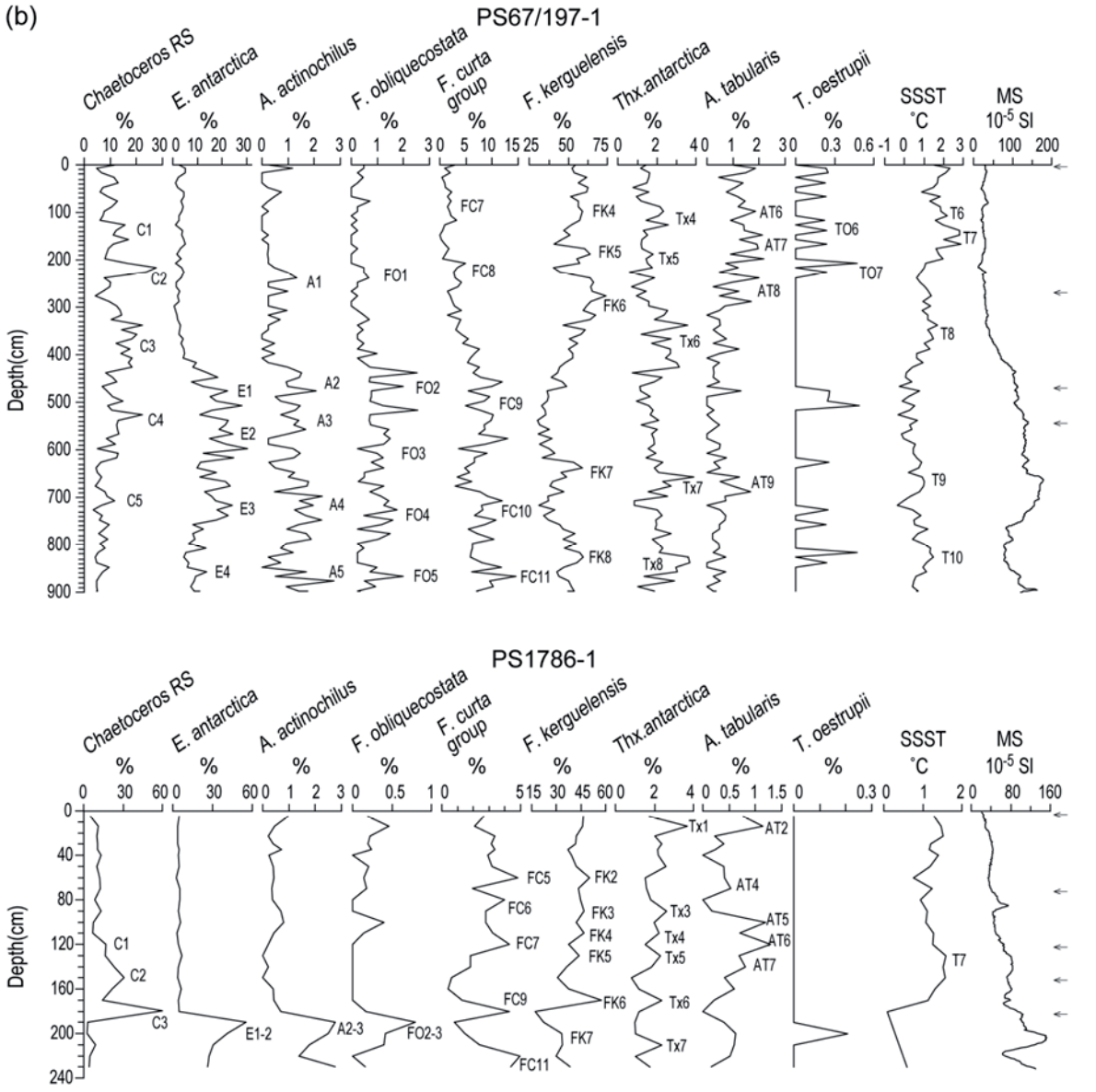
(b)
PS67/197-1
Chaetoceros RS
E. antarctica
A. actinochilus
F. obliquecostata
F. curta group
F. kerguelensis
Thx.antarctica
A. tabularis
T. oestrupii
SSST
MS
%
°C
10-5 SI
Depth(cm)
C1
C2
C3
C4
C5
E1
E2
E3
E4
A1
A2
A3
A4
A5
FO1
FO2
FO3
FO4
FO5
FC7
FC8
FC9
FC10
FC11
FK4
FK5
FK6
FK7
FK8
Tx4
Tx5
Tx6
Tx7
Tx8
AT6
AT7
AT8
AT9
TO6
TO7
T6
T7
T8
T9
T10
PS1786-1
E1-2
A2-3
FO2-3
Tx1
Tx3
AT2
AT4
AT5

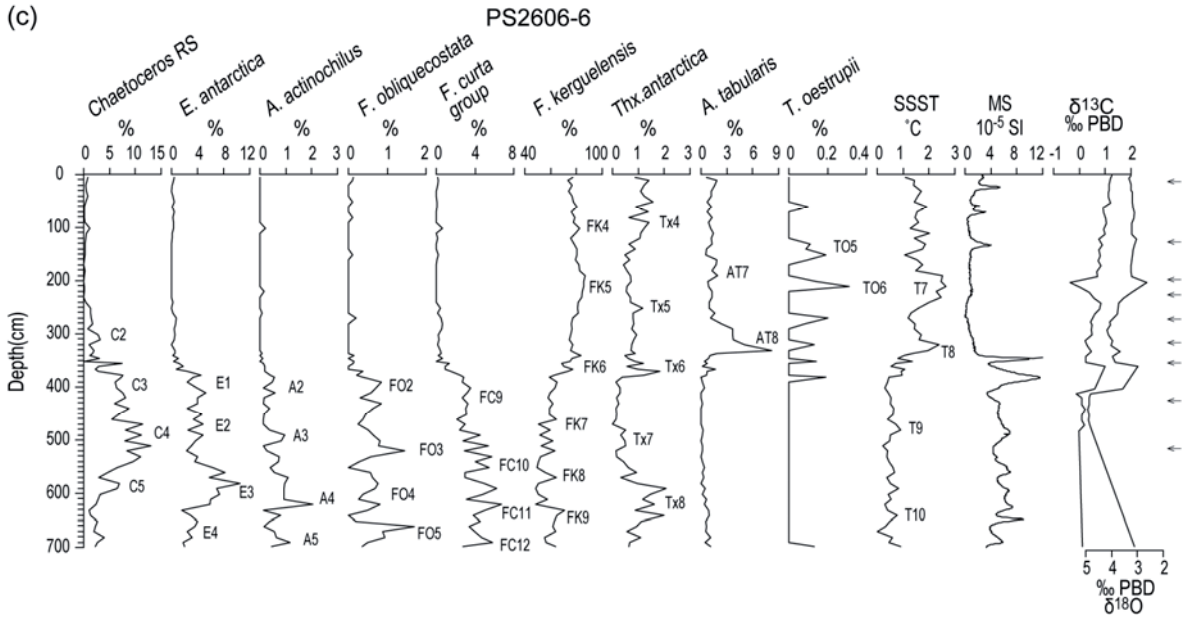

Fig. 5. Relative abundances of relevant diatom species, estimated SSSTs, magnetic susceptibility (MS) records, planktonic foraminifera *N. pachyderma*$_{sin}$ oxygen and carbon isotope records of studied cores from (a) Bouvet Island area; (b) Scotia Sea and (c) western Indian sector, plotted against depth. Arrows indicate the intervals with AMS ^{14}C dating (Table 2). Magnetic susceptibility and isotope records are from http://www.pangaea.de/. Biofluctuation of diatom species and estimated SSSTs used for regional core correlation are numbered.

3.4.3. SSST and sea ice reconstructions

During the last glacial, the estimated SSSTs in Bouvet Island area (Fig. 6) range between 0.2˚C and 1.5˚C across 55˚S (PS1649) and 50˚S (ODP1093), and in western Indian sector (PS2606) average at 0.5˚C and in northern Scotia Sea (PS67/197) at 0.4˚C. In the northeastern Scotia Sea (PS1786), the estimated SSSTs are strongly biased towards warmer temperatures due to the selective opal dissolution, as evidenced by up to 60% of *E. antarctica* in the diatom assemblage. Thus we excluded the biased last glacial SSSTs for this core. The same situation may also occur at the southernmost site PS1649 in the Bouvet Island area, indicated by the lower sea ice species than the northern cores (Fig. 7). The sea ice indicators suggest that, WSI reached 50˚S in the Bouvet Island area, and also covered the northern Scotia Sea at least north of 55˚S and western Indian sector at ca. 41˚E; the summer sea ice occurred at 53.6˚S in the Bouvet Island area and never reached northern Scotia Sea and western Indian sector.

The initial warming started at around 18 cal. ka, with the rapid decline of winter and summer sea ice field (Fig. 6, Fig. 7). At ca. 14 cal. ka, the SSSTs reached at a temporary optimum in the Bouvet Island area at 0.8 – 3.8˚C from south to north and western Indian sector at 2.4˚C. This temporal optimum is best documented at sites ODP1094, ODP1093 and PS2606 with high sample resolution, and the warming is more pronounced in the northern cores than in the southern cores. Different from the other two areas, in the northern Scotia Sea, the SSSTs remained stable at ca. 1.3˚C from 16 to 14 cal. ka after the warming. At this time, WSI retreated south of the western Indian sector site and 53.6˚S (PS1652) in the Bouvet Island area, but persisted in the northern Scotia Sea, summer sea ice retreated south of the studied core sites since then (Fig. 7).

After the temporal warming, the SSSTs dropped at all sites between 12-14 cal. ka. In Bouvet Island area, the amplitudes of cooling were more pronounced at the southern sites than the northern

site at 50˚S, ranged between 0.3 and 3.5˚C across 55 to 50˚S (Fig. 6). In the western Indian sector and northern Scotia Sea, the SSSTs dropped to 1.2 and 0.8˚C, respectively. The cooling is accompanied by the re-occurrence of WSI close to 53˚S in Bouvet Island area, as well slightly increased in the northern Scotia Sea (Fig. 7).

A distinct warming occurred at the early Holocene between 11 and 9 cal. ka and centered at ca. 10 cal. ka. This is especially documented in the southern sites. The SSSTs rose up to 2-4˚C from at 55-50˚S in Bouvet Island area, and 2.8 and 2.7˚C in the northern Scotia Sea and western Indian sector, respectively. Sea ice retreated south of 55˚S in the Bouvet Island area as well as south of northern Scotia Sea and the western Indian sector sites, as indicated by the almost absence of sea ice algae (Fig. 7). This time interval corresponds to the highest sedimentation rates (Fig. 4) and almost pure diatom ooze in the sediments.

The SSSTs started to drop at 8-9 cal. ka after the early Holocene optimum, and persisted in cold conditions during the mid-late Holocene (Fig. 6). The SSSTs dropped to 0.7-3.5˚C in Bouvet Island area (55-50˚S), and averaged at 1.8˚C and 1.7˚C in the northern Scotia Sea and western Indian sector, respectively. This cooling was more prominent in the southern sites (Fig. 6), but at the northern site ODP1093, only small amplitude of oscillations occurred. WSI extended to ca. 53˚S in Bouvet Island area, the maximum expansion occurred at 4.5-7 cal. ka and another increase after 3 cal. ka; in the northern Scotia Sea and western Indian sector, WSI did not reach the core sites (Fig. 7).

Close to site PS1652, core PS1651-1 represents similar SSSTs and sea ice variation to those at site PS1652, but lower WSI species are observed, which leads to slightly colder SSSTs at site PS1652. This is due to the high sedimentation rate and good preservation of lightly silicified cold water species in core PS1652-2, suggested by the WSI indicators in core PS1652-2 are doubled compared to the adjacent cores PS1651-1 and ODP1094.

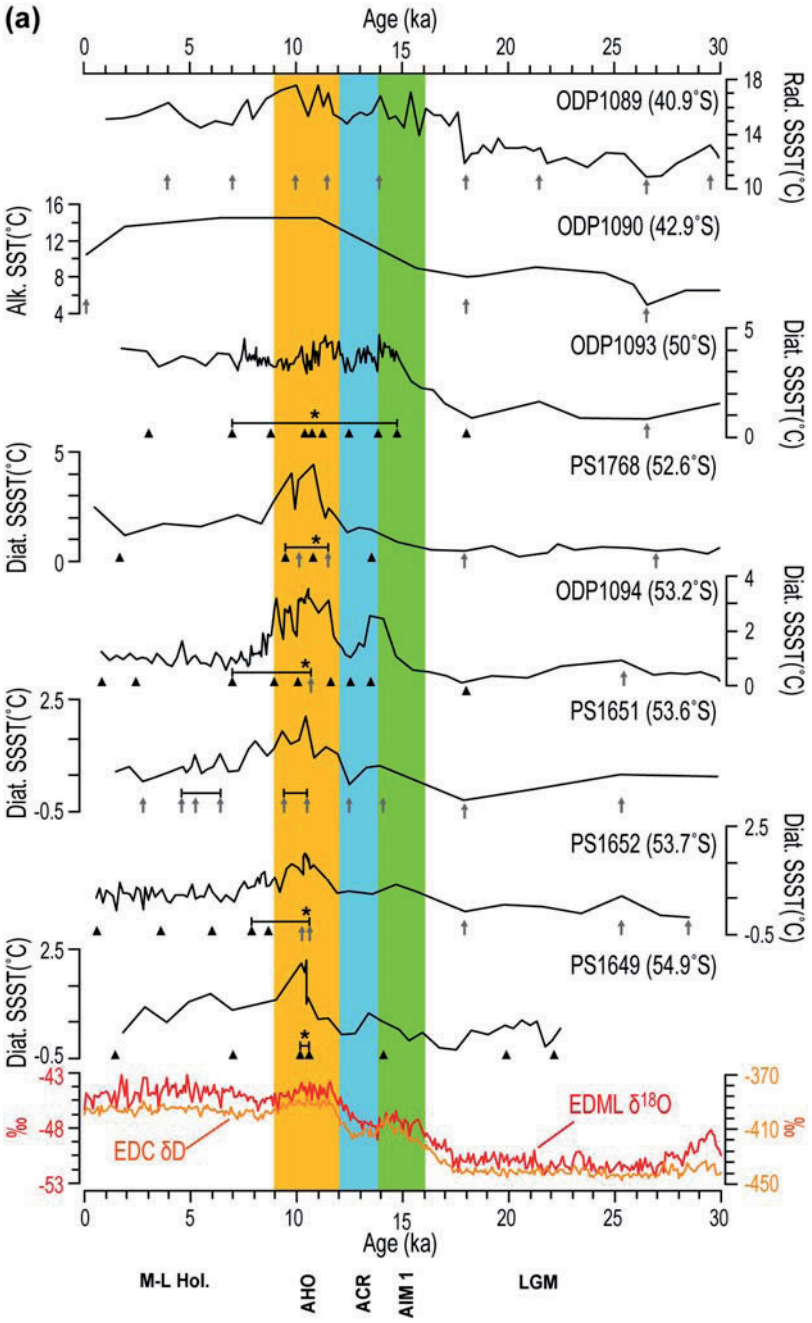
(a)
Age (ka)
ODP1089 (40.9°S)
Rad. SSST(°C)
ODP1090 (42.9°S)
Alk. SST(°C)
ODP1093 (50°S)
Diat. SSST(°C)
PS1768 (52.6°S)
ODP1094 (53.2°S)
PS1651 (53.6°S)
PS1652 (53.7°S)
PS1649 (54.9°S)
EDML δ18O
EDC δD
‰
M-L Hol.
AHO
ACR
AIM 1
LGM

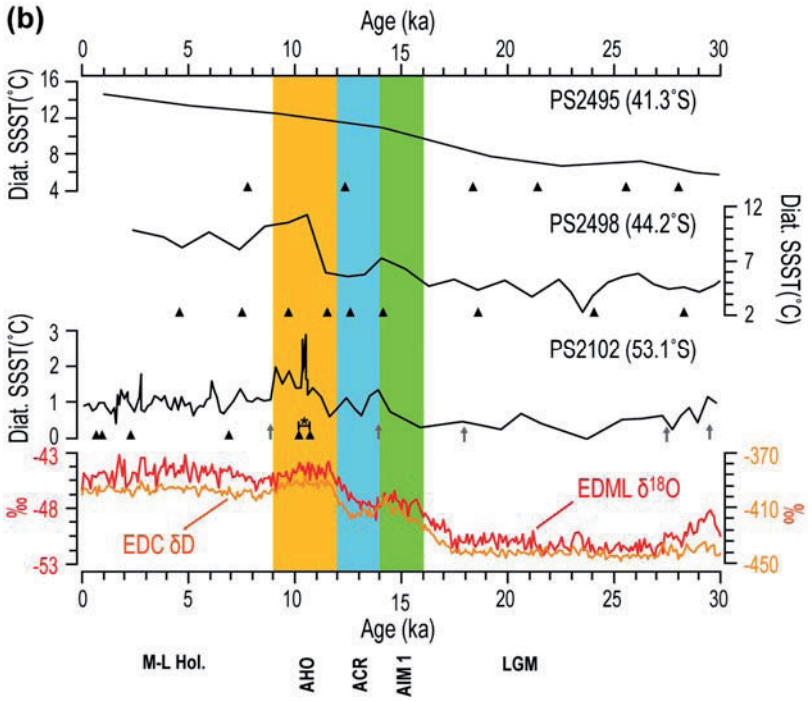
(b)
Age (ka)
0
5
10
15
20
25
30
Diat. SSST(°C)
16
12
8
4
PS2495 (41.3°S)
PS2498 (44.2°S)
12
7
2
Diat. SSST(°C)
PS2102 (53.1°S)
3
2
1
0
Diat. SSST(°C)
-43
-48
-53
‰
EDC δD
EDML δ18O
-370
-410
-450
‰
Age (ka)
M-L Hol.
AHO
ACR
AIM 1
LGM

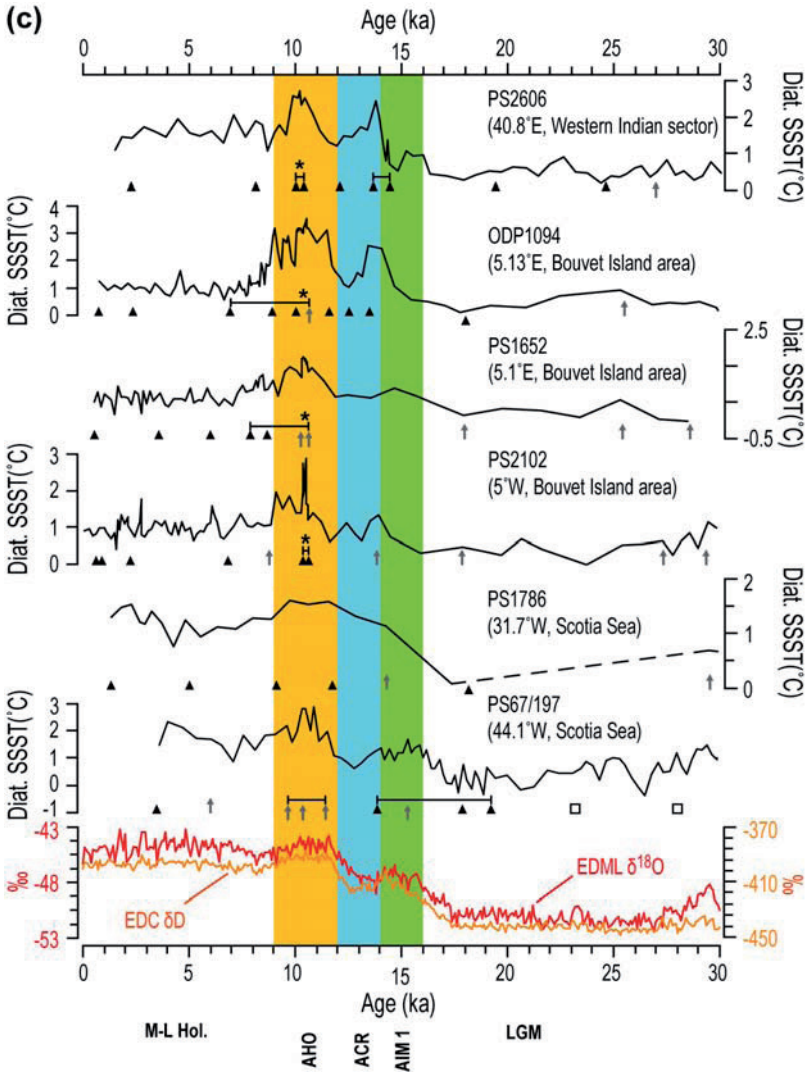

Fig. 6. SSST records from Southern Ocean Atlantic and western Indian sectors comparing to the Antarctic ice cores EDML $\delta^{18}O$ (Epica members, 2006, EDML 1 time scale) and EDC δD (Jouzel et al., 2007, EDC 3 time scale). (a). Bouvet Island area east transect; (b). Bouvet Island area west transect; (c). Longitudinal transect of western Indian sector, Bouvet Island area and Scotia Sea. Data of ODP1089 from Cortese et al. (2007); ODP1090 from Martinez-Garcia et al. (2009); ODP1093 and ODP1094 from Bianchi and Gersonde (2004); PS1768-8 from Zielinski et al. (1998); PS2495-3 and PS2498-1 from Gersonde et al. (2003). AHO: Antarctic early Holocene Optimum; ACR: Antarctic Cold Reversal; AIM 1: Antarctic Isotope Maximum 1 (Epica members, 2006). Bars bracket the intervals with high sedimentation rates with stars mark the maximum sedimentation rate and opal deposition. Solid triangles: intervals of AMS ^{14}C dates; arrows: correlation intervals by diatom biofluctuation and SSST variability; open squares in core PS67/197-1: correlation of MS signal to Antarctic ice core dust proxies (***Chapter 5***).

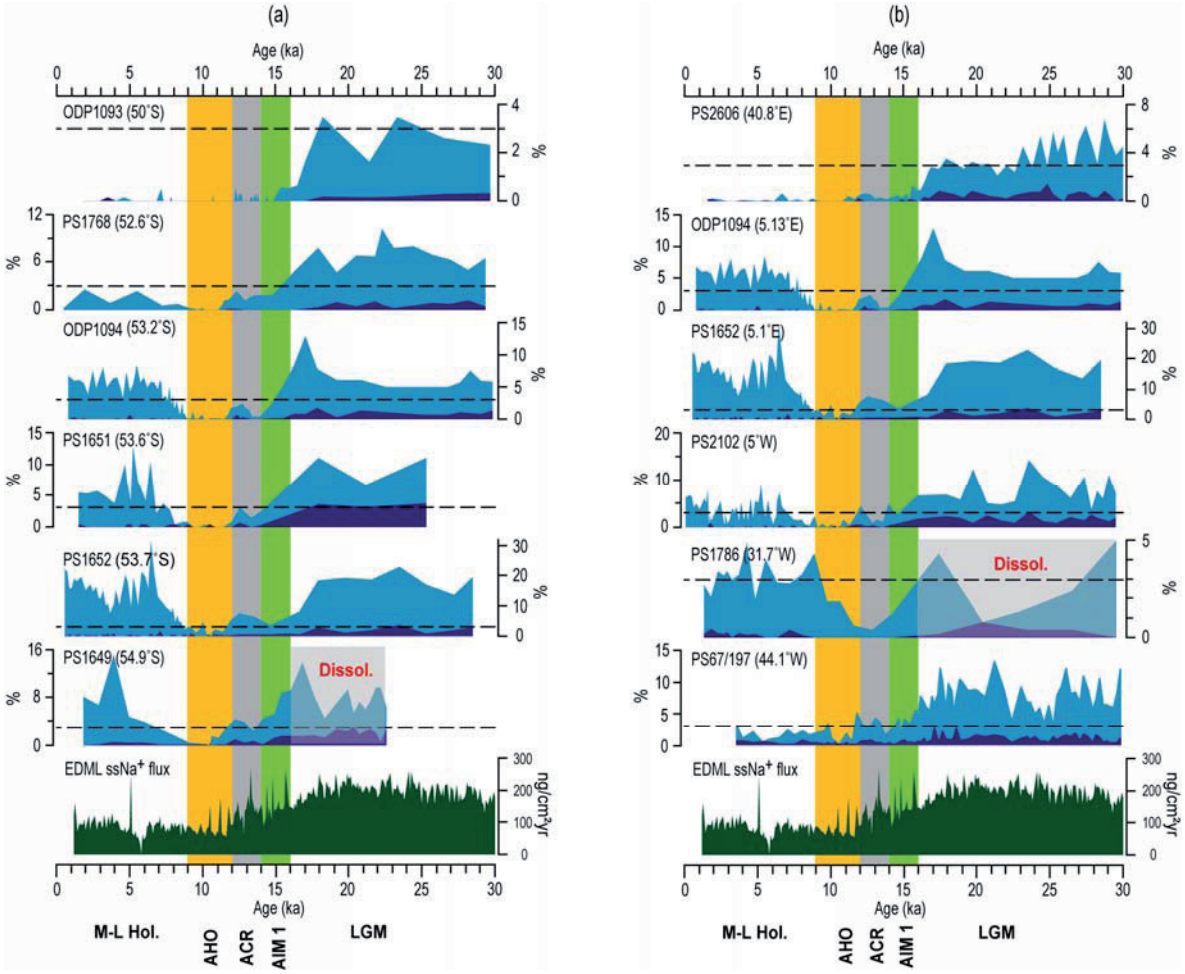

Fig. 7. Spacial distribution of summer (*F. obliquecostata*, dark blue) and winter (*F. curta* group, light blue) sea ice. Dashed line marks 3% as an indication of presence of sea ice. (a). North-south transect in Bouvet Island area; (b). East-west transect across western Indian and Atlantic sectors. EDML sea salt sodium flux ($ssNa^{+}$) presents the sea ice extent proxy from Antarctic ice core (Fischer et al., 2007). Data of ODP1093 and ODP1094 from Bianchi and Gersonde (2004); PS1768-8 from Zielinski et al. (1998).

3.5. Discussion

3.5.1. Last Glacial conditions

Compared to modern conditions, the last glacial SSSTs in our records indicate colder than Holocene conditions by 2-3˚C in sites located south of modern Polar Front. In contrast, the cooling in the modern Subantarctic Zone is ca. 6˚C (Fig. 6). Our data is in agreement with the LGM SSST reconstruction of Gersonde et al., (2003a; 2005), Niebler et al. (2003) and the further summarized Margo (Multiproxy Approach for the Reconstruction of the Glacial Ocean Surface) project (Margo members, 2009) that the strongest cooling occurred in the modern Subantarctic Zone. Recent compilation by Shakun and Carlson (2010) show that the magnitude of the LGM-Holocene warming increases with latitude, with stronger warming in the polar regions and weaker warming in the tropical regions. However, in their compilation the Southern Ocean marine records only include the sites north

of 45˚S (Shakun and Carlson, 2010). The lack of southern high latitude record in their study may neglect the small changes in SSSTs in the area south of the modern Polar Front.

Our records show that, the LG WSI extended northward by ~5˚ latitude compared to modern conditions, to 50˚S in the Bouvet Island area (Fig. 7), which is at the modern Polar Front. The SSI indicator suggests sporadical occurrence of perennial sea ice in the Bouvet Island area, which is in agreement with the reconstructions by Gersonde et al. (2003a; 2005). On the contrary, the maximum summer sea ice extent was deduced similar to its modern position south of 60˚S in the Atlantic sector during the LGM (Crosta et al., 1998b). The difficulties of analyzing the SSI extent are mainly due to the strong opal dissolution in the Weddell Sea that little sediment is available for reconstructions of sea ice extent and SSSTs based on siliceous microfossils (Gersonde et al., 2005). Sea salt flux in the ice core (Wolff et al., 2006; 2010; Fischer et al., 2007) also points to the maximum extension of sea ice field and may be an indicator of seasonal sea ice production. However, at full glacial conditions, this proxy is not as sensitive as the marine proxy (Röthlisberger et al., 2010; Wolff et al., 2010).

Higher occurrence of WSI indicators is evidenced at the western Indian sector site PS2606 at 25-30 cal. ka (Fig. 7), which mirrors the maximum northeastward cold water expansion from the Weddell Sea. This is in agreement with the maximum extent of glaciers in central Patagonia at 27-25 ka (Hein et al., 2010), and broadly synchronous in other areas in Patagonia (McCulloch et al., 2005; Kaplan et al., 2008). Although our records do not show significant colder SSSTs at this time interval, it may support the idea that the coldest time period in the Southern Ocean (Gersonde et al., 2003a; 2005) was prior to LGM, at a time of the lowest sea level between 19 and 22 ka (Yokoyama et al., 2000). Even though, the timing of the lowest sea level stand is also challenged by wider area observations combined with deglacial models (Peltier and Fairbanks, 2006; Clark et al., 2009), indicating the lowest sea level might occur before 26 ka.

The intensively expanded WSI and less expanded SSI would strongly increase the seasonality of the sea ice field compared to modern conditions, allowing the cold and saline deep water production by brine rejection during seasonal sea ice formation (Keeling and Stephens, 2001; Watson and Naveira Garabato, 2006), when the WAIS is grounded on the shelf (Bentley and Anderson, 1998; Anderson et al., 2002; Molosa and Anderson, 2006). The admixing of North Atlantic Deep Water (NADW) into the Circumpolar Deep Water (CDW) occurred farther north than today at 30-40˚S, while the AABW significantly northward extended, in response to an expanded area of deep water formation in the Southern Ocean (Bickert and Mackensen, 2003; Curry and Oppo, 2005; Marchitto and Broecker, 2006). The expanded sea ice field in the South Atlantic would have strongly reduced the heat transport from the Indian Ocean via the warm water route (WWR) south of Africa and from the Pacific Ocean via the cold water route (CWR) at Drake Passage (Gersonde et al., 2003b), which may result in the stronger cooling in the LGM tropical Atlantic than in the tropical Indian and Pacific Oceans (Margo members, 2009).

Gersonde et al. (2003a; 2005) indicate a possible northward shift of 4˚, 4-5˚ and 2-3˚ in latitude of Polar Front, Subantarctic Front and Subtropical Front in the South Atlantic, respectively. The northward extended cold water belt and the stronger sea surface temperature gradient over the modern Subantarctic Zone shift the Southern Westerlies northward (Moreno et al. 2003; Stuut and Lamy, 2004; Kaiser et al., 2005; Toggweiler et al., 2006; Toggweiler and Russell, 2008), which reduced the nutrient supply to the surface waters in the south by wind-driven upwelling. The wind-driven upwelling brings nutrient rich deep waters to the surface south of the Polar Front, it corresponds to the maximum opal deposition (Trull et al., 2001; Anderson et al., 2009). Compared to modern conditions, our records

suggest that the LGM maximum opal deposition zone shifted north of 50˚S in Bouvet Island area, as indicated by low sedimentation rates with low opal content and high magnetic susceptibility of the sediments. This is in agreement with the estimation of Gersonde et al. (2003a) who indicate that the LGM opal belt was shifted to the north by approximately 5˚ in latitude.

As an indicator of intensive bioproductivity and carbon export (Abelmann et al., 2006), high amount of *Chaetoceros* RS occurred in Bouvet Island area (30-40%) and decreased in the western Indian sector (~10%) during the LG (Fig. 9). With the decreased upwelled nutrient supply in the south, this pattern agrees with the mechanism proposed by Abelmann et al. (2006) that sea ice acts as an effective transporter of iron and enhances its bioavailability. The *Chaetoceros* RS pattern in our records generally agrees with the Antarctic dust concentration record (Fig. 9) (Fischer et al., 2007; Lambert et al., 2008). The intensively expanded sea ice in Bouvet Island area provided considerable amount of iron settled on the sea ice which fertilized the upper ocean during the melting season. And to the east, in the western Indian sector, at the maximum eastward expansion of WSI, the iron availability is reduced. Such pattern also mirrors the distance relationship to the dust source region South America that the dust transported by wind also reduced at far distant western Indian sector. However, in the Scotia Sea, the situation is different. Although also covered by WSI, the LGM *Chaetoceros* RS only consists of 5-10% of the diatom assemblage. The reason may be related to the northward shifted Westerlies that the Scotia Sea was away from the dust transport track, thus less dust was settled in the Scotia Sea compared to Bouvet Island area. This may also account for the relatively lower occurrence of the species in the Bouvet Island area at 25-30 ka (Fig. 9). The northward extended *Chaetoceros* RS zone to the modern permanent ocean zone indicates an expanded area of carbon export to the deep ocean to the 50˚S in the Bouvet Island area. The high efficient export of carbon would draw down the atmospheric CO_2 (Kohfeld et al., 2005; Abelmann et al., 2006) that trapped in the deep Southern Ocean by heavy stratification of the surface and deep waters (Stephens and Keeling, 2000; Sigman et al., 2004; Hillenbrand and Cortese, 2006; Bouttes et al., 2009). Thus, our result also supports that the LGM carbon storage in the South Atlantic extended northward (Martínez-Méndez et al., 2009).

Fig. 8. SSST records of western Indian sector, Bouvet Island area and Scotia Sea compared to Southeast Pacific (Lamy et al., 2002; 2007; Kaiser et al., 2005) SST records; South Atlantic bottom water-atmosphere ventilation history (MD07-3076, Skinner et al., 2010, spline-smoothed); bottom-surface water ventilation history (red: benthic-planktic; blue: projection age model) and planktic foraminifera cold water species variation (TN057-21, Barker et al., 2010); AMOC history (GGC5, McManus et al., 2004, red: ^{232}Th based values and blue: ^{238}U based values); Antarctic ice cores EDML $\delta^{18}O$ and accumulation rate (Epica members, 2006; Ruth et al., 2007, EDML1 time scale), EDC δD (Jouzel et al., 2007, EDC3 time scale) and CO_2 (Monnin et al., 2001) records. NGRIP $\delta^{18}O$ record (NGICP members, 2004, GICC05 time scale) is used for revealing the interhemispheric relationship. Holocene glacier advances are modified from Douglass et al. (2005). YD: Younger Dryas; H1: Heinrich stadial 1; B-A: Bølling-Allerød warm interval; AHO: Antarctic early Holocene Optimum; ACR: Antarctic Cold Reversal; AIM 1: Antarctic Isotope Maximum 1 (Epica members, 2006). Horizontal bars bracket the intervals with high sedimentation rates with stars mark the maximum sedimentation rate and opal deposition. Solid triangles: intervals of AMS ^{14}C dates; open triangles: correlation intervals by diatom biofluctuation and SSST variability; open squares in core PS67/197-1: correlation of MS signal to Antarctic ice core dust proxies (***Chapter 5***).

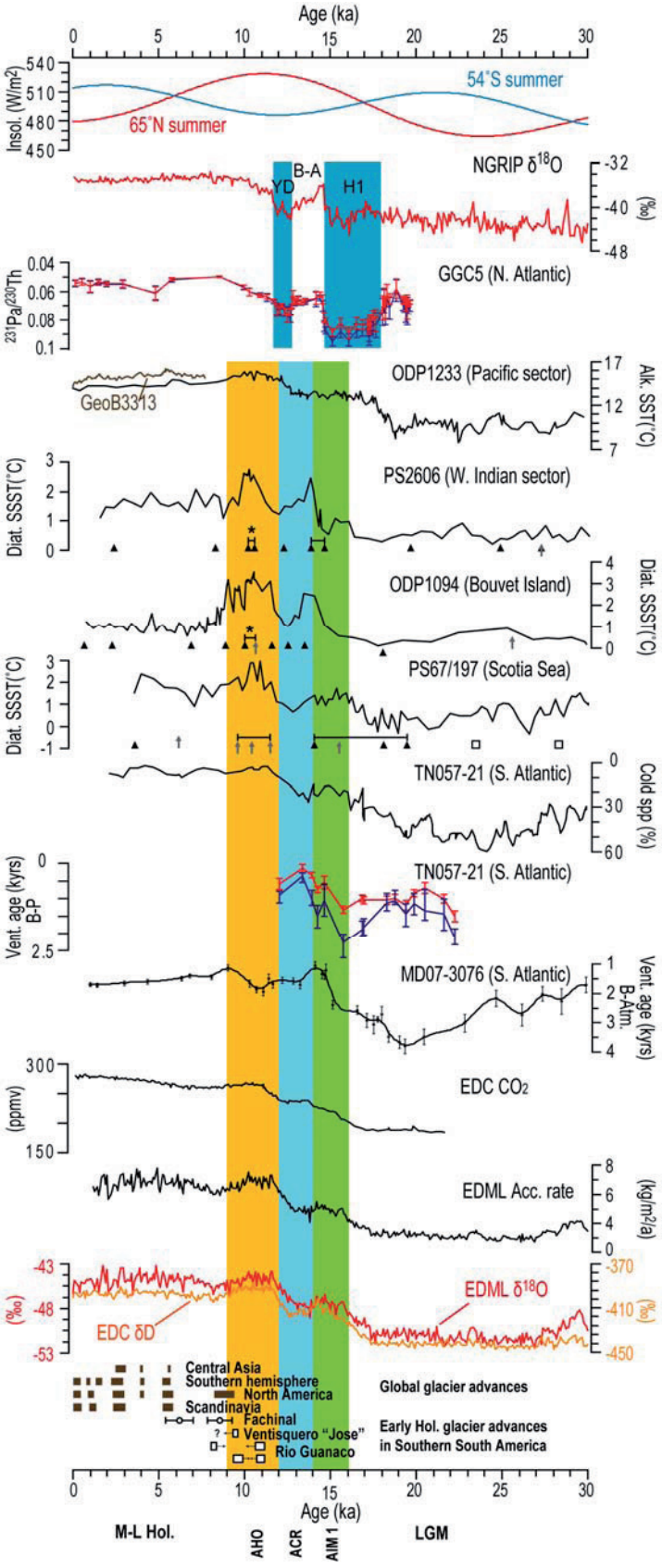
Age (ka)
Insol. (W/m²)
54°S summer
65°N summer
NGRIP δ18O
(‰)
B-A
YD
H1
GGC5 (N. Atlantic)
231Pa/230Th
GeoB3313
ODP1233 (Pacific sector)
Alk. SST(°C)
PS2606 (W. Indian sector)
Diat. SSST(°C)
ODP1094 (Bouvet Island)
PS67/197 (Scotia Sea)
TN057-21 (S. Atlantic)
Cold spp (%)
Vent. age (kyrs) B-P
MD07-3076 (S. Atlantic)
Vent. age (kyrs) B-Alm.
EDC CO2
(ppmv)
EDML Acc. rate
(kg/m²/a)
EDML δ18O
EDC δD
Central Asia
Southern hemisphere
North America
Scandinavia
Fachinal
Ventisquero "Jose"
Rio Guanaco
Global glacier advances
Early Hol. glacier advances in Southern South America
M-L Hol.
AHO
ACR
AIM 1
LGM

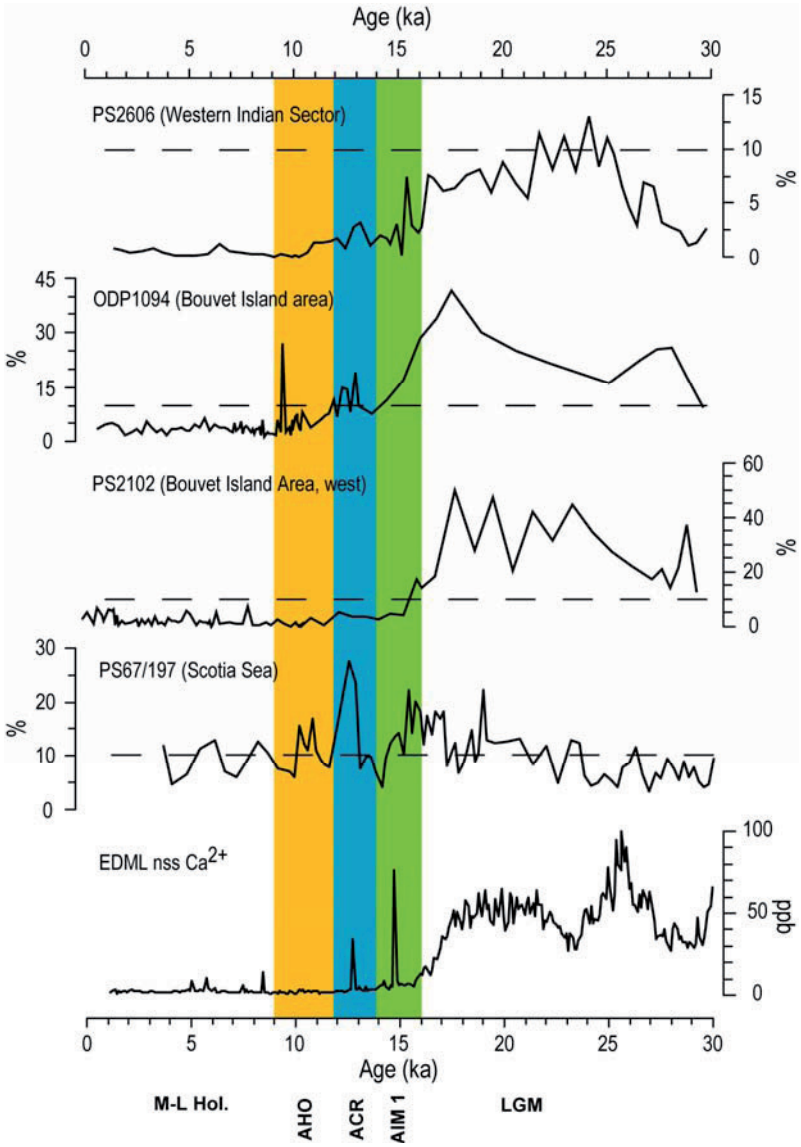

Fig. 9. Relative abundance of *Chaetoceros* RS of western Indian sector, Bouvet Island area and Scotia Sea, compared to EDML dust record (Fischer et al., 2007). Data of ODP1094 from Bianchi and Gersonde (2004). Dashed line marks 10% of the relative abundance. AHO: Antarctic early Holocene Optimum; ACR: Antarctic Cold Reversal; AIM 1: Antarctic Isotope Maximum 1 (Epica members, 2006).

3.5.2. Termination conditions

3.5.2.1. Start of the postglacial warming

Our records show that the LG-Holocene transition in the South Atlantic and western Indian sectors started at around 18 cal. ka, with abrupt SSST rise and sea ice reduction (Fig. 6; Fig. 7). Simultaneously, the planktonic foraminifera lighter $\delta^{18}O$ and heavier $\delta^{13}C$ indicate the freshening of the surface water and enhanced bioproductivity. The timing of postglacial warming is in agreement with the Antarctic ice core records (Epica members, 2006; Jouzel et al., 2007; Lemieux-Dudon et al.,

2010; Stenni et al., 2011), it also coincides with the initial retreat of the grounded ice from the Antarctic Peninsula outer shelf (Heroy and Anderson, 2005; 2007) and various southern mid-latitude glaciers (Alloway et al., 2007; Rodbell et al., 2009; Hein et al., 2010) at 17-18 ka.

In general, the warming phase in our records covaries with the summer insolation in the northern hemisphere (Fig. 8). This may lead to the interpretation of the classic Milankovitch theory that the deglaciation is triggered by northern hemisphere summer insolation (e.g. Kawamura et al., 2007). This has been recently challenged by Laepple et al. (2011), who introduced the local seasonal variations in solar insolation without involving the northern hemisphere forcing. Other mechanisms have been proposed by combining the marine and the Antarctic ice core records and further evaluated by model simulations (Stott et al., 2007; Timmermann et al., 2009). Based on their theory, the initial warming in the Southern Hemisphere is associated to the changes in austral spring insolation, which triggered the early retreat of Southern Ocean sea ice at around 19-18 ka BP, the reducing sea ice field accelerates the deglacial warming through the sea ice albedo feedback and the increase of atmospheric CO_2. Another conceptual model (Wolff et al., 2009) emphasizes that the terminations are led by warming in the southern hemisphere. The authors examined the Antarctic warming intervals (Antarctic isotope maximum: AIM, EPICA members, 2006) and Dansgaard-Oeschger (DO) events in the northern hemisphere, they found out that no equivalent DO event to halt the southern warming at the glacial maxima enables the continuous deglaciation that eventually complete the termination. Although this hypothesis needs further field observation and model test, it provides new insights from the southern point of view.

Along with the early trigger of the termination, the postglacial warming in the Southern Hemisphere is believed to be punctuated by the "bipolar seesaw" mechanism (Rahmstorf, 2002; Stocker, 2003). At the time of Heinrich stadial 1 (H1, 18-15 ka), with a major meltwater discharged into the North Atlantic that prevented the formation of NADW (McManus et al., 2004; Gherardi et al., 2009), and strongly reduced the cross equator transport of warm and saline water from the tropics to the North Atlantic, in consequence the heat was accumulated in the South Atlantic (Seidov and Maslin, 2001). The South Atlantic heat piracy amplified the warming in the Southern Ocean from the surface. The warming phase is abrupt at the northern site ODP1089, and also recognized at the closeby site TN057-21 (Barker et al., 2009), as also recorded in the southeastern Pacific site ODP1233 at similar latitude (Lamy et al., 2007) (Fig. 8). The abrupt warming at TN057-21 is related to the southward shift of the northern front of the ACC (Subtropical Front), with the gradual increase of warm water to the area via the Agulhas Leakage (Barker et al., 2009). Similar situation at the southeast Pacific site is interpreted as a rapid response to the resumption of the AMOC without involving the large thermal inertia of the Southern Ocean. The ACC served as a thermal and dynamical boundary which slowed down the propagation of warming from the north (Barker et al., 2009), as documented in our southern cores.

3.5.2.2. AIM 1 and ACR

The warming process reached a temporal maximum, which is comparable to the early Holocene conditions, at around 14 cal. ka at site PS2606 in the western Indian sector as well as at sites ODP1094 and TN057-13 (Divine et al., 2010) in the Bouvet Island area, and interrupted by a strong cooling between 12 and 14 cal. ka (Fig. 6). The timing is also broadly consistent with the cooling phase in Patagonia and Southern Andes (15-12 ka) (Fogwill and Kubik, 2005; Rodbell et al., 2009; Hein et al.,

2010), and New Zealand (13.8-11.6 ka) (Hajdas et al., 2006; Alloway et al., 2007; Barrows et al., 2007). Our marine records show a lagged cold reversal to the Antarctic ice cores by a few hundred years, which documented that the temporal warming (AIM 1) occurred at ca. 14.5 ka and the cooling afterwards (Antarctic Cold Reversal: ACR) until ca. 12.5 ka (Epica members, 2006; Jouzel et al., 2007; Lemieux-Dudon et al., 2010). The determination of accurate timing of the cold reversal in our marine records is hampered by uncertainties in reservoir effect during the deglaciation. During the warming process, the wind driven upwelling released the ^{14}C depleted CO_2 from the ocean to the atmosphere (Anderson et al., 2009), which may reduce the surface ocean reservoir and possibly bias the climate signal in our records. Besides, the timing in the ice cores also has 200-300 years error in their chronologies (Lemieux-Dudon et al., 2010; Stenni et al., 2010; 2011). Nevertheless, our records confirms the pre Younger Dryas (YD: 12.8-11.5 ka) cooling in the southern high latitudes. The YD actually occurred at the second abrupt warming phase to the Holocene after the coldest period in ACR (Fig. 8). At this time, the bipolar seesaw effect played the role of the abrupt warming in the south when NADW formation was sharply declined (McManus et al., 2004).

The distinct temporal warming is not observed in the northern Scotia Sea (PS67/197) (Fig. 6), instead, the SSSTs remained rather stable between 16 and 14 cal. ka before the small amplitude cooling at 14-12 cal. ka. Our records mark the spacing difference of deglacial warming/cold reversal in the South Atlantic and adjacent western Indian sectors. Interestingly, the slowdown of warming at 16-14 cal. ka at site PS67/197 largely agrees with the $\delta^{18}O$ signal in EDML and Dome F, but differs from that of EDC and Talos Dome with almost constant warming rate (Stenni et al., 2011). Considering the different moisture source regions for the ice cores (Atlantic sector for EDML and Dome F, Indian and Pacific sectors for EDC and Talos Dome), this may give hint to the atmospheric circulation situation (e.g. Westerlies) and related water mass distribution during the Termination.

Little variations of SSSTs are recorded in the southern cores in Bouvet Island area and the warming/cooling amplitude is small (Fig. 6), probably due to the lower sample resolution in these cores (e.g. PS1768-8, north of ODP1094), but more likely indicate a more persistent cold condition that the warming from the north did not extend to the area. This is also indicated by the sea ice diatoms that the small fluctuations of WSI visited the southern sites during the temporal maximum and cold reversal periods (Fig. 7). At the modern Polar Front (ODP1093) and further north, the amplitude of the cold reversal is minor (Fig. 6), also indicated by the little variations of foram cold species at site TN057-21 (Fig. 8) (Barker et al., 2010). In spite of cold reversals recorded in the adjacent land proxies (Hajdas et al., 2006; Alloway et al., 2007), in the Pacific sector, no obvious cold reversal is evidenced in the alkenone SST records off New Zealand (Pahnke and Sachs, 2006). Such difference may be related to the proxy indications: the alkenone estimates are regarded as annual mean SSTs. At the location away from the sea ice influence, the weaker seasonality at the core sites may neglect the strong changes in summer conditions in the high latitude Southern Ocean. Such different climate evolution pattern between the marine and land archives is also observed at deglacial-Holocene around New Zealand (McGlone et al., 2010). This means the area strongly affected by the cold reversal is in a region with strongest variations of cold water/sea ice south of the modern Polar Front.

The start of the Bølling-Allerød (B-A) warming is associated to the “flywheel” in the Southern Ocean which induced a non-linear transition to a strong AMOC warming up the North Atlantic (Knorr and Lohmann, 2003; 2004). Based on our dating, the temporal maximum warming in the South Atlantic is in phase with the early part of B-A warming in the Northern Hemisphere (Fig. 8). Accompanied by the overshoot of AMOC on its resumption after the sharp decline of NADW during

H1 (McManus et al., 2004), the improved bottom-surface water ventilation is observed in the South Atlantic (Fig. 8) (Barker et al., 2010; Skinner et al., 2010). This is resulted from the propagation of NADW to the southern high latitude ocean, which mixes with the CDW and upwells to the surface. In the southern high latitudes, where the propagation of surface warming was slowed down by the ACC front system, the upwelling of relatively warm NADW became the second source of warming, which warmed up the Southern Ocean from below and helped to melt the sea ice. Thus, following the warming through bipolar seesaw during H1, the Southern Ocean was continuously warmed up by upwelled NADW, till ca. 14 cal. ka. The timing is also in agreement with the CO_2 rise recorded in the Antarctic ice cores (Monnin et al., 2001) (Fig. 8). The spatial difference of our SSST records implies that, the intrusion of NADW during this time may have reached the northern Bouvet Island area, western Indian sector, and less pronounced in northern Scotia Sea, but not into the northern Weddell Basin (Fig. 6; Fig. 8). This warming process may have also involved other positive feedbacks such as rise of atmospheric CO_2 content, reduced albedo of retreated sea ice, and the southward shifted Westerlies.

The sharp deterioration of the ventilation, especially the bottom water-atmosphere ventilation, started at ca. 14 cal. ka (Barker et al., 2010; Skinner et al., 2010), at the onset of the cold reversal recorded in our records (Fig. 8). Such condition may be related to the cold water/sea ice re-expansion in the Southern Ocean which prohibited the ventilation between the ocean and the atmosphere.

The ACR was assumed to be related to the meltwater pulse 1a (MWP 1a) discharged from the Antarctic Ice Sheet and the start of the Northern Hemisphere B-A warming at ca. 14.6 ka by the bipolar seesaw (Weaver et al., 2003; Bassett et al., 2005). More recent analysis indicated that the MWP 1a occurred later, at around 14 ka, and thus coincides with the Older Dryas cold event and in fact terminated the Bølling warming (Stanford et al., 2006), which is in agreement with our SSST records. The Antarctic source of MWP 1a was also questioned by Peltier (2005), who suggested the Northern Hemisphere contributed the major part of the melt water. Stanford et al. (2006) emphasized the location of the MWP was not in the critical area that might induce a reduction of the NADW, thus the typical bipolar seesaw effect is not obviously recognized. Even though, there are evidences indicating the retreat of the Western Antarctic Ice Sheet and the melting Antarctic Peninsula ice sheet contributed to the MWP 1a (Heroy and Anderson, 2005; 2007; Clark et al., 2009). With the strongly reduced dust input (Fischer et al., 2007; Lambert et al., 2008), the increases of *Chaetoceros* RS at 14-12 cal. ka in our records, together with the increase of diatom sea ice indicators in all studied sectors, point to a re-expansion of cold water advected from the south and increased stratification (Crosta et al., 1997), which might be related to the melt water input from the Antarctica. The Scotia Sea located at the route of iceberg exporting from the Weddell Sea is primarily affected, evidenced by the abrupt rise of *Chaetoceros* RS observed at site PS67/197 (Fig. 9).

The different amplitude of warming/cooling in the South Atlantic changed the latitudinal SST gradient in different regions, accompanied by the poleward migration of the Westerlies and associated upwelling regions. The EDC CO_2 record (Monnin et al., 2001) indicates that, the two steps of abrupt atmospheric CO_2 increase mainly coincide with the abrupt warming steps in the Southern Hemisphere, including time periods of H1 and YD cold phase in the Northern Hemisphere (Lourantou et al., 2010). Deglacial maximum opal flux (coincides with the maximum warming) mirrors the opal production and Si supply linked to upwelling driven by the Westerlies (Anderson et al., 2009). The wind driven upwelling is also considered as the primary contributor to the deglacial CO_2 rise (Toggweiler et al., 2006). The poleward shifted Westerlies would bring relatively warmer deep water to the surface that

melted the sea ice, and the Southern Ocean and Antarctica were warmed up by increasing eddy transport of heat (Denton et al., 2010). Our records agree with the results of Anderson et al. (2009) that the temporal warming (opal deposition) maximum intruded to 53.2˚S in the Bouvet Island area, along with the southward migration of Westerlies and upwelling zone; furthermore, our records provide additional information that during the cold reversal, all the related features may have shifted northward to ca. 50˚S (ODP1093) (Fig. 4; Fig. 6).

3.5.3. Holocene conditions

3.5.3.1. Holocene trend

Our records show a distinct warming at the early Holocene, and then persistent colder than modern conditions at the southern sites during the mid-late Holocene. Especially at the southern sites of Bouvet Island area, the SSSTs are close to glacial values. Two high resolution diatom based SSST (February) records has been reported at sites TN057-17 (Nielsen et al., 2004; Divine et al., 2010) and TN057-13 (Anderson et al., 2009; Divine et al., 2010), close to sites ODP1093 and ODP1094, respectively. Their SSSTs at TN057-13 is in agreement with our records at ODP1094. In contrast, the SSSTs at TN057-17 show much difference from our records at ODP1093. The initial SSST calculation of TN057-17 is based on Modern Analogue Technique (MAT) method and show large variations of Holocene climate and even warmer glacial SSSTs than modern conditions (Nielsen et al., 2004). Such warm glacial condition is not documented in any of the adjacent area and not likely to be a single site warming in the context of large area cold conditions. Divine et al. (2010) recalculated the SSSTs using Imbrie and Kipp Method (IKM) and showed that the MAT method tends to overestimate the SSSTs. However, both calculations show the same pattern in core TN057-17 with different timing and amplitude of climate change from our records. The high variability of Holocene SSSTs and the late Holocene 2-3˚C warmer than modern conditions in their records are not documented anywhere else in this region. Our records confirm a persistent pattern of small fluctuations during the mid-late Holocene.

Strong decrease of *Chaetoceros* RS is observed in the Holocene South Atlantic. It decreased to trace values at the western Indian sector, maintained at low numbers (<5%) in the Bouvet Island area, and relatively higher values in the northern Scotia Sea (5-15%) (Fig. 9). The decrease is in agreement with the minimum dust flux recorded in the Antarctic ice core (Fig. 9) (Fischer et al., 2007; Lambert et al., 2008). This indicates the iron fertilization by airborne dust is strongly reduced in Holocene.

3.5.3.2. Early Holocene optimum

The early Holocene distinct warming at 9-11 cal. ka in our records is in consistence with the marine records in the Pacific sector of Southern Ocean (Kaiser et al., 2005; Lamy, 2006; Pahnke and Sachs, 2006), as well as the Antarctic ice cores (Masson et al., 2000; Masson-Delmotte et al., 2004). This warming is also synchronous with the tropical Andes (Thompson et al., 1998; 2000), and vast areas in the northern hemisphere (Jansen et al., 2007).

The Antarctic early Holocene optimum exceeds modern SSSTs by 1-2˚C in the Bouvet Island area and close to modern values in the Scotia Sea and western Indian sector. Indicated by the absence of cold water/sea ice diatoms (Fig. 7), the early Holocene ice field retreated far south of 55˚S (PS1649).

It marks the warmest period of the Southern Ocean since last glacial by natural processes. The advances of some Patagonian glaciers during the early Holocene (Ackert et al., 2008; Rodbell et al., 2009) may be attributed to more precipitation due to the shift of the Westerlies (Ackert et al., 2008). Different from the open ocean and the Antarctic ice cores, various East Antarctic coastal oases (Cremer et al., 2007; Wagner and Melles, 2007) and marine record (Denis et al., 2009) show a postponed optimum at the mid-Holocene, where the local deglaciation is still undergoing at the early Holocene.

The early Holocene warming in the Southern Ocean was believed to be related to the reduced AMOC during the YD that kept the heat in the Southern Ocean, and the switch-on of AMOC triggered the cooling following the optimum in the southern high latitudes (Masson et al., 2000). However, this may not explain that such optimum lasts more than 2 kyr (11.5-9 ka), as also recorded in the ice cores (Fig. 8). In contrast, at a time of weakened AABW formation, either by sea ice forming or under the shelf ice, the enhanced production of NADW (McManus et al., 2004) may have intruded into the South Atlantic further south than modern conditions, which introduced relatively warm deep water into the southern high latitudes. In addition, the persisted warmth may be related to the poleward shifted Westerlies which brings heat to the high latitude Southern Ocean (Bentley et al., 2009). Pollen records suggested a southward situated Westerlies before 9.2 cal. ka (McCulloch and Davies, 2001; Mayr et al., 2007). These processes are accompanied by the high atmospheric CO_2 content (Monnin et al., 2001), reduced sea ice albedo, and slow changes in insolation at that time (Fig. 8).

The timing of optimum warming is a little different between the northern and southern cores. The northern cores present longer warming period between 11 and 9 cal. ka whereas in the southern cores it is culminated at 11-10 cal. ka dated in various cores. Compared to the ice cores from the east Antarctic plateau at high altitudes, which present conditions of mid-high latitude Southern Ocean, Taylor Dome ice core better presents conditions of coastal regions of the Southern Ocean Ross Sea sector, also shows slightly shorter optimum at the early Holocene between 11.5 and 10 ka (Steig et al., 1998). This indicates more persistent cold condition in the south, which may be related to the melting of the WAIS, and in Atlantic sector, the cold water is transported to the open ocean by the Weddell Gyre. The major melting of Antarctic Peninsula ice sheets at this time interval (Heroy and Anderson, 2007; Hall, 2009) may also support this idea.

The early Holocene substantially expanded warm ocean would allow the increase of moisture transported to the Antarctic continent, as indicated by the increased accumulation rate in EDML ice core (Fig. 8). The upwelling zones in the Southern Ocean would also shifted poleward with the southward migrated Westerlies. Such enhanced upwelling in the south is recorded by the opal production at site TN057-13 (Anderson et al., 2009). Our records suggest that the early Holocene period of maximum opal flux is confined between 11 and 10 cal. ka, at least in the southern cores, by AMS ^{14}C dating, which corresponds to the maximum sedimentation rates and pure diatom ooze interval in the sediments. The different timing of the maximum opal flux in Anderson et al. (2009) may due to the dating intervals. In their study, 2 datings confined ca. 14-10 cal. ka, thus the maximum opal flux between 11 and 10 cal. ka is not constrained. Our data also suggest that the maximum opal flux zone shifted southward at least to 55˚S (PS1649) in the Bouvet Island area.

3.5.3.3. Mid-late Holocene cooling

The mid-late Holocene cooling is recorded in all the cores south of the modern Polar Front (Fig. 6), started at 8-9 cal. ka, along with the cold water re-expansion in the southern cores (Fig. 7). The SSSTs dropped to low level close to the ACR conditions. This cooling is also recognized in core TN057-13 (Hodell et al., 2001; Divine et al., 2010). In our records, the maximum re-expansion of winter sea ice is between 4.5 and 7 cal. ka, which is slightly different from the TN057-13 at ca. 5 cal. ka (Hodell et al., 2001). The difference may come from the age control point (Bianchi and Gersonde, 2004). Our records show that the mid-late Holocene winter sea ice extended to ca. 53˚S in the Bouvet Island area, and the cooling also covered the Scotia Sea and western Indian sector south of the Polar Front (Fig. 6; Fig. 7). This cooling has been defined as the "neoglaciation" in the Southern Ocean (e.g. Hodell et al., 2001; Divine et al., 2010). However, at the modern Polar Front (ODP1093) and further north, the cooling is minor (Fig. 6). Our records show that the strong cooling in the South Atlantic is only restricted in the area south of the modern Polar Front.

Different from our marine records, the Antarctic plateau ice cores (Epica members, 2006; Jouzel et al., 2007) show relatively warm conditions in the mid Holocene. Modeling studies show that except the coastal ice cores, the moisture sources of east Antarctic plateau ice cores come from the surrounded mid-latitude oceans (e.g. Delaygue et al., 2000), thus these ice cores present the changes of mid-latitude ocean conditions. In the South Pacific off Chile, alkenone records suggest a temporal warming centered at 5.5 cal. ka (Lamy et al., 2002). The warming signal comes from the lower latitude driven by insolation and shifts in position of the Westerlies (Renssen et al., 2005; Bentley et al., 2009).

Based on the different diatom assemblages from the LGM, the high abundance of winter sea ice indicator during the mid-late Holocene was interpreted as a longer growing season, with early spring sea ice retreat and summer blooms not affected by the sea ice (Bianchi and Gersonde, 2004). However, different from the marine records, EDML $ssNa^+$ flux (Fischer et al., 2007) as another sea ice indicator from ice cores represents lowest value at around 6 cal ka. The $ssNa^+$ is not only related to the sea ice coverage, but also influenced by uplift, transport and deposition of the sea salt aerosol (Röthlisberger et al., 2010), these factors may bias the real signal of sea ice conditions. Our marine records provide direct evidence of sea ice occurrence in Bouvet Island area and it marks the strongest cold water expansion in winter since Holocene. Despite of uncertainty of moraine dating, the glacier re-advances in southern Andes (Fig. 8) (Douglass et al., 2005; Rodbell et al., 2009) and several Southern Ocean islands (Hall, 2009) during the mid-late Holocene is clearly documented and loosely synchronous to our sea ice records. The re-advance of Southern Andes glaciers has been interpreted as northward migration of the Westerlies that increased the precipitation and/or decreased the temperature in this area (Douglass et al., 2005). Both are associated with the expanded cold area from the south.

The persistent cold conditions in the high latitudes South Atlantic are different from the lower latitudes, this cooling must come from the cold source in the south, which is the Weddell Gyre and the connected WAIS. Similarly, on the other side of the WAIS, in the Ross Sea sector, at the site Taylor Dome, the precipitation is from cyclonic systems from the nearby Ross Sea and sensitive to local oceanic conditions near Antarctica (Morse et al., 1998). Steig et al. (1998) found evidences of an abrupt cooling and an increase of sea ice cover at ca. 6 ka in the Ross Sea embayment, both in Taylor ice core record and diatom sea ice indicators in the sediments. Other evidences from Siple Dome ice surface melting (Das and Alley, 2008) show that between 8.8 and 6.6ka there was little surface melting,

indicating a cold condition over Ross Embayment. This finding of mid-Holocene cold status is in agreement with the cold conditions in the Atlantic sector.

Glaciology studies show that, the WAIS maintained continuous thinning and retreating during the Holocene, as a response of ice dynamics to an earlier triggering mechanism (Conway et al., 1999; Sugden et al., 2006). Conway et al. (1999) show that most shelf ice grounding line recession in the Ross Sea embayment took place during the mid-late Holocene after 7.6 ka, accompanying by the thinning of the WAIS. The cavity between the shelf ice and the shelf was developed with the retreating grounding line and thinning of the WAIS, allowing the cold water generating beneath the shelf ice and transported to the open ocean. A similar mechanism can be assumed in the Weddell Sea sector which caused the cold conditions documented in our records. However, there is little information of the Holocene grounding line retreat of the Weddell Sea sector shelf ice, more data is strongly needed from both Weddell Sea and Ross Sea sector to fully understand the processes of WAIS variability.

With the developing cavity, AABW was able to be generated similar to modern conditions under the Western Antarctic shelf ice. Together with the more expanded sea ice field, the AABW formation was more enhanced and able to penetrate further north during the mid Holocene compared to the early Holocene. Together with the slightly reduced NADW formation (McManus et al., 2004), the warming by NADW at the southern high latitudes was also reduced. This may contribute to the cooling recorded in our southern sites. Different from the early Holocene CO_2 increase, modeling studies (Joos et al., 2004; Elsig et al., 2009) suggest the 20 ppmv increase of atmospheric CO_2 during the mid-late Holocene is mainly contributed from carbonate compensation of earlier land-biosphere uptake and coral reef formation.

3.5.4. Recent warming

The young sediments of core PS1652-1 are expected to document the recent warming of the Southern Ocean. However, no significant changes of the diatom assemblages are found compared to the mid-late Holocene as recorded in gravity core PS1652-2, nor the estimated SSSTs.

Did the Southern Ocean surface water respond to the recent warming? Ship-based hydrological survey since 1930s are combined with detailed studies of the global sea ice cover by satellite observation since 1970s (Zwally et al., 1983; Gloersen and Campbell, 1988; 1991; Comiso, 2003; Gille, 2002; 2008), which provides comprehensive long term and areal coverage at a relatively high temporal resolution. A 22-year (1979-2000) observation shows insignificant trend of 0.4±0.3% per decade sea ice increase for the entire southern hemisphere and -1.2±0.8% per decade decrease at the Weddell Sea sector (Comiso, 2003). Longer record of summer sea ice extent around Antarctica is available by whaling industry. De La Mare (1997) stated a decline in sea ice cover by 25% between the mid 1950s and early 1970s, corresponding to a southward shift of sea ice edge by 2.8˚ latitude; contradictory conclusion has been made by Ackley et al. (2003) that no significant deviations in the mean ice extents from the pre-1950s to the post 1970s. Even though, in the long term trend of warming, the presence of cyclical components of sea ice extent variations was recognized (Zwally et al., 1983), as an increase in sea ice extent from 1966 to 1972 and followed by a remarkable decrease during the mid-1970s, and rebound afterwards particularly in the Weddell Sea. Gloersen and Campbell (1988; 1991) also stated there was no significant trend in sea ice extent in the Antarctic during the period 1978-1987.

The recent warming is not well presented in core PS1652-1 may due to the following reasons: firstly, the core was recovered in 1988, when the warming is not markedly detected in the Southern Ocean with a big heat capacity and the signal of warming might be lagged, although there was evidence of sea ice thinning, retreating and less duration; secondly, according to the sedimentation rate, 1 cm of sediment may be accumulated for around 5-20 years, thus even the core top sample may represent the long term climate signal for 2 decades, the warming trend may be leveled off by the former colder intervals and the subdecadal oscillations is not presented. The non-existence of recent warming in our record may indicate a retreat of cold water and sea ice after 1990s.

Fig. 10. Schematic illustration of climate development in the LG-Holocene South Atlantic: (A). present; (B). 30-18 ka; (C). H1/YD; (D). 14 ka; (E). ACR; (F). 11-10 ka; (G). 9-0 ka. F & R: Filchner & Ronne shelf ice; SSI: summer sea ice; WSI: winter sea ice; WG: Weddell Gyre; CWR: cold water route; WWR: warm water route; AAIW: Antarctic intermediate water; CDW: Circumpolar Deep Water; NADW: North Atlantic Deep Water; AABW: Antarctic Bottom Water; PF: Polar Front.

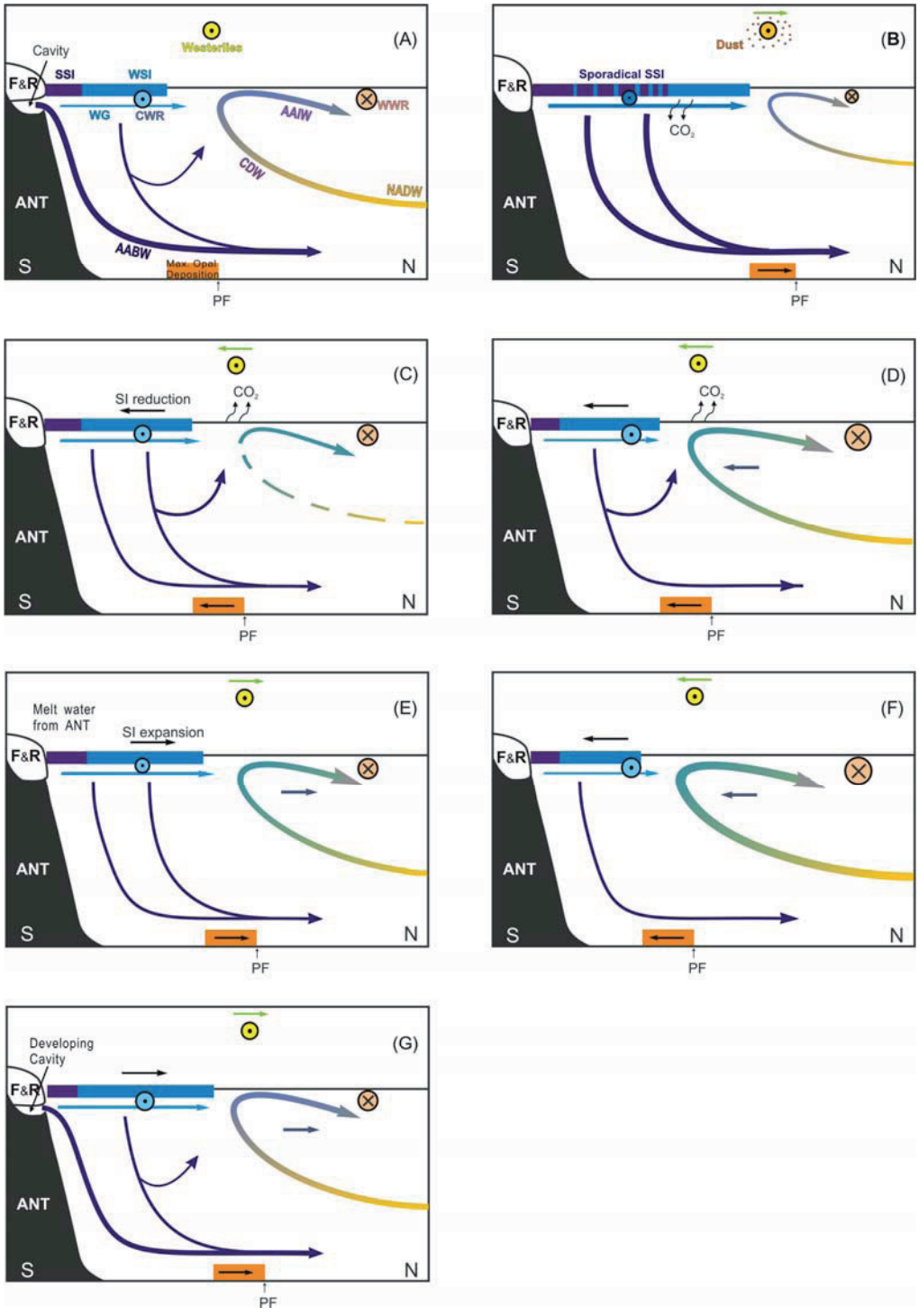

3.6. Conclusions

We provide comprehensive new high resolution diatom based records from the high latitude Atlantic and western Indian sectors of the Southern Ocean. By integration of other records from this region, we are able to establish a detailed climate development covering the past 30 kyr (Fig. 10). The

climate development of the South Atlantic is in concert with the changes in summer sea surface temperature, sea ice extension, surface and deep water formation, shift of the Westerlies and the associated upwelling/opal deposition zones. It is closely related to the cold water extent from the Weddell Sea, which is connected to the Western Antarctic Ice Sheet.

Compared to modern conditions, the LG South Atlantic is characterized by 2-3˚C cooling in the area south of the modern Polar Front, however, the strongest LG cooling (ca. 6˚C) is in the modern Subantarctic zone. Winter sea ice expanded by 5˚ in latitude in the Bouvet Island area. Along with the Westerlies and the upwelling zone, the maximum opal deposition also shifted to north of 50˚S. Enhanced AABW production via sea ice formation and the reduced NADW formation in the North Atlantic composed the glacial mode of deep water circulation. On the sea surface, the heat and water mass exchange from the Indian and Pacific basins to the South Atlantic were reduced due to the expanded sea ice field as a response to the extended cold-water sphere. This also results in the stronger cooling in the tropical Atlantic than other tropical oceans. Our data support that, during the LG, the Southern Ocean became a carbon sink due to the intensive carbon export to the stratified deep ocean. The extended area of carbon export to the deep ocean is characterized by high occurrence of diatom species *Chaetoceros* resting spores.

The deglacial warming started at ca. 18 cal. ka. The two step warming is coherent with the strong reduction of NADW formation during the H1 and YD in the North Atlantic, suggesting the bipolar seesaw mechanism played a major role in the warming in the Southern Ocean. In addition, the overshoot of NADW intruded further south during the early B-A stage provided a second warming source which warm up the southern high latitudes ocean from below. The two warming steps were at times of abrupt rise of atmospheric CO_2 related to the poleward migrated Westerlies that released the CO_2 stored in the deep ocean during the glacial times. The cold reversal started at ca. 14 cal. ka, only affected the region south of the modern Polar Front, which may be caused by melt water from the Antarctica.

Distinct warming in the southern cores during the early Holocene optimum marks the warmest time period since last deglaciation with the strongest reduction of cold water field in the south. The sea ice distribution is probably far south of its modern conditions. The shorter period of optimum in the south may be attributed to the melting of Antarctic ice sheet. The reduced production of AABW and enhanced production of NADW allowed the further south propagation of NADW into the South Atlantic which may also contribute the warming in the south. The Westerlies shifted southwards and marks the maximum opal deposition southward expanded to at least 55˚S between 11 and 10 cal. ka. Mid-late Holocene cooling started at 9-8 cal. ka after the early Holocene optimum, together with the Westerlies northward shifted. With the developing cavity between the shelf ice and shelf, AABW formation gradually developed close to modern conditions. The Holocene maximum sea ice cover occurred at 4.5-7 cal. ka, with a winter sea ice edge displaced northward by ca. 3˚ latitude in Bouvet Island area compared to present situation. The recent warming is not observed in our records, this may indicate the retreat of cold water and sea ice was after 1990s in the Atlantic sector.

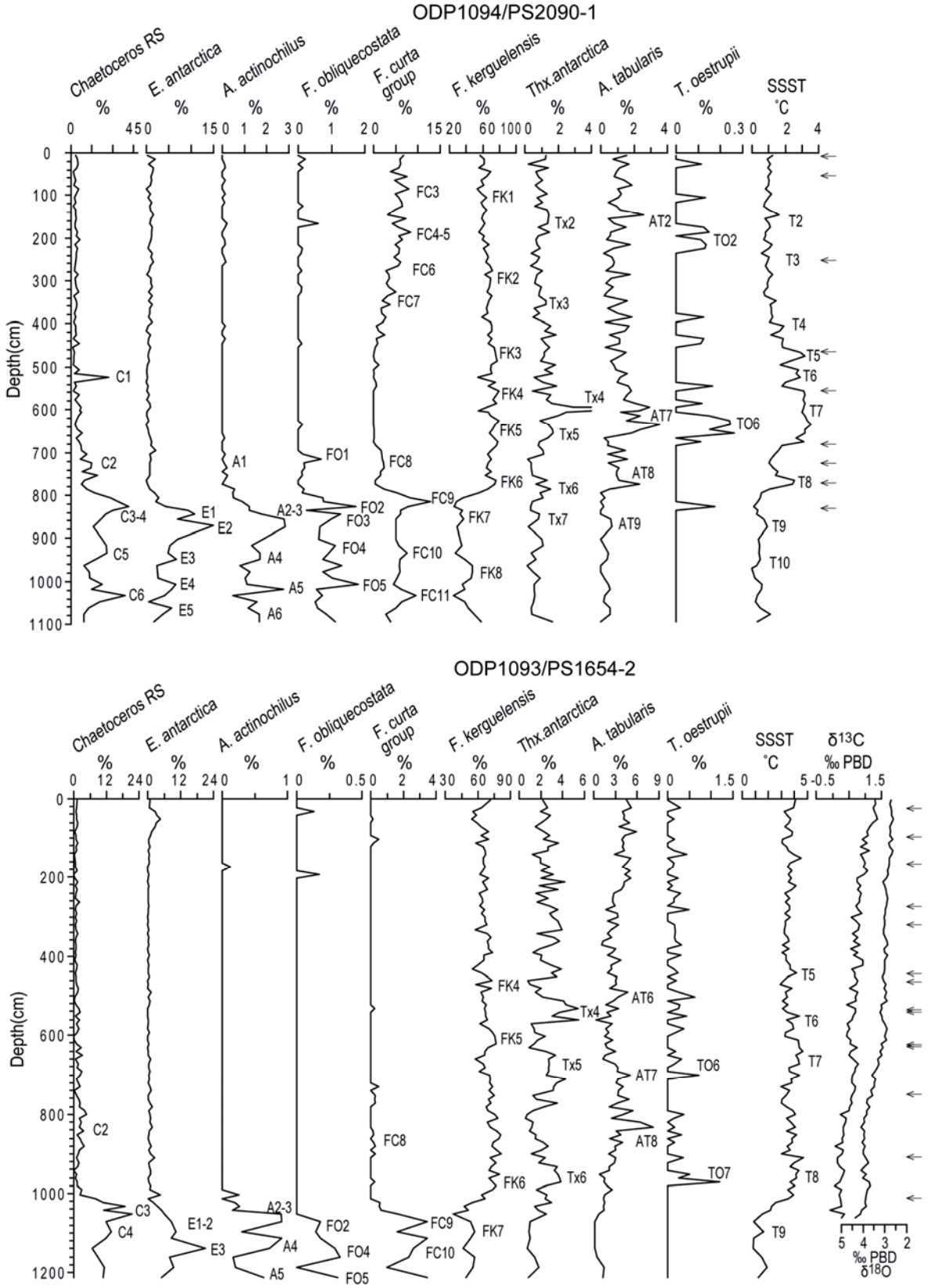
ODP1094/PS2090-1
Chaetoceros RS
E. antarctica
A. actinochilus
F. obliquecostata
F. curta group
F. kerguelensis
Thx.antarctica
A. tabularis
T. oestrupii
SSST
Depth(cm)
ODP1093/PS1654-2
δ13C
‰ PBD
δ18O

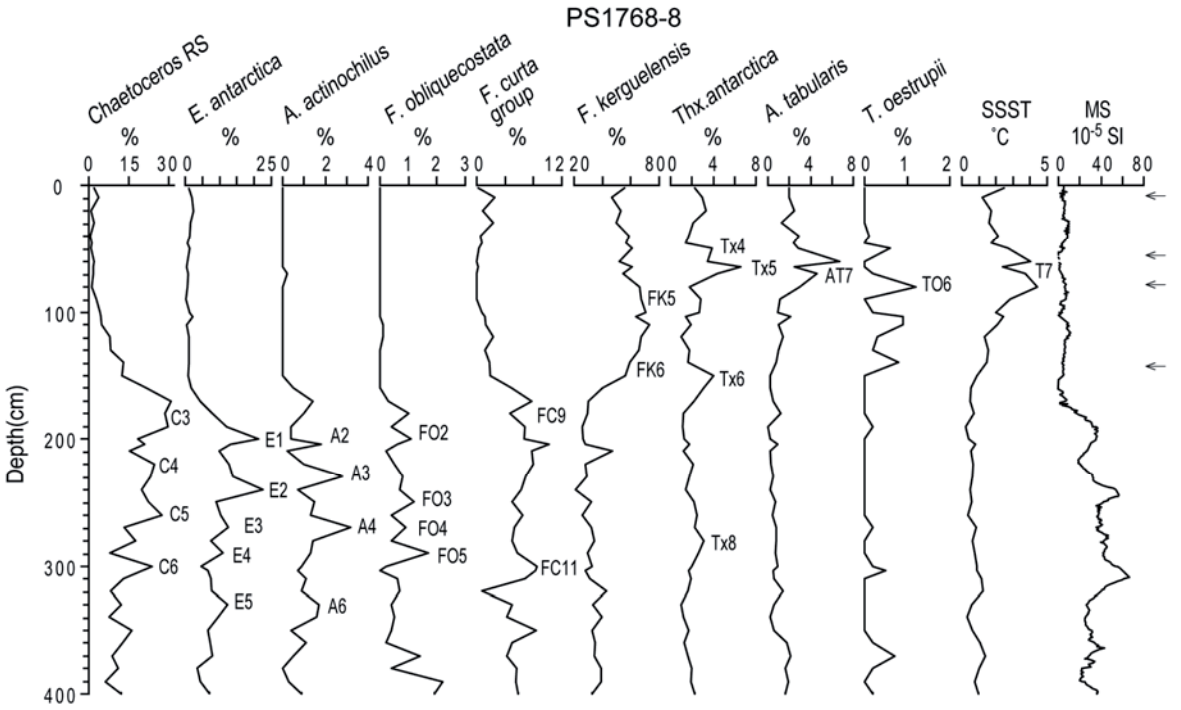

Supplimentary figure. Relative abundances of relevant diatom species, estimated SSSTs, magnetic susceptibility (MS) records, planktonic foraminifera *N. pachyderma*$_{sin}$ oxygen and carbon isotope records of cores ODP1093, ODP1094 (Bianchi and Gersonde, 2004) and PS1768-8 (Zielinski et al., 1998). Arrows indicate the AMS ^{14}C dating intervals. Biofluctuation of diatom species and estimated SSSTs used for regional core correlation are numbered.

Chapter 4. Centennial-scale climate variability of the Holocene Scotia Sea (Atlantic Southern Ocean)

Wenshen Xiao[a], Rainer Gersonde[a], Thomas Frederichs[b]

a. Stiftung Alfred-Wegener-Institut für Polar- und Meeresforschung in der Helmholtz-Gemeinschaft, 27568 Bremerhaven, Germany
b. Fachbereich Geowissenschaften der Universität Bremen, 28334 Bremen, Germany

To be submitted to *Paleoceanography*

Abstract

Holocene climate variability in the high latitude Southern Ocean is little studied due to the lack of high resolution records. Centennial-scale climate variability has been revealed by diatom based high resolution records from the Scotia Sea. Our study shows that, other than the northern Scotia Sea which displays similar climate development to the open Southern Ocean, the central and southern Scotia Sea remained stable during the Holocene with frequently visited winter sea ice, even at the Southern Ocean climate optimum during the early Holocene. This may be attributed to the melting of Antarctic Peninsula ice sheet which induced persistent cold conditions in the south. Upwelled nutrients sustained the diatom productivity during the early Holocene due to the enhanced upwelling at that time. The Holocene reservoir change in the Scotia Sea is in agreement with the South Atlantic ventilation, the lowered $\Delta^{14}C_{atm}$ after the release of CO_2 from the Southern Ocean during the pre-Holocene warming substantially contributed to the early Holocene low reservoir at the core site. The centennial scale climate variability may be attributed to solar activity and sea ice induced freshwater variability. The Holocene megascopic ash layer in the Scotia Sea is dated at 8.1 ka, which provides an additional age marker for further studies in this area.

4.1. Introduction

As the most intensively studied current interglacial, the Holocene (0-11.5 ka: kyr BP) was generally considered as a stable warm period, however, rapid and complex climate changes show big spatial variability which are documented in various paleoclimate archives in response to significant changes in climate forcing (Jansen et al., 2007). To understand the complexity of the Holocene climate, efforts have been made through achieving high resolution Holocene climate records as well as model studies. High resolution records from the southern high latitudes are best documented in the Antarctic ice cores, which show an early Holocene optimum between 11.5 and 9 ka, and followed by a cooling (Masson et al., 2000; Masson-Delmotte et al., 2004). Mid Holocene warming is documented in some ice cores from Antarctic plateau at high altitudes (Epica members, 2006; Jouzel et al., 2007), whereas cooling is recorded in some coastal ice cores (Steig et al., 1998; Masson et al., 2000). The differences also imply the complexity of climate variability in the southern high latitudes.

Other than Antarctic ice cores, high resolution marine records from the high latitude Southern Ocean are remarkably few. In the open ocean South Atlantic, high resolution climate records indicate similar variability as recorded in the Antarctic ice cores (Bianchi and Gersonde, 2004; ***Chapter 3***). High sedimentation rates have been reported in several Holocene sediments from the Antarctic coastal

regions, with lamination documenting seasonality changes of diatom production, especially the early Holocene (Leventer et al., 2002; Denis et al., 2006; Madisson et al., 2006). Long term and short term cyclicities have been related to different forcings such as solar and lunar variability (Warner and Domack, 2002) and thermohaline circulation (Crosta et al., 2007). These records are retrieved from the coastal regions and the local deglaciation strongly influences the core sites. And the interpretations of the climate records are strongly dependent on the core age models which are mainly based on AMS ^{14}C dating.

However, uncertainties of carbon reservoir change and contamination of fossil carbon significantly influence the reliability of the core stratigraphy based on AMS ^{14}C dating. Reservoir change through glacial/interglacial transition (Sarnthein et al., 2007) as well as Holocene (Ascough et al., 2007; 2009; Druffel et al., 2008; McGregor et al., 2008) is well noticed in the northern latitudes and tropical regions. In the Atlantic Southern Ocean, van Beek et al. (2002) estimated a mid-late Holocene reservoir of ca. 1100 years and almost doubled (1900 years) at the early Holocene by comparing the ^{14}C and ^{226}Ra-in-barite ages. However, the authors indicated that the large early Holocene reservoir may be biased by the high sedimentation rates (van Beek et al., 2002). Recently, the Southern Ocean ventilation history for the past 30 kyrs was investigated through comparing planktic and benthic foraminifera ages (Skinner et al., 2010), their study indicates ventilation changes through Holocene, which is directly related to the possible reservoir changes of the Southern Ocean.

Located at the “cold water route” (Seidov and Maslin, 2001) of South Atlantic Ocean, the Antarctic Circumpolar Current (ACC) transports Pacific waters into the South Atlantic via the Scotia Sea; cold water generated in the Weddell Sea is imported by the Weddell Gyre from the south. The Scotia Sea represents a key region of the Atlantic Meridional Overturning Circulation. However, Holocene climate changes of the Scotia Sea are little investigated due to lack of high resolution record.

In this study, we present the first diatom based centennial scale climate variability of the Holocene Scotia Sea. By combining with other records from this region, we reveal the unique climate development, and establish the reservoir changes of Holocene Scotia Sea.

4.2. Materials and Methods

With a length of 23.62 m, piston core PS67/206-1 (KOL) was retrieved from the central Scotia Sea at water depth of 3206 m during the R/V Polarstern cruise ANT XXII/4 in 2005. The core represents the first high resolution Holocene record from the Scotia Sea. It mainly consists of diatom ooze with discontinuous laminations occurring at 16.7-17.2 m and 18.2-22 m. A very pronounced ash layer marks at 14.64-14.7 m, and a disseminated ash layer was also observed at 17.43m. In the northern Scotia Sea, piston core PS67/197-1 (KOL) was recovered from the same cruise, an ash layer was found at 80 cm core depth. Both cores are located south of the modern Polar Front and north of the modern winter sea ice edge. In the southern Scotia Sea, gravity core PS2319-1 (GC) was taken from a small basin north of South Orkney Islands during R/V Polarstern cruise ANT X/5 in 1992. Ash was found at 75 cm core depth. The core is located south of the Southern ACC Front and modern winter sea ice edge (WSI). With a north-south transect (Fig. 1; Table 1), we are able to reconstruct the detailed Holocene climate variability of the Scotia Sea.

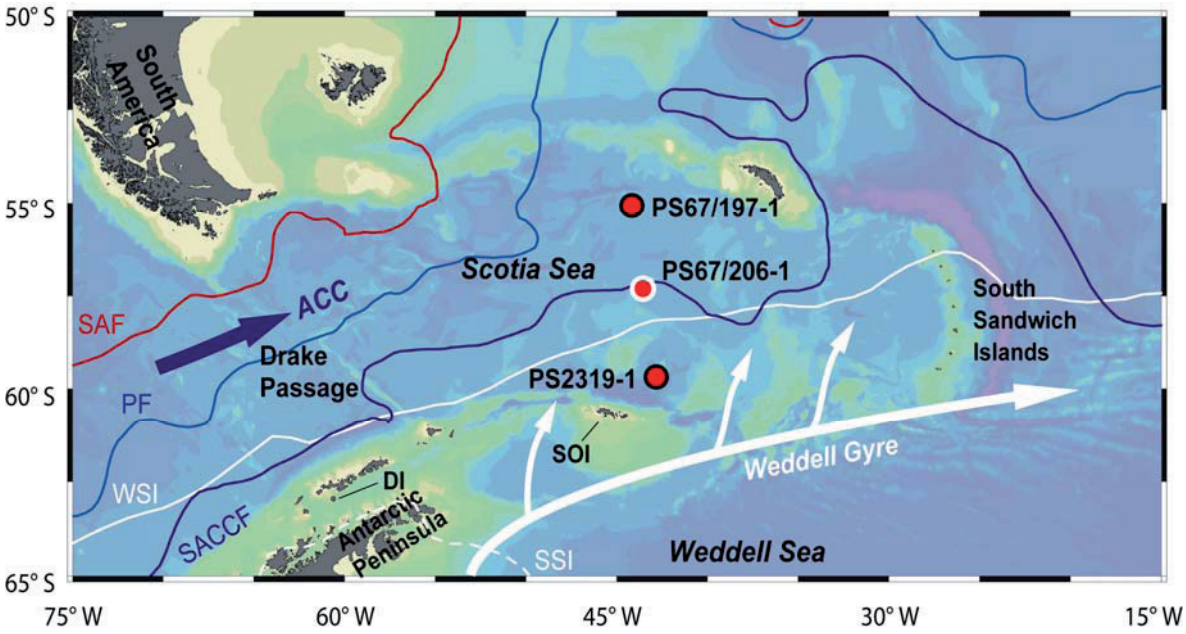

Fig. 1. Core locations and oceanographic frontal system and sea ice distribution map of Scotia Sea. High resolution record PS67/206-1 is highlighted. SACCF: Southern ACC Front; PF: Polar Front; SAF: Subantarctic Front; WSI: modern winter sea ice edge; DI: Deception Island. Front positions are from Orsi et al. (1995), sea ice distribution from (Comiso, 2003).

Table 1. Locations and water depths of studied cores.

Station	Latitude	Longitude	Water depth (m)	Coring device
PS67/197-1	55° 8.24' S	44° 6.28' W	3837	KOL
PS67/206-1	57° 24.67' S	43° 27.5' W	3206	KOL
PS2319-1	59° 47.3'S	42° 41'W	4323	GC

Coring device: KOL-piston core; GC-gravity core

Samples were taken at 10 cm intervals and freeze dried. For sample treatment and diatom slide preparation, the standard procedure developed at Alfred-Wegener Institute (AWI)-Bremerhaven (Gersonde and Zielinski, 2000) was applied. The slides were examined under a Zeiss light microscope at a magnification of 1000×. At least 400 diatom valves were counted in each sample. The counting method was according to Schrader and Gersonde (1978) and the taxonomy was according to Zielinski and Gersonde (1997).

The Imbrie and Kipp transfer function method (IKM: Imbrie and Kipp, 1971; Zielinski et al., 1998; Esper and Gersonde, in prep.) was applied for Summer Sea Surface Temperature (SSST) estimation. The SSSTs of the hydrographic reference data set represent average summer values (December to March) measured at 10 m below sea surface (Olbers et al., 1992). The reference data set includes 133 sites from the Southern Ocean Atlantic sector with 28 diatom texa or texa groups for SSST calculation (Esper and Gersonde, in prep.). We note that at the lower part of core PS67/206-1, where high abundant *Rhizosolenia antennata f. semispina* occurs, induces non-analogue conditions in the SSST calculation, thus we excluded this species from the reference data set for the SSST calculation of this core. A standard error of the estimates regression with the new reference data set is 0.5 ˚C. A related software package (Sieger et al. 1999) was used for calculations. The communalities for the estimates generally range between 0.8 and 0.9.

Diatom sea ice indicator species were used for sea ice reconstructions (Gersonde and Zielinski, 2000). Over 3% of the relative abundance of *Fragilariopsis curta* and *Fragilariopsis cylindrus*, combined as *F. curta / F. cylindrus* group (*F. curgr*), indicates the presence of winter sea ice. Distinct drop in biogenic sedimentation rate and over 3% of the deep-temperature species *Fragilariopsis obliquecostata* represents the occurrence of perennial sea ice.

Geomagnetic samples were taken at 10 cm intervals from core PS67/206-1 with 2.2 cm × 2.2 cm × 1.8 cm plastic cubes and analyzed in the palaeomagnetic laboratory at the Department of Geosciences, University of Bremen. Palaeomagnetic directions and magnetic intensities of natural remanent magnetization (NRM), anhysteretic remanent magnetization (ARM) and isothermal remanent magnetization were measured stepwise with a maximum alternating field (AF) demagnetization intensity of 100_{mT} on a cryogenic magnetometer (model 2G Enterprises 755HR). Relative paleointensity (RPI) was calculated as ratios NRM_{20mT} / ARM_{20mT} (RPI-ARM_{20mT}) and NRM_{20mT} / IRM_{20mT} (RPI-IRM_{20mT}) using an AF demagnetization level of 20mT for each type of remanence.

In order to decipher the short term climate variability of the Scotia Sea, spectral analysis was performed on core PS67/206-1 using the software Redfit 3.8 (Schulz and Muldesee, 2002), which can process unevenly spaced time series, with 1000 Monte-Carlo simulations, an oversampling factor of 4 for the Fourier transform, three segments with 50% overlapping, and a Welch window. Red-noise spectrum of 90% was selected to define significant frequencies.

4.3. Stratigraphy

In order to establish the stratigraphy of core PS67/206-1, ^{210}Pb activities were measured on core top sediments to determine the modern deposition; AMS ^{14}C dating on organic matter of the bulk sediment samples gives a detailed ^{14}C chronology; geomagnetic RPI record correlating to regional and global reference curves provides independent chronology for the core; the age model was also created based on correlation between estimated SSSTs and Antarctic ice core Epica Dronning Maudland (EDML) δ^{18}O record (Epica members, 2006).

The stratigraphy of core PS67/197-1 is based on a combination of AMS ^{14}C chronology, MS correlated to Antarctic ice cores, diatom biostratigraphy and geomagnetic paleointensity chronology (***Chapter 5***), and also regionally correlated to records from open ocean Atlantic Southern Ocean (***Chapter 3***). Holocene section of core PS2319-1 is based on regional correlation by diatom biofluctuations (Fig. 7).

4.3.1. ^{210}Pb excess chronology

Approximately 10g of freeze-dried core top sediments of PS67/206-1 at 3-5 cm intervals were weighed and packed into a plastic lid, pressed and sealed in radon proof foil for 3 weeks to establish radioactive equilibrium between ^{226}Ra and ^{222}Rn before measurement. Then the samples were analyzed by low-level low-background gamma spectroscopy using a coaxial HPGe detector (Canberra Industries). Activity concentrations of ^{210}Pb and ^{137}Cs were determined. The determination was performed at the Institute of Environmental Physics, University of Bremen.

$^{210}Pb_{ex}$ is well recorded in the surface sediment with a down-core decreasing profile down to 15-20 cm (Fig. 2), clearly showing that it is not significantly modified by erosion or mixing and not older

than 100 yr. A simple exponential fit through $^{210}Pb_{ex}$ data gives an estimated sedimentation rate of 2.4 ± 0.7 m/kyr of the core top sediment. The ^{137}Cs was also measured, which implies the most recent 60 years, but the ^{137}Cs is under detection limit in all measured samples. This is probably due to the nonexistence in the sediments or very little deposition of ^{137}Cs in this region of southern hemisphere (UNSCEAR, 2000). Thus, whether the surface sediment of PS67/206-1 is younger than 60 years is unclear.

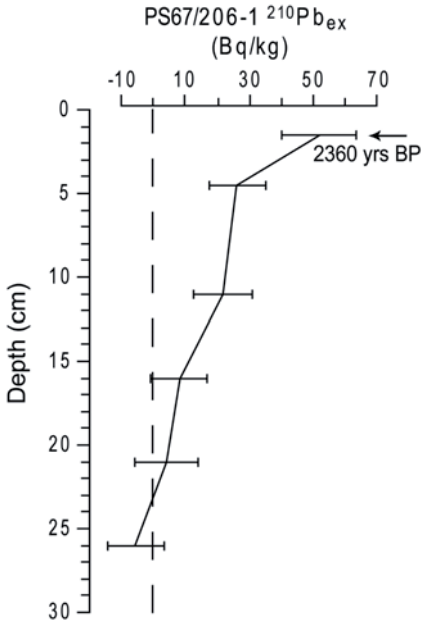

Fig. 2. Surface sediments ^{210}Pb excess of core PS67/206-1. Dashed line indicates the 0 excess of ^{210}Pb. Bars show the measurement errors. Arrow indicates surface ^{14}C age on humic fraction (Table 2).

4.3.2. AMS ^{14}C chronology

For AMS ^{14}C chronology, 16 bulk sediment samples were taken from piston core PS67/206-1 (KOL), and in addition the surface sediment of trigger core at the same site (Table 2). ^{14}C ages were obtained from both humic acid and residue fractions of organic matter for each sample (Table 2). The sample preparation and the AMS ^{14}C measurements were performed at the Poznan Radiocarbon Laboratory, Poland.

The residue ^{14}C ages are systematically older than humic ages (Fig. 3), the age differences are from 1000 to up to 4000 years, and age reversals occur, suggesting that the residue fraction is strongly affected by old stable carbon which may result from reworking of the sediment, as also highlighted by Heroy and Anderson (2007). To the contrary, the humic ages represent consistent increasing ages according to depth. In the Bouvet Island area of Southern Ocean Atlantic sector, the humic ages are comparable to the ages dated on foraminifera during the Holocene (Bianchi and Gersonde, 2004; ***Chapter 3***). Therefore, the ^{14}C chronology is based on the humic ages.

Table 2. AMS ^{14}C dating of core PS67/206-1 using a calibration program Calib 6.0.1 (Stuiver and Reimer, 1993; Reimer et al., 2009) by applying different General Reservoir (GR) values. C sources for dating are: H: humic acid fraction; R: residue fraction.

Core	Depth (cm)	Lab ID	C source	^{14}C age (yr BP)	GR=400 yr Calib. age (yr BP)	GR=1300 yr Calib. age (yr BP)	GR=2300 yr Calib. age (yr BP)
TC	6-9	Poz-31350	H	2435 ± 35	2074	1092	172
	6-9	Poz-31351	R	6660 ± 50	7194	6185	5015
KOL	0-5	Poz-31290	H	2360 ± 35	1982	1004	72
	0-5	Poz-31291	R	3445 ± 35	3326	2220	1102
	71-75	Poz-31292	H	3040 ± 35	2805	1732	689
	71-75	Poz-31293	R	7430 ± 110	7889	7036	5919
	157-160	Poz-31294	H	3370 ± 35	3245	2123	1014
	157-160	Poz-31296	R	4630 ± 40	4851	3654	2435
	365-368	Poz-31297	H	4180 ± 50	4266	3119	1892
	365-368	Poz-31298	R	6000 ± 40	6412	5469	4150
	651-654	Poz-31300	H	5080 ± 40	5440	4267	2979
	651-654	Poz-31301	R	6630 ± 50	7163	6146	4968
	862-865	Poz-31302	H	5710 ± 40	6125	5104	3757
	862-865	Poz-31303	R	7650 ± 60	8107	7282	6168
	1067-1070	Poz-31304	H	6230 ± 40	6679	5686	4463
	1067-1070	Poz-31305	R	7350 ± 50	7816	6942	5821
	1258-1261	Poz-31329	H	6850 ± 70	7365	6366	5289
	1258-1261	Poz-31330	R	8750 ± 50	9429	8319	7367
	1361-1364	Poz-31331	H	7190 ± 40	7652	6746	5646
	1361-1364	Poz-31524	R	9480 ± 70	10336	9231	8044
	1470-1473	Poz-31333	H	8195 ± 35	8692	7756	6752
	1470-1473	Poz-31335	R	10300 ± 70	11297	10254	9002
	1557-1560	Poz-31336	H	8470 ± 50	9091	8030	7088
	1557-1560	Poz-31337	R	10440 ± 60	11532	10399	9179
	1758-1761	Poz-31339	H	8920 ± 50	9578	8477	7511
	1758-1761	Poz-31340	R	10610 ± 70	11895	10571	9381
	1958-1961	Poz-31341	H	9320 ± 60	10166	9033	7882
	1958-1961	Poz-31342	R	10630 ± 60	11942	10588	9406
	2058-2061	Poz-31525	H	9860 ± 60	10761	9628	8424
	2058-2061	Poz-31344	R	11880 ± 70	13334	12478	10944
	2258-2261	Poz-31345	H	11420 ± 60	12891	11707	10376
	2258-2261	Poz-31346	R	13620 ± 80	16129	14329	13205
	2358-2362	Poz-31347	H	11990 ± 120	13443	12589	11051
	2358-2362	Poz-31349	R	15190 ± 90	17992	16962	15416

The surface ^{14}C age of core PS67/206-1 (2360 ± 35 yrs BP) reasonably agrees with the surface age of the trigger core at the same site (2435 ± 35 yrs BP, Table 2) and another core close by (PS67/219-1 TC, 2660 ± 35 yrs BP, ***Chapter 5***). The $^{210}Pb_{ex}$ activities show that the surface sediments of PS67/206-1 are modern deposition not older than 100 years. However, previous studies show that ^{14}C in the Weddell Sea and Scotia Sea (Weiss et al., 1979; Stuiver and Östlund, 1980; Schlosser et al., 1989) at different water depth or in various life forms (Gordon and Harkness, 1992; Berkman and Forman, 1996) point to a maximum correction of 1300 ± 100 year for the reservoir effect in modern conditions. This means, despite the old ^{14}C age of modern sediment, fossil carbon may also exist in the humic fraction. The different fossil carbon contamination in the humic fraction in the Scotia Sea sediments from those in Bouvet Island area may due to the core location, where re-suspension of sediment occurs and more terrigeneous input from the adjacent land in the Scotia Sea. In that case, the core top correction for ^{14}C includes the reservoir effect and fossil carbon contamination and referred as General Reservoir (GR).

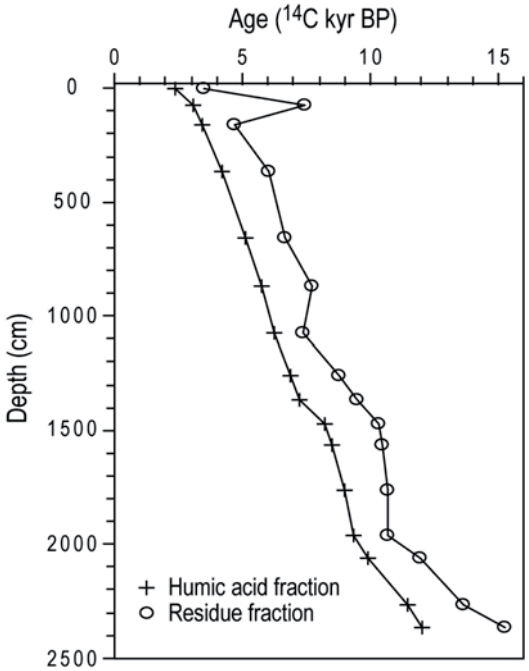

Fig. 3. AMS ^{14}C dating of core PS67/206-1.

In the Southern Ocean, very complex carbon reservoir effects are reported caused by low exchange of CO_2 between atmosphere and ocean induced by sea ice cover and stratified water column, and vary in different sea ice and ocean circulation conditions through time (e.g. Sikes et al., 2000; van Beek et al., 2002). At the Antarctic Peninsula region and adjacent area, a reservoir age of 1200-1300 years was applied in previous studies, and the extracted core top age was applied down core for the ^{14}C correction (e.g. Berkman and Forman 1996; Domack et al., 2001; Heroy and Anderson, 2005; Hillenbrand et al., 2009; Pugh et al., 2009). We notice that a core top humic ^{14}C age of 2350 ± 40 yr BP is also reported in a high resolution Holocene record from Adélie Land, East Antarctica, and a reservoir age of 1300 was applied, explained as core top sediment loss during the coring process (e.g. Crosta et al., 2005; Denis et al., 2009). Similarly, a core top age of 2260 ± 55 yr BP obtained by dating on organic carbon from the Palmer Deep also attributed to core top sediment loss (Leventer et al., 1996); some other core top ages from the same region however show 1200-1300 yr BP (Domack et al., 2001). This implies the complexity of correction for dating on organic carbon from coastal regions around Antarctica. Detailed dating (e.g. $^{210}Pb_{ex}$) is needed to quantify the real core top correction which contains both carbon reservoir effect and fossil carbon contamination.

The ^{14}C ages were calculated to calendar ages (Table 2) using a calibration program Calib 6.0.1 (Stuiver and Reimer, 1993; Reimer et al., 2009). However, the changes in GR through time are not well quantified, large uncertainties still remain. In order to verify the possible GR change, a series of GR values (400 yrs, 1300 yrs and 2300 yrs) were applied.

4.3.3. Geomagnetic paleointensity chronology

Independent from radiocarbon dating, the geomagnetic paleointensity provides a unique time series which can be correlated interhemisphericly between marine, land and ice archives (e.g. Channell

et al., 2000; Stoner et al., 2002; Lund et al., 2006; Raisbeck et al., 2007). In the Antarctic Peninsula region, a recently derived high resolution RPI record (Willmott et al., 2006) has been tuned to St. Lawrence Estuary RPI record, which was AMS ^{14}C dated and can be well correlated to the GISP2 ^{10}Be record with an maximum age uncertainty of 200 yrs (St-Onge et al., 2003). This RPI record enables us a detailed correlation for the past 9 kyrs. In addition, our RPI record was also correlated to the global reference curve of virtual axial dipole moment (VADM) covering the past 50 kyrs, which was established by a compiled GEOMAGIA50 geomagnetic paleointensity data set (Knudsen et al., 2008). The correlation indicates that core PS67/206-1 extends back to ca. 12.5 ka (Fig. 4).

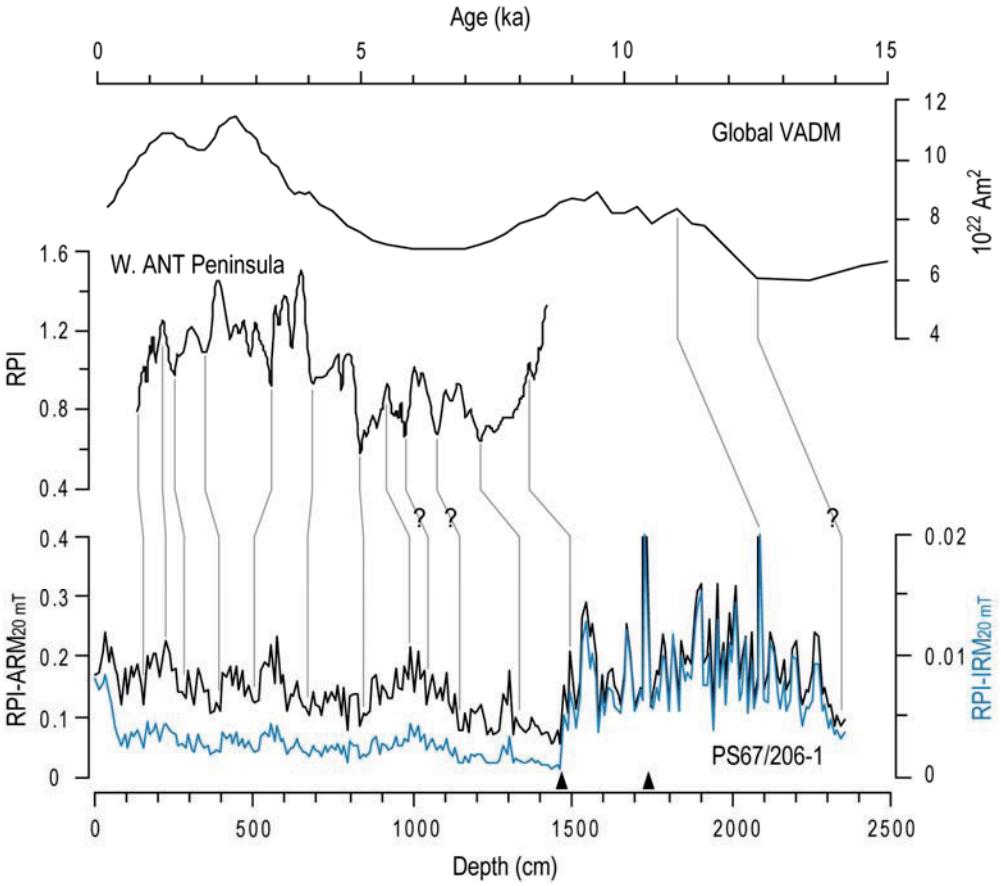

Fig. 4. Correlation between relative paleointensity record of PS67/206-1 and the reference curves from Western Antarctic Peninsula (Willmott et al., 2006) and global VADM (Knudsen et al., 2008). Two ash layers are marked by solid triangles. The blue curve represents the RPI-IRM$_{20\ mT}$ record.

4.3.4. Stratigraphy by SSST correlating to EDML $\delta^{18}O$ record

Although with the estimation error of 0.5 ˚C, the high temporal SSST variability of core PS67/206-1 may document the similar climate signal to the Antarctic ice core records. With the constrain of RPI age model, an additional age model was made by correlation of diatom based SSST to EDML ice core $\delta^{18}O$ record (Epica members, 2006) (Fig. 5) in order to refine the RPI age model.

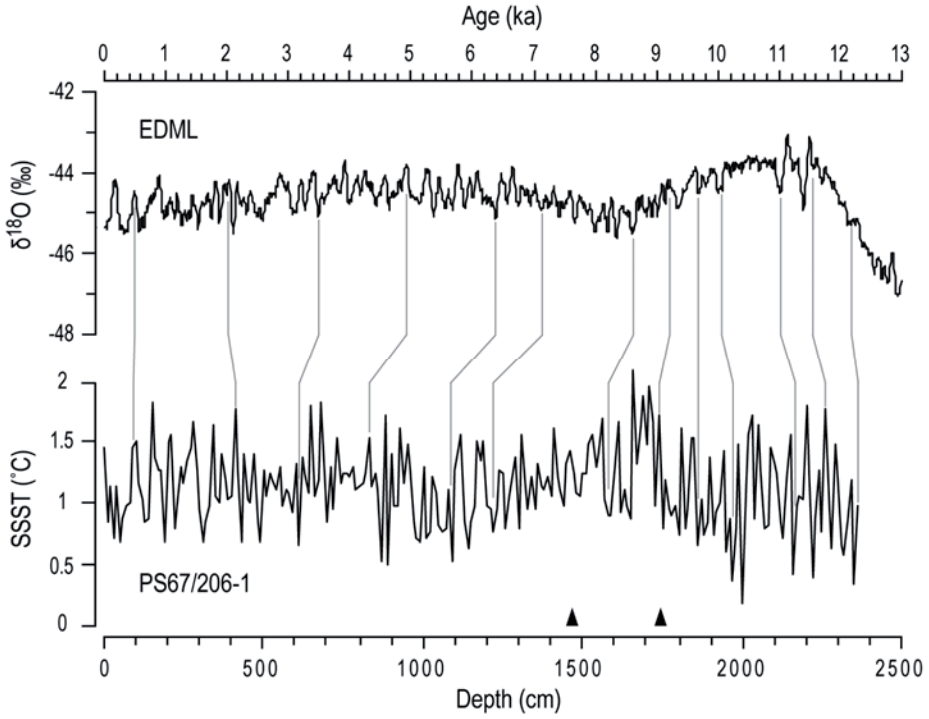

Fig. 5. Diatom based SSST record of core PS67/206-1 correlates to EDML $\delta^{18}O$ record (Epica members, 2006). Solid triangles mark the ash layer intervals.

4.3.5. Core stratigraphy

The ^{14}C chronology can be strongly affected by changes in reservoir effect and fossil carbon contamination (GR), which is not quantified in this area. The RPI and SSST-EDML age models clearly point out that the GR changes throughout the Holocene. Considering that the SSSTs present more detailed variability that can be correlated to EDML, we apply the SSST-EDML age model as the core age model, the core top age regards to 0 as dated by $^{210}Pb_{ex}$. Age error between the SSST-EDML and the RPI age models is mainly below 200 yrs, larger errors of ca. 600 yrs may occur at ca. 2.7 ka according to the SSST-EDML age model and 300-400 yrs at the lower part of the core (Fig. 6).

According to the SSST-EDML age model, relatively low sedimentation rate of ca. 160 cm/kyr is presented at 11-12 ka; it is elevated between 7 and 11 ka of more than 200 cm/kyr, with maximum centered at 9 and 10 ka over 250 cm/kyr. The sedimentation rate drops at 7 ka and maintains between 140 to 170 cm/kyr till 2 ka; afterwards, it rises during the last 2 millennia up to ca. 200 cm/kyr. The core top sedimentation rates reasonably agree with the $^{210}Pb_{ex}$ chronology. Based on the age model, the megascopic ash layer was dated at 8.1 ka and the second ash layer at 9.2 ka.

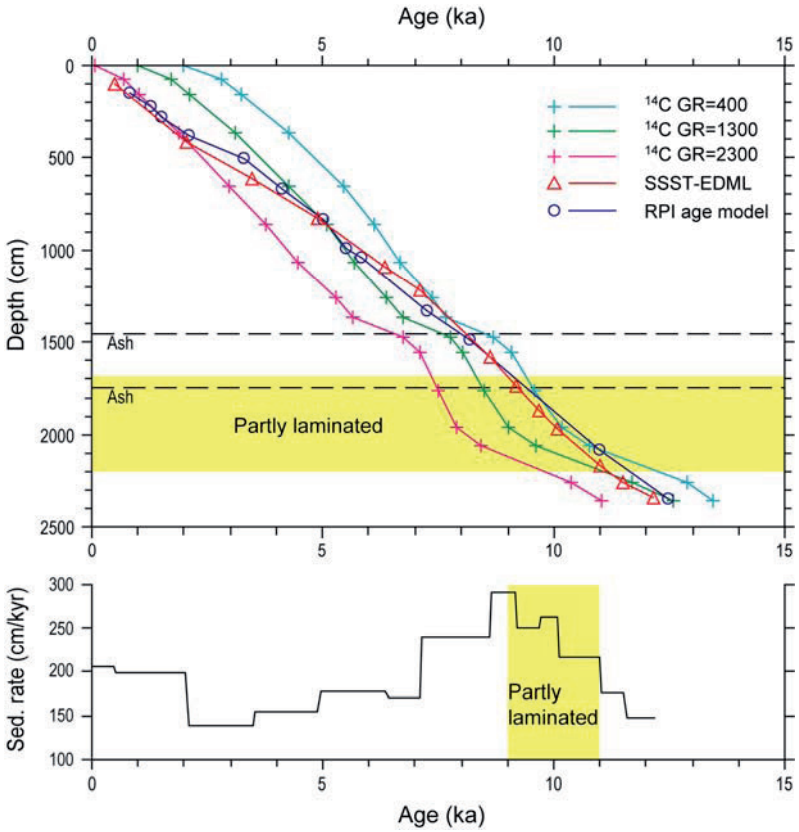

Fig. 6. Age model comparison of core PS67/206-1. GR ages of 400, 1300 and 2300 yrs were applied in calibration of humic ^{14}C ages to calendar ages (Table 2). The sedimentation rates were calculated based on the SSST-EDML age model.

4.4. Results

4.4.1. Diatom assemblages, summer sea surface temperature and sea ice extension

At the southernmost site PS2319-1 (Fig. 7), *Chaetoceros* resting spores (RS) dominate the diatom assemblage by more than 80% at the early Holocene, as well as relatively high occurrence of *Rhizosolenia antennata f. semispina*; other species persist at low levels. The *Chaetoceros* RS drop to 50-70% at mid-Holocene accompanied by the increases of other species.

At the central Scotia Sea site PS67/206-1 (Fig. 7), the diatom assemblage of early Holocene between 12 and 10 ka is characterized by more than 50% of *Chaetoceros* RS as well as ca. 10% *R. antennata f. semispina*; *Eucampia antarctica* is at low values between 0 and 3%; open ocean species *Fragilariopsis kerguelensis* range between 10 and 20%. After 10 ka, *Chaetoceros* RS drop distinctly and accounts for 10 to 25% at 9 ka and rise to a temporal peak at ca. 40% at around 8 ka, after that, this species remain stable during the mid-late Holocene averaging at ca. 25%. Another *R. antennata f. semispina* elevation occurs at ca. 9 ka peaking at 30 %, then this species drops to below 10% during

Fig. 7. Diatom composition and estimated SSSTs of studied cores. Arrows in core PS67/206-1 indicate the intervals with AMS ^{14}C dating. Solid triangles mark the ash layers in the studied cores. Diatom species features are labeled for regional correlation.

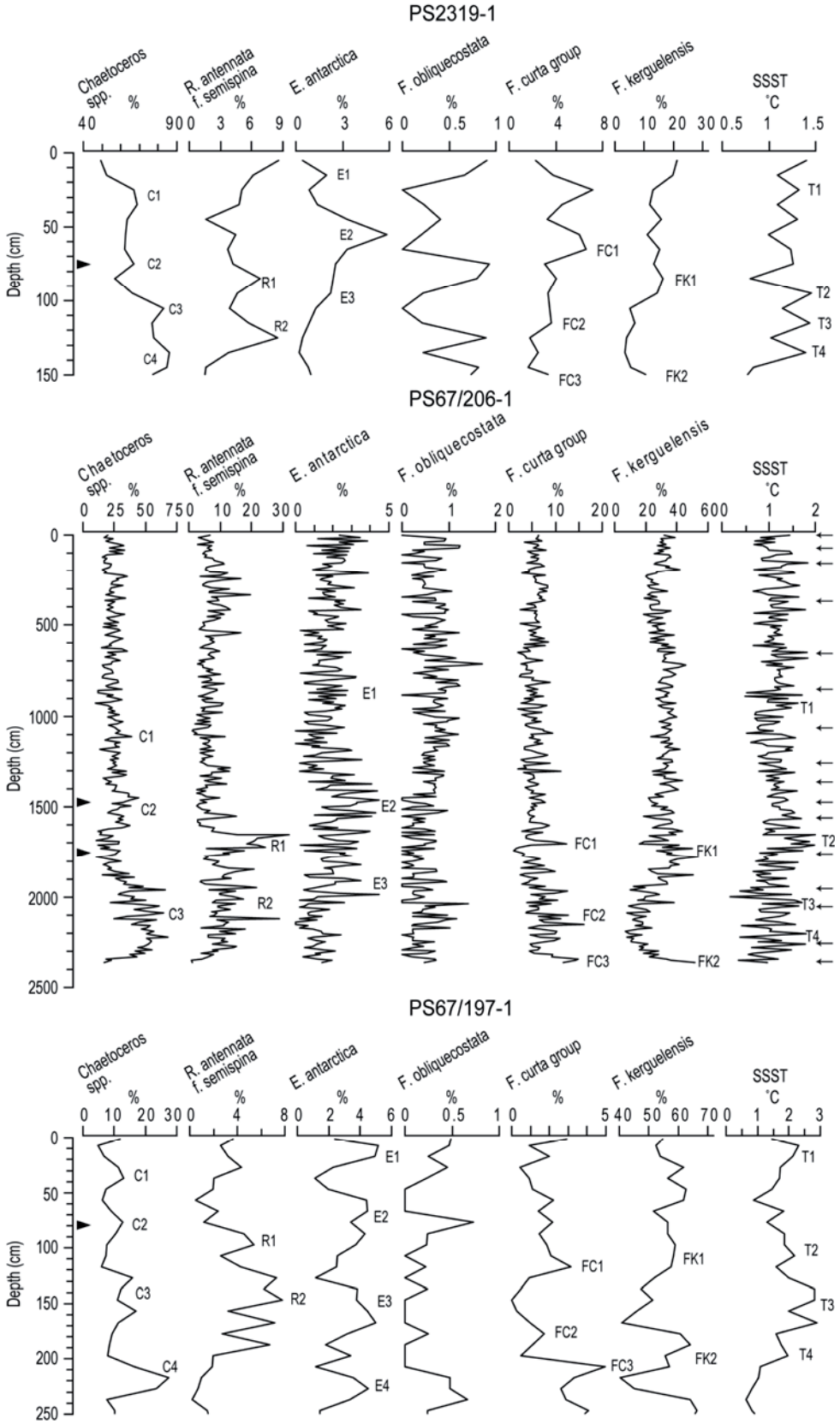
PS2319-1
Chaetoceros spp. %
R. antennata f. semispina %
E. antarctica %
F. obliquecostata %
F. curta group %
F. kerguelensis %
SSST °C
Depth (cm)
C1
C2
C3
C4
R1
R2
E1
E2
E3
FC1
FC2
FC3
FK1
FK2
T1
T2
T3
T4
PS67/206-1
PS67/197-1

the mid-Holocene. The mid-late Holocene *E. antarctica* fluctuates between 0 and 5% at the core site. *F. kerguelensis* peaks at around 9 ka and fluctuates between 20 and 40%.

Lower than in the southern cores, *Chaetoceros* RS fluctuate between 5 and 17%, and peak at 15-17% during the early Holocene at the northern site PS67/197-1 (Fig. 7). *R. antennata f. semispina* peaks at the early Holocene up to 8% and drops to less than 4% during mid-late Holocene. Cold water species represent lowest amount at the early Holocene and take larger composition during the mid-Holocene.

The Holocene SSSTs vary between 1 and 1.5˚C at the southern site, remaining rather constant averaging at ca. 1.2˚C. At the central site the SSSTs also remain stable, fluctuating between 0 and 2˚C with a temporal maximum of ca. 2˚C at 9 ka. At a few points the central site show lower SSSTs than the southern site, where selective dissolution may play a role that the lightly silicified cold species may have dissolved due to the low sedimentation rate at the southern site, also supported by higher winter sea ice species *F. curta* group at the central site (Fig. 7; Fig. 9b). At the northern site, the SSSTs are marked by a strong warming up to 3˚C between 10 and 11 ka, and followed by a cooling trend towards 7 ka of ca. 1˚C, the SSST rose again after 7 ka.

Less than 3% of *F. obliquecostata* throughout the Holocene in all 3 cores indicates the summer sea ice never reached studied area during the Holocene. In contrast, winter sea ice (>3% of *F. curta* group) persisted in the central Scotia Sea and only occurred prior to 12 ka at the northern site (Fig. 7; Fig. 9b). The early Holocene winter sea ice signal is suppressed at the southern site due to the dominance of *Chaetoceros* RS in the diatom assemblage.

4.4.2. Spectral analysis

In order to avoid mis-transfer the frequency signal between sections with different resolution, the spectral analysis was performed on split section of 0-7 ka and 7-12 ka according to the estimated sedimentation rates of core PS67/206-1 (Fig. 8). For 0-7 ka interval, Redfit analysis identifies cyclicities above 90% confidence level of 320, 210, 185 and 135 yr in SSSTs; 360, 290 and 160 yr in *Chaetoceros* RS; 390 and 190 yr in *F. curta* group. For 7-12 ka interval, cyclicities of 175 yr is estimated in SSSTs; 205, 130 and 95 yr are recognized in *Chaetoceros* RS; 210, 155 and 115 yr in *F. curta* group.

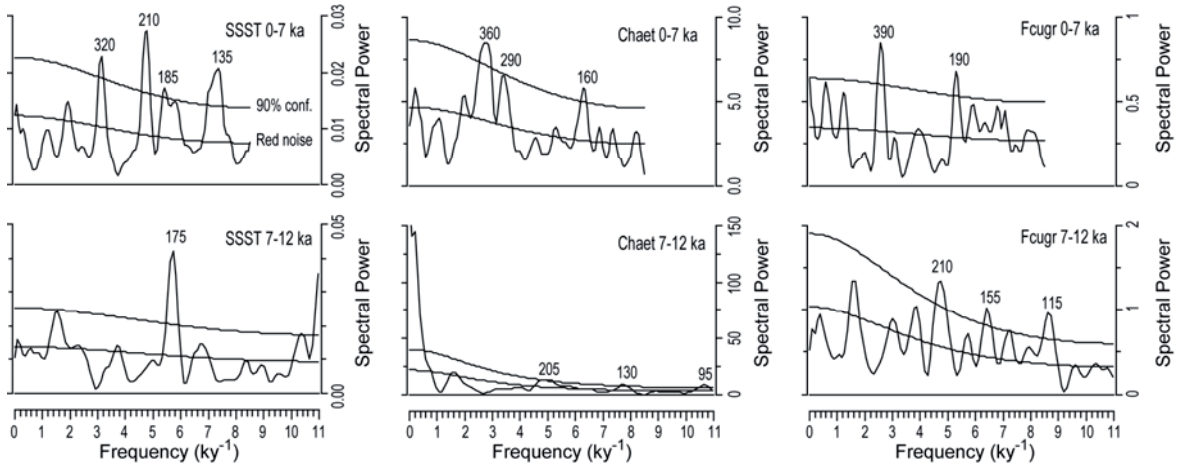

Fig. 8. Spectral analysis of core PS67/206-1, performed on SSST, *Chaetoceros* RS and F. curta group on split time intervals. Numbers indicate the significant cyclicities (yrs) above 90% confidence lines.

4.5. Discussion

4.5.1. Holocene climate variability in the Scotia Sea

The early Holocene optimum marks between 9 and 11.5 ka in various Antarctic ice cores (Masson et al., 2000), and at ca. 10-11 ka in the northern Scotia Sea (PS67/197-1) as well as in the southern cores from the South Atlantic open ocean (Bianchi and Gersonde, 2004; ***Chapter 3***) (Fig. 9a). However, our records show that in the central Scotia Sea (PS67/206-1), the optimum occurred later, at ca. 9 ka; further in the south (PS2319-1), no clear sign of an optimum existed. The more persistent cold conditions in the early Holocene central and southern Scotia Sea is also indicated by sea ice conditions (Fig. 9b). In the context of lowest sea ice concentration in the early Holocene open ocean South Atlantic (Bianchi and Gersonde, 2004; ***Chapter 3***), winter sea ice continuously extended to the central Scotia Sea (PS67/206-1) (Fig. 9b). The early Holocene higher than mid-late Holocene occurrence of *F. curta* group may be attributed to the good preservation where lamination occurred. The low relative abundance of *F. curta* group in the southern site (PS2319-1) is biased by the dominant species *Chaetoceros* RS, which make up to 80% of the diatom assemblage. Different from those of open ocean South Atlantic, this north-south pattern in the Scotia Sea suggests that cold water from the south persisted in the central and southern Scotia Sea during the early Holocene.

Relatively cold early Holocene was previously observed in the Palmer Deep in the Antarctic Peninsula region, characterized by increased primary productivity and ice rafting at ca. 11.5-9.07 cal. kyr BP (Domack et al., 2001; Domack, 2002). The recently derived TEX_{86} SST from the same core indicates an early Holocene optimum (up to 6-10 ˚C, Shevenell et al., 2011), interpreted as the spring intermittent meltwater-induced stratification in the regional fjords, and the big amplitude early Holocene warming responded to the high early Holocene insolation. However, the warm early Holocene in the Palmer Deep is not supported by any strong increase of warm water diatom species (Taylor and Sjunneskog, 2002). The SST calibration in this region may be complicated by the covariation of the TEX_{86} and *Chaetoceros* RS, which reflects spring bioproductivity.

Although the early Holocene optimum is characterized both in Antarctic ice cores and open Southern Ocean Atlantic sector (e.g. Masson et al., 2000; Bianchi and Gersonde, 2004; ***Chapter 3***), the Antarctic ice sheets were still undergoing deglaciation (Hall, 2009). In the Antarctic Peninsula, Bentley et al. (2005a) proposed that Marguerite Bay was deglaciated at least by ca. 9 ^{14}C ka (ca. 10 cal. kyr BP), by extrapolation of ^{14}C dates; another study showed that George VI Ice Shelf was absent beginning at ca. 9.6 cal. kyr BP (Bentley et al., 2005b). Domack et al. (2005) suggested Larsen Ice Shelf-A and B deglaciated between 11 and 10 ka. Heroy and Anderson (2007) suggested that the retreat of the Antarctic Peninsula Ice Sheet started on the outer shelf before ca. 18 to 9 cal. kyr BP and continued to retreat from the inner shelf by ca. 13 to 7 cal. kyr BP, generally in two steps at ca. 14 and 11 cal. kyr BP and they are suggested to have contributed to the global sea level rises at the melt water pulses (MWP 1a and 1b). The timing of the deglaciation was constrained by AMS ^{14}C dating in various cores. Although the glacial retreat in individual cores may vary by up to 1100 years, and the dating is affected by uncertainty of the ^{14}C correction before calibration (Heroy and Anderson, 2007), their data clearly suggest the undergoing melting process during the early Holocene. By exporting meltwater to the open ocean, the melting of APIS could also induce regional cool conditions in the adjacent area (Bentley et al., 2009), e.g. the central and southern Scotia Sea, where the Southern Ocean early Holocene optimum was suppressed along with the persistent occurrence of winter sea ice.

(a)

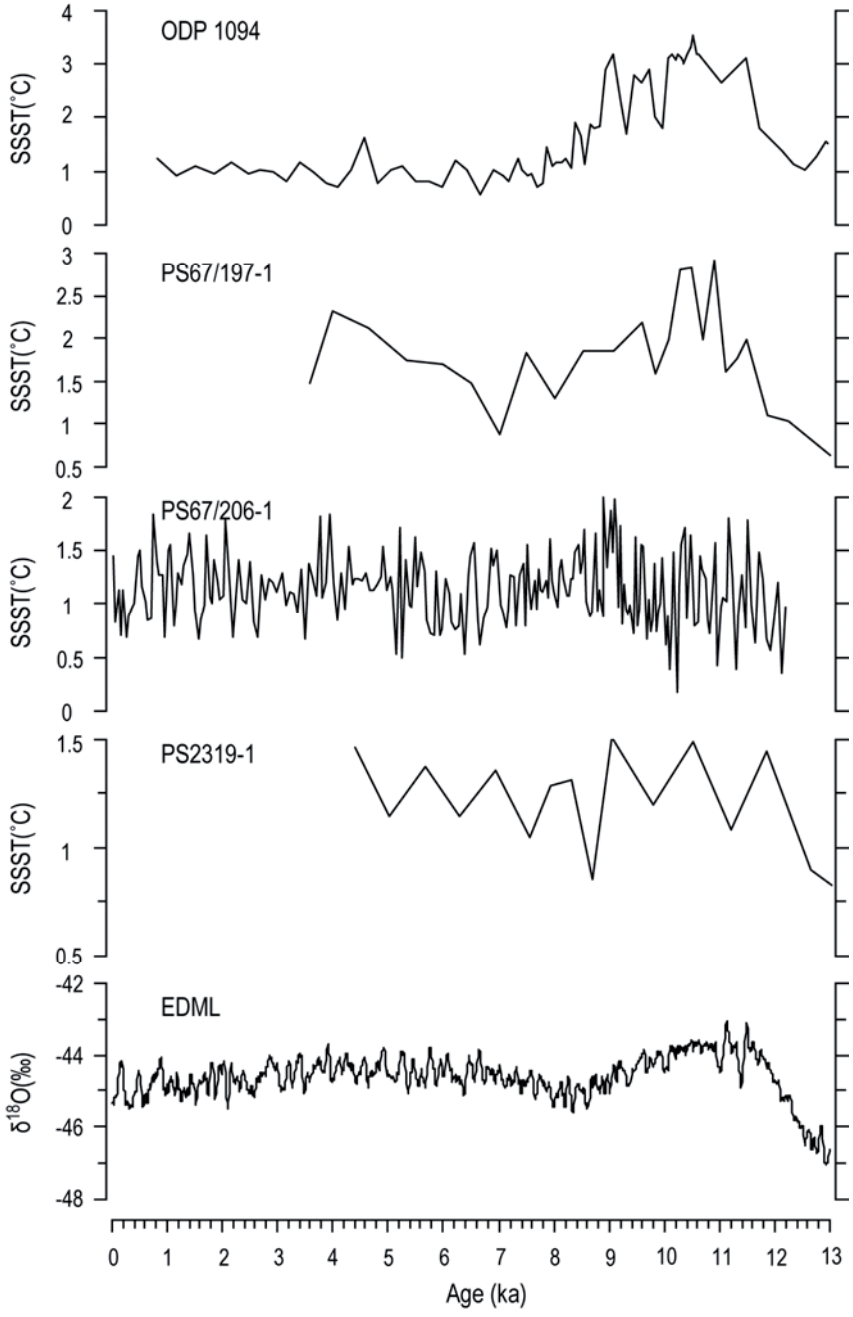
ODP 1094
SSST(°C)
PS67/197-1
SSST(°C)
PS67/206-1
SSST(°C)
PS2319-1
SSST(°C)
EDML
δ18O(‰)
Age (ka)

(b)

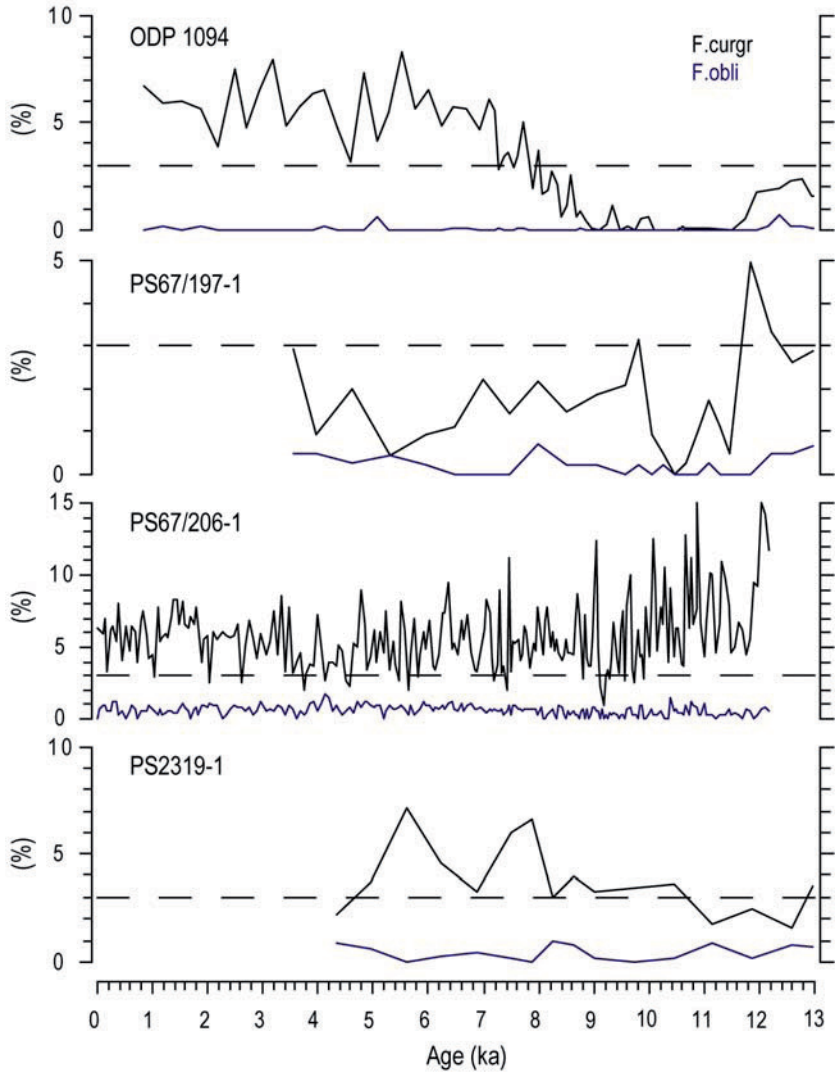

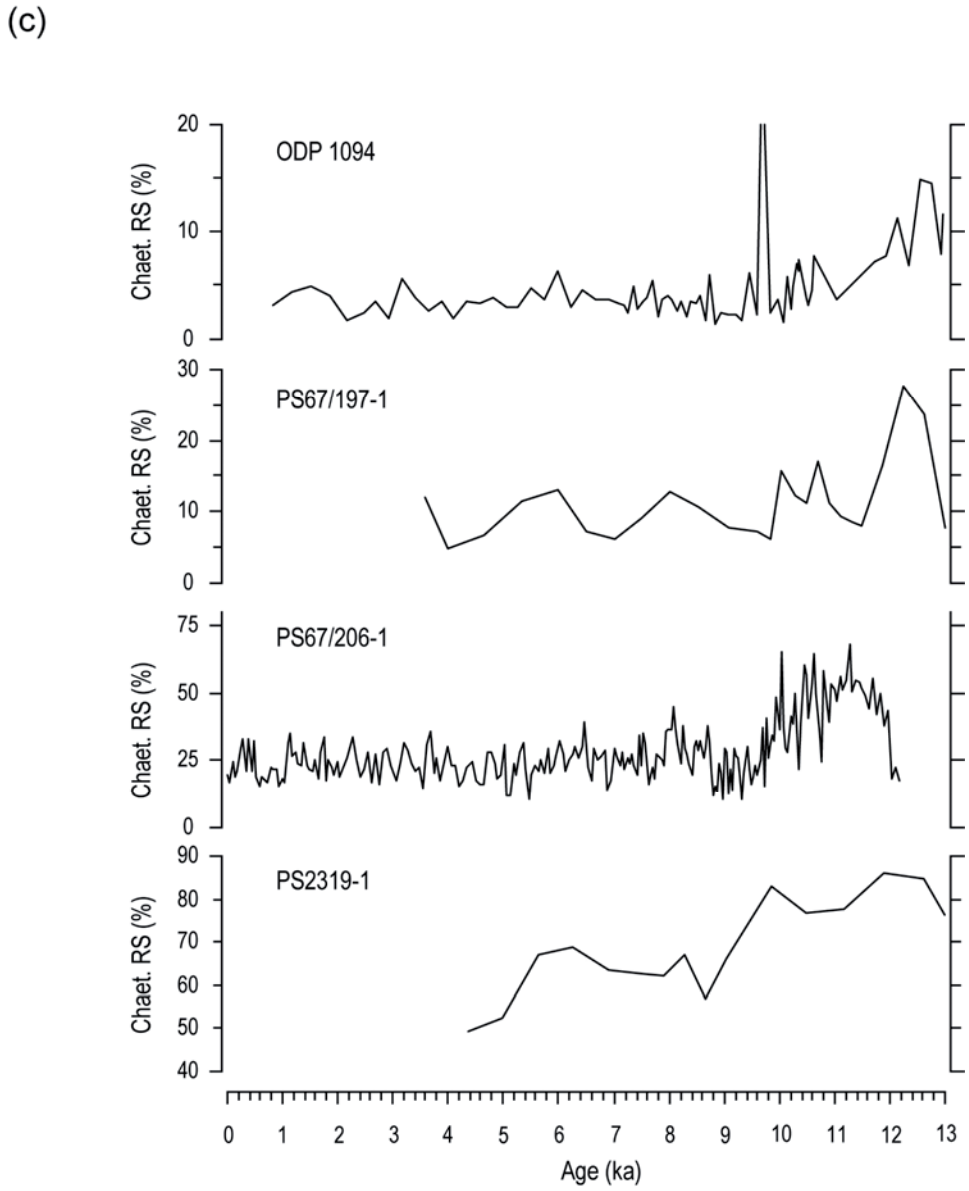

Fig. 9. Holocene Scotia Sea climate records compared to open ocean South Atlantic and Antarctic ice core. (a) SSSTs; (b) relative abundances of summer (*F. obliquecostata*) and winter (*F. curta* group) sea ice indicators, dashed lines (3%) indicate the presence of sea ice; (c) relative abundance of *Chaetoceros* spp. Data of ODP 1094 from Bianchi and Gersonde (2004) and Xiao et al. (***Chapter 3***); EDML from Epica community members (2006).

4.5.2. Nutrient supply of the Holocene Scotia Sea

Compared to the cores from open ocean South Atlantic (Bianchi and Gersonde, 2004; ***Chapter 3***), another significant feature of the Holocene Scotia Sea is the high occurrence of *Chaetoceros* RS, as well as *R. antennata f. semispina* (Fig. 7; Fig. 9c). The *Chaetoceros* RS dominates the diatom assemblage in the early Holocene biogenic laminae. Such feature is also observed in other Southern Ocean marine coastal records, e.g. Palmer Deep in the Antarctic Peninsula region (Leventer et al., 2002), Mac. Robertson Shelf (Stickley et al., 2005), Mertz Ninnis Trough (Maddison et al., 2006) and

Adélie Land (Denis et al., 2006; Crosta et al., 2008), East Antarctica. Similarly, a slight increase of *Chaetoceros* RS is also observed in the open ocean South Atlantic (Fig. 9c).

Chaetoceros RS often dominate the diatom assemblages in the Antarctic coastal sediments (Stockwell, 1991; Crosta et al., 1997; Zielinski and Gersonde, 1997), the Antarctic Peninsula region documents the highest occurrence of *Chaetoceros* RS and related to high primary productivity. Sediment trap investigations suggest that *Chaetoceros* RS blooms are associated with the melting sea ice in austral spring (Leventer, 1991). The spring Antarctic coastal regions are characterized by high nutrient and stratified surface water, and thus the high occurrence of *Chaetoceros* RS has also been proposed as an indicator of stratified water column, and therefore the amount of meltwater (Crosta et al., 1997; 2008). Our Scotia Sea records generally agree with such scenario, with higher abundance of *Chaetoceros* RS in the south with higher sea ice concentration, and the *Chaetoceros* RS covaries with the winter sea ice species most of the time (Fig. 7; Fig. 9).

The sea-ice melting induced stratified surface water provides a favorable environment of water column stability for the formation of *Chaetoceros* RS, but it is not the controlling factor. More importantly, the blooming of *Chaetoceros* is highly related to nutrient availability and represents high primary productivity (Stockwell, 1991; Abelmann et al., 2006). Smetacek (1985) suggested that the formation of *Chaetoceros* RS was associated with nutrient depletion in the water column after the bloom of vegetative cells. In contrast, Alldredge et al. (1995) reported that the *Chaetoceros* RS form in the aggregates prior to nutrient depletion, the deposition results from self-sedimentation (Grimm et al., 1997). They are better preserved in the sediment than the vegetative cells because of their thick wall and more resistance from dissolution and grazing. High occurrence of *Chaetoceros* in the southern Argentine Basin was interpreted as imported from the shallow Falkland Plateau which is away from the sea ice influence (Zielinski and Gersonde, 1997). Similarly, high numbers of *Chaetoceros* RS in the Falkland Through also have been attributed to the Falkland Plateau source transported by the overflow of North Atlantic Deep Water (Allen et al., 2005). *Chaetoceros* RS also dominate the laminated sediments from Santa Barbara Basin, they are formed by self-sedimentation and related to high nutrient supply by upwelling (Grimm et al., 1996; 1997). These studies indicate that the *Chaetoceros* RS represent high productivity in response to nutrient availability rather than surface water stratification by ice melting.

Studies from the Gulf of California and Eastern Mediterranean (Kemp et al., 2000) suggest that *Rizosolenia spp.* live beneath a strong seasonal thermocline as they are able to migrate downwards to take advantage of higher nutrient at depth and migrate upwards to better light conditions for photosynthesis. Investigations of Southern Ocean surface sediments (Zielinski and Gersonde, 1997; Armand and Zielinski, 2001) show relatively high abundant *R. antennata f. semispina* between the winter sea ice and the Polar Front. The *Rhizosolenia spp.* sublaminae was reported occurring at the beginning of summer (Stickley et al., 2005; Denis et al., 2006), and implying nutrient limitation of a surface pycnocline. The settlement of these species records the breakdown of the pycnocline with the deepening of the surface mixed layer, and the upwelled nutrients sustain the bloom of such species.

For diatom growth and reproduction, nutrients such as silicic acid, nitrate and phosphate are required; micro nutrient iron stimulates diatom production (de Baar et al., 1995) and modulate the nutrient uptake ratios and carbon sequestration (Blain et al., 2007; Mosseri et al., 2008). One source of the nutrients is that, the accumulated dust on the sea ice and iceberg unload to the water during ice melting; another source is the upwelled UCDW enriched in dissolved nutrient including iron (Sambrotto et al., 2003; Stickley et al., 2005; Blain et al., 2007), and it has been suggested that the

dissolved iron supply from the upwelling water is more important than that released from the sea ice (Watson et al., 2000).

For the Holocene period, low dust concentrations are recorded in the Antarctic ice cores (Delmonte et al., 2002; Fischer et al., 2007), especially the early Holocene at the climate optimum. Although large part of the airborne iron is readily soluble (Edwards and Sedwick, 2001), the dust records suggest that the sea ice melting released nutrients to the water column might be limited. On the other hand, the terrigeneous input by the icesheet melting and glacial runoff also did not contribute much to the spring diatom bloom at the core location, because the ice sheet melting mainly occurs in summer, as reported that the terrigeneous laminae were deposited during summer (Leventer et al., 2002; Stickley et al., 2005; Denis et al., 2006; Maddison et al., 2006). Thus, the upwelled UCDW became the more important nutrient source during the early Holocene. Prézelin et al. (2000) reported that the intrusion of upwelled UCDW to the Antarctic Peninsula shelf area provides a reservoir of nutrient rich, warmer water that stimulates the bloom of diatom, and in the absence of the upwelled water, the nutrients are not sufficient for diatoms to achieve high abundance or community dominance. Also suggested by other authors (Edward and Sedwick, 2001; Sambrotto et al., 2003; Blain et al., 2007) that the upwelled iron, as well as other major nutrients sustain the surface phytoplankton production rather than the sea ice released nutrients. Maddison et al. (2006) further indicated that, the nutrients supplied during the winter upwelling are trapped in the sea-ice induced stratified surface water, and allow the spring bloom of *Chaetoceros* RS.

Similarly, the enhanced early Holocene upwelling in the summer also favored the bloom and deposition of *Rhizosolenia spp.* A strong peak of *R. antennata f. semispina* occurred at ca. 9ka in all the Scotia Sea cores when the abundances of *Chaetoceros* RS are relatively low. This is also a time of climate optimum in the central Scotia Sea, with lowest sea ice concentration. This implies a relatively short duration of sea ice melting and *Chaetoceros* bloom season in spring, and strong upwelling in the following summer that induced the mass production of *Rhizosolenia spp*.

Early Holocene is characterized by the rapid resumption of NADW formation after the sharp decline during the Younger Dryas (McManus et al., 2004). And the production of Antarctic Bottom Water (AABW) was at low stand due to the intensively reduced sea ice formation and unformed cavity under the shelf ice, where the modern AABW is formed (Hall, 2009; Nicholls et al., 2009; ***Chapter 3***). In such conditions, NADW would have further propagated to the high latitude Southern Ocean and merged into the ACC. This overflow of relatively warm NADW would also induce stronger upwelling in the high latitude Southern Ocean.

In summary, during the early Holocene, the upwelling zone poleward shifted accompanied by the Westerlies (Anderson et al., 2009). With relatively little contribution from the sea ice released dust to the water column, the enhanced upwelling at the high latitudes ocean brought nutrient from depth that fertilized the surface ocean and enhanced the diatom productivity. Such scenario is different from the glacial times when sea ice plays a more important role transporting iron and enhancing the bioavailability (Abelmann et al., 2006).

4.5.3. Changes in General Reservoir in the Holocene Scotia Sea

Changes in GR in the Scotia Sea through the Holocene can be clearly identified by comparing the RPI and SSST-EDML age models with the AMS ^{14}C chronology of core PS67/206-1 (Fig. 6). Accroding to the SSST-EDML age model, the GR decreased from 1600 to 540 yrs between 12 and 10

ka, then rose slightly to 940 yrs till 8 ka, after another drop to ca. 400 yrs at 7.6 ka, the GR steadily rose up to more than 2000 yrs till the late Holocene (Fig. 10). In general, low GR is presented at the early Holocene between 11 and 7 ka.

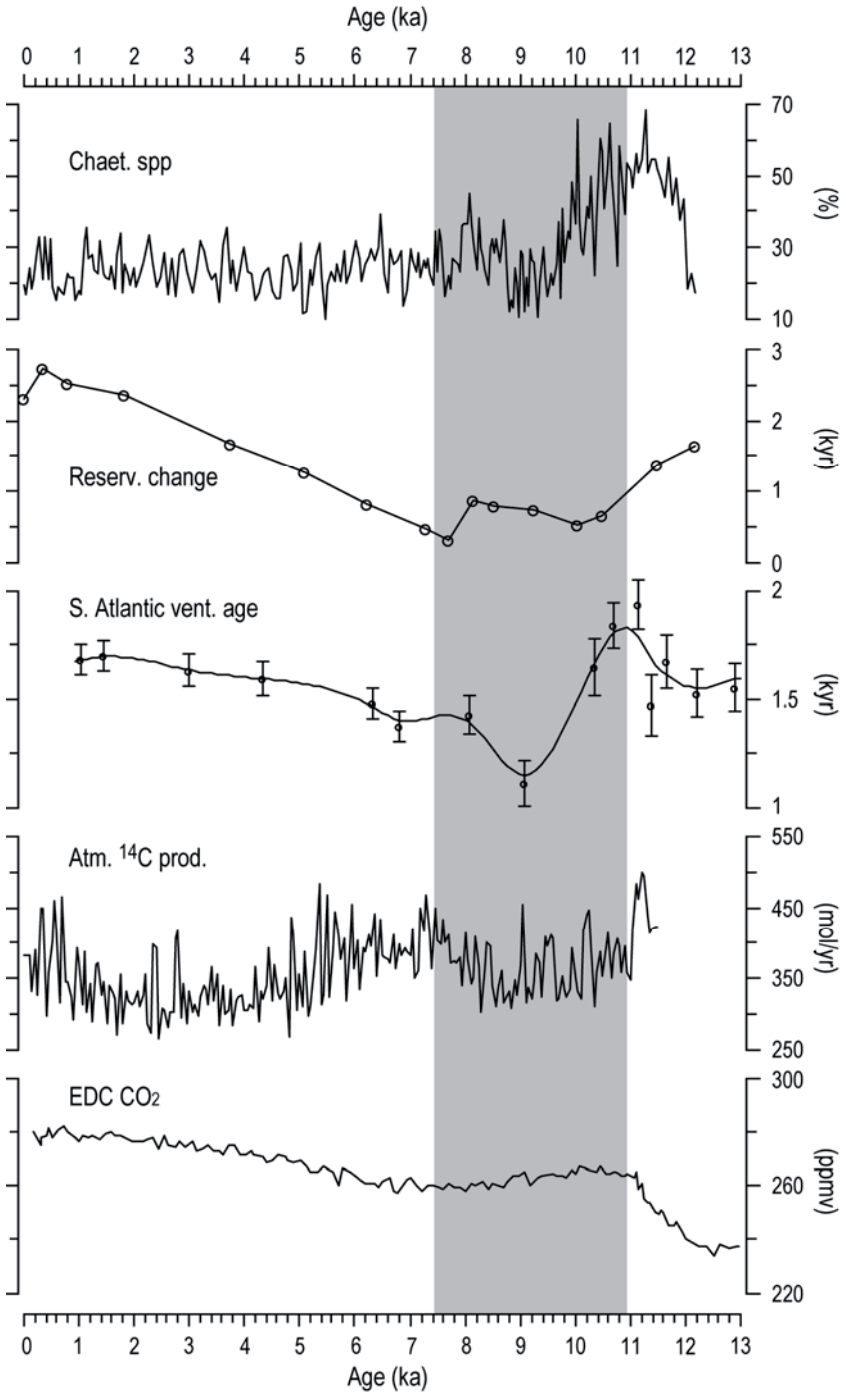

Fig. 10. Changes in General Reservoir (GR) of core PS67/206-1. Shaded area indicates relatively low GR at the early Holocene. Shaded area indicates the early Holocene low reservoir. Data of South Atlantic ventilation ages are from Skinner et al., 2010; atmospheric ^{14}C production from Marchal, 2005; EDC CO_2 concentration from Monnin et al., 2001.

The marine reservoir effect is the offset between the ^{14}C activity in the atmosphere and oceanic carbon reservoir, thus in turn is related to the atmospheric ^{14}C production and the ocean circulation conditions (e.g. Hughen et al., 2004a; Franke et al., 2008). At times of high atmospheric ^{14}C production, the $\Delta^{14}C_{atm}$ increase leads to a larger atmosphere-ocean ^{14}C difference because of the slow response of the ocean, and subsequently an increase in reservoir age, and vice versa. Hughen et al. (2004b) estimated the Holocene reservoir correction according to the atmospheric ^{14}C production for the ^{14}C calibration. On the other hand, ocean circulation affects the reservoir in different ways. For example, deep water production will transport more ^{14}C into the deep ocean and reduce the $\Delta^{14}C_{atm}$, and the other way around (Delaygue et al., 2003; Muscheler et al., 2004); the stratified surface water reduces the gas exchange between the atmosphere and the ocean, resulting in accumulated ^{14}C in the atmosphere and more depleted ^{14}C in the isolated deep ocean. This is especially the case in areas with sea ice cover such as the Southern Ocean.

The low GR between 11 and 7 ka in our record generally corresponds to the low atmospheric ^{14}C production at that time (Marchal, 2005; Hughen, 2006). This suggests a direct impact of ^{14}C production on the reservoir changes in the Southern Ocean. However, the ^{14}C production did not work alone. At the time of postglacial warming, atmospheric CO_2 rose in two steps at times of Heinrich Event 1 and Younger Dryas (Monnin et al., 2001), when the North Atlantic Deep Water formation was sharply declined (McManus et al., 2004) and subsequent warming in the Southern Ocean (Bianchi and Gersonde, 2004; ***Chapter 3***). Along with the abrupt warming, ^{14}C depleted CO_2 from the deep Southern Ocean was released to the atmosphere by wind driven upwelling and in consequence increased the ocean-atmosphere gas exchange, lowered the $\Delta^{14}C_{atm}$ and improved the deep water ventilation (Toggweiler et al., 2006; Broecker and Barker, 2007; Anderson and Carr, 2010; Skinner et al., 2010). The two steps of $\Delta^{14}C_{atm}$ drop during the last deglaciation coincide with the rapid jumps in CO_2 rather than the changes in ^{14}C production (Skinner et al., 2010). After the pre-Holocene abrupt release of CO_2, the atmospheric CO_2 level maintained stable in the early Holocene (Monnin et al., 2001). Better ventilation conditions persisted with the warm climate, strongest reduction of sea ice, poleward shifted Westerlies and associated upwelling (Skinner et al., 2010; ***Chapter 3***). Thus, the lowered $\Delta^{14}C_{atm}$ intensively contributed to the low reservoir age of the early Holocene Southern Ocean.

Our data show that, the GR change in central Scotia Sea generally in agreement with the South Atlantic deep water ventilation (Skinner et al., 2010) (Fig. 10). Both records represent lowered GR/better ventilation during the early Holocene and increased GR/reduced ventilation after 7 ka. The early Holocene GR change is in line with the relative abundance of *Chaetoceros* RS (Fig. 10). As the early Holocene blooming of *Chaetoceros* RS is strongly associated to the nutrient availability by upwelling, this indicates the early Holocene GR changes at our core location are closely related to the upwelling pulses in the central Scotia which brought old carbon to the surface ocean.

The GR continuously increased from 7-8 ka till the late Holocene. This is in agreement with the mid-late Holocene cooling in the high latitude Atlantic Southern Ocean, accompanied by strong re-expansion of winter sea ice (Bianchi and Gersonde, 2004; ***Chapter 3***). This is related to the enhanced cold water production under the Western Antarctic Ice Shelf. The expansion of sea ice resulted in more stratified surface ocean, which limited the gas exchange in the entire Southern Ocean. The mid-late Holocene GR increase is also in agreement with the reduced South Atlantic ventilation (Skinner et al., 2010), suggesting the oceanic circulation played a significant role in the reservoir change.

Such lowered reservoir effect in the Southern Ocean may have also occurred during postglacial warming at ca. 15 ka (Epica members, 2006), which was also a period of intensive warming and enhanced upwelling in the Southern Ocean, after the first step of abrupt CO_2 release from the Southern Ocean (Anderson et al., 2009). The mechanism caused low reservoir at the early Holocene might also play a role. The first step of Southern Ocean postglacial warming corresponds to Heinrich Event 1, with strong reduction of the deep water formation and Atlantic overturning circulation in the North Atlantic, the gas exchange was limited in the North Atlantic and led to increased reservoir (Sarnthein et al., 2007). This implies that the reservoir changes vary at different regions according to the local circulation pattern, rather than synchronous globally.

The General Reservoir change in the Scotia Sea may also exist in the adjacent area (e.g. the Antarctic Peninsula region) and other areas in the high latitude Southern Ocean. Thus the core stratigraphies and related timing of climate variability may need to be reconsidered in previous studies, which only based on ^{14}C chronology using constant ^{14}C correction.

4.5.4. Short term climate variability of Holocene Scotia Sea

The spectral analysis largely depends on the quality of the age model. Since our age model is based on correlations between the SSST record and Antarctic ice core record, the tie points would significantly influence the spectral analysis. Although this method avoids the uncertainty of ^{14}C correction, errors in smaller variations may also occur, especially concerning the small amplitude of SSST variability. However, the cyclicities derived from our records may also give us hints of the mechanisms driving the Holocene climate changes in the Scotia Sea.

In general our Scotia Sea Holocene cyclicities range between 95 to 390 yr. Centennial periodicities were also frequently observed in other Holocene records. Cyclicities of 200-300 yr were found in productivity record of Antarctic Peninsula region (Leventer et al., 1996). Periodicities of 240, 200, 180, 150, 120-110, 100-70 yr were found in isotopic and dust size records of Antarctic ice cores (Yiou et al., 1997; Masson et al., 2000; Delmonte et al., 2005). Nielsen et al. (2004) described cycles of 1220, 1070, 400 and 150 yr in the open ocean South Atlantic. These cyclicities have been associated to solar variability. Wavelet and Redfit spectral analysis have been applied in the diatom records from Adélie Land, East Antarctica (Crosta et al., 2007), they identified cyclicities of 1250, 1050, 570, 310, 230, 150-125, 110, 90, and 66 yr. Cyclicities of 360, 500-530, 270-290, 420-450 and 210 yr were extracted from the Eastern Australian lakes (Skilbeck et al., 2005). The 500-550 yr cycles are proposed to be related to NADW variations (Stuiver and Braziunas, 1993; Chapman and Shackleton, 2000), which is not evidenced in our Scotia Sea records. An internal forcing with periodicities of 320-360 yr is proposed in the polar regions, by freshwater influencing thermohaline circulation in terms of stratification and sea ice melting (Pierce et al., 1995; Crosta et al., 2007). Such cyclicities are also shown in our records in 0-7 ka, which is in agreement with Crosta et al. (2007) at the same time interval. Besides, other centennial cyclicities have been widely attributed to solar activities, as also can be seen in the ^{14}C and ^{10}Be records (e.g. Stuiver and Braziunas, 1993; Vonmoos et al., 2006; Crosta et al., 2007). The cyclicities found in the Holocene Scotia Sea are very close to those from other Holocene records, it may indicate a prevailing drive of solar activity in Holocene climate variability.

4.5.5. Age of the megascopic ash layer

The Holocene megascopic ash layer in PS67/206-1 is also recorded in various Scotia Sea sediment cores (Moreton, 1999; ***Chapter 5***), which is regionally correlated. In the northern core PS67/197-1, although cannot be well identified by the magnetic susceptibility signal, the ash was also observed with diatom and smear slides under the microscope, the core location is in the farthest distribution area of this tephra (Moreton, 1999). The correlation of this ash in core PS67/197-1 and the prominent ash layer in core PS67/206-1 is also supported by the biofluctuation pattern of diatom species (Fig. 7). In core PS67/206-1, the ^{14}C dating right below the megascopic ash layer gives a humic ^{14}C age of 8195 year, and calculated to calendar years with different GR correction, resulting in ages between 6.7 and 9.3 cal kyr BP (Table 2). Our dating shows younger ages than the datings by Moreton (1999), which gave an age of ~10 cal. kyr BP. Moreton (1999) took samples right above and below the megascopic ash layer for ^{14}C dating from various cores. The ^{14}C measurements were based on bulk samples, which have high potential of fossil carbon contamination, resulting from sediment reworking or redeposition. By applying a reservoir correction of 1300 years, Moreton (1999) summarized all the ^{14}C ages from different cores by taking average value of the above and below ash layer ages. The various fossil carbon contamination conditions in different cores may result in inaccurate ages, as the ^{14}C ages of above and below the ash layer show big variability in different cores (Moreton, 1999).

Several ash layers were found in Holocene sediment records from northern Antarctic Peninsula region (Willmott et al., 2006). The last tephra in their study was dated at 6.5 ka ^{14}C age by interpolation of 2 ^{14}C dates located 12 m apart in the core (Keller et al., 2003; Willmott et al., 2006). This age is not reliable due to the possible inconstant sedimentation rate. Based on the tuned RPI age model of Willmott et al. (2006), This ash was determined at ca. 7.8 ka (we note that the age of this ash layer presented in their paper is wrong based on their own tuned age model). Geochemical analysis show that this ash layer is from the same origin (Deception Island) as the one preserved in our core (Moreton, 1999; Willmott et al., 2006). We determined the age of this prominent ash layer in our cores at ca. 8.1 ka, both in RPI and SSST- EDML age models, this is also well in agreement with the result of Willmott et al. (2006).

Further in Antarctic ice cores, an Holocene ash layer in Vostok ice core is dated at 6.87 ka with an unknown source (Basile et al., 2001); and in Epica Dome C (EDC) at 3.5 and 10.7 ka originated from South Sandwich Islands (Narcisi et al., 2005). No visible Holocene ash was found in Dome Fuji ice core (Kohno et al., 2004). Severi et al. (2007) synchronized the volcanic activities recorded in EDML and EDC, which were detected by sulfate spikes. However, various volcanic signals were recorded in the time interval between 7 and 10 ka, thus we still have no solid evidence to prove the correlation between our marine tephra to the ice core recorded volcanic activities. Nevertheless, due to the limited volcanic ash distribution (Moreton, 1999), this volcanic eruption recorded in the Scotia Sea Holocene sediments is not a major one. Even though, we provide an age marker for the Scotia Sea Holocene records in future study.

4.6. Conclusion

Based on high resolution records, our study show that, the Holocene climate in the central and southern Scotia Sea remained stable and frequently visited by winter sea ice; whereas the northern Scotia Sea documents similar climate variability to the open Southern Ocean Atlantic sector. The

persistent early Holocene cold conditions in the central and southern Scotia Sea may be attributed to the melting of Antarctic Peninsula ice sheet. The enhanced diatom productivity during the early Holocene was mainly sustained by increased nutrient availability via enhanced upwelling, and the stratified surface water by ice melting provided favorable conditions for the growing of diatom cells.

Holocene reservoir changes are observed in the Scotia Sea, with lowered reservoir in the early Holocene and increase during the mid-late Holocene. This is in agreement with the South Atlantic ventilation history. The low early Holocene reservoir in the Scotia Sea is caused by a combination of low atmospheric ^{14}C productivity and more importantly, the lowered $\Delta^{14}C_{atm}$ after the release of CO_2 from the Southern Ocean during the pre-Holocene warming process. Such effect may have also occurred after the first step of postglacial warming, at ca. 15 ka. The increase of mid-late Holocene reservoir is related to the reduced ventilation in the Southern Ocean accompanied with the re-expansion of sea ice field. The changes in Holocene reservoir suggest that, age models established only by ^{14}C dating and calculated by applying constant reservoir should be carefully reconsidered.

Spectral analysis shows that, periodicities similar to those found in other Holocene records are also observed in the Scotia Sea, which are mainly ascribed to cyclic solar activity. Internal forcing by sea ice variability is also evidenced.

The widely distributed Holocene megascopic ash layer in the Scotia Sea has been dated at 8.1 ka, this provides an additional age marker for further studies in this area.

Chapter 5. Scotia Sea stratigraphy and environmental changes of the past 300 kyrs

Wenshen Xiao[a], Rainer Gersonde[a], Thomas Frederichs[b], Gerhard Kuhn[a]

a. Stiftung Alfred-Wegener-Institut für Polar- und Meeresforschung in der Helmholtz-Gemeinschaft, 27568 Bremerhaven, Germany
b. Fachbereich Geowissenschaften der Universität Bremen, 28334 Bremen, Germany

To be submitted to *Earth and Planetary Science Letters*

Abstract

The establishment of sediment core stratigraphy in southern high latitudes is hampered by lack of calcareous microfossils, which can be well dated, and the isotope signature can be globally correlated. Based on multi-proxy approaches, high resolution records retrieved from the Scotia Sea enable us to establish detailed sediment core stratigraphy in this region and validate the reliability of different approaches.

The core stratigraphies are based on radiocarbon chronology, diatom biostratigraphy, correlations between sediment magnetic susceptibility (MS) and Antarctic ice cores dust/climate signals, and geomagnetic chronology. The integrated approaches of different methods improve the reliability of our age models, and they show good agreement of the core stratigraphies. However, the AMS ^{14}C chronology is complicated by the uncertainty of marine carbon reservoir effect and fossil carbon contamination at this southern high latitude area. Diatom biostratigraphies of the studied cores constrain the basic frame of core stratigraphy. The relative abundance fluctuations of diatom species *Eucampia antarctica* is a useful stratigraphic tool to identify the past 6 marine isotope stages (MIS) in the Scotia Sea, but the fluctuation weakens during MIS 7 and 8, and alternatively diatom concentration serves to distinguish the cold/warm intervals. The high variability of MS in the Scotia Sea sediments enables detailed correlation to signals recorded in Antarctic ice cores up to millennial scale. High variability of MIS 3 is also documented in the MS signal, which allows detailed correlation to Antarctic ice dust and climate records. Such high efficiency correlation results from high sedimentation rates in the Scotia Sea and high sensitivity to changes of surrounding source regions and current systems, as well as changes in bioproductivity. The geomagnetic paleointensity records can be well correlated to the global and regional reference curves that support the validity of MS-Antarctic ice core age models. However, the reliability is affected in low sedimentation rate conditions. Correlations of ash layers are established between Scotia Sea sediments and East Antarctic ice cores; they can be used as additional age markers for further studies in this area.

5.1. Introduction

Stratigraphic age assignment is a crucial prerequisite of paleoceanographic studies to place the paleoceanographic history in a time frame at highest possible accuracy and as a baseline for accurate correlation of marine records among each other but also with climate records obtained from land and ice cores. In Southern Ocean sedimentary records the application of the well-established oxygen stratigraphy (e.g. Lisiecki and Raymo, 2005) is hampered by the lack of continuous planktic and

benthic foraminifera records in most of the sedimentary basins. This also accounts for records radiocarbon dating based on calcareous microfossils. Alternatively, the radiocarbon chronology has been accomplished by dating the bulk acid insoluble organic carbon (AIO) (e.g. Domack et al., 2001; Hillenbrand et al., 2010; Pugh et al., 2009) or the humic acid and residue fractions of organic carbon (e.g. Bianchi and Gersonde, 2004; Denis et al., 2009). However, the application of the radiocarbon chronology is restricted to the past 40-50 kyrs and can be complicated in Southern Ocean sediments by temporal and spatial changes of the marine carbon reservoir effect (Bard, 1988; Sikes et al., 2000; van Beek et al., 2002; Reimer et al., 2009; Skinner et al., 2010). Contamination with ^{14}C-inactive fossil carbon may further disturb the down-core radiocarbon profile.

Considering the urgent need to generate reliable and robust chronostratigraphies for Southern Ocean Quaternary sediment cores, alternative methods have been developed and tested successfully. This includes down-core variability patterns of magnetic susceptibility (MS) having potential to delineate glacial/interglacial intervals (Bareille et al., 1994; Dezileau et al., 2000; O'Cofaigh et al., 2001; Crosta and Shemesh, 2002; Schmieder, 2004). The magnetic components in the sedimentary record that represent ice rafted debris (IRD) and aeolian input can be related to cold climate (Bareille et al., 1994; Diekmann et al., 2000; Crosta and Shemesh 2002). Pugh et al. (2009) have documented the close resemblance of downcore MS with dust records obtained from Antarctic ice cores allowing for the transfer of ice-core age models to marine sediment records. Such correlation can be complicated by the occurrence of IRD or volcanic ash layers. However, the occurrence of increased ferromagnetic minerals in ash layers resulting in distinct MS-peaks can also be used for exact ash layer correlation at regional scale.

Ash layers are widely deposited on the Antarctic continent and in the surrounding Southern Ocean during the late Quaternary, they have high potential for correlating and dating palaeoenvironmental archives such as ice, lake and marine sediment cores (e.g. Hodgson et al., 1998; Moreton and Smellie, 1998; Smellie, 1999; Narcisi et al., 2005), and provide important age markers to refine age models for these archives (e.g. Parrenin et al., 2007; Hillenbrand et al., 2008). Several recently active volcanoes are located in the Antarctic Peninsula region, which disperse the tephra across the Scotia Sea by prevailing eastward oceanic and atmospheric circulation (Björck et al., 1991). Moreton (1999) identified several wide spread ash layers in Scotia Sea and Bellingshausen Sea-Amundsen Sea sediments, however, the volcanic shards were difficult to be separated from the surrounding sediment allowing independent ^{40}Ar/^{39}Ar dating.

Another method establishing core stratigraphy is based on the occurrence pattern of siliceous microfossils widespread and well preserved in Southern Ocean sediments. Abundance fluctuations of the radiolarian species *Cycladophora davisiana* represent a long-standing stratigraphic method in Quaternary Southern Ocean sediments and have been calibrated with the global oxygen isotope record (Morley and Hays, 1979; Martinson et al., 1987; Brathauer et al., 2001). Down-core records of diatom species *Eucampia antarctica* display increased abundance in glacial intervals and have been correlated tentatively with the oxygen isotope record (Burckle and Cooke, 1983; Burckle and Burak, 1988). Age control points can be defined based on the occurrence ranges of diatom or radiolarian biostratigraphic marker species calibrated with the geomagnetic polarity record or oxygen isotope stratigraphy (e.g. Hays, 1965; Baldauf and Barron, 1991; Gersonde and Barcena, 1998; Zielinski et al., 2002; Zielinski and Gersonde, 2002). Measurements of changes in Earth's magnetic field recorded as geomagnetic dipole intensity and cosmogenic ^{10}Be flux in marine sediments and ice cores present another approach to generate higher resolution age assignments in Quaternary records and allow for inter-hemispheric

correlation (Stoner et al., 2002; Laj et al., 2004; Raisbeck et al., 2007; Parrenin et al., 2007; Roberts, 2008; Yamazaki et al., 2008; Channell et al., 2009). Studies on geomagnetic paleointensity in the southern high latitudes are remarkably few (e.g. Stoner et al., 2003). Exception is the Antarctic Peninsula region with studies on the Holocene-Last Glacial Maximum period (Brachfeld et al., 2003; Willmott et al., 2006; Hillenbrand et al., 2010), the past 160 ka (Sagnotti et al., 2001) and 270 kyrs (Macri et al., 2006). These records can be well correlated to global geomagnetic intensity stacks, and prove that this method represents a useful stratigraphic tool in Southern Ocean sediment records.

Although the different proxies have been applied to establish the core stratigraphy from the southern high latitudes, there is a lack of detailed comparison to validate the consistency and reliability of these methods. To fill the gap of such knowledge, in this paper, continuous sediment sequences from the Scotia Sea are selected, which are mainly composed of biosiliceous microfossils and abundant terrigenous materials, allowing the multi-proxy approaches to achieve best accuracy and detailed comparison for the chronology. In this study, we establish high resolution stratigraphy for the Scotia Sea sediments for the past 300 kyrs, by means of radiocarbon chronology, magnetic susceptibility, diatom biostratigraphy and geomagnetic paleointensity. We show that the changes in proxies are closely related to the surrounding environment/climate changes. We also establish the possible correlation of ash layers found in the Scotia Sea sediments and the Antarctic ice cores.

5.2. Materials and methods

5.2.1. Regional settings

The Scotia Sea is the cold-water route connecting the Pacific Ocean and Atlantic Ocean in southern high latitude (Seidov and Maslin, 2001). The Antarctic Circumpolar Current (ACC) driven by the southern Westerlies flows eastward through the Drake Passage bounded by South America in the north and Antarctic Peninsula in the south. Three deep oceanic fronts are presented in the Drake Passage and the Scotia Sea, from south to north are the Southern ACC front (SACCF), the Polar Front (PF) and the Subantarctic Front (SAF) (Orsi et al., 1995) (Fig. 1). The Weddell Sea Deep Water (WSDW) introduces northward from the cold Weddell Gyre in the south (Maldonado et al., 2003). The phytoplankton blooms start in early spring when increased water column stability induced by ice-melting processes (Fryxell and Kendrick, 1988) and the phytoplankton distribution pattern is strongly affected by the frontal system, ice edge and the grazing pressure (Treguer et al., 1991; Gonzalez, 1992; Socal et al., 1997). The central Scotia Sea is isolated from major sources of sediment supply at the continental margins (Maldonado et al., 2003), but receives terrigenous sediment by ice rafting, currents and aeolian input (Pudsey and Howe, 1998; O'Cofaigh et al., 2001).

5.2.2. Materials

Sediment cores PS67/197-1, PS67/205-2, PS67/206-1, PS67/219-1 and PS67/224-1 were collected from the Scotia Sea during the R/V Polarstern cruise ANT XXII/4 in 2005. Two other Polarstern cores PS2319-1 and PS2515-3 were recovered during cruises ANT X/5 (1992) and ANT XI/2 (1994), respectively (Table 1). The cores are located south of the Polar Front on a north-south transect across the central Scotia Sea. The southernmost core PS2319-1 was recovered from a small basin north of the South Orkney Islands and located south of the SACCF and modern winter sea ice edge (WSI); the

northernmost core PS2515-3 was taken on the southern flank of the North Scotia Ridge (Diekmann et al., 2000) (Fig. 1).

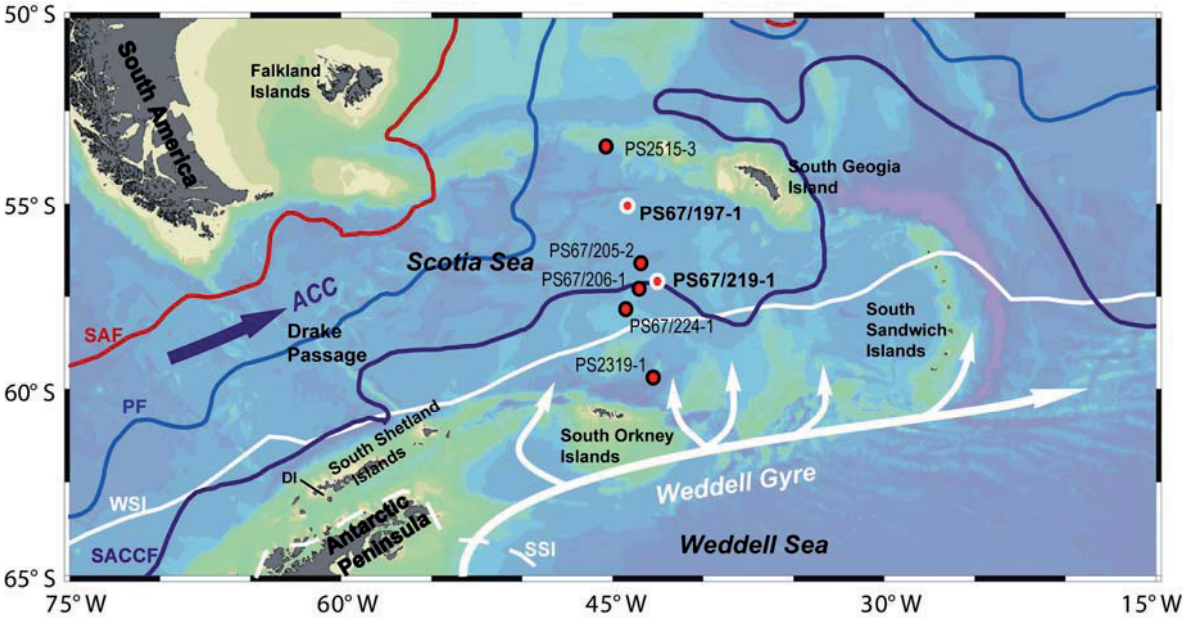

Fig. 1. Core locations, oceanographic features and sea ice distribution map of the Scotia Sea. Cores PS67/197-1 and PS67/219-1 are highlighted. DI: Deception Island; SAF: Subantarctic Front; PF: Polar Front; SACCF: Southern ACC Front; WSI: modern winter sea ice; SSI: modern summer sea ice. Locations of oceanic fronts are from Orsi et al., 1995; sea ice distribution is from Comiso, 2003. Pathways of Weddell Sea water into the Scotia Sea are modified from Heywood et al. (2002).

Table 1. Core locations of Scotia Sea sediment cores and Antarctic ice cores.

Station	Latitude	Longitude	Water Depth (m)	Recovery (m)	Reference
PS67/197-1	55° 8.24' S	44° 6.28' W	3837	23.31	this study
PS67/205-2	56° 42.11' S	43° 21.45' W	3790	19.27	this study
PS67/206-1	57° 24.67´ S	43° 27.5' W	3206	23.62	this study
PS67/219-1	57° 13.22' S	42° 28.02' W	3619	20.71	this study
PS67/224-1	57° 56.57' S	44° 11.79' W	2868	22.01	this study
PS2319-1	59° 47.3' S	42° 41' W	4323	11.54	Diekmann et al., 2000
PS2515-3	53° 32.7' S	45° 17.5' W	3467	13.07	Diekmann et al., 2000

This study focuses on cores PS67/197-1 and PS67/219-1 (both piston and trigger cores: KOL and TC). Both cores consist of biogenic intervals with olive to olive gray diatom ooze and terrigenous intervals with olive gray to gray diatomaceous mud and diatom bearing mud. Big grains of IRD and drop stones frequently scatter in core PS67/219-1, the size ranges from a few millimeters to 2-3 cm, while sediments in core PS67/197-1 are generally fine grained (Fig. 4). In core PS67/219-1, a very pronounced ash layer occurs at 61 cm core depth, which is clearly in accordance with the ash layer found in core PS67/206-1 at 1470 cm and in core PS67/205-2 at 285 cm, and less pronounced in core PS67/197-1 at 80 cm and in core PS2319-1 at 75 cm, which proved as the same ash layer by correlations of diatom species biofluctuation (***Chapter 4***). Other disseminated ashes were observed in core PS67/219-1 under the microscope at 540 cm, 623 cm, 786 cm, 998 cm, 1175cm, 1648 cm, 1891 cm and 2003 cm core depth. Ashes were also observed in core PS67/197-1 at depth of 543 cm, 664 cm,

894 cm, 1580 cm and 2050cm. These distinguishable ashes were also found in other cores in the Scotia Sea by smear slides observation, which can be very well regionally correlated in this area (Table 2; Fig. 4).

Table 2. Core depth of ash layers (Fig. 4) found in Scotia Sea cores.

	67/197-1	67/205-2	67/206-1	67/219-1	67/224-1	2319-1	2515-3
AS 1	80 cm	285 cm	1470 cm	61 cm		75 cm	
AS 1.1			1743 cm				
AS 2	543 cm	515 cm		540 cm	145 cm	236 cm	156 cm
AS 3	664 cm	555 cm		623 cm	185 cm	290 cm	260 cm
AS 4	894 cm	655 cm		786 cm	235 cm	350 cm	433 cm
AS 5	1580 cm	785 cm		998 cm	495 cm	485 cm	658 cm
AS 6	2050 cm	1645 cm		1175 cm	750 cm	660 cm	900 cm
AS 7				1648 cm	1395 cm	1082 cm	
AS 8				1891 cm	1625 cm		
AS 9				2003 cm	1915 cm		
AS 10					2025 cm		

5.2.3. Methods

Multiple proxies are combined to establish a detailed Scotia Sea stratigraphy: ^{210}Pb excess of surface sediments is measured to determine the modern deposition; AMS ^{14}C is measured for the upper interval of studied cores; magnetic susceptibility is correlated to Antarctic ice cores; diatom biostratigraphy and geomagnetic paleointensity chronology are also applied.

In order to determine if the surface sediments represent the modern deposition, core top samples were taken from both KOL and TC cores of PS67/197-1 and PS67/206-1 to measure the ^{210}Pb activities. Approximately 10 g of freeze-dried sediments at 3-5 cm intervals were packed into a plastic lid, pressed and sealed in radon proof foil for 3 weeks to establish radioactive equilibrium between ^{226}Ra and ^{222}Rn before measurement. Then the samples were analyzed by low-level low-background gamma spectroscopy using a coaxial HPGe detector (Canberra Industries). Activity concentrations of ^{210}Pb were determined at the *Institute of Environmental Physics, University of Bremen*.

Due to the lack of carbonate in the sediment, 12 bulk sediment samples from core PS67/197-1 and 16 from core PS67/219-1 were selected for Accelerator Mass Spectrometry (AMS) ^{14}C dating on both humic acid fraction and residue fraction of organic material in each sample (Table 2). In addition, 2 surface samples from the trigger and piston cores and one sample right below the megascopic ash layer were dated from core PS67/206-1 (Table 3, ***Chapter 4***). The dating was carried out in *Poznan Radiocarbon Laboratory* in Poland. Although the marine reservoir effect may change through time (Sikes et al., 2000; van Beek et al., 2002; Skinner et al., 2010; ***Chapter 4***), we roughly applied a constant reservoir effect of 1300 years in calculation to calendar years as normally used in this area (e.g. Domack et al., 2001; Pugh et al., 2009) retrieved from modern organisms (Berkman and Forman, 1996), using the calibration program CALIB 6.0.1 with updated calibration dataset (Stuiver and Reimer, 1993; Reimer et al., 2009) (Table 3).

For diatom analysis, subsamples were taken at 10-cm intervals from cores PS67/197-1 and PS67/219-1 and freeze-dried for diatom slides preparation. The sample treatment and slide preparation followed the standard procedure developed at AWI-Bremerhaven (Gersonde and Zielinski, 2000). The slides were examined under a Zeiss light microscope at a magnification of 1000×. The counting method is according to Schrader and Gersonde (1978). For taxonomy we followed Zielinski and

Gersonde (1997; 2002). For statistic reliability, more than 400 specimens were counted for each sample. Relative abundances of each species were calculated, and the total diatom abundances are calculated as concentration of valves/gram of dry sediment (Fig. 7).

High-resolution magnetic susceptibility (MS; volume-specific), was measured at 1-cm intervals on the split half cores PS67/206-1 and PS67/219-1 using a GEOTEK multisensor core logger at the AWI-Bremerhaven with a Bartington MS2F-Probe. The other cores were measured on board prior to core splitting with a MS2C-Sensor. MS is presented as dimensionless SI units of volume-specific magnetic susceptibility (κ_{lf}) of the bulk sediment.

Samples for geomagnetic investigations (comprising determination of intensity and direction of the Earth's magnetic field in the past) were taken at 5-cm intervals from cores PS67/197-1 and PS67/219-1 with 2.2 cm×2.2 cm×1.8 cm plastic cubes. The discrete samples were analyzed in the palaeomagnetic laboratory at the Department of Geosciences, University of Bremen. Palaeomagnetic directions and magnetization intensities of natural remanent magnetization (NRM), anhysteretic remanent magnetization (ARM) generated in a peak alternating field of 100 mT and a biasing DC field of 40 μT as well as isothermal remanent magnetization (IRM) generated in a DC field of 100 mT were measured on a cryogenic magnetometer (model 2G Enterprises 755 HR). NRM was measured on each sample before these were subjected to a systematic demagnetization treatment involving 16 steps for each sample with a maximum alternating field (AF) intensity of 100 mT. A detailed vector analysis was applied to the results (Kirschvink, 1980) in order to determine the characteristic remanent magnetisation (ChRM). Samples showing no systematic demagnetisation pattern were rejected. Due to the fact that the remanence vector of samples from such high latitudes is mostly represented by the vertical component, we present and discuss only results referring to the inclination. Relative paleointensity (RPI) was calculated as ratios NRM_{20mT} / ARM_{20mT}, NRM_{20mT} / IRM_{20mT} using an AF demagnetization level of 20 mT for each type of remanence. For magnetic grain size, we calculated the ratio between ARM / IRM (Maher, 1988; Verosub and Roberts, 1995; Willmott et al., 2006; Mazaud et al., 2002; 2007) imparted at fields of 100 mT respectively.

5.3. Results

5.3.1. ^{210}Pb determination

A few centimeters of the TC core top sediments from cores PS67/197-1 and PS67/206-1 are missing. Nevertheless, no clear signal of ^{210}Pb excess was found in surface sediments of core PS67/197-1 KOL and the analytical errors are high. The same case is shown in PS67/206-1 TC. In contrast, ^{210}Pb excess is well recorded in the core top sediments of PS67/206-1 KOL with a down-core decreasing profile clearly showing that the surface sediments are not modified by erosion or mixing. With a half-life of 22.3 years, the ^{210}Pb chronology is generally valid for the recent 150 years (7 half-life, only 0.8% of the original activity left), and most reliable for the recent 100 years (5 half-life, 3% of the original activity left) (Appleby, 2001). The downcore profile suggests that the core top 20 cm of PS67/206-1 KOL representing modern deposition not older than 100 years (Fig. 2). The occurrence of negative values does not have any real physical sense.

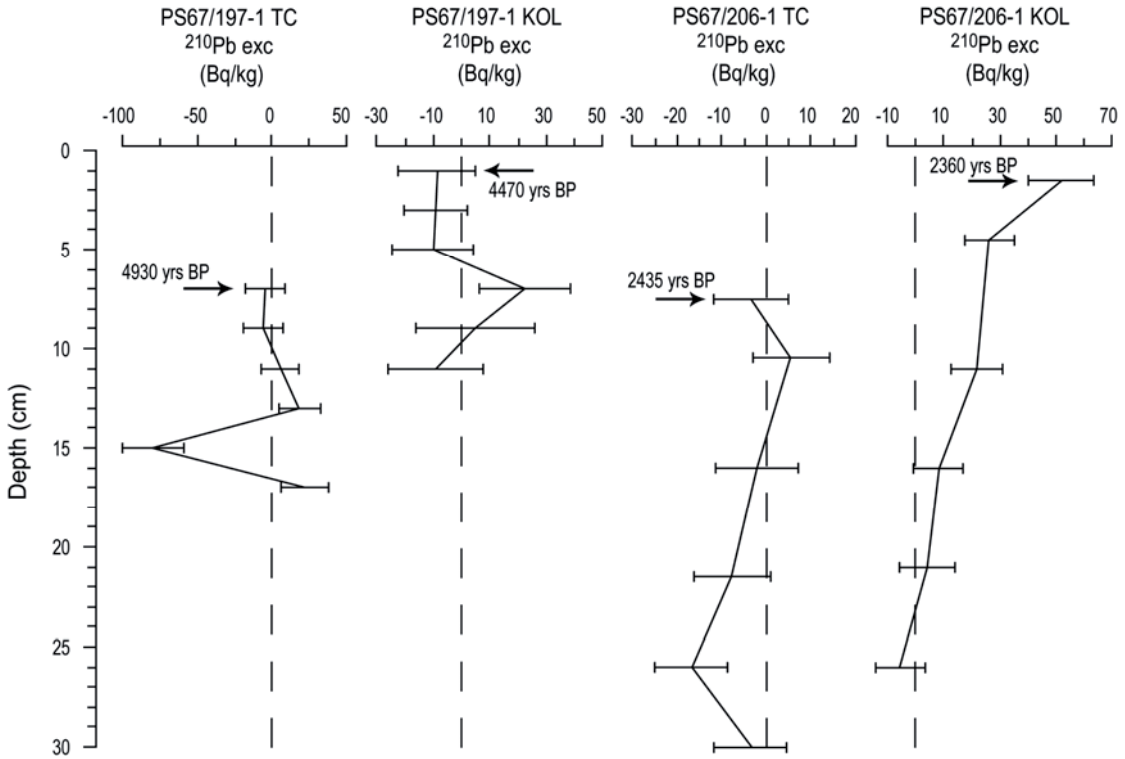

Fig. 2. ^{210}Pb excess of core top samples PS67/197-1 and PS67/206-1. The dashed lines mark the zero excess of ^{210}Pb, values above the zero line indicate the existence of ^{210}Pb excess. Bars indicate the analytical errors for each measurement, representing 1 sigma uncertainty. Arrows indicate core top ^{14}C ages on humic acid fraction (Table 3).

5.3.2. Radiocarbon dating

The AMS ^{14}C results of core PS67/219-1 show systematically higher residue ages than humic ages. Both residue and humic ages show down-core age reversals, but the residue ages show much more frequent and big amplitudes. The reversals occur at 190-193 cm on both humic acid and residue fractions, claiming that they were not caused by "laboratory effects". In general, the humic ages show more constant age-depth relationship. The PS67/197-1 radiocarbon chronologies show much more deviation between the two fractions. The residue ages are significantly older than the humic ages throughout the core except the lowermost sample. A large age reversal of humic age occurs at 329-332 cm and a smaller reversal occurs at 663-666 cm (Table 3; Fig. 3).

In the southern core PS67/219-1, the core top age difference between the 2 fractions is less than 1 kyr and increase to a temporal maximum at ca. 9 ka (kyr BP) humic age; the age differences remained between 1 and 2 kyr till ca. 15 ka humic age and deviate significantly until 22 ka humic age. For the northern core PS67/197-1, significant old surface humic age (older than 4 ka) is presented in both trigger and piston cores. There is also a remarkable rise of age differences (up to 8 kyrs) between the two fractions at 10 ka humic ^{14}C age. The age starts to deviate at ca. 16 ka humic age, large difference remains till ca. 21 ka humic age. In both cores, at 21-22 ka humic age, the ages dated on humic and residue fractions show smallest deviation.

Table 3. Radiocarbon dating of cores PS67/197-1, PS67/206-1 and PS67/219-1. The conversion to calendar ages are obtained using the calibration program CALIB 6.0.1 (Stuiver and Reimer, 1993; Reimer et al., 2009), with a reservoir age and contamination correction of 1300 years (ΔR=900 years) as normally applied in this area. TC: trigger core; KOL: piston core. C sources for dating are: H: humic acid fraction; R: residue fraction.

Core	Depth (cm)	Lab ID	C source	^{14}C age (yrs BP)	Error (yrs)	Calib. Age (cal. yrs BP)
PS67/197-1 TC	6-9	Poz-32666	H	4930	40	4047
	6-9	Poz-32810	R	17390	90	19208
	96-99	Poz-32674	H	6650	50	6173
	96-99	Poz-32812	R	9010	80	8589
PS67/197-1 KOL	0-4	Poz-32667	H	4470	40	3460
	0-4	Poz-32738	R	7260	40	6829
	80-83	Poz-32672	H	10310	70	10266
	80-83	Poz-32813	R	18230	90	20110
	200-203	Poz-32668	H	13590	130	14309
	200-203	Poz-32739	R	16290	80	18254
	270-273	Poz-32669	H	13350	110	13903
	270-273	Poz-32740	R	16720	80	18654
	329-332	Poz-32670	H	8630	60	8203
	329-332	Poz-32742	R	15010	90	16837
	470-473	Poz-32671	H	16020	160	17914
	470-473	Poz-32849	R	17700	140	19544
	542-545	Poz-32693	H	17370	130	19182
	542-545	Poz-32743	R	20580	120	22971
	663-666	Poz-32694	H	16950	130	18804
	663-666	Poz-32744	R	21100	200	23662
	718-721	Poz-32798	H	18270	150	20135
	718-721	Poz-32811	R	21660	130	24280
	780-783	Poz-32799	H	21400	160	24017
	780-783	Poz-32850	R	20500	190	22892
PS67/206-1 TC	6-9	Poz-31350	H	2435	35	1092
	6-9	Poz-31351	R	6660	50	6185
PS67/206-1 KOL	0-5	Poz-31290	H	2360	35	1004
	0-5	Poz-31291	R	3445	35	2220
	1470-1473	Poz-31333	H	8195	35	7756
	1470-1473	Poz-31335	R	10300	70	10254
PS67/219-1 TC	1-5	Poz-32802	H	2660	35	1307
	1-5	Poz-32851	R	4160	40	3093
	82-86	Poz-32805	H	7060	50	6594
	82-86	Poz-32872	R	7780	50	7394
PS67/219-1 KOL	1-5	Poz-32807	H	5730	50	5128
	1-5	Poz-32873	R	6520	50	6021
	63-66	Poz-32866	H	9140	80	8773
	63-66	Poz-32816	R	12570	60	13171
	91-94	Poz-32806	H	9880	70	9660
	91-94	Poz-32817	R	10970	60	11085
	131-134	Poz-32801	H	11770	60	12379
	131-134	Poz-32852	R	13490	90	14049
	190-193	Poz-32803	H	10750	60	10744
	190-193	Poz-32888	R	11480	60	11836
	240-243	Poz-32804	H	12590	70	13185
	240-243	Poz-32814	R	14740	80	16598
	275-278	Poz-32853	H	13500	110	14082
	275-278	Poz-32855	R	10700	70	10678
	321-324	Poz-32856	H	15620	100	17407

Core	Depth (cm)	Lab ID	C source	^{14}C age (yrs BP)	Error (yrs)	Calib. Age (cal. yrs BP)
PS67/219-1 KOL	321-324	Poz-32857	R	17970	140	19814
	381-384	Poz-32859	H	15420	120	17183
	381-384	Poz-32860	R	18020	150	19867
	471-474	Poz-32861	H	16650	130	18605
	471-474	Poz-32889	R	22390	180	25189
	541-544	Poz-32862	H	17250	250	19115
	541-544	Poz-32863	R	20550	360	22965
	624-627	Poz-32864	H	20930	360	23420
	624-627	Poz-32865	R	23420	270	26594
	651-654	Poz-32867	H	21510	210	24120
	651-654	Poz-32869	R	21550	170	24159
	721-724	Poz-32870	H	22610	230	25473
	721-724	Poz-32871	R	25370	290	28900

At close locations, the surface ages from trigger and piston cores of PS67/206-1 are similar to the age of PS67/219-1 trigger core surface sample ranging between 2300 to 2600 yrs (Table 3). In contrast, while the surface humic ages are constant, the surface residue ages are always more than one thousand years older than the humic ages and vary at different locations, indicating that the residue ages are significantly affected by reworking of old carbon (as discussed below). As the humic ages represent better age-depth relationship and regional consistency, we assume the humic ages can better represent the true ^{14}C age and used for ^{14}C chronology. This is the same case in Bouvet Island area in the Southern Ocean Atlantic sector, where the humic ages are comparable to those dated on foraminifers (Bianchi and Gersonde, 2004; ***Chapter 3***). The residue ages are more like the AIO ages determined in the same area (Pugh et al., 2009).

The ages dated on humic fraction are used for ^{14}C chronology (Fig. 3). The variation of reservoir effect in Holocene and last glacial is not well understood in this area, and the contamination of relic carbon cannot be quantified down-core at the moment. Thus, although with a surface age of ca. 2300 yrs BP, we roughly apply a correction of 1300 yrs as normally applied in this area for the calculation to calendar ages (Table 3). We note that this may also introduce a calibrated age error of ca. 1000 years.

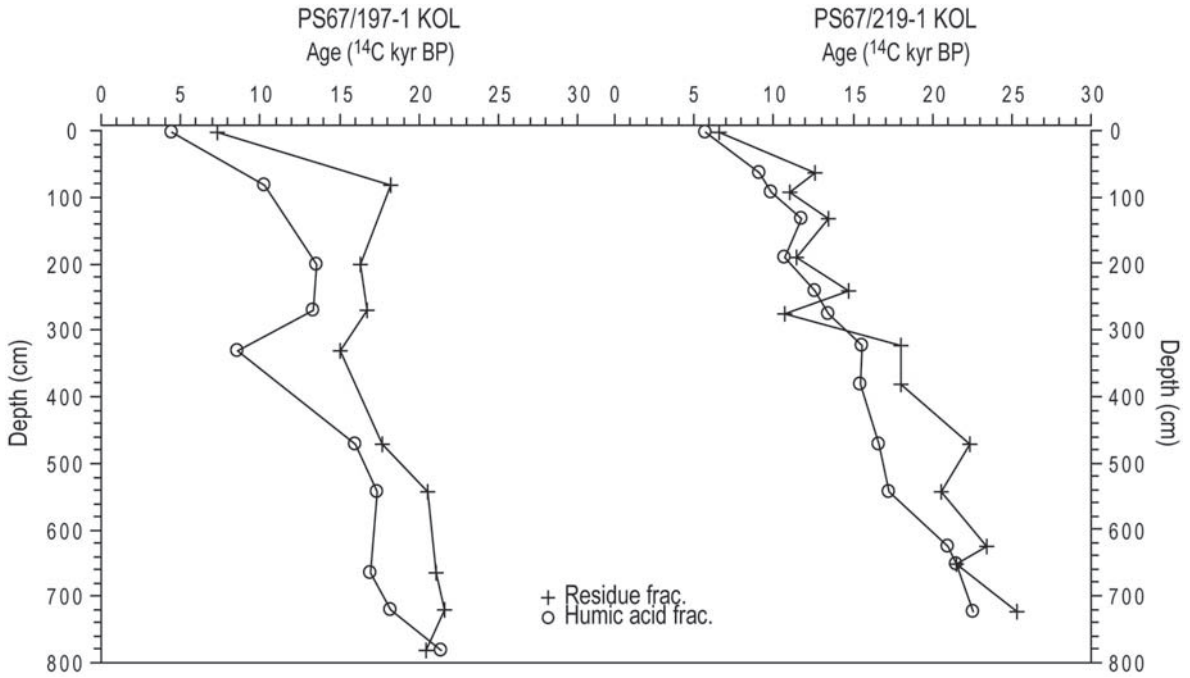

Fig. 3. Radiocarbon dating of cores PS67/197-1 and PS67/219-1.

5.3.3. Magnetic susceptibility age model

The MS records from the Scotia Sea show strong pattern of low and high MS values (Fig. 4), corresponding to the olive gray diatom ooze and gray diatomaceous mud to diatom bearing mud units, respectively. Several sharp MS peaks coincide with the ash layers and drop stones observed under the microscope or by bear eyes (Fig. 4). Drop stones were especially recognized in the southern core PS67/219-1, indicating the influence of ice rafted debris from the south, especially during cold periods. Across the south-north transect of Scotia Sea, all the cores show consistent pattern of the MS variability, enable us to make a regional correlation based on the MS records over the area, and strongly claims that there was no significant sediment disturbance during deposition.

Fig. 4. Scotia Sea magnetic susceptibility correlation. Ashes were identified in the cores. Several ash layers can be very well regionally correlated (Table 2) and are labeled AS (Scotia Sea Ash). Large IRDs and drop stones were observed during visual core description, which are labeled D. Shaded areas mark the estimated glacial intervals of MIS 2, MIS 4, MIS 6 and MIS 8.

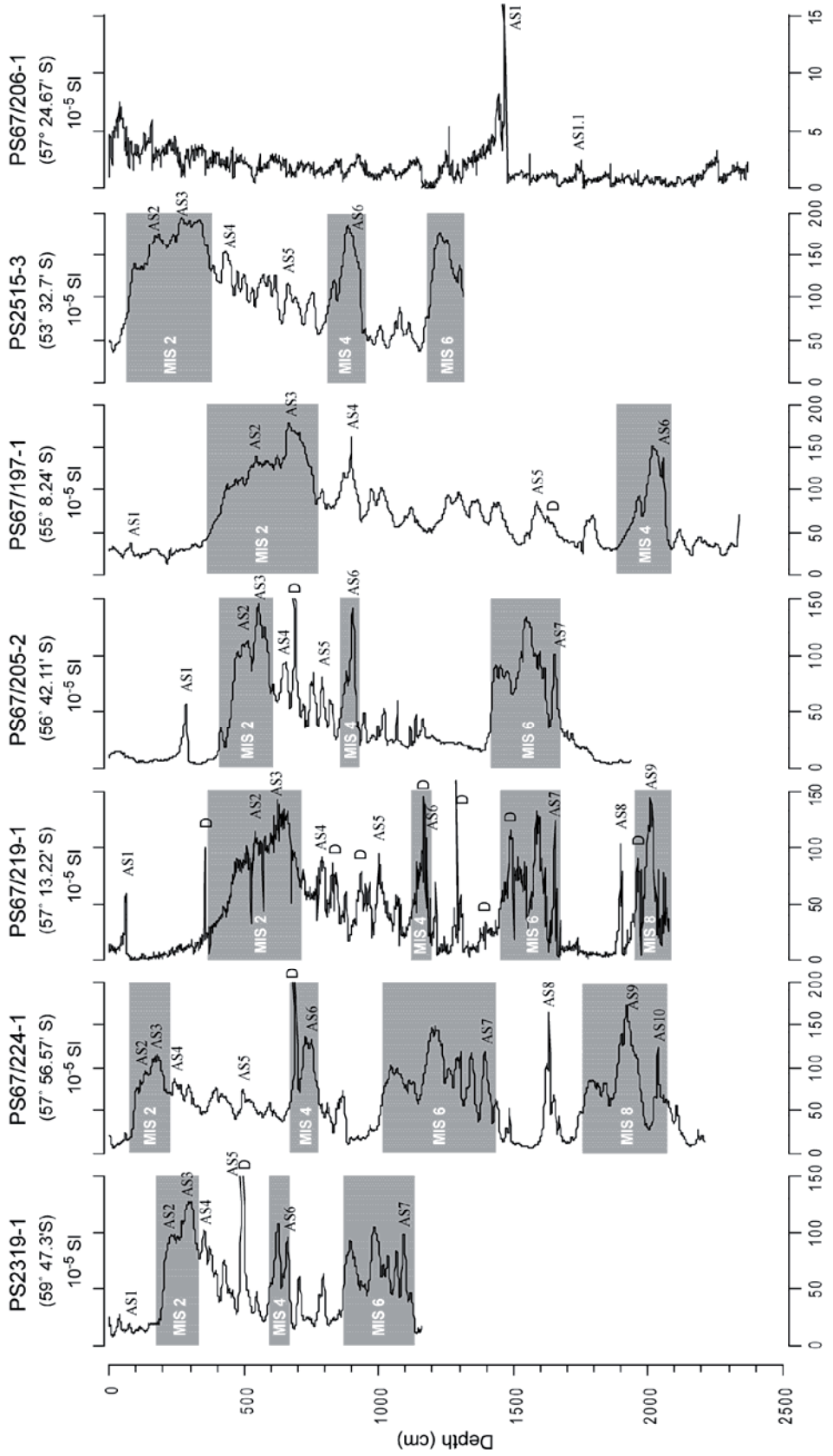
PS67/206-1
(57° 24.67' S)
10-5 SI
PS2515-3
(53° 32.7' S)
10-5 SI
PS67/197-1
(55° 8.24' S)
10-5 SI
PS67/205-2
(56° 42.11' S)
10-5 SI
PS67/219-1
(57° 13.22' S)
10-5 SI
PS67/224-1
(57° 56.57' S)
10-5 SI
PS2319-1
(59° 47.3'S)
10-5 SI
MIS 2
MIS 4
MIS 6
MIS 8
AS1
AS1.1
AS2
AS3
AS4
AS5
AS6
AS7
AS8
AS9
AS10
D
Depth (cm)
0
500
1000
1500
2000
2500

The MS signals of Scotia Sea cores show remarkable similarities to variations of dust concentrations and climate variations in Antarctic ice cores (Fig. 5). Our high resolution records enable us to establish a detailed correlation between the marine MS signal and the Antarctic ice core dust concentrations (Epica members, 2006; Fischer et al., 2007; Jouzel et al., 2007; Lambert et al., 2008) up to millennial scale.

We correlate the MS records of core PS67/197-1 and upper 14 m of core PS67/219-1 to Epica Dronning Maud Land (EDML) ice core atmospheric non sea salt Ca^{2+} ($nssCa^{2+}$) concentration record, as an indicator of dust emission from Patagonia (Fischer et al., 2007), and the $\delta^{18}O$ record (Epica members, 2006), which represents high resolution climate changes linked to the Atlantic sector of the Southern Ocean. The lower part of core PS67/219-1 is correlated to Epica Dome C (EDC) ice core dust concentration record (Lambert et al., 2008) and deuterium record (Jouzel et al., 2007) for climate variations with a longer time span. The two ice core records show consistent development of climate over both sites with different time scales, reliable age models have been developed for both ice cores (Ruth et al., 2007; Parrenin et al., 2007). The AnalySeries software (Paillard et al., 1996) was applied for graphic correlation.

The correlation of MS to ice core records show that PS67/197-1 extends back to ca. 86 ka and PS67/219-1 extends back to ca. 300 ka. Core PS67/197-1 shows much higher resolution than the upper 1300 cm interval of PS67/219-1 (Fig. 5). 14 tie points were applied in the correlation between core PS67/197-1 MS and EDML $nssCa^{2+}$ and yield a correlation coefficiency of 0.89; 29 tie points were used to correlate core PS67/219-1 MS signal to EDML/EDC dust proxies, resulting in a correlation coefficiency of 0.83.

Fig. 5. MS records of cores PS67/197-1 and PS67/219-1 correlate to Antarctic ice dust/climate records, the ash layers and main tie points are shown. EDML $nssCa^{2+}$ from Fischer et al. (2007), $d^{18}O$ from Epica members (2006); EDC dust concentration from Lambert et al. (2008), deuterium record from Jouzel et al. (2007). Intervals of Vostok, Dome F and EDC ash layers are from Basile et al. (2001), Kohno et al. (2004) and Narcisi et al. (2005), respectively.

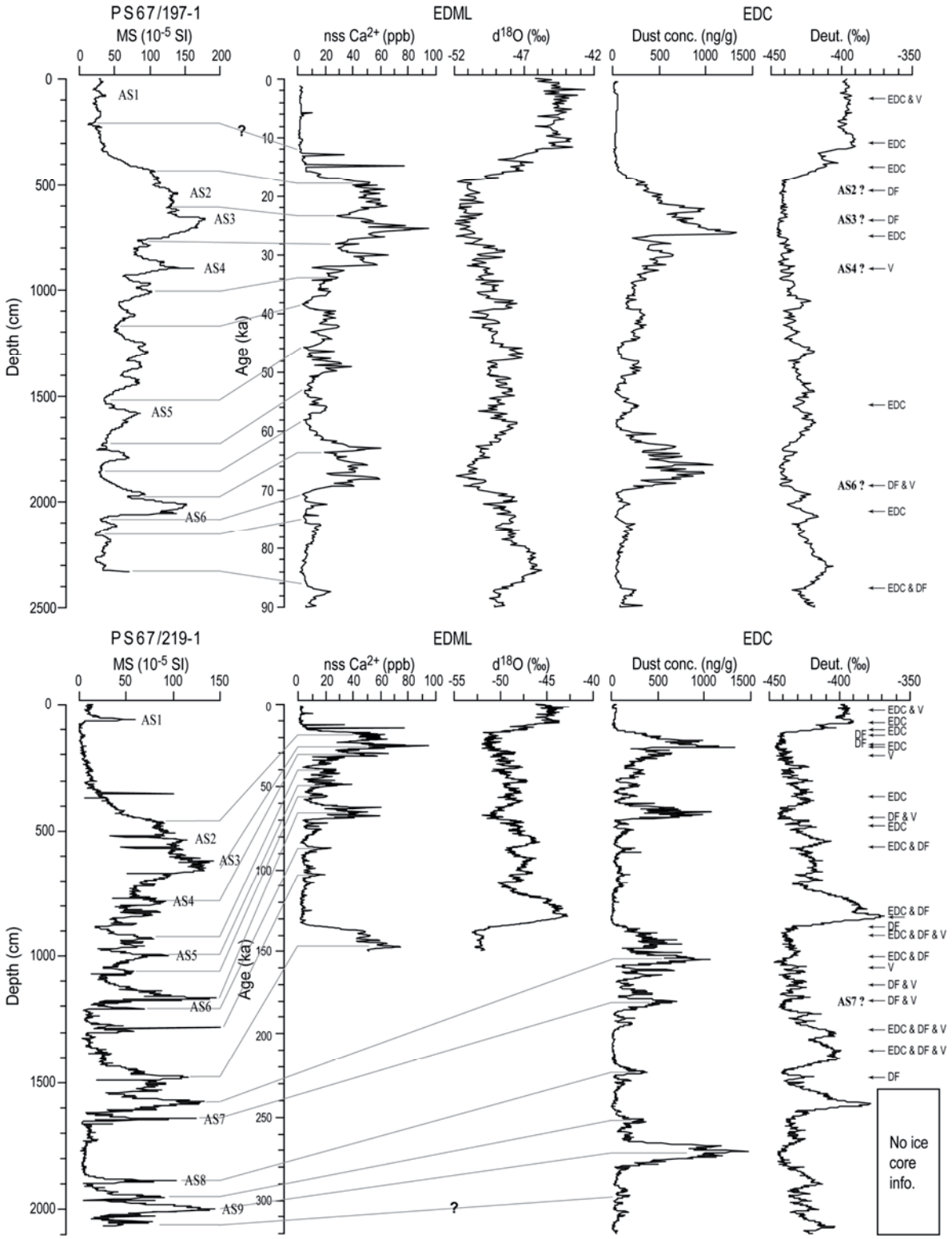
PS67/197-1
EDML
EDC
MS (10-5 SI)
nss Ca2+ (ppb)
d18O (‰)
Dust conc. (ng/g)
Deut. (‰)
Depth (cm)
Age (ka)
AS1
AS2
AS3
AS4
AS5
AS6
EDC & V
EDC
DF
V
EDC & DF
PS67/219-1
AS7
AS8
AS9
DF & V
EDC & DF & V
No ice core info.

5.3.4. Diatom biofluctuation stratigraphy

The initial biostratigraphies of PS2319-1 and PS2515-3 have been established by relative abundance fluctuations of *C. davisiana* with high values during glacial times (Diekmann et al., 2000). PS2319-1 extends back to ca. 200 ka and PS2515-3 extends back to ca. 150 ka (Fig. 6). These age models generally agree with the MS based age models and help to constrain the basic frame of the stratigraphies of other cores by regional core correlation. The radiolarian stratigraphies of the other cores have not been investigated yet.

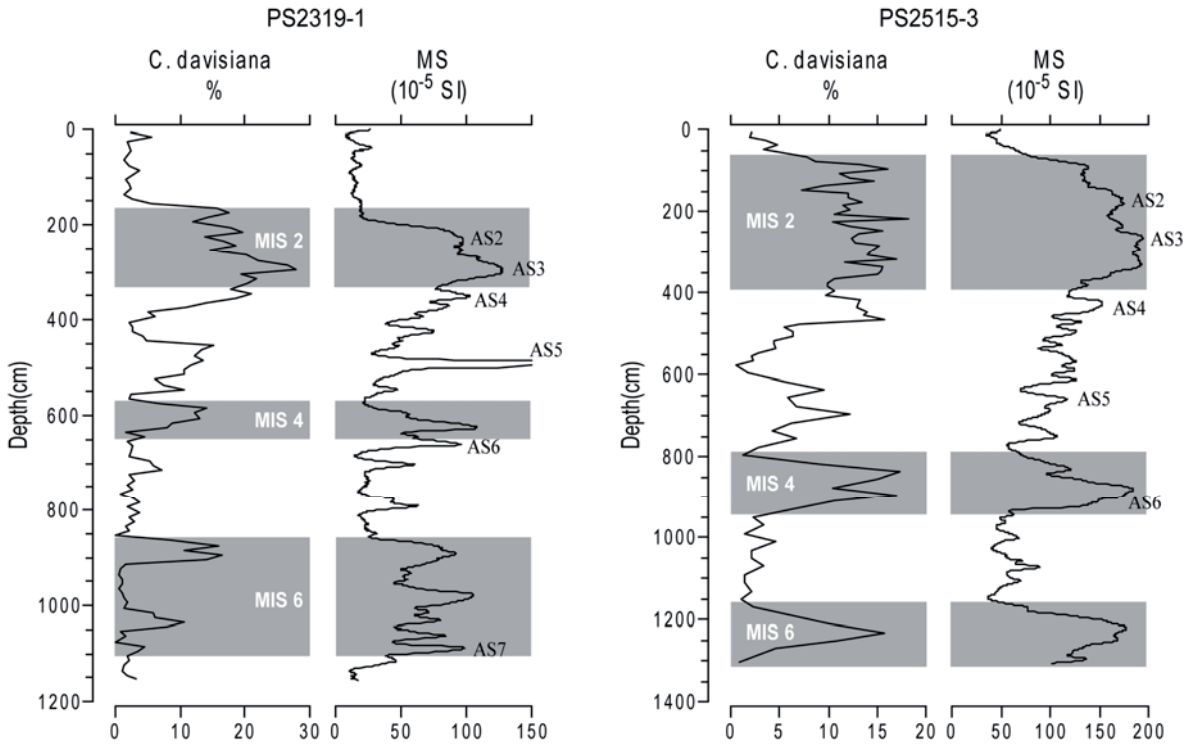

Fig. 6. Radiolarian stratigraphies of cores PS2319-1 and PS2515-3 based on C. davisiana relative abundances (Diekmann et al., 2000) compared to their MS records. Ash layers are indicated.

Relative abundances of diatom species *Eucampia antarctica* and *Flagilariopsis kerguelensis*, and diatom concentration are used for diatom biofluctuation stratigraphy (Fig. 7). In core PS67/197-1, *E. antarctica* ranges between 0 to 30%, temporal maxima occur at intervals of 447-737 cm and 1907-2077 cm, other smaller peaks are also presented (Fig. 7). High abundances of *F. kerguelensis* are presented throughout the core ranging from 30 to 75% of the total diatom assemblage; strong fluctuation of the species largely fits the variability of the MS record. The diatom concentration varies between 10^6 and 2×10^7 valves/gram, with temporal maximum at 0 to 4 m and 11.5 to 13 m, temporal minimum at 4 to 8 m and 19 to 21 m. The fluctuation of the concentration follows the pattern of *F. kerguelensis*. In core PS67/219-1, *E. antarctica* varies between 0 and 45%, with the temporal maxima occurring at 500-670 cm, 1110-1200 cm, 1430-1650 cm (Fig. 7). *F. kerguelensis* ranges between 10 to 60%, with fluctuations comparable to the MS record in the upper 12 meters, but varies in the lower part. Other two stratigraphic marker species occur at the lower part of the core. The last occurrence (LO) of *Rouxia leventerae* is at core depth 1300 cm. The last occurrence datum (LOD) of this species

was proposed at the upper boundary of MIS 6 (~130-140 ka, Zielinski et al., 2002), estimated from a series of cores from the eastern South Atlantic. However, based on the MS-Antarctic ice core age model, the LOD of this species is within MIS 5 at ca. 110 ka in our Scotia Sea core. At core depth 1670 cm, the last occurrence of *Hemidiscus karstenii* roughly marks the boundary of MIS 6 and MIS 7 (~190-200 ka, Zielinski and Gersonde, 2002). The diatom concentration ranges between 8×10^6 and 1.8×10^7 valves/gram, with temporal maximum at 0 to 4 m, 12 to 14 m and 16.5 to 19 m, temporal minimum at 4 to 7 m, 11 to 12 m, 14 to 16.5 m and 19 to 20.7 m.

The comparison of the two cores clearly shows that the southern core PS67/219-1 has much stronger occurrence of *E. antarctica*, together with lower relative abundances of *F. kerguelensis* than the northern core PS67/197-1. The biofluctuations of diatom species of PS67/197-1 can be well correlated to those of the upper 1200 cm of core PS67/219-1, as is the same case of the MS record (Fig. 7).

E. antarctica has been significantly regarded as a biostratigraphic marker for the late Quaternary Southern Ocean (Trinchitella and Dinkelman, 1980; Burckle and Cooke, 1983; Burckle and Burak, 1988). This species is most abundant in neritic-like environments, and related to sea ice conditions (Burckle, 1984). We correlate the *E. antarctica* relative abundance peaks to glacial intervals with maximum sea ice extent. A detailed *E. antarctica* stratigraphy can be established for core PS67/197-1 for the youngest 4 marine isotope stages (MIS 1 to MIS 4), and well in line with the top 1200 cm of core PS67/219-1. The lower part (older than MIS 4) of *E. antarctica* stratigraphy is based on core PS67/219-1 with relatively lower resolution. The MIS 1 to MIS 6 *E. antarctica* stratigraphy is well in agreement with the *C. davisiana* stratigraphies in cores PS2319-1 and PS2515-3 (Diekmann et al., 2000). However, continuous low relative abundances of *E. antarctica* in the intervals older than MIS 6 in core PS67/219-1, even though small fluctuations occur. This has been also recognized in the Kerguelen Plateau region of the Southern Ocean Indian sector (Kaczmarska et al., 1993) where the *E. antarctica* maximum is poorly developed at the glacial interval MIS 8, not allowing the identification of this cold stage.

As an alternative proxy of diatom productivity, diatom concentration is strongly related to the sea ice conditions and the shifting of opal belt. South of the Polar Front, the opal belt shifted to the north with a wider sea ice extension during glacial periods, whereas during interglacial periods more opal deposition to the south is in response to the reduction of sea ice (Diekmann, 2007). Thus, despite of the indistinguishable *E. antarctica* in the lower part of core PS67/219-1, MIS 7 and 8 can be well recognized by the diatom concentration signal.

Fig. 7. Diatom stratigraphies of core PS67/197-1 and PS67/219-1, compared to their MS records. Ash layers are indicated. The relative abundance peaks of certain species for regional correlation are labeled with numbers. LO: last occurrence.

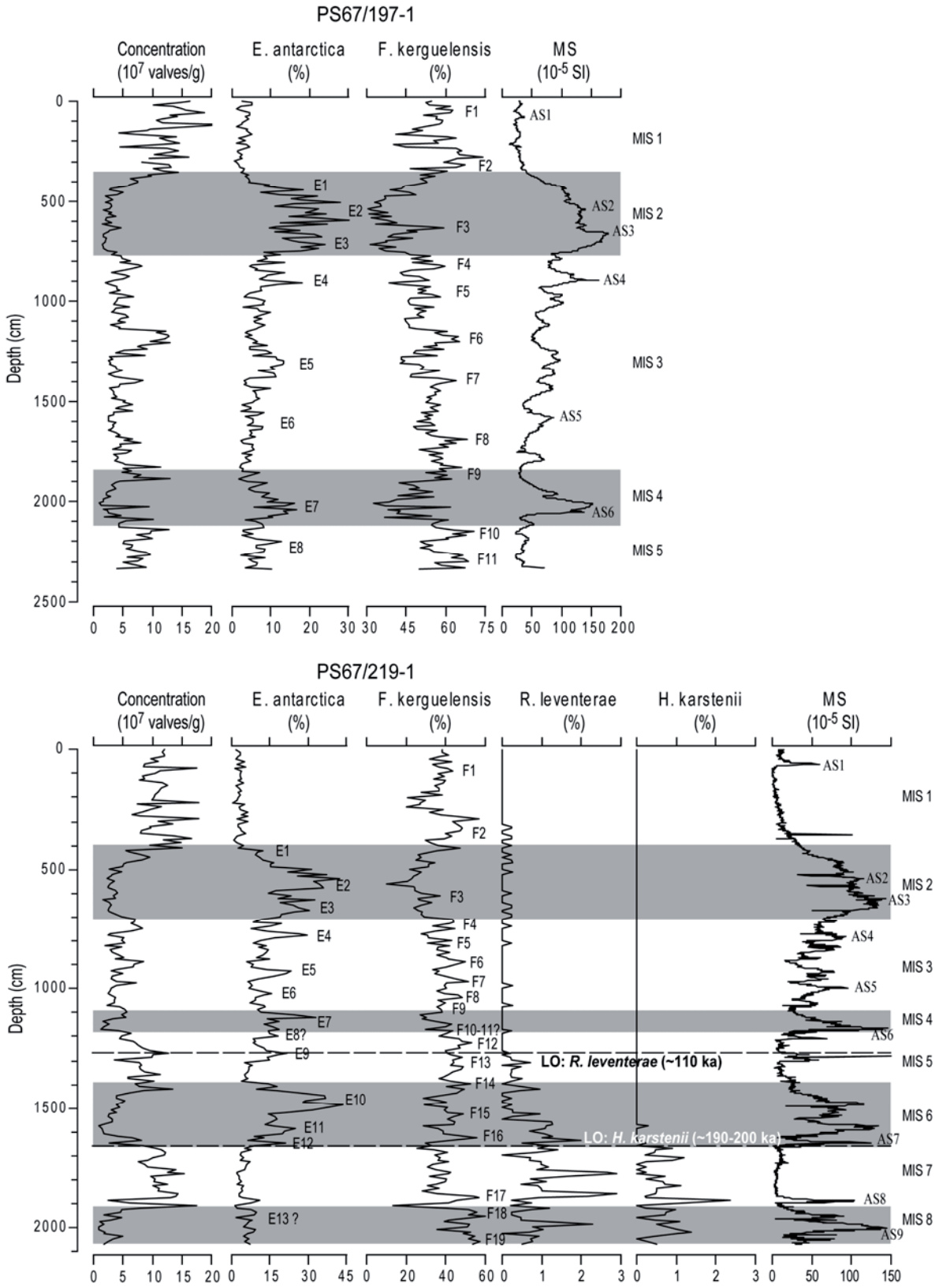
PS67/197-1
Concentration (10^7 valves/g)
E. antarctica (%)
F. kerguelensis (%)
MS (10^-5 SI)
Depth (cm)
MIS 1
MIS 2
MIS 3
MIS 4
MIS 5
PS67/219-1
Concentration (10^7 valves/g)
E. antarctica (%)
F. kerguelensis (%)
R. leventerae (%)
H. karstenii (%)
MS (10^-5 SI)
Depth (cm)
LO: R. leventerae (~110 ka)
LO: H. karstenii (~190-200 ka)
MIS 1
MIS 2
MIS 3
MIS 4
MIS 5
MIS 6
MIS 7
MIS 8

5.3.5. Geomagnetic directional information and relative paleointensity (RPI)

Inclination of core PS67/197-1 demonstrates generally normal polarity for the Brunhes Chron, oscillating from -88˚ to -11˚ with a mean inclination of -65° which is slightly shallower than the expected inclination of -74.4° of an axial geomagnetic dipole at the site location (Fig. 8). The core top's lower inclination values may attribute to the reorientation of magnetic particles during or after core recovery in response to the high water content of the surface sediments (Hillenbrand et al., 2010). Two excursions occur at 1014 cm and 1299 cm. Based on the constrains by biostratigraphy and MS stratigraphy, we related them to Mono Lake (ca. 34.2 ka) and Laschamp (ca. 41.2 ka) excursions (Laj et al., 2004), respectively. In contrast, no clear evidence for geomagnetic excursions was found in core PS67/219-1 (Fig. 8). The inclination generally fluctuates between -86˚ to -22˚ with a mean inclination of -61° which is slightly shallower than the expected inclination of -75.9° of an axial geomagnetic dipole at the site location.

Excluding the ash layer intervals, the NRM, ARM, IRM and ARM/IRM ratios of core PS67/197-1 generally range from 8 to 101 mA/m, 30-250 mA/m, 1-16 A/m and 0.013-0.05, respectively (Fig. 8). Highest values for concentration-dependent parameters NRM, ARM, and IRM were determined in core depths between 2009 and 2049 cm. A remarkable increase in intensity of all concentration dependent parameters is found for core depths 300 to 700 cm. This increase is accompanied with a coarsening of the magnetic grain size as indicated by lower ARM/IRM ratios. The core interval from 300 to about 2050 cm is characterized by a coarser overall average magnetic grain size (lower ARM/IRM ratio) than the stratigraphic units above and below this section. Nevertheless, ARM and IRM vary by less than one order of magnitude (since higher values were found only within an ash layers around 2049 cm core depth). Grain size variability as expressed by ARM/IRM is low as well. Median destructive field of ARM (MDFarm, not shown here) representing the alternating field amplitude at which the ARM intensity is reduced to half its value ranges from 20 to 33 mT with a mean of 27 mT indicating that the ARM was acquired by a low-coercive mineral like magnetite (Sagnotti et al., 2001). In summary, the magnetic mineral properties of core PS67/197-1 meet the requirements of Tauxe (1993) for sediments suitable for paleointensity investigations.

In core PS67/219-1 we determined NRM, ARM, IRM and ARM/IRM ratios ranging from 2 to 104 mA/m, 9-300 mA/m, 0.3-18 A/m and 0.001 to 0.027, respectively (Fig. 8). Highest values for concentration-dependent parameters NRM, ARM, IRM and κ_{lf} occur at core depths 1173, 1583 and 2003 cm. Variability of the concentration-dependent magnetic parameters of this core expressed as standard deviations is higher than compared to PS67/197-1 while magnetic grain size (ARM/IRM) and coercivity (MDFarm, not shown here) show variations in almost the same range as the other core.

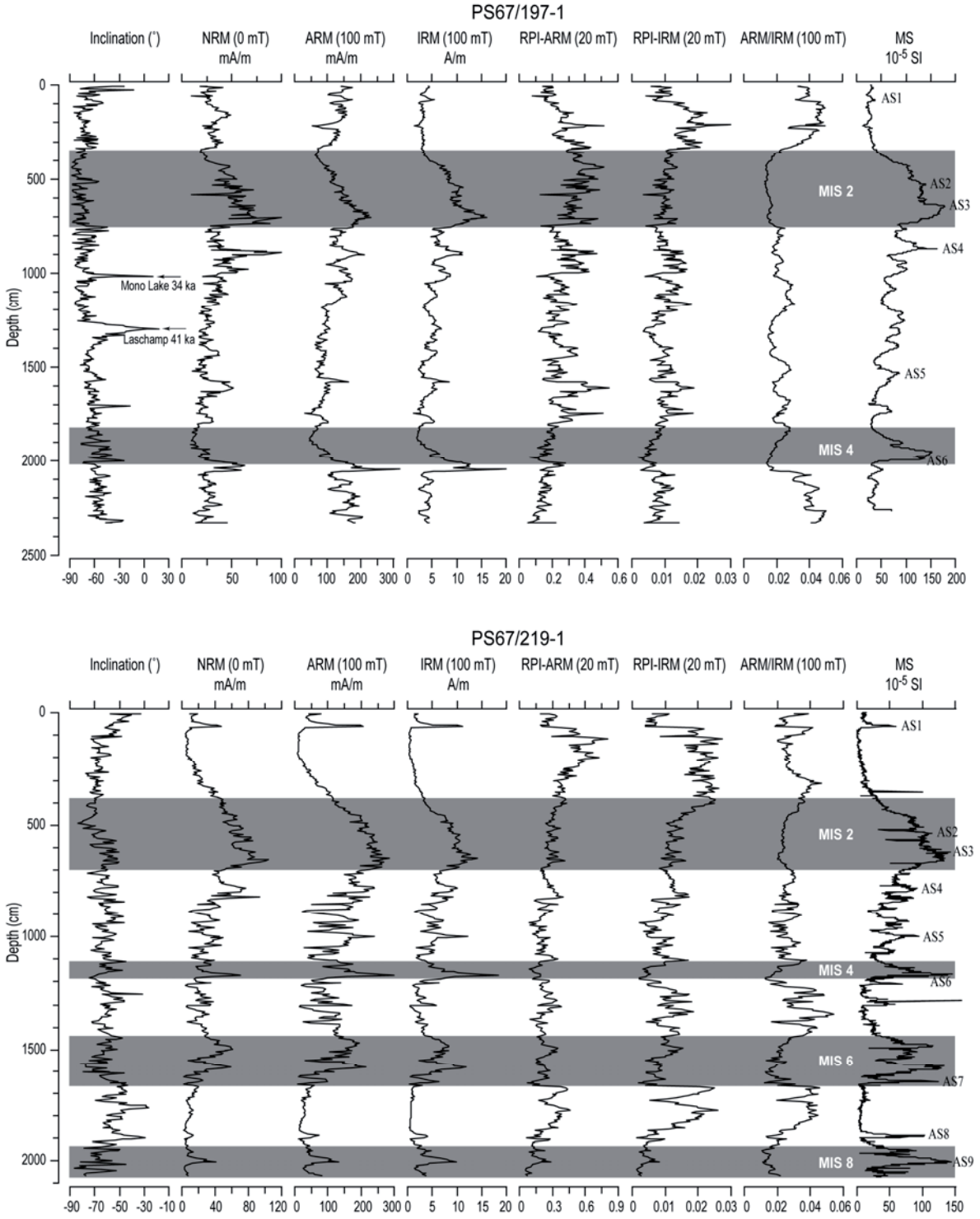

Fig. 8. Geomagnetic paleointensity records of core PS67/197-1 and PS67/219-1. Two inclination reversals occur at 1014 cm and 1299 cm in core PS67/197-1 correspond to geomagnetic excursions Mono Lake and Laschamp events, respectively. Ash layers are indicated.

Comparing the records of both cores (Fig. 8), the values of concentration dependent parameters increase from the top down to about 700 cm and 650 cm in core PS67/197-1 and PS67/219-1, respectively. This points to a decreasing terrigenous input upcore for this interval. Interestingly ARM and IRM representing only the remanence carrying minerals as magnetite demonstrate almost the same mean intensity in both cores (ARM 121±42 and 108±74 mA/m, IRM 5±3 and 4±3 A/m for PS67/197-1 and PS67/219-1, respectively) but MS which is affected by the bulk sediment composition is higher in core PS67/197-1 (17-192×10^{-5} SI) compared to core PS67/219-1 (3-160×10^{-5} SI). This might indicate that at the location of core PS67/197-1, sediment is deposited that originates from two different sources. The first source that brings the remanence carrying material might be the same at both sites. But site PS67/197-1 receives additional material from a second source that contains only minor amounts of remanence carrying minerals but mostly paramagnetic (possibly clay minerals). Mean magnetic grain size and magnetic coercivity is again more or less identical for both cores (mean ARM/IRM is 0.025±0.010 and 0.027±0.009, mean MDFarm I 26±2 mT and 27±2 mT for cores PS67/197-1 and PS67/219-1, respectively) pointing to a similar magnetic mineralogy.

In order to calculate the relative paleointensity (RPI) we followed other paleomagnetic studies from southern high latitudes (Macri et al., 2006, Willmott et al., 2006, Hillenbrand et al., 2010) and calculated RPI by dividing NRM intensity AF-demagnetized at 20 mT (NRM_{20mT}) by ARM intensity AF-demagnetized at 20 mT (ARM_{20mT}) and IRM intensity AF-demagnetized at 20 mT (IRM_{20mT}) for normalization. The RPI records calculated as NRM_{20mT}/ARM_{20mT} (RPI-ARM_{20mT}) and NRM_{20mT}/IRM_{20mT} (RPI-IRM_{20mT}) exhibit similar but not identical variations for each core (Fig. 8).

5.4. Discussion

5.4.1. Reworked old carbon and radiocarbon calibration

For the calibration to calendar ages of Antarctic sediments, a reservoir age of 1300 years is obtained by carbonate and various biogenic components (Gordon and Harkness, 1992; Berkman and Forman 1996). This reservoir age has been widely applied in this region (Domack et al., 2001; Heroy and Anderson, 2005; Pugh et al., 2009; Hillenbrand et al., 2010). The ages obtained from bulk acid-insoluble organic (AIO) material have been used to establish radiocarbon chronology around Antarctica in many previous studies (e.g. Domack et al., 2001; Pudsey et al., 2006; Pugh et al., 2009; Hillenbrand et al., 2010). However, most of the Antarctic surface sediments show significant old ages ranging from less than 2 ka to more than 10 ka, even recognized as modern deposition by ^{210}Pb dating (Andrews et al., 1999; Pudsey et al., 2006). As the sediment has a mixture of different carbon sources, reworking of old carbon is generally considered as the reason for old surface ages. The application of AIO ages for the age model requires the following prerequisites (Licht et al., 1998): 1. Relatively high influx of biogenic material; 2. Low influx of terrigenous material; 3. Little reworked old carbon. In regions where reworking of old carbon is unavoidable, a local contamination offset of the fossil carbon age is applied, by assuming that the contamination is constant through time (e.g. Hillenbrand et al., 2010). However, this assumption may not hold true for the Antarctic Peninsula region and the adjacent area.

The potential sources of reworked carbon are the admixture of old sediments by bottom current, and the input of terrigenous old carbon from adjacent land. The geographic and oceanographic settings were much different during the Last Glacial Maximum (LGM) from those of Holocene. Sea level was

ca. 120-130 m lower, ice sheets and sea ice were much more expanded during the LGM compared to present situation (Clark and Mix, 2002; Gersonde et al., 2005), more terrigenous detritus were supplied into the area by ice rafting as well as by wind and current transport. In the Holocene, the relic carbon for the northern site may be mainly transported by wind or wind driven current; the southern site may also be affected by a second source from Antarctica via ice transportation and deep flow from the Weddell Sea. During the LGM and the following termination 1, ice transportation and deep flow from the south may play a growing important role because sea ice also expanded to the northern site (Gersonde et al., 2005; ***Chapter 3***); moreover, the northern core may also receive IRDs from southern Patagonia glaciers due to expanded ice field and low sea level stands.

The variation of age differences of the two fractions show similarities in both cores. At ca. 9-10 ka and 15-21 ka humic ^{14}C age, temporal maximum of age difference between the two fractions occur in both cores, indicating enhanced reworked carbon supplied to the region during these periods. This time period corresponds to termination 1 marking the transition from the LGM to the Holocene, accompanying the major melting of ice sheets in Western Antarctica and Patagonia which brought terrigenous detritus from land. The southward shifted Westerlies during the warming process (Anderson et al., 2009; ***Chapter 3***) resulting in more vigorous currents might have also introduced more reworked carbon to the residue fraction.

Significant old surface humic age (ca. 4.5 ka) occurs at the northern site PS67/197-1, which is in agreement with another undisturbed core top sediment from Falkland Through, north of Scotia Sea, dated at 4 ka ^{14}C age on bulk organic carbon (Allen et al., 2005). This is much older than can be explained by the reservoir effect in this region. Allen et al. (2005) attributed the old surface age to enhanced ACC flow over the site that prevents the settling of the sediment and winnows the surface sediments. As indicated by the ^{210}Pb excess analysis, the core top sediments of PS67/197-1 (both KOL and TC) are not from the modern deposition. This may be also related to the enhanced ACC, but considering the 1 m recovery of the TC (as the maximum recovery is 1 m), it is likely that the TC over-penetrated the surface, so the surface sediments might be lost during coring.

The ca. 2300 yrs BP surface ^{14}C ages in the southern cores also seem to be a regional phenomenon. ^{210}Pb excess analysis shows that the surface sediments of core PS67/206-1 KOL are younger than 100 years, with a estimated sedimentation rate of 2.4±0.7 m/kyr by a simple exponential fit through ^{210}Pb excess data, which is comparable to the age model of PS67/206-1 (***Chapter 4***). This leads us to assume that the modern carbon reservoir effect in this region is ~2300 years, which is much larger than the conventionally used 1300 years. However, previous Southern Ocean ^{14}C studies suggest that either ^{14}C in the Weddell Sea or Scotia Sea water at different depth (Weiss et al., 1979; Stuiver and Östlund, 1980; Schlosser et al., 1989) or in various life forms (Gordon and Harkness, 1992; Berkman and Forman, 1996) points to a maximum correction factor of 1300±100 year for the reservoir. That indicates that fossil carbon may also exist in the humic fraction. Compared to Bouvet Island area (Bianchi and Gersonde, 2004; ***Chapter 3***), the sediments from the Scotia Sea have higher potential receiving fossil carbon from terrigenous detritus and reworking of sediments than those from Bouvet Island area, as we can see from the almost pure diatom ooze of Holocene sediment in Bouvet Island area, where the humic and residue ages are quite similar in the Holocene, and diverse towards LGM (Bianchi and Gersonde, 2004; ***Chapter 3***). Due to the more consistency of humic ages, here we propose that both humic and residue ages can be affected by relic carbon, but the humic fraction may be less affected.

The reservoir effect may change in different time intervals, which is closely related to the ocean ventilation (Sikes et al., 2000; Waelbroeck et al., 2001; Delaygue et al., 2003; Butzin et al., 2005; Skinner et al., 2010). The age reversals occurring in our records may be also affected by the temporal change of reservoir during the termination (e.g. Sarnthein et al., 2007; Skinner et al., 2010). But the extremely young humic age at 329-332 cm in core PS67/197-1 may be contaminated by modern carbon absorption due to the highly active opal surface (Zheng et al., 2002). The Holocene reservoir effect may be not constant in the Southern Ocean. van Beek et al. (2002) estimated a doubled early Holocene reservoir compared to mid-late Holocene conditions in the eastern part of Southern Ocean Atlantic sector, however, such deduction may be biased by high early Holocene sedimentation rates of the estimated core. To the contrary, a decreasing reservoir towards the early Holocene and increasing to glacial times is found in the Scotia Sea, which is in agreement with the Southern Ocean ventilation history (Skinner et al., 2010; ***Chapter 4***).

5.4.2. Validity of the correlation of MS signal from Scotia Sea to Antarctic ice core dust/climate records

Detailed correlation between Scotia Sea MS records and Antarctic dust can be made because of the high sedimentation rates in the Scotia Sea and abundant terrigenous material input predominantly bearing the magnetic signal. This correlation is not constrained to the Scotia Sea, in fact a circum-Antarctica correlation between marine MS and Antarctic ice core dust flux has been established in regionally different markedness (Pugh et al., 2009). Yet the authors claimed that west of the Scotia Sea, the correlation between the sediment's MS and the Antarctic dust concentration weakens, by listing a number of cores from southwest Scotia Sea (Yoon et al., 2007), northwest Drake Passage (Bae et al., 2003) and Pacific continental rise of the Antarctic Peninsula (Hillenbrand et al., 2008). However, by re-evaluating the age models of Yoon et al. (2007) and Bae et al. (2003), we found that their age models are actually inaccurate due to an erroneously correlation to the incomplete MS reference record of Palmer Deep core ODP 1098 (Yoon et al., 2007) and a presumably incorrect interpretation of the marine isotope stages (Bae et al., 2003). The variability of their MS records are consistent with our records from the Scotia Sea and their wrong age models led to the conclusion of Pugh et al. (2009) that west of the Scotia Sea, the correlation weakens. On the other hand, the situation on the Pacific continental rise of the Antarctic Peninsula (Hillenbrand et al., 2008) is complicated by active volcanic input, temporal discharge of icebergs releasing IRD and turbidity supplied sediments. Thus MS signals present higher variability in cores collected from such regions; even though, the general pattern of the MS record is also in line with the ones from Scotia Sea. Further to the east in the open ocean Atlantic, the MS signal weakens that detailed correlation is hampered in areas with lower sedimentation rates and lack of terrigenous supply.

High efficiency correlation (>0.8) between the Scotia Sea MS records and Antarctic ice core dust/climate records suggests a close relationship between the proxies. The primary causes of the variations in MS are changes in the input amount and nature of terrigenous material to the core site and changes in grain size associated with sorting by ocean currents and/or aeolian processes. These factors are ultimately related to climate and tectonics, and in many cases can be correlated to the $\delta^{18}O$ record (Verosub and Roberts, 1995). The MS records show clear glacial/interglacial cycles in the Scotia Sea with high values in glacial periods and low values in interglacial times (Pudsey and Howe, 1998; Diekmann et al., 2000; Pugh et al., 2009). This indicates a strong supply of terrigenous material

enriched in magnetic particles maybe resulting from changes in detrital contribution from different sources during glacial times. Geochemical and mineralogical analyses indicate that terrigenous sediments mainly originate from nearby terrestrial sources or are introduced from adjacent seas by interbasinal sediment transfer (Diekmann et al., 2000). The northern Scotia Sea sediment points to a Patagonian supply as well as an influx from the southeast Pacific through the Drake Passage; while in the southern Scotia Sea, sediment suspension from Weddell Sea is considered as the main terrigenous source and an increase of mud influx from the Antarctic Peninsula also contributes during glacial times (Diekmann et al., 2000). Another important contributor to the MS signal in Scotia Sea sediments is the aeolian dust from Patagonia (Diekmann, 2007). Similarly, the isotopic signatures show that East Antarctic dust is transported by wind mainly from Patagonia (Fischer et al., 2007; Lambert et al., 2008; Delmonte et al., 2008; Vallelonga et al., 2010; Wolff et al., 2010) with a small contribution from East Australia during interglacial times (Revel-Rolland et al., 2006).

A climatically driven link between the MS signal in Southern Ocean sediments and the Antarctic dust flux is proposed by Pugh et al. (2009). The authors suggested that more vigorous glacial winds had driven a stronger ACC that transported more Patagonian sediment to the Scotia Sea, and the material carrying the magnetic signal was either all transported by wind or was supplemented by wind-driven current transport. Similar conclusion has been previously made by Pudsey and Howe (1998), and Hofmann (1999). Pudsey and Howe (1998) investigated the distribution and changes of sediment texture in the Scotia Sea, and proposed stronger ACC flow in the Scotia Sea during the LGM with the evidence from the sortable silt. However, their interpretation is confusing due to the fact that they did not exclude the biogenic component in the grain size analysis. Higher sortable silt content during glacials in core PS2319-1 was found by Hofmann (1999), and it was also interpreted as stronger wind driven ACC in the area. In fact, core PS2319-1 is located south of the modern SACCF and more close to land, thus it is controlled by the northward extension of the Weddell Gyre, and the deep inflow from the Weddell Sea; moreover, the terrigenous input by more intensive ice rafting during glacial times may complicate the grain size signal.

Proxy studies (Stuut and Lamy, 2004; Kaiser et al., 2007; Anderson et al., 2009) and model simulations (Williams and Bryan, 2006; Toggweiler et al., 2006; Drost et al., 2007; Toggweiler, 2009; Rojas, et al., 2009) suggest that during glacial time, the Southern Westerlies shifted towards the equator, although whether the wind intensity is stronger is under debate. For the ocean current system, new evidence from isotopic studies (Hemming et al., 2007) suggests a slight northward shift of the southern boundary of the ACC during glacials. The Antarctic fronts could have been also shifted northward during glacial times (Gersonde et al., 2005), if so, the axis of ACC would also be displaced northward. Other authors (Moore et al., 1999; 2000; Pollard and Read, 2001) suggested that the ACC position is grounded by the bathymetry, e.g. in the Scotia Sea with strong topographic features. In this case, the Westerlies would have had a weaker impact on the southern part of the ACC. Nevertheless, a glacial weaker ACC current at high southern latitudes would be expected compared to interglacial conditions, also indicated by diatom evidences from the Falkland Trough (Allen et al., 2005) that stronger ACC flow during the Holocene rather than during the LGM. Thus, the assumption of a high influx of particles dominating MS into the Scotia Sea caused by a stronger wind driven ACC during glacial times (Pugh et al., 2009) would be questionable. In addition, in the modern Southern Ocean, sediments with high MS values are from regions south of the winter sea ice edge which is south of the highest current velocity zone of ACC, namely the Polar Front. In contrast, the area between winter sea ice edge and Polar Front represents the highest opal deposition with the lowest MS signal in the

sediments (Diekmann, 2007). Thus, the glacial high input of MS signal is not necessary related to high ACC velocity at the core sites.

Sedimentological studies show that terrigenous accumulation generally increases over a wide region of Atlantic Southern Ocean during glacial times (Diekmann et al. 1999; 2003), except several cores close to land that may be affected by local iceberg discharge. This is in agreement with the glacial increase of MS signal. Pugh et al. (2009) also proved the glacial increased MS by terrigenous input. Instead of interpreted as stronger ACC, such increase is primarily attributed to enhanced input of terrigenous materials. Aeolian input and current transport are the two candidate sources.

Antarctic ice core nssCa^{2+}/dust records confirm that dust originating from South America closely mirrors Antarctic climate. Mineral dust emissions in Patagonia are strongly but not linearly related to temperature changes recorded in Antarctica (Wolff et al., 2006; 2010). Such relationship is also found in our MS records (Fig. 5). During warm periods such as Holocene, warm intervals of MIS 5 and 7, the MS signal represents minimum values and low variations, as well as low dust concentration in Antarctic ice cores. Thus the correlation weakens during the warm periods. During glacial times, more aridity conditions in Patagonia and more exposed source regions due to the low sea level stand would increase the aeolian supply to the Antarctic continent and the surrounding Southern Ocean. Approximately 10 times higher glacial dust influx than interglacial influx has been recorded in Antarctic ice cores (e.g. Lambert et al., 2008). Smaller climate fluctuations are also synchronous to changes (reduced aridity and/or lower wind speeds) in the Patagonian source regions during temporal warming periods in MIS 3 (as recorded as AIMs in Antarctic ice cores) (Epica members, 2006). Thus, the dust signal from Patagonian sources is enhanced both in Antarctic ice cores and marine sediments in the Southern Ocean during cold time intervals. Secondly, during cold intervals, the longer coastlines due to the lower sea level enable more terrigenous input by current erosion.

The strength of deep water currents which suspend the terrigenous material is controversial. Hall et al. (2001) suggested intensified deep Pacific inflow during glacial times which may be directly related to the enhanced production of AABW. However, the core site (ODP 1123) of their study located north of the modern Subtropical Front (Orsi et al, 1995), and whether the relatively shallow water depth (3290m) is bathed in the AABW during glacial and interglacial times is questionable (Reid, 1986). The intensified deep water flow is likely related to the northward displacement of Westerlies and related structure of the ACC during glacial times. Isotopic and clay mineralogical evidences indicate a northward expansion of southern deep water during glacial times, possibly through mechanism of intensive sea ice formation in more extensive areas than interglacial times (Bickert and Mackensen, 2003; Diekmann et al., 2003; Watson and Naveira Garabato., 2006). Although the strength of bottom water flow may be stronger during interglacials generated under the shelf ice (Kuhn and Diekmann, 2002; Diekmann et al., 2003), the point is that more terrigenous material was loaded during glacial times.

In addition, more expanded sea ice conditions suppress bioproductivity, biosiliceous organisms as the dominant biomass in Southern Ocean contribute inversely to the MS signal. The strong dilution effect of such biogenic component reduces MS to minimum values during interglacial times, and vice versa, the missing dilution further amplifies the MS during glacial times.

5.4.3. Geomagnetic paleointensity age model

The ARM and IRM normalized RPI record of both cores show similar but not identical variations for each core. The RPI-IRM of both cores correlates very well based on other proxies such as MS and biofluctuations of diatom species. The biggest differences between the RPI-ARM and RPI-IRM in both cores occur at the interval of termination 1 to Holocene. The difference variations of RPI-ARM and RPI-IRM may result from different composition of particles carrying magnetic signal. ARM is principally linked to small magnetic grains, with size around 0.1-5μm, while IRM is sensitive to a wider range of magnetic grain size (Verosub and Roberts, 1995; Mazaud et al., 2007). Thus, the different variations between RPI-ARM and RPI-IRM imply source changes of magnetic particles at the core locations, especially the small size fraction. The decreasing values of RPI-ARM in core PS67/197-1 after the LGM indicate reduced supply of small magnetic particles in the northern Scotia Sea, and to the contrary, the increasing RPI-ARM values in core PS67/219-1 indicate increased supply of small magnetic particles. Such variations may suggest Holocene enhanced circumpolar current in the northern Scotia Sea, which is in agreement with Allen et al. (2005).

The RPI records of both cores are compared with RPI reference curves. We used the high-resolution global geomagnetic paleointensity stack curve of the past 75 kyr (GLOPIS-75) (Laj et al., 2004) and the synthetic paleointensity stack SINT-800 which integrated 33 records into a composite curve spanning the past 800 kyr (Guyodo and Valet, 1999) and the PISO-1500 stack (Channell et al., 2009) as reference curves. Due to the nature of a stacked curve that the features of variations are smoothed and detailed variability is leveled off, we also choose the RPI record from ODP site 1089 as a regional reference curve, which spans the past ~580 kyrs and preferentially located in the Southern Ocean Atlantic sector with a good age model (Stoner et al. 2003).

Geomagnetic excursions of Mono Lake (ca. 34.2 ka) and Laschamp (ca. 41.2 ka) (Laj et al., 2004) are very well recognized in core PS67/197-1 as indicated by reversals of inclination (Fig. 8). Such inclination reversals are not evidenced in core PS67/219-1. The lack of clear excursion in this core may result from lower sedimentation rates, bioturbation effects and the acquisition of the post-depositional remanence (Roberts and Winklhofer, 2004) at the excursion intervals. This is also the case in a sediment core from the western continental rise of the Antarctic Peninsula (Macri et al., 2006). However, these excursions are expressed as minima in the RPI curves documented in core PS67/219-1, as can also be related to other excursions such as Blake (ca. 120 ka), Iceland Basin (ca. 190) and Pringle Falls (ca. 220 ka) (Channell, 2006; Lund et al., 2006) (Fig. 9).

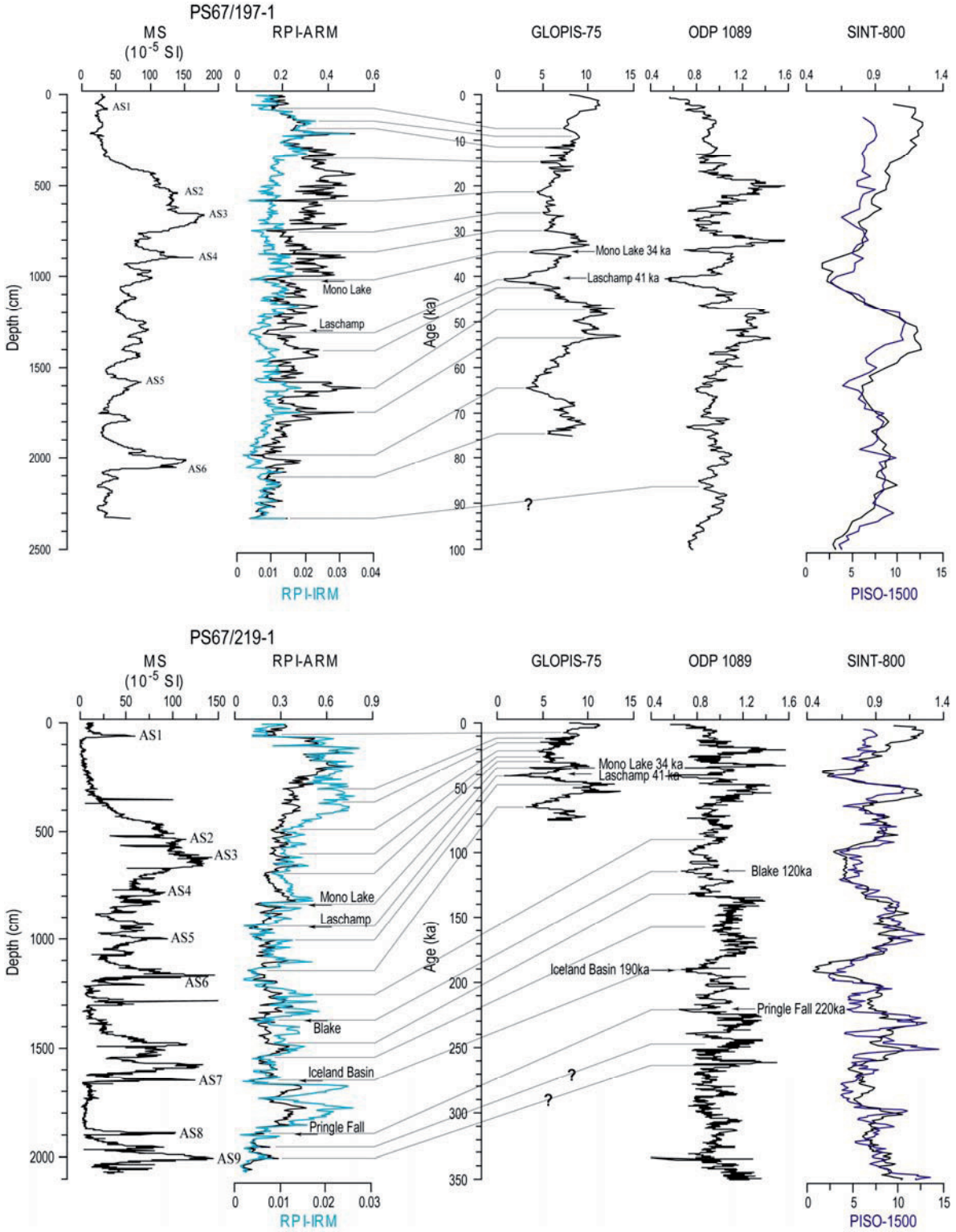

Fig. 9. ARM and IRM normalized relative paleointensity (RPI-ARM and RPI-IRM, respectively) records of cores PS67/197-1 and PS67/219-1 correlate to reference curves GLOPIS-75 (Laj et al., 2004), SINT-800 (Guyodo and Valet, 1999) PISO-1500 (Channell et al., 2009) and RPI record of ODP 1089 (Stoner et al., 2003). Ages of geomagnetic excursions are from Laj et al. (2004), Channell et al. (2006) and Lund et al. (2006).

5.4.4. Age model comparison and validation

The AMS ^{14}C dating covers a relatively short period of time. The lower intervals of the ^{14}C ages are significantly younger than those from the age models based on MS, diatom biostratigraphy and geomagnetic paleointensity (Fig. 10). The ^{14}C ages of last dating interval in both cores are 4-5 kyrs younger than the other chronologies. Such young glacial ^{14}C ages were also found in Pugh et al. (2009) at similar MS intervals. As discussed in Pugh et al. (2009), we also attribute these young ages to the absorption of modern carbon to the active opal surface of diatom valves during sample preparation for ^{14}C dating (Zheng et al., 2002), especially the old intervals with low ^{14}C concentration. The unusual large humic age reversal at 329-332 cm of PS67/197-1 and the residue age at 275-278 cm of PS67/219-1, which is significantly younger than the humic ages, may also be affected by such effect.

For core PS67/197-1 exists a good agreement between the MS/Antarctic ice core correlation age model, biostratigraphy and geomagnetic chronology throughout the full time interval covered by the core (Fig. 10) implying that the developed age models are reliable. The RPI record of core PS67/219-1 demonstrates a fairly good correlation with all literature data from about 5 ka back to an age of 70 ka (corresponding to core depth of ~1200 cm), but differs in the lower part (Fig. 10). The poor agreement might be related to the significantly lower sedimentation rates at the lower part of the core. McMillan and Constable (2006) evaluate correlations between individual RPI records and find out a systematical degradation of the correlations with decreased sedimentation rate and increased magnitude of age errors. Roberts and Winklhofer (2004) suggest minimum sedimentation rates above 10 cm/kyr as required for a reliable RPI records. In the upper part of core PS67/219-1, the sedimentation rates vary between 6 and 37 cm/kyr with a mean of 16 cm/kyr according to our age model. For deeper strata, sedimentation rates range from 1 and 12 cm/kyr with a mean of only 4 cm/kyr. The low sedimentation rate in the lower part of the core may cause an incomplete recording of the variations of the Earth's magnetic field. It is not a simple time delay between sedimentation and fixation of the magnetic signal as mentioned by Macri et al (2006) which causes the differences to other RPI reference curves, but a partly inverse correlation of the RPI record of PS67/219-1 with literature reference data.

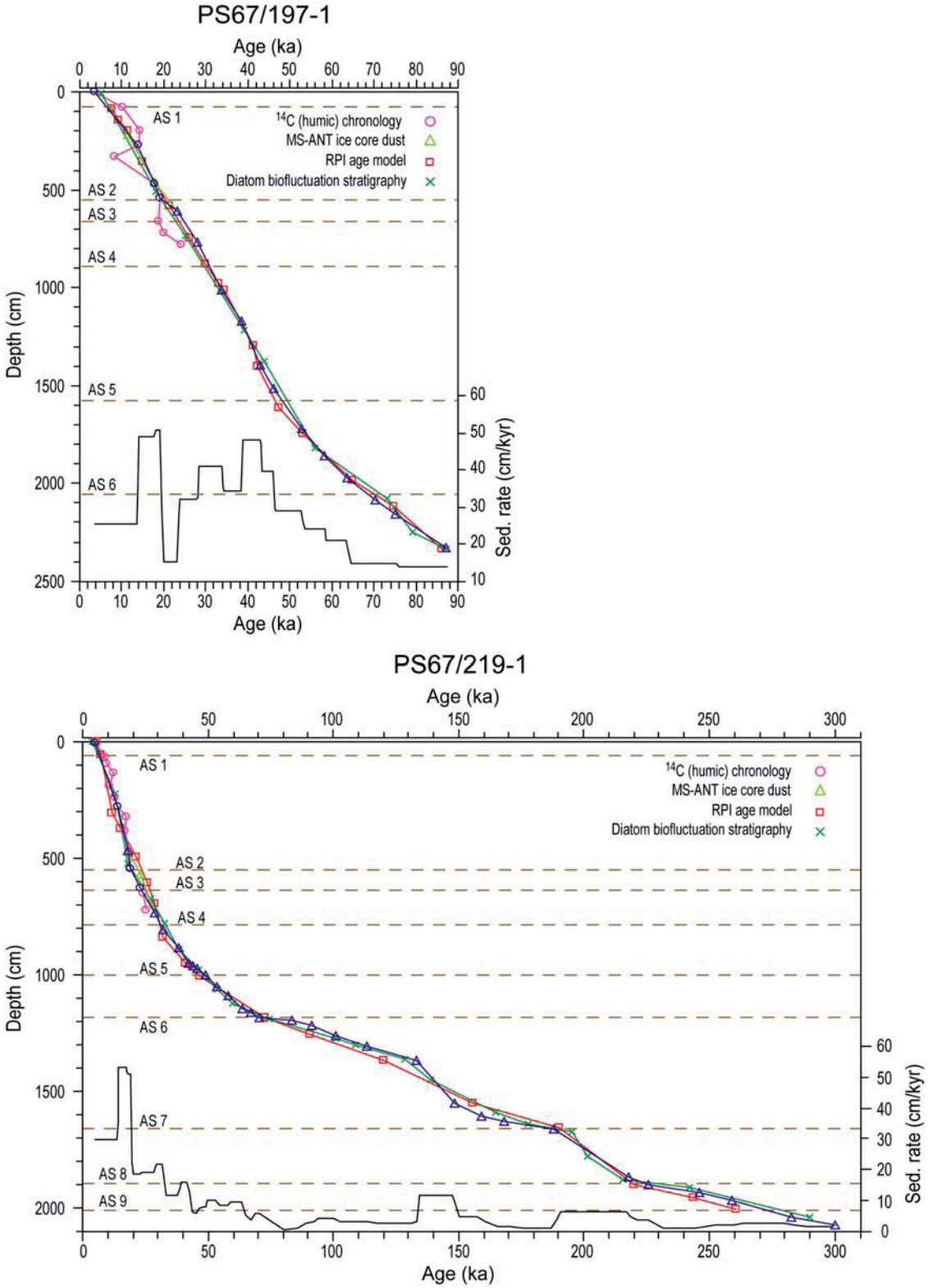

Fig. 10. Age model comparison of cores PS67/197-1 and PS67/219-1 based on radiocarbon chronology (circle), MS-Antarctic ice core age model (triangle), diatom biostratigraphy (plus) and geomagnetic chronology (square). Integrated age models are marked blue. Sedimentation rates are calculated based on integrated age models.

According to the MS/Antarctic ice core age models, the depths of geomagnetic excursions Mono Lake and Laschamp defined by RPI age models are dated at 33.9 ka and 41.0 ka for core PS67/197-1, 34.6 ka and 42.2 ka for core PS67/219-1, respectively. In the lower part of core PS67/219-1, depths of geomagnetic excursions Blake, Iceland Basin and Pringle Falls are dated by MS/Antarctic ice core age model at ages of 133.5 ka, 185.8 ka and 225.3 ka, respectively. The ages are generally in good agreement with the ages given in the literature (Laj et al., 2004; Channell, 2006; Lund et al., 2006; Roberts, 2008; Macri et al., 2010) except the Blake excursion which is supposed to be at ca. 120 ka. The deviation may caused by decreased sedimentation rate at this time interval. In summary, the paleomagnetic age models provide further support for the MS/Antarctic ice correlation age models we present here.

The integrated age model for cores PS67/197-1 and PS67/219-1 (Table 4) are mainly according to the MS/Antarctic ice core age model, which presents high efficiency correlation between the MS and ice core dust/climate proxies; ^{14}C datings were supplemented to the upper section of the cores, where the ^{14}C ages from both cores show similar ages.

Table 4. Integrated age models of cores PS67/197-1 and PS67/219-1.

Core	Depth (cm)	Age (ka)	Source
PS67/197-1			
	0	3.5	^{14}C
	271.5	13.9	^{14}C
	471.5	17.9	^{14}C
	543.5	19.2	^{14}C
	608.49	23.2	MS-Ant. ice core dust
	766.41	28	MS-Ant. ice core dust
	1009.33	33.8	MS-Ant. ice core dust
	1171.25	38.4	MS-Ant. ice core dust
	1396.17	43	MS-Ant. ice core dust
	1517.63	46	MS-Ant. ice core dust
	1720.55	52.8	MS-Ant. ice core dust
	1856.47	58.2	MS-Ant. ice core dust
	1973.93	63.6	MS-Ant. ice core dust
	2080.39	70.4	MS-Ant. ice core dust
	2153.85	75	MS-Ant. ice core dust
	2331.31	86	MS-Ant. ice core dust
PS67/219-1			
	3	5.1	^{14}C
	276.5	14.1	^{14}C
	465	17.6	MS-Ant. ice core dust
	542.5	19.1	^{14}C
	625.5	23.4	^{14}C
	733	28.8	MS-Ant. ice core dust
	808	32.2	MS-Ant. ice core dust
	885	38.4	MS-Ant. ice core dust
	948	42.2	MS-Ant. ice core dust
	962	44.2	MS-Ant. ice core dust
	972	45.8	MS-Ant. ice core dust
	1000	49	MS-Ant. ice core dust
	1048	53.6	MS-Ant. ice core dust
	1088	58	MS-Ant. ice core dust
	1144	63.6	MS-Ant. ice core dust

Core	Depth (cm)	Age (ka)	Source
PS67/219-1			
	1160	67.2	MS-Ant. ice core dust
	1181	70.6	MS-Ant. ice core dust
	1193	83.8	MS-Ant. ice core dust
	1217	91.6	MS-Ant. ice core dust
	1263	100.8	MS-Ant. ice core dust
	1308	113.2	MS-Ant. ice core dust
	1367	133.4	MS-Ant. ice core dust
	1548	148.2	MS-Ant. ice core dust
	1607	159	MS-Ant. ice core dust
	1625	168	MS-Ant. ice core dust
	1662	188	MS-Ant. ice core dust
	1864	217.6	MS-Ant. ice core dust
	1901	226	MS-Ant. ice core dust
	1932	245.8	MS-Ant. ice core dust
	1966	259	MS-Ant. ice core dust
	2038	282.8	MS-Ant. ice core dust
	2071	300.4	MS-Ant. ice core dust

5.4.5. Ash layers correlate to Antarctic ice core

The occurrence of volcanic ash is a common phenomenon in the cores from the Antarctic Peninsula region, as the wide distribution of active volcanoes in this area. Ashes are deposited in marine sediments while they are also transported to the Antarctic continent by wind, and preserved in the ice. In this study, ashes were identified from the sediments during core description and under the microscope from both smear slides and diatom slides. Based on the integrated age models of cores PS67/197-1 and PS67/219-1, ages of the Scotia Sea ashes are calculated (Table 5). We try to establish a correlation between the marine ash layers and the Antarctic ice core volcanic signals.

The prominent Holocene ash layer (AS1, Fig. 4) preserved in core PS67/206-1, PS67/219-1 and PS67/205-2 is also found in other Scotia Sea cores and associated to Deception Island source (Moreton and Smellie, 1998; Moreton, 1999). This ash layer has been dated at 8.1 ka and the ash below it (AS1.1, Fig. 4) at 9.2 ka from core PS67/206-1 by multi-proxy approaches and suggesting a lowered early Holocene reservoir at the core site (***Chapter 4***). However, the ^{14}C dates of this ash layer from cores PS67/197-1 and PS67/219-1 are 1-2 kyr older than from core PS67/206-1. The older ages from cores PS67/197-1 and PS67/219-1 may be attributed to lower sedimentation rates, therefore lower fresh to old organic carbon ratios, and possible bioturbation effect at the core sites, and this may be also the reason that the second Holocene ash layer (AS1.1) preserved in core PS67/206-1 is not well recognized in other cores. The Holocene ash layers in the Scotia Sea sediments cannot be well correlated to East Antarctic ice core ashes (***Chapter 4***).

According to Moreton (1999), the two ash layers (AS2 and AS3, Fig. 4) in LGM were dated at 21.6 and 26.4 cal kyr BP, respectively, both are originated from Deception Island. The ages are older than our ^{14}C dating (in core PS67/219-1, 19.1 and 23.4 cal kyr BP, respectively; in core PS67/197-1, 19.2 cal kyr BP for AS2, calibrated with reservoir correction of 1300 yrs, and 24.9 ka for AS3 according to integrated age model. Table 3; Table 5), as the AIO ages may be strongly affected by the fossil carbon contamination as discussed before. In contrast, our datings show similar ages to two ash layers in Dome Fuji (19 ka and 24 ka) (Kohno et al., 2004), and the South Shetland Islands (including Deception Island) are considered as the source region. Thus, the two LGM ashes in our records are

likely the same ones preserved in Dome Fuji ice core (Fig. 4), and may indicate a reservoir effect of ~1300 yrs for the LGM at the core sites.

No AMS ^{14}C dating is available for the lower part of the cores; the ash ages are calculated by the integrated age model for each core. The ash AS4 (Fig. 4) is best preserved in core PS67/197-1 and also observed in the southern cores. Our age model for core PS67/197-1 suggests an age of 31.1 ka, and 31.2 ka in core PS67/219-1 (Table 5), which is close to one ash layer in Vostok dated at 32.2 ka and South Sandwich Islands have been defined as the source region (Basile et al., 2001). Ash AS5 (Fig. 4) is widely recorded in Scotia Sea cores, as also noticed by Moreton (1999), geochemical analysis also points to Deception Island origin. Our age models suggest an age of ~48.1 ka and ~48.8 ka for AS5 in cores PS67/197-1 and PS67/219-1, respectively (Table 5). No visible ash layers at this time interval have been recorded in the reference Antarctic ice cores yet (Basile et al., 2001; Kohno et al., 2004; Narcisi et al., 2005). The age by Moreton (1999) is much too young (35.4 cal kyr BP) based on ^{14}C dating. This may due to the fact that this interval is close to the limit of ^{14}C dating, low content of ^{14}C in the sediment is easily biased toward young ages by absorption of young ^{14}C. AS6 occurs at depth of 2050 cm in core PS67/197-1 and 1175 cm in core PS67/219-1, given an age of 68.5 ka and 69.6 ka, respectively (Table 5). This ash may be related to one ash in Dome Fuji at 68 ka or 70 ka (Kohno et al., 2004) (Fig. 4). For AS7, the age model of core PS67/219-1 suggests an age of 180.4 ka (Table 5). At similar time interval, an ash layer was found in Vostok dated at 179.3 ka and South Sandwich Islands are considered as the origin (Basile et al., 2001), as well as the one in Dome Fuji ice core at 177 ka (Kohno et al., 2004). In the lower part of core PS67/219-1, two ash layers (AS8 and AS9, Fig. 4) can be clearly identified. Our age model suggests ages of 223.7 ka and 271.2 ka for these two ashes, respectively (Table 5). But no ice core ash layer information is available yet in the relevant time interval (Narcisi et al., 2005; 2010).

Ash particles are also found in some other intervals of MIS 3-4, and frequently in MIS 6 and 8. However, they are difficult to correlate between different cores because no clear sign of a layer exists. Such problems often occur at glacial times especially at low sedimentation rate conditions. At glacial times, volcanic ashes are mixed with other terrigenous particles, which also bear strong MS signals and at the first place make it difficult to distinguish them either from MS variations or under the microscope. Second, in the glacial, the timing is not only related to the eruption, but also to the deposition. They are not only transported by wind, but also by sea ice or icebergs, and only released to the water when the ice melts, which causes a delayed signal of eruption. And in that case, the ice may be loaded with ashes from different eruptions and carry mixed signals.

Concrete correlation of ash layers between different cores and archives lay on geochemical evidences. In this study, the geochemical composition of the tephra is not measured. However, tephra in the marine sediments are still geochemically difficult to correlate (Hillenbrand et al., 2008): 1. chemical composition of tephra changes through time even from the same source; 2. similarities of tephra particles from different volcanic source; 3. alteration by submarine weathering in marine cores. From this aspect, geochemical identification of tephra is also difficult to differentiate between the tephra preserved in marine sediments and in ice cores, because the tephra in ice cores are sorted by wind and only fine grained particles can reach the ice core sites. In this case, only very strong geochemical fingerprint may show convincible evidence of correlation.

Table 5. Ages of Scotia Sea ash layers based on integrated age models of cores PS67/197-1 and PS67/219-1. Ages of AS 1 and AS 1.1 are according to age model of PS67/206-1 (***Chapter 4***).

	Age (ka)		
Scotia Ash	PS67/197-1	PS67/219-1	PS67/206-1
AS 1			8.1
AS 1.1			9.2
AS 2	19.2	19.1	
AS 3	24.9	23.4	
AS 4	31.0	31.2	
AS 5	48.1	48.8	
AS 6	68.5	69.6	
AS 7		180.4	
AS 8		223.7	
AS 9		271.2	

5.5. Conclusions

Detailed Scotia Sea stratigraphy of the past 300 kyr is established by a combination of AMS ^{14}C chronology, diatom biostratigraphy, correlation of magnetic susceptibility to signals in Antarctic ice cores, and geomagnetic chronology. The multi-proxy approach improves the fidelity of our age models.

A generally good consistency between the different approaches to Scotia Sea stratigraphy indicates the validity of these proxies applied in this area. However, the AMS ^{14}C chronology is complicated by the uncertainty of marine carbon reservoir effect and fossil carbon contamination at this southern high latitude area, and they are related to changes in ocean ventilation and sources of detritus. A modern ^{14}C correction of ~2300 yrs is found in the Scotia Sea surface sediments but a correction of ~1300 years is more reasonable during the LGM and was used for our dating throughout the cores.

Diatom biostratigraphies of the studied cores constrain the basic frame of core stratigraphy. The relative abundance fluctuations of diatom species *Eucampia antarctica* is a useful stratigraphic tool for the past 6 marine isotope stages (MIS) in the Scotia Sea, but the fluctuation weakens during MIS 7 and 8, in this case, diatom concentration can be a alternative proxy to distinguish the cold/warm intervals.

High efficiency correlation between the magnetic susceptibility in the Scotia Sea sediments and the Antarctic ice cores indicates close relationship between the Scotia Sea MS and ice core proxies. The strong fluctuations in MIS 3 are also clearly documented in the MS signal and can be very well correlated to the dust and climate records in Antarctic ice cores. Such high efficient correlation results from high sedimentation rates in the Scotia Sea and high sensitivity to changes of surrounding source regions and current systems, as well as changes in bioproductivity. Changes in source are suggested to be the primary factor. The MS-Antarctic ice core correlation weakens during warm periods.

The geomagnetic paleointensity records can be well correlated to the global and regional reference curves which supports the validity of MS-Antarctic ice core age models. However, the reliability is affected in low sedimentation rate conditions.

Based on our age model, most of the ash layers found in Scotia Sea sediments can be correlated to East Antarctic ice core ash layers, which provide additional age markers for further studies in this area.

Fig. 11. Stratigraphic parameters of cores PS67/197-1 and PS67/219-1 compared with dust records from EDML (Fischer et al., 2007) and EDC (Lambert et al., 2008), respectively, and geomagnetic paleointensity record of ODP1089 (Stoner et al., 2003). Antarctic ice core ash information are from Basile et al. (2001), Kohno et al. (2004) and Narcisi et al. (2005). Possible correlation of Scotia Sea ash (AS) and ice core ash are indicated.

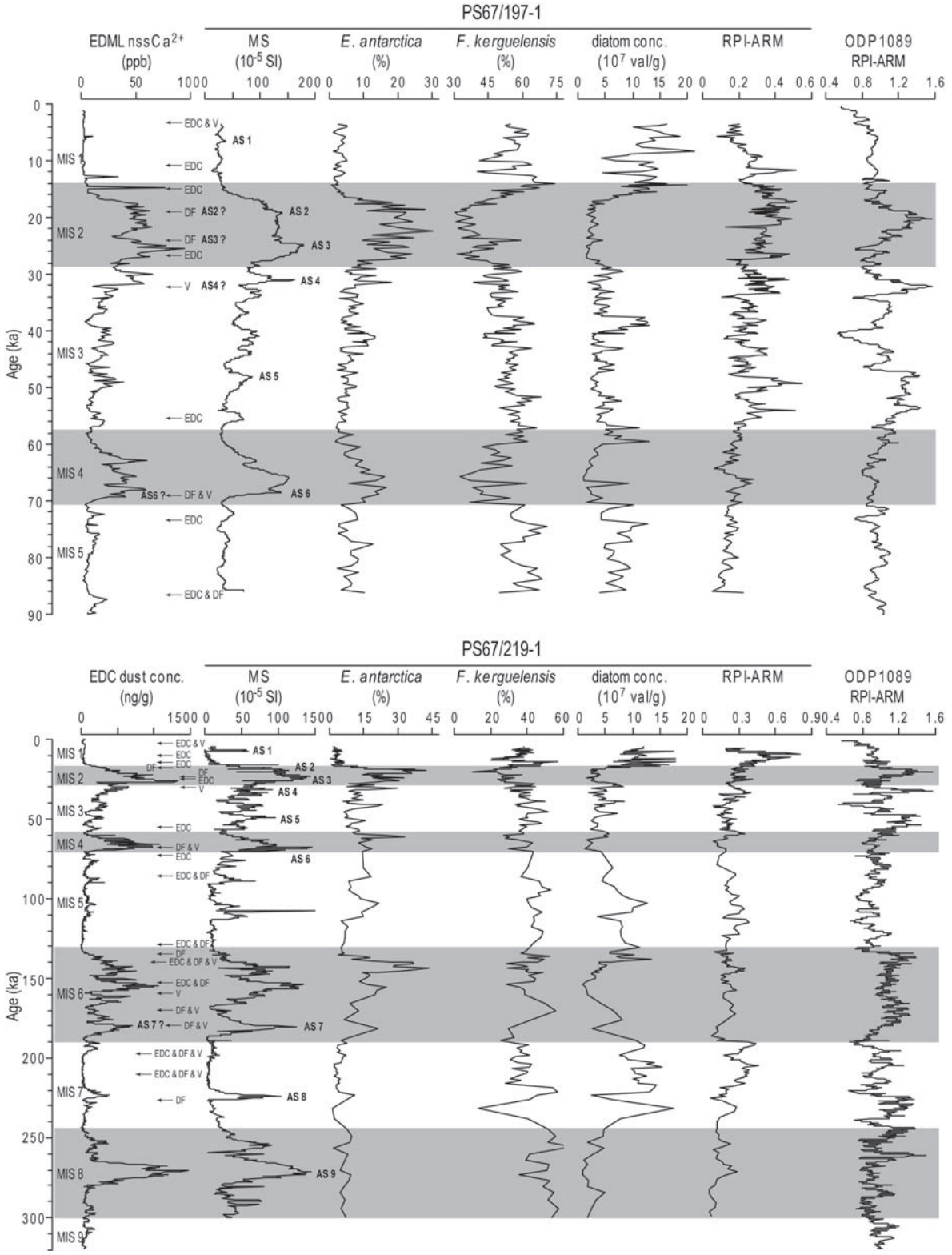
PS67/197-1
EDML nssCa2+ (ppb)
MS (10-5 SI)
E. antarctica (%)
F. kerguelensis (%)
diatom conc. (107 val/g)
RPI-ARM
ODP1089 RPI-ARM
Age (ka)
MIS 1
MIS 2
MIS 3
MIS 4
MIS 5
AS 1
AS 2
AS 3
AS 4
AS 5
AS 6
EDC & V
EDC
DF
V
DF & V
EDC & DF
PS67/219-1
EDC dust conc. (ng/g)
MIS 6
MIS 7
MIS 8
MIS 9
AS 7
AS 8
AS 9

Chapter 6. Conclusions and future perspectives

6.1. Conclusions

The studies performed in this PhD project generated a number of new diatom based records from the Southern Ocean Atlantic sector, and provide new insights into the climate and environment changes in the late Quaternary Southern Ocean.

The new records retrieved from the Bouvet Island area and Scotia Sea were combined with other records from the Southern Ocean Atlantic and Western Indian sectors, which provide comprehensive information to reconstruct the detailed climate variability in the South Atlantic for the past 30 kyrs (***Chapter 3***). A detailed regional age model has been established by AMS ^{14}C chronology and regional core correlations. Compared to modern conditions, Last Glacial cooling of 2-3˚C was found in the area south of the modern Polar Front; winter sea ice northward expanded by 5˚ in the Bouvet Island area. Then intensively expanded winter sea ice resulted in northward shifted maximum opal deposition and expanded area of carbon export to the deep ocean. The deglacial warming started at ca. 18 cal. ka (kyr BP). The bipolar seesaw mechanism warmed up the Southern Ocean in two steps during the Heinrich stadial 1 and Younger Dryas cold periods in the northern hemisphere, and the southward intruded North Atlantic Deep Water (NADW) provided the second source of warming that extended the first step warming till ca. 14 cal. ka. A cold reversal between 14 and 12 cal. ka is probably related to the melt water input from the Antarctica. The deglacial warming supports the Southern Ocean control of the deglacial atmospheric CO_2 rise. The early Holocene optimum occurred at 11-9 cal. ka and restricted at 11-10 cal. ka in the southern cores, with the winter sea ice retreated and the maximum opal deposition expanded to south of 55˚S. The further south propagation of NADW due to its strong production may also contribute to the warming in the south. The mid-late Holocene cooling started at 9-8 cal. ka, which is related to the developing cavity under the West Antarctic Shelf Ice where the cold water is generated and transported to the open ocean by the Weddell Gyre.

A closer investigation of the high resolution Holocene record from the Scotia Sea (***Chapter 4***) suggests that, during the Southern Ocean early Holocene optimum, the persisted “cold” conditions and frequently visited winter sea ice in the southern and central Scotia Sea may be related to the melting of Antarctic Peninsula ice sheet. The enhanced upwelling of nutrient favors diatom productivity. Change of Holocene carbon reservoir in the Scotia Sea is evidenced, and it is in agreement with the South Atlantic ventilation history. The early Holocene low reservoir may be ascribed to the release of CO_2 stored in the Southern Ocean that lowered the $\Delta^{14}C$ difference between the atmosphere and the surface ocean. Multi-centennial cyclicities were identified in the SSST, bioproductivity and winter sea ice signals, which are possibly attributed to solar activities, and superimposed by sea ice variability forcing.

Detailed stratigraphies of Scotia Sea sediments for the past 300 kyrs were established by multi proxy approaches performed on cores PS67/197-1 and PS67/219-1 (***Chapter 5***). The generally good consistency between the proxies enhances the reliability of the stratigraphies. However, changes marine carbon reservoir and fossil carbon contamination complicates the radiocarbon chronology. A modern ^{14}C correction of ~2300 yrs is found in the Scotia Sea surface sediments but a correction of ~1300 years is more reasonable for the Last Glacial Maximum. Diatom species *Eucampia antarctica* appears to be useful to identify glacial/interglacial intervals for the past 6 marine isotope stages (MIS) in the Scotia Sea, and diatom concentration can be used to distinguish the cold/warm periods. The

magnetic susceptibility (MS) signal of Scotia Sea sediments can be well correlated to Antarctic ice core dust and climate records. The high efficiency correlation results from high sedimentation rates and high sensitivity to changes in surrounding source regions, current systems, and bioproductivity, and primarily related to the changes in source. The reliability of geomagnetic chronology is affected in low sedimentation rate conditions. Possible correlations between the ash layers found in Scotia Sea sediments and Antarctic ice core ash layers are established based on our stratigraphy, which provide additional age markers for further studies in this area.

6.2. Future perspectives

6.2.1. Determination of chronology

The paleoclimate study in the southern high latitudes is hampered by difficulties of a reliable age model. This problem is also encountered in this study. Although with abundant radiocarbon dating, the uncertainties of changes in reservoir as well as fossil carbon contamination through time, especially the Last Glacial to Holocene transition, to some extent trouble the determination of precise timing of climate development. To overcome this problem, we tried to establish additional age models based on other parameters (***Chapter 4*** and ***5***) and generated all the information possible to minimize the errors (***Chapter 3***). More investigation is needed for understanding the detailed changes in reservoir which is related to ocean ventilation and carbon storage in the Southern Ocean.

6.2.2. Ash layer determination

Correlations of ash layers between Scotia Sea sediments and Antarctic ice cores have been established for the past 300 kyrs (***Chapter 5***). However, some ashes in the lower interval of our sediment cores did not find the counter parts in the ice cores due to the lack of information in the ice core ash layers. More detailed investigation of ice core ash layers will enhance the correlation to our records. To have solid evidence for these correlations, geochemical analysis is needed to investigate both sediment core and ice core ashes.

6.2.3. Long term Climate development in the Scotia Sea

The Scotia Sea sites PS67/197-1 and PS219-1 are located at the Cold Water Route (Seidov and Maslin, 2001) of the South Atlantic Ocean, also at the southern end of the Atlantic Meridional Overturning Circulation. The stratigraphies of Scotia Sea cores PS67/197-1 and PS67/219-1 have been established by multi-proxy approaches (***Chapter 5***), which extend back to ca. 87 ka and 300 ka, respectively. The age models enable the paleoceanography and paleoclimate reconstructions in the Scotia Sea of the past glacial-interglacial cycles at high resolution. The SSSTs have been calculated using the diatom based IKM method (Imbrie and Kipp, 1971; Zielinski et al., 1998; Esper and Gersonde, 2011, in prep.) (Fig. 1); and the sea ice conditions have been reconstructed by diatom proxies (Gersonde and Zielinski, 2000) (Fig. 2).

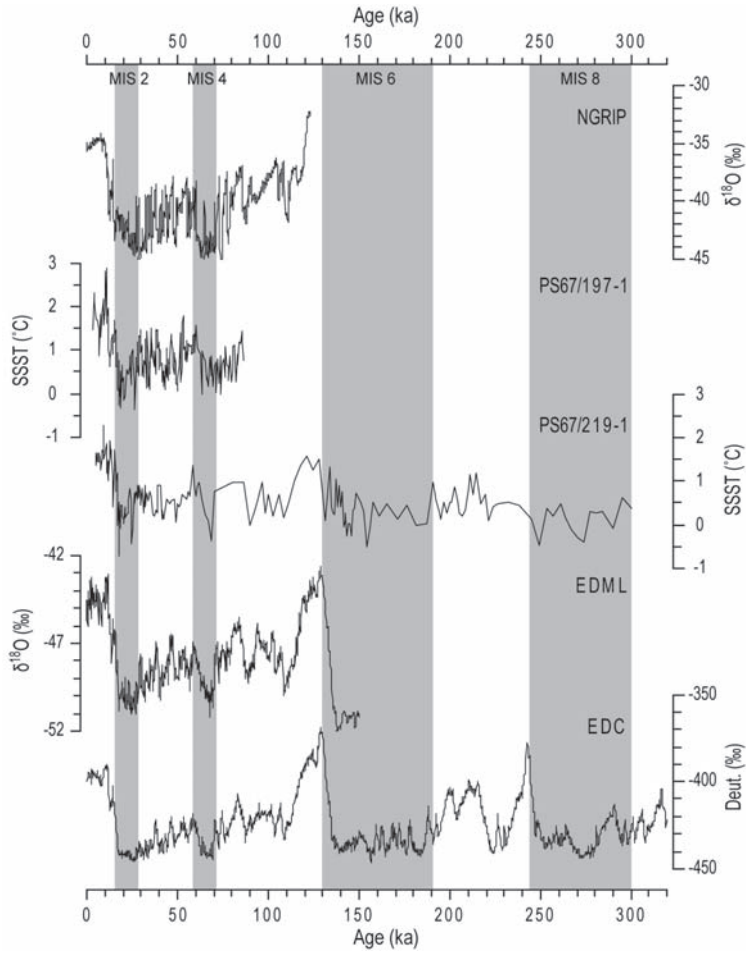

Fig. 1. SSST records of Scotia Sea cores PS67/197-1 and PS67/219-1, compared to Greenland (NGRIP, NGICP members, 2004) and Antarctic (EDML, EPICA members, 2006; EDC, Jouzel et al., 2007) ice core records.

Core PS67/197-1 covers the last glacial including MIS 3 with high climate variability (Fig. 1). This record represents the first high resolution SSST record from this area, it shows similar changes to that documented in the Antarctic ice cores, which can be coupled with the Greenland ice core proxies (Epica members, 2006). It provides new insights of the "bipolar seesaw" mechanism from the Southern Ocean marine sediments. The southern core PS67/219-1 documents climate changes at longer time span (Fig. 1). At Termination 2 (transition of MIS 6 to MIS 5), high SSST variability is observed in the core, cold rebound occurred as also recorded in the open ocean core ODP1094 (Bianchi and Gersonde, 2002).

The spatial distribution of sea ice in the Scotia Sea is closely related to the cold water expansion from the Weddell Sea, where the cold deep and surface water is generated under the Western Antarctic Shelf Ice today. It has great impact on the bioproductivity, water mass formation, ocean ventilation, etc. The diatom sea ice proxies (Fig. 2) indicate that, summer sea ice reached the southern site PS67/219 during MIS 8 and persisted south of the site afterwards. Winter sea ice covered the southern site most of time for the past 300 kyr except the warm periods of MIS 7, MIS 5 and sporadically occurred during the early Holocene. It also covered the northern site PS67/197 during the last glacial but retreated at the Holocene.

The new generated records will be combined with other existing records, to establish a detailed climate development in the southern high latitudes area.

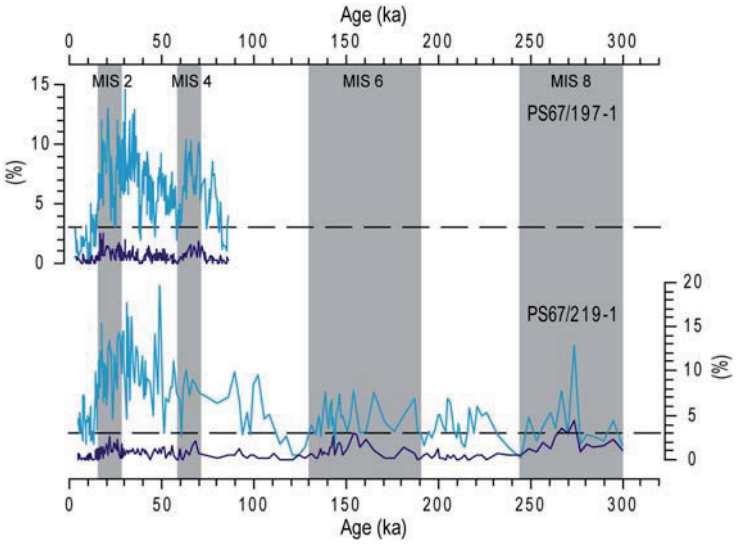

Fig. 2. Sea ice records of Scotia Sea cores PS67/197-1 and PS67/219-1. Light blue curves represent relative abundances of diatom winter sea ice indicators and dark blue curves for summer sea ice indicator. Dashed lines indicate the presence of sea ice.

6.2.4. Climate records from other Southern Ocean sectors

The South Atlantic Ocean is an unique area for understanding the climate development, not only because it is located at the southern end of the AMOC, modulating heat and water mass transport across the ocean basins, another important feature is the cold Weddell Gyre which connects the Western Antarctic Ice Sheet (WAIS). Thus the sea ice distribution and cold water expansion in the South Atlantic is closely related to the dynamics of the Antarctic ice sheet. On the other side of the WAIS, the Ross Sea plays similar role in the Pacific sector. Such feature results in the different latitudinal distribution of sea ice as well as oceanic front system in different sectors of the Southern Ocean. This PhD project focuses on the Atlantic sector, the future study to retrieve new records from the Pacific and Indian sectors, especially the region south of the Polar Front, is of great interest. These records will help to generate an overview of the Southern Ocean climate development, and will also give hints to interpret the differences between the Antarctic ice core records, which face to different source regions.

References

Abelmann, A., Gersonde, R., 1991. Biosiliceous particle flux in the Southern Ocean. Marine Chemistry, 35, 503-536.

Abelmann, A., Gersonde, R., Cortese, G., Kuhn, G., Smetacek, V., 2006. Extensive phytoplankton blooms in the Atlantic sector of the glacial Southern Ocean. Paleoceanography 21, PA1013, doi: 10.1029/2005PA001199.

Ackert Jr., R.P., Becker, R.A., Singer, B.S., Kurz, M.D., Caffee, M.W., Mickelson, D.M., 2008. Patagonian glacier response during the late glacial-Holocene transition. Science, 321, 392-395.

Ackley, S., Wadhams, P., Comiso, J.C., Worby, A.P., 2003. Decadal decrease of Antarctic sea ice extent inferred from whaling records revisited on the basis of historical and modern sea ice records. Polar Research, 22(1), 19-25.

Alldredge, A.L., Gotschalk, C., Passow, U., Riebesell, U., 1995. Mass aggregation of diatom blooms: Insights from a mesocosm study. Deep-Sea Research II, 42(1), 9-27.

Allen, C.S., Pike, J., Pudsey, C.J., Leventer, A., 2005. Submillennial variations in ocean conditions during deglaciation based on diatom assemblages from the southwest Atlantic. Paleoceanography, 20, PA2012, doi:10.1029/2004PA001055.

Alloway, B.V., Lowe, D.J., Barrell, D.J.A., Newnham, R.M., Almond, P.C., Augustinus, P.C., Bertler, N.A.N., Carter, L., Litchfield, N.J., McGlone, M.S., Shulmeister, J., Vandergoes, M.J., Williams, P.W., NZ-INTIMATE members, 2007. Towards a climate event stratigraphy for New Zealand over the past 30000 years (NZ-INTIMATEproject). Journal of Quaternary Science, 22, 9-35.

Anderson, J., Shipp, S., Lowe, A., Wellner, J.S., Mosola, A., 2002. The Antarctic Ice Sheet during the last glacial maximum and its subsequent retreat history: a review. Quaternary Science Reviews, 21, 49-70.

Anderson, R.F., Ali, S., Bradtmiller, L.I., Nielsen, S.H.H., Fleisher, M.Q., Anderson, B.E., Burckle, L.H., 2009. Wind driven upwelling in the Southern Ocean and the deglacial rise in atmospheric CO2. Science, 323, 1143-1148.

Anderson, R.F. and Carr, M.-E., 2010. Uncorking the Southern Ocean's vintage CO_2. Science, 328, 1117-1118.

Andrews, J.T., Domack, E.W., Cunningham, W.L., Leventer, A., Licht, K.J., Jull, A.J.T., DeMaster, D.J., Jennings, A.E., 1999. Problems and possible solutions concerning radiocarbon dating of surface marine sediments, Ross Sea, Antarctica. Quaternary Research, 52, 206-216.

Appleby, P., 2001. Chronostratigraphic techniques in recent sediments. In Tracking Environmental Change Using Lake Sediments, vol. 1, Last, W.M. and Smol, J.P. (eds.), Kluwer Acad., Dordrecht, Netherlands, 171-203.

Armand, L.K. and Zielinski, U., 2001. Diatom species of the genus *Rhizosolenia* from Southern Ocean sediments: distribution and taxonomic notes. Diatom Research, 16(2), 259-294.

Ascough, P.L., Cook, G.T., Dugmore, A.J., Scott, E.M., 2007. The North Atlantic marine reservoir effect in the Early Holocene: Implications for defining and understanding MRE values. Nuclear Instruments and Methods in Physics Research B, 259, 438-447.

Ascough, P.L., Cook, G.T., Dugmore, A.J., 2009. North Atlantic marine ^{14}C reservoir effects: Implications for late-Holocene chronological studies. Quaternary Geochronology, 4, 171-180.

Bae, S.H., Yoon, H.I., Park, B.K., Kim, Y., 2003. Late Quaternary stable isotope record and melt water discharge anomaly events to the south of the Antarctic Polar Front, DrakePassage. Geo-Marine Letters, 23,110–116.

Baldauf, J.G. and Barron, J.A., 1991. Diatom biostratigraphy : Kerguelen Plateau and Prydz Bay regions of the Southern Ocean. In Barron, J.A. and Larsen, B. (eds). Proceedings of the Ocean Drilling Program, Scientific Results 119. College Station, TX (Ocean Drilling Program), 547-598.

Bard, E., 1988. Correction of accelerator mass spectrometry ^{14}C ages measured in planktic foraminifera: paleoceanographic implications. Paleoceanography, 3, 635-645.

Bareille, G., Grousset, F.E., Labracherie, M., Labeyrie, L.D.,Petit, J.R., 1994. Origin of detrital fluxes in the southeast Indian Ocean during the last climate cycles. Paleoceanography, 9, 799-819.

Barker, P.F., Dalziel, I.W.D., Storey, B.C., 1991. Tectonic development of the Scotia Arc region. In: Tingey, R.J. (Ed.), The Geology of Antarctica. Oxford University Press, Oxford, 215-248.

Barker, P.F. and Thomas, E., 2004. Origin, signature and palaeoclimatic influence of the Antarctic Circumpolar Current. Earth-Science Reviews, 66, 143-162.

Barker, P.F., Diekmann, B., Escutia, C., 2007. Onset of Cenozoic Antarctic glaciations. Deep-Sea Research II, 54, 2293-2307.

Barker, S., Diz, P., Vautravers, M.J., Pike, J., Knorr, G., Hall, I.R., Broecker, W.S., 2009. Interhemispheric Atlantic seesaw response during the last deglaciation. Nature, 457, 1097-1102.

Barker, S., Knorr, G., Vautravers, M.J., Diz, P., Skinner, L.C., 2010. Extreme deepening of the Atlantic overturning circulation during deglaciation. Nature Geoscience, 3, 567-571.

Barrows, T.T., Lehman, S.J., Fifield, L.K., Deckker, P.D., 2007. Absence of cooling in New Zealand and the adjacent ocean during the Younger Dryas chronozone. Science, 318, 86-89.

Basile, I., Petit, J.R., Touron, S., Grousset, F.E., Barkov, N., 2001. Volcanic layers in Antarctic (Vostok) ice cores: Source identification and atmospheric implications. Journal of Geophysical Research, 106, 31915-31931.

Bassett, S.E., Milne, G.A., Mitrovica, J.X., Clark, P.U., 2005. Ice sheet and solid earth influences on far-field sea-level histories. Science, 309, 925-928.

Belkin, I.M. and Gordon, A.L., 1996. Southern Ocean fronts from the Greenwich meridian to Tasmania. Journal of Geophysical Research, 101(C2), 3675-3696.

Bentley, M. and Anderson, J., 1998. Glacial and marine geological evidence for the ice sheet configuration in the Weddell Sea-Antarctic Peninsula region during the last glacial maximum. Antarctic Science, 10, 309-325.

Bentley, M., Hodgson, D., Smith, J.A., Cox, N., 2005a. Relative sea-level curves for the South Shetland Islands and Marguerite Bay, Antarctic Peninsula. Quaternary Science Reviews, 24, 1203-1216.

Bentley, M., Hodgson, D., Sugden, D., Roberts, S., Smith, J., Leng, M., Bryant, C., 2005b. Early Holocene retreat of the George VI Ice Shelf, Antarctic Peninsula. Geology, 33, 173-176.

Bentley, M., Hodgson, D.A., Smith, J.A., Ó Cofaigh, C., Domack, E.W., Larter, R.D., Roberts, S.J., Brachfeld, S., Leventer, A., Hjort, C., Hillenbrand, C-D., Evans, J., 2009. Mechanisms of Holocene palaeoenvironmental change in the Antarctic Peninsula region. The Holocene, 19(1), 51-69.

Berkman, P. A. and Forman, S. L., 1996. Pre-bomb radiocarbon and the reservoir correction for calcareous marine species in the Southern Ocean. Geophysical Research Letters, 23(4), 363-366.

Bianchi, F., Boldrin, A., Cioce, F., Dieckmann, G., Kuosa, H., Larsson, A.-M., Nöthig, E.-M., Sehstedt, P.-I., Socal, G., Syvertsen, E.E., 1992. Phytoplankton distribution in relation to sea ice, hydrography and nutrients in the northwestern Weddell Sea in early spring 1988 during EPOS. Polor Biology, 12, 225-235.

Bianchi, C., Gersonde, R., 2002. The Southern Ocean surface between Marine Isotope Stages 6 and 5d: Shape and timing of climate changes. Palaeogeography, Palaeoclimatology, Palaeoecology, 187, 151-177.

Bianchi, C. and Gersonde, R., 2004. Climate evolution at the last deglaciation-the role of the Southern Ocean. Earth and Planetary Science Letters, 228, 407-424.

Bickert, T. and Mackensen, A., 2003. Last glacial to Holocene changes in South Atlantic deep water circulation. In Wefer, G., Mulitza, S., Ratmeyer, V. eds. The South Atlantic in the Late Quaternary: Reconstruction of material budget and current systems. Berlin: Springer, 671-693.

Björck, S., Sandgren, P., Zale, R., 1991. Late Holocene Tephrochronology of the Northern Antarctic Peninsula. Quaternary Research, 36(3), 322-328.

Blain, S., Quéguiner, B., Armand, L., et al., 2007. Effect of natural iron fertilization on carbon sequestration in the Southern Ocean. Nature, 446, 1070-1074.

Bouttes, N., Roche, D.M., Paillard, D., 2009. Impact of strong deep ocean stratification on the glacial carbon cycle. Paleoceanography, 24, PA3203, doi: 10.1029/2008PA001707.

Brachfeld, S., Acton, G.D., Guyodo, Y., Banerjee, S.K., 2003. High-resolution paleomagnetic records from Holocene sediments from the Palmer Deep, Western Antarctic Peninsula. Earth and Planetary Science Letters, 181, 429-441.

Brathauer, U., Abelmann, A., Gersonde, R., Niebler, H.-S., Fütterer, D.K., 2001. Calibration of *Cycladophora davisiana* events versus oxygen isotope stratigraphy in the subantarctic Atlantic Ocean - a stratigraphic tool for carbonate-poor Quaternary sediments. Marine Geology, 175, 167-181.

Broecker, W. and Barker, S., 2007. A 190‰ drop in atmosphere's $\Delta^{14}C$ during the "Mystery Interval" (17.5-14.5 kyr). Earth and Planetary Science Letters, 256, 90-99.

Brovkin, V., Kim, J.-H., Hofmann, M., Schneider, R., 2008. A lowering effect of reconstructed Holocene changes in sea surface temperatures on the atmospheric CO2 concentration. Global Biogeochemical Cycles, 22, GB1016, doi: 10.1029/2006GB002885.

Bryden, H.L. and Cunningham, S.A., 2003. How wind forcing and the air-sea heat exchange determine meridional temperature gradient and stratification for the Antarctic Circumpolar Current. Journal of Geophysical Research, 108. doi:10.1029/2001JC001296.

Burckle, L.H. and Cooke, D.W., 1983. Late Pleistocene Eucampia antarctica abundance stratigraphy in the Atlantic sector of the Southern Ocean. Micropaleontology, 29(1), 6-10.

Burckle, L.H., 1984. Ecology and paleoecology of the marine diatom Eucampia antarctica (Castr.) Mangin. Marine Micropaleontology, 9, 77-86.

Burckle, L.H. and Burak, R.W., 1988. Fluctuations in Late Quaternary diatom abundances: stratigraphic and paleoclimatic implications from subantarctic deep sea cores. Palaeogeography, Palaeoclimatology, Palaeoecology, 67, 147-156.

Butzin, M., Prange, M., Lohmann, G., 2005. Radiocarbon simulations for the glacial ocean: The effects of wind stress, Southern Ocean sea ice and Heinrich events. Earth and Planetary Science Letters, 235, 45-61.

Channell, J.E.T., Stoner, J.S., Hodell, D.A., Charles, C.D., 2000. Geomagnetic paleointensity from the subantarctic South Atlantic: a tool for inter-hemispheric correlation. Earth and Planetary Science Letters, 175, 145–160.

Channell, J.E.T. and Stoner, J.S., 2002. Plio-Pleistocene magnetic polarity stratigraphies and diagenetic magnetite dissolution at ODP Leg 177 Sites (1089, 1091, 1093 and 1094). Marine Micropaleontology, 45, 269-290.

Channell, J.E.T., 2006. Late Brunhes polarity excursions (Mono Lake, Laschamp, Iceland Basin and Pringle Falls) recorded at ODP Site 919 (Irminger Basin). Earth and Planetary Science Letters, 244, 378-393.

Channell, J.E.T., Xuan, C., Hodell, D.A., 2009. Stacking paleointensity and oxygen isotope data for the last 1.5 Myr (PISO-1500). Earth and Planetary Science Letters, 283, 14-23.

Chapman, M.R. and Shackleton, N.J., 2000. Evidence of 550-year and 1000-year cyclicities in North Atlantic circulation patterns during the Holocene. The Holocene, 10(3), 287-291.

Clark, P.U. and Mix, A.C., 2002. Ice sheets and sea level of the Last Glacial Maximum. Quaternary Science Reviews, 21, 1-7.

Clark, P.U., Dyke, A.S., Shakun, J.D., Carlson, A.E., Clark, J., Wohlfarth, B., Mitrovica, J.X., Hostetler, S.W., McCabe, A.M., 2009. The Last Glacial Maximum. Science, 325, 710-714.

Clement, A.C. and Peterson, L.C., 2008. Mechanisms of abrupt climate change of the last glacial period. Reviews of Geophysics, 46, RG4002, doi: 10.1029/2006RG000204.

Comiso, J. C., 2003. Large-scale characteristics and variability of the global sea ice cover. In: Thomas, D. N., Diekmann, G. S. (Eds.), Sea ice an introduction to its physics, chemistry, biology and geology. Blackwell, Oxford, 112-142.

Comiso, J.C., 2010. Variability and trends of the global sea ice cover. In: Thomas, D.N. and Diekmann, G.S. (Eds.), Sea Ice (second edition). Blackwell, Oxford, 205-246.

Conway, H., Hall, B., Denton, G., Gades, A., Waddington, E., 1999. Past and future grounding-line retreat of the West Antarctic Ice Sheet. Science, 286, 280–283.

Cortese, G., Abelmann, A., Gersonde, R., 2007. The last five glacial-interglacial transitions: A high-resolution 450,000-year record from the subantarctic Atlantic. Paleoceanography, 22, PA4203, doi:10.1029/2007PA001457.

Cremer, H., Heiri, O., Wagner, B., Wagner-Cremer, F., 2007. Abrupt climate warming in East Antarctica during the early Holocene. Quaternary Science Reviews, 26, 2012-2018.

Crosta, X., Pichon, J.J., Labracherie, M., 1997. Distribution of *Chaetoceros* resting spores in modern peri-Antarctic sediments. Marine Micropaleontology, 29, 283-299.

Crosta, X., Pichon, J.J., Burckle, L.H., 1998a. Application of the modern analog technique to marine Antarctic diatoms: reconstruction of maximum sea-ice extent at the Last Glacial Maximum. Paleoceanography, 13(3), 284-297.

Crosta, X., Pichon, J.J., Burckle, L.H., 1998b. Reappraisal of Antarctic seasonal sea-ice at the Last Glacial Maximum. Geophysical Research Letters 25(14), 2703-2706.

Crosta, X. and Shemesh, A., 2002. Reconciling down core anticorrelation of diatom carbon and nitrogen isotopic ratios from the Southern Ocean. Paleoceanography, 17(1), doi: 10.1029/2000PA000565.

Crosta, X., Sturm, A., Armand, L., Pichon, J-J., 2004. Late Quaternary sea ice history in the Indian sector of the Southern Ocean as recorded by diatom assemblages. Marine Micropaleontology, 50, 209-223.

Crosta, X., Crespin, J., Billy, I., Ther, O., 2005. Major factors controlling Holocene $\delta^{13}C_{org}$ changes in a seasonal sea-ice environment, Adélie Land, East Antarctica. Global Biogeochemical Cycles, 19, GB4029, doi:10.1029/2004GB002426.

Crosta, X., Debret, M., Denis, D., Courty, M.A., Ther, O., 2007. Holocene long- and short-term climate changes off Adelie Land, East Antarctica. Geochemistry, Geophysics, Geosystems, 8(11), doi: 10.1029/2007GC001718.

Crosta, X., Debret, M., Denis, D., Courty, M.A., Ther, O., 2007. Holocene long- and short-term climate changes off Adelie Land, East Antarctica. Geochemistry, Geophysics, Geosystems, 8(11), doi: 10.1029/2007GC001718.

Crosta, X., Denis, D., Ther, O., 2008. Sea ice seasonality during the Holocene, Adélie Land, East Antarctica. Marine Micropaleontology, 66, 222-232.

Cunningham, S.A., Alderson, S.G., King, B.A., Brandon, M.A., 2003. Transport and variability of the Antarctic Circumpolar Current in Drake Passage. Journal of Geophysical Research, 108(C5), 8084, doi:10.1029/2001JC001147.

Cunningham, S.A. and Pavic, M., 2007. Surface geostrophic currents across the Antarctic circumpolar current in Drake Passage from 1992 to 2004. Progress in Oceanography, 73, 296-310.

Curry, W.B. and Oppo, D.W., 2005. Glacial water mass geometry and the distribution of $\delta^{13}C$ of ΣCO_2 in the western Atlantic Ocean. Paleoceanography, 20, PA1017, doi: 10.1029/2004PA001021.

Das, S.B. and Alley, R.B., 2008. Rise in frequency of surface melting at Siple Dome through the Holocene: Evidence for increasing marine influence on the climate of West Antarctica. Journal of Geophysical Research, 113, D02112, doi:10.1029/2007JD008790.

de Baar, H.J.W., de Jong, J.T.M., Bakker, D.C.E., Löscher, B.M., Veth, C., Bathmann, U., Smetacek, V., 1995. Importance of iron for plankton blooms and carbon dioxide draw down in the Southern Ocean. Nature, 373, 412-415.

De La Mare, W.K., 1997. Abrupt mid-twentieth-century decline in Antarctic sea-ice extent from whaling records. Nature, 389, 57-60.

De La Rocha, C.L., Brzezinski, M.A., DeNiro, M.J., Shemesh, A., 1998. Silicon-isotope composition of diatoms as an indicator of past oceanic change. Nature, 395, 680-683.

Delaygue, G., Masson, V., Jouzel, J., Koster, R.D., Healy, R., 2000. The origin of Antarctic precipitation: a modeling approach. Tellus, 52B, 19-36.

Delaygue, G., Stocker, T.F., Joos, F., Plattner, G.-K., 2003. Simulation of atmospheric radiocarbon during abrupt oceanic circulation changes: trying to reconcile models and reconstructions. Quaternary Science Reviews, 22, 1647-1658.

Delmonte, B., Petit, J.R., Maggi, V., 2002. Glacial to Holocene implications of the new 27,000-year dust record from the EPICA DomeC (EastAntarctica) ice core. Climate Dynamics, 18, 647-660.

Delmonte, B., Petit, J.R., Krinner, G., Maggi, V., Jouzel, J., Udisti, R., 2005. Ice core evidence for secular variability and 200-year dipolar oscillations in atmospheric circulation over East Antarctica during the Holocene. Climate Dynamics, 24, 641-654.

Delmonte, B., Andersson, P.S., Hansson, M., Schöberg, H., Petit, J.R., Basile-Doelsch, I., Maggi, V., 2008. Aeolian dust in East Antarctica (EPICA-Dome C and Vostok): Provenance during glacial ages over the last 800 kyr. Geophysical Research Letters, 35, L07703, doi:10.1029/2008GL033382.

Denis, D., Crosta, X., Zaragosi, S., Romero, O., Martin, B., Mas, V., 2006. Seasonal and sub-seasonal climate changes recorded in laminated diatom ooze sediments, Adélie Land, East Antarctica. The Holocene, 16(8), 1137-1147.

Denis, D., Crosta, X., Schmidt, S., Carson, D.S., Ganeshram, R.S., Renssen, H., Bout-Roumazeilles, V., Zaragosi, S., Martin, B., Cremer, M., Giraudeau, J., 2009. Holocene glacier and deep water dynamics, Adelie Land region, East Antarctica. Quaternary Science Reviews, 28, 1291-1303.

Denton, G.H., Alley, R.B., Comer, G.C., Broecker, W.S., 2005. The role of seasonality in abrupt climate change. Quaternary Science Reviews, 24, 1159-1182.

Denton, G.H., Anderson, R.F., Toggweiler, J.R., Edwards, R.L., Schaefer, J.M., Putnam, A.E., 2010. The last glacial termination. Science, 328, 1652-1656.

de Vernal, A., Rosell-Melé, A., Kucera, M., Hillaire-Marcel, C., Eynaud, F., Weinelt, M., Dokken, T., Kageyama, M., 2006. Comparing proxies for the reconstruction of LGM sea-surface conditions in the northern North Atlantic. Quaternary Science Reviews, 25, 2820-2834.

Dezileau, L., Bareille, G., Reyss, J.L., Lemoine, F.,2000. Evidence for strong sediment redistribution by bottom currents along the southeast Indian ridge. Deep-Sea Research I, 47, 1899-1936.

Diekmann, B., Kuhn, G., Mackensen, A., Petschick, R., Fütterer, D.K., Gersonde, R., Rühlemann, C., Niebler, H.-S., 1999. Kaolinite and chlorite as tracers of modern and late Quaternary deep water circulation in the South Atlantic and adjoining Southern Ocean. In: Fischer, G., Wefer, G. (Eds.), Use of Proxies in Paleoceanography: Examples from the South Atlantic. Springer-Verlag, Berlin, pp. 285-313.

Diekmann, B., Kuhn, G., Rachold, V., Abelmann, A., Brathauer, U., Fütterer, D.K., Gersonde, R., Grobe, H., 2000. Terrigenous sediment supply in the Scotia Sea (Southern Ocean): response to Late Quaternary ice dynamics in Patagonia and on the Antarctic Peninsula. Palaeogeography, Palaeoclimatology, Palaeoecology, 162, 357-387.

Diekmann, B., Fütterer, D.K., Grobe, H., Hillenbrand, C.D., Kuhn, G., Michels, K., Petschick, R., Pirrung, M., 2003. Terrigenous sediment supply in the polar to temperate South Atlantic: Land-ocean links of environmental changes during the late Quaternary. In: Wefer,G., Mulitza,S., Ratmeyer,V. (Eds.). The South Atlantic in the Late Quaternary: Reconstruction of Material Budget and Current Systems. Berlin: Springer, 375-399.

Diekmann, B., 2007. Sedimentary patterns in the late Quaternary Southern Ocean. Deep-Sea Research II, 54, 2350-2366.

Divine, D.V., Koç, N., Isaksson, E., Nielsen, S., Crosta, X., Godtliebsen, F., 2010. Holocene Antarctic climate variability from ice and marine sediment cores: Insights on ocean-atmosphere interaction. Quaternary Science Reviews, 29, 303-312.

Domack, E.W., Leventer, A., Dunbar, R., Taylor, F., Brachfeld, S., and Sjunneskog, C., and ODP Leg 178 Scientific Party, 2001. Chronology of the Palmer Deep site, Antarctic Peninsula: A Holocene palaeoenvironmental reference for the circum-Antarctic. The Holocene, 11(1), 1–9.

Domack, E.W., 2002: A synthesis for site 1098: Palmer Deep. In Barker, P.F., Camerlenghi, A., Acton, G.D. and Ramsay, A.T.S., (eds), Proceedings of the ocean drilling program, scientific results. Ocean Drilling Program, Texas A&M University.

Domack, E.W., Duran, D., Leventer, A., Ishman, S., Doane, S., McCallum, S., Amblas, D., Ring, J., Gilbert, R., Prentice, M., 2005. Stability of the Larsen B ice shelf on the Antarctic Peninsula during the Holocene epoch. Nature, 436, 681-685.

Dong, S., Sprintall, J., Gille, S.T., 2006. Location of the Polar Front from AMSR-E satellite sea surface temperature measurements. Journal of Physical Oceanography, 36, 2075-2089.

Douglass, D.C., Singer, B.S., Kaplan, M.R., Ackert, R.P., Mickelson, D.M., Caffee, M.W., 2005. Evidence of early Holocene glacial advances in southern South America from cosmogenic surface-exposure dating. Geology, 33(3), 237-240.

Douglass, D.C., Singer, B.S., Kaplan, M.R., Mickelson, D.M., Caffee, M.W., 2006. Cosmogenic nuclide surface exposure dating of boulders on last-glacial and late-glacial moraines, Lago Buenos Aires, Argentina: Interpretive strategies and paleoclimate implications. Quaternary Geochronology, 1, 43-58.

Drost, F., Renwick, J., Bhaskaran, B., Oliver, H., McGregor, J., 2007. Features of the zonal mean circulation in the Southern Hemisphere during the Last Glacial Maximum. Journal of Geophysical Research, 112, D02101, doi: 10.1029/2005JD006811.

Druffel, E.R.M., Robinson, L.F., Griffin, S., Halley, R.B., Southon, J.R., Adkins, J.F., 2008. Low reservoir ages for the surface ocean from mid-Holocene Florida corals. Paleoceanography, 23, PA2209, doi:10.1029/2007PA001527.

Edwards, R. and Sedwick, P., 2001. Iron in East Antarctic snow: Implications for atmospheric iron deposition and algal production in Antarctic waters. Geophysical Research Letters, 28(20), 3907-3910.

Elsig, J., Schmitt, J., Leuenberger, D., Schneider, R., Eyer, M., Leuenberger, M., Joos, F., Fischer, H., Stocker, T.F., 2009. Stable isotope constraints on Holocene carbon cycle changes from an Antarctic ice core. Nature, 461, 507-510.

Epica community members, 2004. Eight glacial cycles from an Antarctic ice core. Nature, 429, 623-628.

Epica community members, 2006. One-to-one coupling of glacial climate variability in Greenland and Antarctica. Nature, 444, 195-198.

Esper, O. and Gersonde, R., 2011. Quaternary surface water temperature estimations: New diatom transfer functions for the Southern Ocean. In prep.

Fahrbach, E., Rohardt, G., Schroeder, M., Strass, V., 1994. Transport and structure of the Weddell Gyre. Annals of Geophysics, 12, 840-855.

Fairbanks, R.G., Mortlock, R.A., Chiu, T.-C., Cao, L., Kaplan, A., Guilderson, T.P., Fairbanks, T.W., Bloom, A.L., Grootes, P.M., Nadeau, M.-J., 2005. Radiocarbon calibration curve spanning 0 to 50,000 years BP based on paired $^{230}Th/^{234}U/^{238}U$ and ^{14}C dates on pristine corals. Quaternary Science Reviews, 24, 1781-1796.

Fischer, G., Fütterer, D., Gersonde, R., Honjo, S., Ostermann, D., Wefer, G., 1988. Seasonal variability of partical flux in the Weddell Sea and its relation to ice cover. Nature, 335, 426-428.

Fischer, G., Gersonde, R., Wefer, G., 2002. Organic carbon, biogenic silica and diatom fluxes in the Northern Seasonal Ice Zone in the Polar Front Region in the Southern Ocean (Atlantic Sector): Interannual variation and changes in composition. Deep Sea Research II, 49, 1721-1745.

Fischer, H., Fundel, F., Ruth, U., Twarloh, B., Wegner, A., Udisti, R., Becagli, S., Castellano, E., Morganti, A., Severi, M., Wolff, E., Littot, G., Röthlisberger, R., Mulvanev, R., Hutterli, M.A., Kaufmann, P., Federer, U., Lambert, F., Bigler, M., Hansson, M., Jonsell, U., de Angelis, M., Boutron, C., Siggaard-Andersen, M.-L., Steffensen, J.P., Barbante, C., Gaspari, V., Gabrielli, P., Wagenbach, D., 2007. Reconstruction of millennial changes in dust emission, transport and regional sea ice coverage using the deep EPICA ice cores from the Atlantic and Indian Ocean sector of Antarctica. Earth and Planetary Science Letters, 260, 340-354.

Fodvik, A., Gammelsrod, T., Osterhus, S., et al., 2004. Ice shelf water overflow and bottom water formation in the southern Weddell Sea. Journal of Geophysical Research, 109, C02015, doi: 10.1029/2003JC002008.

Fogwill, C.J. and Kubik, P.W., 2005. A glacial stage spanning the Antarctic Cold Reversal in Torres del Paine (51°S), Chile, based on preliminary cosmogenic exposure ages. Geografiska Annaler, 87A(2), 403-408.

Foster, T.D. and Middleton, J.H., 1980. Bottom water formation in the western Weddell Sea. Deep-Sea Res. 27, 367-381.

Frank, M., Gersonde, R., Rutgers van der Loeff, M., Bohrmann, G., Nürnberg, C.C., Kubik, P.W., Suter, M. and Mangini, A., 2000. Similar glacial and interglacial export bioproductivity in the Atlantic sector of the

Southern Ocean: Multiproxy evidence and implications for glacial atmospheric CO_2. Paleoceanography, 15, 642-658.

Franke, J., Paul, A., Schulz, M., 2008. Modeling variations of marine reservoir ages during the last 45000 years. Climate of the Past, 4, 125-136.

Fryxell, G.A. and Kendrick, G.A., 1988. Austral spring microalgae across the Weddell Sea ice edge: spatial relationships found along a northward transect during AMERIEZ 83. Deap-Sea Research, 35, 1-20.

Geibert, W., Rutgers van der Loeff, M.M., Usbeck, R., Gersonde, R., Kuhn, G., Seeberg-Elverfeldt, J., 2005. Quantifying the opal belt in the Atlantic and southeast Pacific sector of the Southern Ocean by means of ^{230}Th normalization. Global Biogeochemical Cycles, 19, GB4001, doi: 10.1029/2005GB002465.

Gersonde, R. and Wefer, G., 1987. Sedimentation of biogenic siliceous particles in Antarctic waters from the Atlantic sector. Marine Micropaleontology 11, 311-332.

Gersonde, R. and Barcena, M.A., 1998. Revision of the upper Pliocene-Pleistocene diatom biostratigraphy for the northern belt of the Southern Ocean. Micropaleontology, 44(1), 84-98.

Gersonde, R., Hodell, D., Blum, P., (ed), et al., 1999. Proceedings of the Ocean Drilling Program, Initial Reports, Leg 177. College Station, Texas (ODP), doi: 10.2973/odp.proc.ir.177.1999.

Gersonde, R. and Zielinski, U., 2000. The reconstruction of late Quaternary Antarctic sea-ice distribution—the use of diatoms as a proxy for sea-ice. Palaeogeography, Palaeoclimatology, Palaeoecology, 162, 263-286.

Gersonde, R., Abelmann, A., Brathauer, U., Becquey, S., Bianchi, C., Cortese, G., Grobe, H., Kuhn, G., Niebler, H.-S., Segl, M., Sieger, R., Zielinski, U., Fütterer, D.K., 2003a. Last glacial sea surface temperatures and sea-ice extent in the Southern Ocean (Atlantic-Indian sector): A multiproxy approach. Paleoceanography, 18(3), 1061, doi: 10.1029/2002PA000809.

Gersonde, R., Abelmann, A., Cortese, G., Becquey, S., Bianchi, C., Brathauer, U., Niebler, H.-S., U. Zielinski, and Pätzold, J. 2003b. The late Pleistocene South Atlantic and Southern Ocean surface waters - A summary of time-slice and time series.studies. In Wefer G, Mulitza S, Ratmeyer V (ed), The South Atlantic in the Late Quaternary: reconstruction of Material Budget and Current Systems, Springer Berlin, pp. 499-529.

Gersonde, R., Crosta, X., Abelmann, A., Armand, L., 2005. Sea-surface temperature and sea ice distribution of the Southern Ocean at the EPILOG Last Glacial Maximum – a circum-Antarctic view based on siliceous microfossil records. Quaternary Science Reviews, 24, 869–896.

Gherardi, J.-M., Labeyrie, L., Nave, S., Francois, R., McManus, J.F., Cortijo, E., 2009. Glacial-interglacial circulation changes inferred from ^{231}Pa/^{230}Th sedimentary record in the North Atlantic region. Paleoceanography, 24, PA2204, doi: 10.1029/2008PA001696.

Gille, S.T., 1994. Mean sea surface height of the Antarctic Circumpolar Current from Geosat data: method and application. Journal of Geophysical Research, 99, 18255-18273.

Gille, S. T., 2002. Warming of the Southern Ocean since the 1950s. Science, 295, 1275-1277.

Gille, S. T., 2008. Decadal-scale temperature trends in the southern hemisphere ocean. Journal of Climate, 21, doi: 10.1175/2008JCLI2131.1.

Gloersen, P. and Campbell, W.J., 1988. Variations in the Arctic, Antarctic, and Global Sea Ice Covers During 1978–1987 as Observed With the Nimbus 7 Scanning Multichannel Microwave Radiometer. Journal of Geophysical Research, 93, C9, 10666-10674.

Gloersen, P. and Campbell, W.J., 1991. Recent variations in Arctic and Antarctic sea-ice covers. Nature, 352, 33-36.

Goldstein, S.J., Lea, D.W., Chakraborty, S., Kashgarian, M., Murrell, T., 2001. Uranium-series and radiocarbon geochronology of deep-sea corals: implications for Southern Ocean ventilation rates and the oceanic carbon cycle. Earth and Planetary Science Letters, 193(1-2), 167-182.

Gonzalez, H.E., 1992. The distribution and abundance of krill faecal material and oval pellets in the Scotia and Weddell Seas (Antarctica) and their role in particle flux. Polar Biology, 12, 81-91.

Gordon, J.E. and Harkness, D.D., 1992. Magnitude and geographic variation of the radiocarbon content in Antarctic marine life: Implications for reservoir corrections in radiocarbon dating. Quaternary Science Reviews, 11, 697-708.

Grimm, K.A., Lange, C.B., Gill, A.S., 1996. Biological forcing of hemipelagic sedimentary laminae: evidence from ODP site 893, Santa Barbara Basin, California. Journal of Sedimentary Research, 66(3), 613-624.

Grimm, K.A., Lange, C.B., Gill, A.S., 1997. Self-sedimentation of phytoplankton blooms in the geologic record. Sedimentary Geology, 110, 151-161.

Guillou, H., Singer, B.S., Laj, C., et al., 2004. On the age of the Laschamp geomagnetic excursion. Earth and Planetary Science Letters, 227, 331-343.

Guyodo, Y. and Valet, J.-P., 1999. Global changes in intensity of the earth's magnetic field during the past 800 kyr. Nature, 399, 249-252.

Hajdas, I., Lowe, D.J., Newnham, R.M., Bonani, G., 2006. Timing of the late-glacial climate reversal in the Southern Hemisphere using high-resolution radiocarbon chronology for Kaipo bog, New Zealand. Quaternary Research, 65, 340-345.

Hall, I.R., McCave, N., Shackleton, N.J., Weedon, G.P., Harris, S.E., 2001. Intensified deep Pacific inflow and ventilation in Pleistocene glacial times. Nature, 412, 809-812.

Hall, B.L., 2009. Holocene glacial history of Antarctica and the sub-Antarctic islands. Quaternary Science Reviews, 28, 2213-2230.

Hays, J.D., 1965. Quaternary sediments of the Antarctic Ocean. Progress in Oceanography, 4, 117-131.

Hays, J.D., Imbrie, J., Shackleton, N.J., 1976. Variations in the earth's orbit: pacemaker of the ice ages. Science, 194, 1121-1132.

Hein, A.S., Hulton, N.R.J., Dunai, T.J., Sugden, D.E., Kaplan, M.R., Xu, S., 2010. The chronology of the Last Glacial Maximum and deglacial events in central Argentine Patagonia. Quaternary Science Reviews, 29, 1212-1227.

Hellmer, H.H., 2004. Impact of Antarctic ice shelf basal melting on sea ice and deep ocean properties. Geophysical Research Letters, 31, L10307, doi:10.1029/2004GL019506.

Hemming, S.R., van de Flierdt, Goldstein, S.L., Franzese, A.M., Roy, M., Gastineau, G., Landrot, G., 2007. Strontium isotope tracing of terrigenous sediment dispersal in the Antarctic Circumpolar Current: Implications for constraining frontal positions. Geochemistry Geophysics Geosystems, 8, Q06N13, doi: 10.1029/2006GC001441.

Heroy, D.C. and Anderson, J.B., 2005. Ice-sheet extent of the Antarctic Peninsula region during the Last Glacial Maximum (LGM) – insights from glacial geomorphology. Geological Society of America Bulletin, 117, 1497–512.

Heroy, D.C. and Anderson, J.B., 2007. Radiocarbon constraints on Antarctic Peninsula Ice Sheet retreat following the Last Glacial Maximum (LGM). Quaternary Science Reviews, 26, 3286-3297.

Heywood, K.J., Garabato, A.C.N., Stevens, D.P., 2002. High mixing rates in the abyssal Southern Ocean. Nature, 415, 1011-1014.

Hillenbrand, C.-D. and Cortese, G., 2006. Polar stratification: A critical view from the Southern Ocean. Palaeogeography, Palaeoclimatology, Palaeoecology 242, 240-252.

Hillenbrand, C.-D., Moreton, S.G., Caburlotto, A., et al., 2008. Volcanic time-markers for Marine Isotopic Stages 6 and 5 in Southern Ocean sediments and Antarctic ice cores: implications for tephra correlations between palaeoclimatic records. Quaternary Science Reviews, 27, 518-540.

Hillenbrand, C.-D., Smith, J.A., Kuhn, G., Esper, O., Gersonde, R., Larter, R.D., Maher, B., Moreton, S.G., Shimmield, T.M., Korte, M., 2009. Age assignment of a diatomaceous ooze deposited in the western Amundsen Sea Embayment after the Last Glacial Maximum. Journal of Quaternary Science, ISSN 0267-8179.

Hodell, D.A., Kanfoush, S.L., Shemesh, A., Crosta, X., Charles, C.D., Guilderson, T.P., 2001. Abrupt cooling of Antarctic surface waters and sea ice expansion in the South Atlantic sector of the Southern Ocean at 5000 cal yr B.P. Quaternary Research, 56, 191-198.

Hodgson, D.A., Dyson, C.L., Jones, V.J., Smellie, J.L., 1998. Tephra analysis of sediments from Midge Lake (South Shetland Islands) and Sombre Lake (South Orkney Islands), Antarctica. Antarctic Science, 10, 13-20.

Hofmann, A., 1999. Kurzfristige Klimaschwankungen im Scotiameer und Ergebnisse zur Kalbungsgeschichte der Antarktis wahrend der letzten 200.000 Jahre. PhD thesis, Institut für Polar und Meeresforschung, Bremerhaven, Berichte zu Polarforschung, 345, 1-162.

Howe, J.A., Livermore, R.A., Maldonado, A., 1998. Mudwave activity and current-controlled sedimentation in the Powell Basin, northern Weddell Sea, Antarctica. Marine Geology, 149, 229-241.

Hughen, K.A., Lehman, S., Southon, J., Overpeck, J., Marchal, O., Herring, C., Turnbull, J., 2004a. ^{14}C activity and global carbon cycle changes over the past 50,000 years. Science, 303, 202-207.

Hughen, K.A., Baillie, M.G.L., Bard, E., Beck, J.W., Bertrand, C.J.H., Blackwell, P.G., Buck, C.E., Burr, G.S., Cutler, K.B., Damon, P.E., Edwards, R.L., Fairbanks, R.G., Friedrich, M., Guilderson, T.P., Kromer, B., McCormac, G., Manning, S., Ramsey, C.B., Reimer, P.J., Reimer, R.W., Remmele, S., Southon, J.R., Stuiver, M., Talamo, S., Taylor, F.W., van der Plicht, J., Weyhenmeyer, C.E., 2004b. Marine04 marine radiocarbon age calibration, 0-26 cal kyr BP. Radiocarbon, 46(3), 1059-1086.

Hughen, K.A., 2006a. Cosmogenic isotope ^{14}C: Production and carbon cycle. PAGES News, 14(3), 6-7.

Hughen, K., Southon, J., Lehman, S., Bertrand, C., Turnbull, J., 2006b. Marine-derived ^{14}C calibration and activity record for the past 50,000 years updated from the Cariaco Basin. Quaternary Science Reviews, 25, 3216-3227.

Huhn, O., Hellmer, H.H., Rhein, M., Rodehacke, C., Roether, W., Schodlok, M.P., Schröder, M., 2008. Evidence of deep- and bottom-water formation in the western Weddell Sea. Deep-Sea Research II, 55, 1098-1116.

Imbrie, J. and Kipp, N.G., 1971. A new micropaleontological method for Quantitative Paleoclimatology: Application to a late Pleistocene Caribbean Core. In: Turekian, K.K. (Ed.), The Late Cenozoic Glacial Ages. Yale University Press, New York, Conn., 71-181.

Jacot Des Combes, H., Esper, O., De La Rocha, C.L., Abelmann, A., Gersonde, R., Yam, R., Shemesh, A., 2008. Diatom d13C, d15N, and C/N since the Last Glacial Maximum in the Southern Ocean: Potential impact of species composition, Paleoceanography, 23, PA4209, doi:10.1029/2008PA001589.

Jansen, E., et al., 2007. Chapter 6, Paleoclimate, Intergovernmental Panel on Climate Change (IPCC) report 2007, in Climate Change 2007 – The Physical Science Basis. Cambridge University Press, Cambridge. 433-497.

Joos, F., Gerber, S., Prentice, I.C., Otto-Bliesner, B.L., Valdes, P.J., 2004. Transient simulations of Holocene atmospheric carbon dioxide and terrestrial carbon since the Last Glacial Maximum. Global Biogeochemical cycles, 18, GB2002, doi: 10.1029/2003GB002156.

Jordan, R.W. and Pudsey, C.J., 1992. High-resolution diatom stratigraphy of Quaternary sediments from the Scotia Sea. Marine Micropaleontology, 19, 201-237.

Jouzel, J., Masson-Delmotte, V., Cattani, O., Dreyfus, G., Falourd, S., Hoffmann, G., Minster, B., Nouet, J., Barnola, J.M., Chappellaz, J., Fischer, H., Gallet, J.C., Johnsen, S., Leuenberger, M., Loulergue, L., Luethi, D., Oerter, H., Parrenin, F., Raisbeck, G., Raynaud, D., Schilt, A., Schwander, J., Selmo, E., Souchez, R., Spahni, R., Stauffer, B., Steffensen, J.P., Stenni, B., Stocker, T.F., Tison, J.L., Werner, M., Wolff, E.W., 2007. Orbital and millennial Antarctic climate variability over the Past 800,000 years. Science, 317, 793-796.

Kaczmarska, I., Barbrick, N.E., Ehrman, J.M., Cant, G.P., 1993. Eucampia index as an indicator of the Late Pleistocene oscillations of the winter sea-ice extent at the ODP Leg 119 Site 745B at the Kerguelen Plateau. Hydrobiologia, 269/270, 103-112.

Kaiser, J., Lamy, F., Hebbeln, D., 2005. A 70-kyr sea surface temperature record off southern Chile (Ocean Drilling Program Site 1233). Paleoceanography, 20 PA4009, doi: 10.1029/2005PA001146.

Kaiser, J., Lamy, F., Arz, H.W., Hebbeln, D., 2007. Dynamics of the millennial-scale sea surface temperature and Patagonian Ice Sheet fluctuations in southern Chile during the last 70 kyr (ODP Site 1233). Quaternary International, 161, 77-89.

Kaplan, M.R., Fogwill, C.J., Sugden, D.E., Hulton, N., Kubik, P.W., Freeman, S., 2008. Southern Patagonian glacial chronology for the Last Glacial period and implications for Southern Ocean climate. Quaternary Science Reviews, 27, 284-294.

Kaspi, Y., Sayag, R., Tzipermann, E., 2004. A "triple sea-ice state" mechanism for the abrupt warming and synchronous ice sheet collapses during Heinrich events. Paleoceanography 19, PA3004, doi: 10.1029/2004PA001009.

Kawamura, K., Parrenin, F., Lisiecki, L., Uemura, R., Vimeux, F., Severinghaus, J.P., Hutterli, M.A., Nakazawa, T., Aoki, S., Jouzel, J., Raymo, M.E., Matsumoto, K., Nakata, H., Motoyama, H., Fujita, S., Goto-Azuma, K., Fujii, Y., Watanabe, O., 2007. Northern hemisphere forcing of climatic cycles in Antarctica over the past 360,000 years. Nature, 448, 912-916.

Keeling, R.F. and Stephens, B.B., 2001. Antarctic sea ice and the control of Pleistocene climate instability. Paleoceanography, 16(1), 112-131.

Keller, R., Domack, E.W., Drake, A., 2003. Potential for tephrochronology of marine sediment cores from Bransfield Strait and the Northwestern Weddell Sea. XVI INQUA Congress. Reno, USA.

Kemp, A.E.S., Pike, J., Pearce, R.B., Lange, C.B., 2000. The "Fall dump" – a new perspective on the role of a "shade flora" in the annual cycle of diatom production and export flux. Deep-Sea Research II, 47, 2129-2154.

Kirschvink, J.L., The least-squares line and plane and the analysis of paleomagnetic data: examples from Siberia and Morocco. Geoph. J. Royal Astr. Soc. 62, 699-718.

Kohfeld, K.E., Le Quéré, C., Harrison, S.P., Anderson, R.F., 2005. Role of marine biology in glacial-interglacial CO2 cycles. Science, 308, 74-78.

Knorr, G. and Lohmann, G., 2003. Southern Ocean origin for the resumption of Atlantic thermohaline circulation during deglaciation. Nature, 424, 532-536.

Knorr, G. and Lohmann, G., 2004. The Southern Ocean as the flywheel of the oceanic conveyor belt circulation. PAGES News, 12, 11-13.

Knudsen, M.F., Riisager, P., Donadini, F., Snowball, I., Muscheler, R., Korhonen, K., Pesonen, L.J., 2008. Variations in the geomagnetic dipole moment during the Holocene and the past 50 kyr. Earth and Planetary Science Letters, 272, 319-329.

Kohfeld, K.E., Le Quéré, C., Harrison, S.P., Anderson, R.F., 2005. Role of marine biology in glacial-interglacial CO_2 cycles. Science, 308, 74-78.

Kohno, M., Fuji, Y., Hirata, T., 2004. Chemical composition of volcanic glasses in visible tephra layers found in a 2503 m deep ice core from Dome Fuji, Antarctica. Annals of Glaciology, 39, 576-584.

Kuhn, G. and Diekmann, B., 2002. Late Quaternary variability of ocean circulation in the southeastern South Atlantic inferred from the terrigenous sediment record of a drift deposit in the southern Cape Basin (ODP Site 1089). Palaeogeography, Palaeoclimatology, Palaeoecology, 182, 287-303.

Kunz-Pirrung, M., Gersonde, R., Hodell, D.A., 2002. Mid-Brunhes century-scale diatom sea surface temperature and sea ice records from the Atlantic sector of the Southern Ocean (ODP Leg 177, sites 1093, 1094 and core PS2089-2). Palaeogeography, Palaeoclimatology, Palaeoecology, 182, 305-328.

Labeyrie, L.D., Pichon, J.J., Labracherie, M., Ippolito, P., Duprat, J., Duplessy, J.C., 1986. Melting history of Antarctica during the past 60,000 years. Nature, 322, 701-706.

Laepple, T., Werner, M., Lohmann, G., 2011. Synchronicity of Antarctic temperatures and local solar insolation on orbital time scales. Nature, 471, 91-94.

Laj, C., Kissel, C., Mazaud, A., Michel, E., Muscheler, R., Beer, J., 2002. Geomagnetic field intensity, North Atlantic Deep Water circulation and atmospheric $\Delta^{14}C$ during the last 50 kyr. Earth and Planetary Science Letters, 200, 177-190.

Laj, C., Kissel, C., Beer, J., 2004. High resolution global paleointensity stack since 75 kyr (GLOPIS-75) calibrated to absolute values. In: Channell, J.E.T., Kent, D.V., Lowrie, W., Meert, J.G. (Eds), Timescales of the Paleomagnetic Field, AGU Geophysical Monograph, 145, 255-265.

Lambert, F., Delmonte, B., Petit, J.R., Bigler, M., Kaufmann, P.R., Hutterli, M.A., Stocker, T.F., Ruth, U., Steffensen, J.P., Maggi, V., 2008. Dust-climate couplings over the past 800,000 years from the EPICA Dome C ice core. Nature, 452, 616-619.

Lamy, F., Rühlemann, C., Hebbeln, D., Wefer, G., 2002. High- and low-latitude climate control on the position of the southern Peru-Chile Current during the Holocene. Paleoceanography, 17, 1028, doi: 10.1029/2001PA000727.

Lamy, F., 2006. Postglacial South Pacific. Encyclopedia of Quaternary Science, 1855-1866.

Lamy, F., Kaiser, J., Arz, H.W., Hebbeln, D., Ninnemann, U., Timm, O., Timmermann, A., Toggweiler, J.R., 2007. Modulation of the bipolar seesaw in the Southeast Pacific during Termination 1. Earth and Planetary Science letters, 259, 400-413.

Lamy, F., Kilian, R., Arz, H.W., Francois, J.-P., Kaiser, J., Prange, M., Steinke, T., 2010. Holocene changes in the position and intensity of the southern westerly wind belt. Nature Geoscience, 3, 695-699.

Lawver, L.A., Gahagan, L.M., Coffin, M.F., 1992. The development of paleoseaways around Antarctica. In: Kennett, J.P., Warnke, D.A. (Eds.), The Antarctic Paleoenvironment: A Perspective on Global Change, vol. 56. AGU Antarctic Research Series, 7-30.

Lawver, L.A. and Gahagan, L.M., 2003. Evolution of Cenozoic seaways in the circum-Antarctic region. Palaeogeography, Palaeoclimatology, Palaeoecology, 198, 11-38.

Lemieux-Dudon, B., Blayo, E., Petit, J.-R., Waelbroeck, C., Svensson, A., Ritz, C., Barnola, J.-M., Narcisi, B.M., Parrenin, F., 2010. Consistent dating for Antarctic and Greenland ice cores. Quaternary Science Reviews, 29, 8-20.

Leventer, A., 1991. Sediment trap diatom assemblages from the northern Antarctic Peninsula region. Deep-Sea Research Part A, 38 (8-9), 1127-1143.

Leventer, A., Domack, E.W., Ishman, S.E., Brachfeld, S., McClennen, C.E., Manley, P., 1996. Productivity cycles of 200–300 years in the Antarctic Peninsula region: Understanding linkages among the sun, atmosphere, oceans, sea ice, and biota. GSA Bulletin, 108, 1626-1644.

Leventer, A., Domack, E., Barkoukis, A., McAndrews, B., Murray, J., 2002. Laminations from the Palmer Deep: A diatom-based interpretation. Paleoceanography, 17(2), 8002, doi: 10.1029/2001PA000624.

Licht, K.J., Cunningham, W.L., Andrews, J.T., Domack, E.W., Jennings, A.E., 1998. Establishing chronologies from acid-insoluble organic ^{14}C dates on Antarctic (Ross Sea) and Arctic (North Atlantic) marine sediments. Polar Research, 17, 203-216.

Lifton, N., Smart, D.F., Shea, M.A., 2008. Scaling time-integrated in situ cosmogenic nuclide production rates using a continuous geomagnetic model. Earth and Planetary Science Letters, 268, 190-201.

Lisiecki, L.E. and Raymo, M.E., 2005. A Pliocene-Pleistocene stack of 57 globally distributed benthic $\delta^{18}O$ records. Paleoceanography, 20, PA1003, doi: 10.1029/2004PA001071.

Livermore, R., McAddo, D., Marks, K., 1994. Scotia Sea tectonics from high-resolution satellite gravity. Earth and Planetary Science Letters, 123, 255-268.

Locarnini, R.A., Whitworth, T., III, Nowlin, W.D.J., 1993. The importance of the Scotia Sea on the out flow of Weddell Sea Deep Water. Journal of Marine Research, 51, 135-153.

Lourantou, A., Lavrič, J.V., Köhler, P., Barnola, J.-M., Paillard, D., Michel, E., Raynaud, D., Chappellaz, J., 2010. Constraint of the CO_2 rise by new atmospheric carbon isotopic measurements during the last deglaciation. Global Biogeochemistry Cycles, 24, GB2015, doi: 10.1029/2009GB003545.

Lund, S., Stoner, J.S., Channell, J.E.T., Acton, G., 2006. A summary of Brunhes paleomagnetic variability recorded in Ocean Drilling Program cores. Physics of the Earth and Planetary Interiors, 156, 194-204.

Macri, P., Sagnotti, L., Lucchi, R.G., Rebesco, M., 2006. A stacked record of relative geomagnetic paleointensity for the past 270 kyr from the western continental rise of the Antarctic Peninsula. Earth and Planetary Science Letters, 252, 162-179.

Mackensen, A. 2004. Changing Southern Ocean palaeocirculation and effects on global climate. Antarctic Science, 16, 369-386.

Macri, P., Sagnotti, L., Lucchi, R.G., Rebesco, M., 2006. A stacked record of relative geomagnetic paleointensity for the past 270 kyr from the western continental rise of the Antarctic Peninsula. Earth and Planetary Science Letters, 252, 162-179.

Macri, P., Sagnotti, L., Dinares-Turell, J., Caburlotto, A., 2010. Relative geomagnetic paleointensity of the Brunhes Chron and the Matuyama-Brunhes precursor as recorded in sediment core from Wilkes Land Basin (Antarctica). Physics of the Earth and Planetary Interiors, 179, 72-86.

Maddison, E.J., Pike, J., Leventer, A., Dunbar, R., Brachfeld, S., Domack, E.W., Manley, McClennen, C., 2006. Post-glacial seasonal diatom record of the Mertz Glacier Polynya, East Antarctica. Marine Micropaleontology, 60, 66-88.

Maher, B.A., 1988. Magnetic properties of some synthetic sub-micron magnetites. Geophysical Journal, 94, 83-96.

Maher, B.A., Prospero, J.M., Mackie, D., Gaiero, D., Hesse, P.P., Balkanski, Y., 2010. Global connections between aeolian dust, climate and ocean biogeochemistry at the present day and at the last glacial maximum. Earth-Science Reviews, 99, 61-97.

Maldonado, A., Barnolas, A., Bohoyo, F., et al., 2003. Contourite deposits in the central Scotia Sea: the importance of the Antarctic Circumpolar Current and the Weddell Gyre flows. Palaeogeography, Palaeoclimatology, Palaeoecology, 198, 187-221.

Marchal, O., 2005. Optimal estimation of atmospheric ^{14}C production over the Holocene: paleoclimate implications. Climate Dynamics, 24, 71-88.

Marchitto, T.M. and Broecker, W.S., 2006. Deep water mass geometry in the glacial Atlantic Ocean: A review of constraints from the paleonutrient proxy Cd/Ca. Geochemistry, Geophysics, Geosystem, 7, Q12003, doi: 10.1029/2006GC001323.

Margari, V., Skinner, L.C., Tzedakis, P.C., Ganopolski, A., Vautravers, M., Shackleton, N.J., 2010. The nature of millennial-scale climate variability during the past two glacial periods. Nature Geoscience, 3, 127-131.

Margo members, 2009. Constraints on the magnitude and patterns of ocean cooling at the Last Glacial Maximum. Nature Geoscience 2, 127-132.

Markgraf, V., Dodson, J.R., Kershaw, A.P., McGlone, M.S., Nicholls, N., 1992. Evolution of late Pleistocene and Holocene climates in the circum-South Pacific land areas. Climate Dynamics, 6, 193-211.

Martínez-Méndez, G., Molyneux, E.G., Hall, I.R., Zahn, R., 2009. Variable water column structure of the South Atlantic on glacial-interglacial time scales. Quaternary Science Reviews, 28, 3379-3387.

Martinson, D.G., Pisias, N.G., Hays, J.D., Imbrie, J., Moore Jr., T.C., Shackleton, N.J., 1987. Age dating and the orbital theory of the ice ages: development of a high-resolution 0 to 300,000-year chronostratigraphy. Quaternary Research, 27, 1-29.

Masson, V., Vimeux, F., Jouzel, J., Morgan, V., Delmotte, M., Ciais, P., Hammer, C., Johnsen, S., Lipenkov, V.Y., Mosley-Thompson, E., Petit, J.-R., Steig, E.J., Stievenard, N., Vaikmae, R., 2000. Holocene Climate Variability in Antarctica Based on 11 Ice-Core Isotopic Records. Quaternary Research, 54, 348-358.

Masson-Delmotte, V., Stenni, B., Jouzel, J., 2004. Common millennial-scale variability of Antarctic and Southern Ocean temperatures during the past 5000 years reconstructed from the EPICA Dome C ice core. Holocene, 14, 145-151.

Mayewski, P., Rohling, E., Stager, C., Karlén, W., Maasch, K.A., Meeker, L.D., Meyerson, E.A., Gasse, F., van Kreveld, S., Holmgren, K., Lee-Thorp, J., Rosqvist, G., Rack, F., Staubwasser, M., Schneider, R.R., Steig, E.J., 2004. Holocene climate variability. Quaternary Research 62, 243-255.

Mayr, C., Wille, M., Haberzettl, T., Fey, M., Janssen, S., Lücke, A., Ohlendorf, C., Oliva, G., Schäbitz, F., Schleser, G.H., Zolitschka, B., 2007. Holocene variability of the Southern Hemisphere westerlies in Argentinean Patagonia (52°S). Quaternary Science Reviews, 26, 579-84.

Mazaud, A., Sicre, M.A., Ezat, U., Pichon, J.J., Duprat, J., Laj, C., Kissel, C., Beaufort, L., Michel, E., Turon, J.L., 2002. Geomagnetic-assisted stratigraphy and sea surface temperature changes in core MD94-103 (Southern Indian Ocean): possible implications for North–South climatic relationships around H4. Earth and Planetary Science Letters, 201, 159-170.

Mazaud, A., Kissel, C.,Laj, C., Sicre, A., Michel, E., 2007. Variations of the ACC-CDW during MIS3 traced by magnetic grain deposition in mid latitude South Indian Ocean cores: connections with the northern hemisphere and with central Antarctica. Geochem. Geophys. Geosyst., 8, Q05012, doi:10.1029/2006GC001532.

McCulloch, R.D. and Davies, S.J. 2001: Late-glacial and Holocene palaeoenvironmental change in the central Strait of Magellan, southern Patagonia. Palaeogeography, Palaeoclimatology, Palaeoecology, 173, 143-73.

McCulloch, R.D., Fogwill, C.J., Sugden, D.E., Bentley, M.J., Kubik, P.W., 2005. Chronology of the last glaciations in central Strait of Magellan and Bahia Inutil, southernmost South America. Geografiska Annaler, 87A, 289-312.

McGlone, M.S., 2002. A Holocene and latest Pleistocene pollen record from Lake Poukawa, Hawke's Bay, New Zealand. Global and Planetary Change, 33, 283-299.

McGlone, M.S., Turney, C.S.M., Wilmshurst, J.M., Renwick, J., Pahnke, K., 2010. Divergent trends in land and ocean temperature in the Southern Ocean over the past 18,000 years. Nature Geoscience, 3, 622-626.

McGregor, H.V., Gagan, M.K., McCulloch, M.T., Hodge, E., Mortimer, G., 2008. Mid-Holocene variability in the marine ^{14}C reservoir age for northern coastal Papua New Guinea. Quaternary Geochronology, 3, 213-225.

McManus, J.F., Francois, R., Gherardi, J.-M., Keigwin, L.D., Brown-Leger, S., 2004. Collapse and rapid resumption of Atlantic meridional circulation linked to deglacial climate change. Nature, 428, 834-837.

McMillan, D.G., Constable, C.G., 2006. Limitations in correlation of regional relative geomagnetic paleointensity. Geochemistry, Geophysics, Geosystems, 7, Q09009, doi: 10.1029/2006GC001350.

Meredith, M.P., Locarnini, R.A., van Scoz, K.A., Watson, A.J., Heywood, K.J., King, B.A., 2000. On the sources of Weddell Gyre Antarctic Bottom Water. Journal of Geophysical Research, 105(C1), 1093-1104.

Molosa, A.B. and Anderson, J.B., 2006. Expansion and rapid retreat of the West Antarctic Ice Sheet in eastern Ross Sea: possible consequence of over-extended ice streams? Quaternary Science Reviews, 25, 2177-2196.

Monnin, E., Indermühle, A., Dällenbach, A., Flückiger, J., Stauffer, B., Stocker, T., Raynaud, D., Barnola, J.-M., 2001. Atmospheric CO_2 concentrations over the last glacial termination. Science, 291, 112-114.

Moore, J.K., Abbott, M.R. and Richman, J.G., 1997. Variability in the location of the Antarctic Polar Front (90˚-20˚W) from satellite sea surface temperature data. Journal of Geophysical Research, 102(C13), 27825-27833.

Moore, J.K., Abbott, M.R., Richman, J.G., 1999. Location and dynamics of the Antarctic Polar Front from satellite sea surface temperature data. Journal of Geophysical Research, 104(C2), 3059-3073.

Moore, J.K., Abbott, M.R., Richmann, J.G., Nelson, D.M., 2000. The Southern Ocean at the last glacial maximum: A strong sink for atmospheric carbon dioxide. Global Biogeochemical Cycles, 14(1), 455-475.

Moreno, P.I., and León, A.L., 2003. Abrupt vegetation changes during the Last Glacial to Holocene transition in mid-latitude South America, Journal of Quaternary Science, 18, 787-800.

Moreton, S.G. and Smellie, J.L., 1998. Identification and correlation of distal tephra layers in deep-sea sediment cores, Scotia Sea, Antarctica. Annals of Glaciology, 27, 285–289.

Moreton, S.G., 1999. Quaternary tephrochronology of the Scotia Sea and Bellingshausen Sea, Antarctica. Ph.D. Thesis, British Antarctic Survey, Cambridge, UK, 191pp.

Morse, D.L., Waddington, E.D. and Steig, E.J., 1998. Ice age storm trajectories inferred from radar stratigraphy at Taylor Dome, Antarctica. Geophysical Research Letters, 25(17), 3383-3386.

Morley, J.J. and Hays, J.D., 1979. *Cycladophora davisiana*: a stratigraphic tool for Pleistocene North Atlantic and interhemispheric correlation. Earth and Planetary Science Letters, 44, 383-389.

Mosseri, J., Quéguiner, B., Armand, L., Cornet-Barthaux, V., 2008. Impact of iron on silicon utilization by diatoms in the Southern Ocean: A case study of Si/N cycle decoupling in a naturally iron-enriched area. Deep-Sea Research II, 55, 801-819.

Mudelsee, M., 2001. The phase relations among atmospheric CO2 content, temperature and global ice volume over the past 420 ka. Quaternary Science Reviews, 20, 583-589.

Muscheler, R., Beer, J., Wagner, G., Laj, C., Kissel, C., Raisbeck, G.M., Yiou, F., Kubik, P.W., 2004. Changes in the carbon cycle during the last deglaciation as indicated by the comparison of ^{10}Be and ^{14}C records. Earth and Planetary Science Letters, 219, 325-340.

Narcisi, B., Petit, J.R., Delmonte, B., Basile-Doelsch, I., Maggi, V., 2005. Characteristics and sources of tephra layers in the EPICA-Dome C ice record (East Antarctica): implications for past atmospheric circulation and ice core stratigraphic correlations. Earth and Planetary Science Letters, 239, 253-265.

Narcisi, B., Petit, J.R., Delmonte, B., 2010. Extended East Antarctic ice-core tephrostratigraphy. Quaternary Science Reviews, 29, 21-27.

NGICP members, 2004. High-resolution record of Northern Hemisphere climate extending into the last interglacial period. Nature, 431, 147-151.

Nicholls, K.W., Østerhus, S., Makinson, K., Grammelsrød, T., Fahrbach, E., 2009. Ice-ocean processes over the continental shelf of the southern Weddell Sea, Antarctica: a review. Reviews of Geophysics, 47, RG3003, doi: 10.1029/2007RG000250.

Niebler,H.-S., Arz, H.W., Donner, B., Mulitza, S., Pätzold, J., Wefer, G., 2003. Sea surface temperatures in the equatorial and South Atlantic Ocean during the Last Glacial Maximum (23–19ka). Paleoceanography, 18(3), 1069, doi:10.1029/2003PA000902.

Nielsen, S.H.H., Koç, N., Crosta, X., 2004. Holocene climate in the Atlantic sector of the Southern Ocean: controlled by insolation or oceanic circulation? Geology 32(4), 317-320.

Nowlin Jr, W.D. and Klinck, J.M., 1986. The physics of the Antarctic Circumpolar Current. Review of Geophysics, 24, 469-491.

O'Cofaigh, C.O., Dowdeswell, J.A., Pudsey, C.J., 2001. Late Quaternary Iceberg Rafting along the Antarctic Peninsula Continental Rise and in the Weddell and Scotia Seas. Quaternary Research, 56, 308-321.

Olbers, D., Gouretski, V., SeiM, G., Schroeter, J., 1992. Hydrographic Atlas of the Southern Ocean. Alfred Wegener Institute for Polar and Marine Research, Bremerhaven.

Olbers, D., Borowski, D., Voelker, C., Woelff, J.-O., 2004. The dynaical balance, transport and circulation of the Antarctic Circumpolar Current. Antarctic Science, 16(4), 439-470.

Orsi, A.H., Nowlin Jr, W.D., Whitworth III, T., 1993. On the circulation and stratification of the Weddell Gyre. Deep-Sea Research I, 40(1), 169-203.

Orsi, A.H., Whitworth, T., Nowlini Jr., W.D., 1995. On the meridional extent and fronts of the Antarctic Circumpolar Current. Deep Sea Research, 42(5), 641-673.

Orsi, A.H., Johnson, G.C., Bullister, J.L., 1999. Circulation, mixing, and production of Antarctic Bottom Water. Progress in Oceanography, 43, 55–109.

Pahnke, K. and Sachs, J., 2006. Sea surface temperatures of southern midlatitudes 0-160 kyr B.P. Paleoceanography, 21, PA2003, doi:10.1029/2005PA001191.

Paillard, D., Laeyrie, L., Yiou, P., 1996. Macintosh program performs time-series analysis. EOS Transactions American Geophysical Union, Washington D.C., 77, 379.

Parrenin, F., Barnola, J.-M., Beer, J., Blunier, T., Castellano, E., Chappellaz, J., Dreyfus, G., Fischer, H., Fujita, S., Jouzel, J., Kawamura, K., Lemieux-Dudon, B., Loulergue, L., Masson-Delmotte, V., Narcisi, B., Petit, J.-R., Raisbeck, G., Raynaud, D., Ruth, U., Schwander, J., Severi, M., Spahni, R., Steffensen, J. P., Svensson, A., Udisti, R., Waelbroeck, C., Wolff, E., 2007. The EDC3 chronology for the EPICA Dome C ice core. Climate of the Past, 3, 485-497.

Peltier, W.R., 2005. On the hemispheric origins of meltwater pulse 1a. Quaternary Science Reviews, 24, 1655-1671.

Peltier, W.R. and Fairbanks, R.G., 2006. Global glacial ice volume and Last Glacial Maximum duration from an extended Barbados sea level record. Quaternary Science Reviews, 25, 3322-3337.

Peterson, R.G. and Whitworth, T., III, 1989. The Subantarctic and Polar Fronts in relation to deep water masses through the Southwestern Atlantic. Journal of Geophysical Research, 94, 10817-10838.

Pierce, D.W., Barnett, T.P., Mikolajewicz, U., 1995. Competing roles of heat and freshwater flux in forcing thermohaline oscillations. Journal of Physical Oceanography, 25, 2046-2064.

Pollard, R.T. and Read J.F., 2001. Circulation pathways and transports of the Southern Ocean in the vicinity of the southwest Indian Ridge. Journal of Geophysical Research, 106, 2881-2898.

Prézelin, B.B., Hofmann, E.E., Mengelt, C., Klinck, J.M., 2000. The linkage between Upper Circumpolar Deep Water (UCDW) and phytoplankton assemblages on the west Antarctic Peninsula continental shelf. Journal of Marine Research, 58, 165-202.

Pudsey, C.J. and Howe, J.A., 1998. Quaternary history of the Antarctic Circumpolar Current- evidence from the Scotia Sea. Marine Geology, 148, 83-112.

Pudsey, C.J., Murray, J.W., Appleby, P., Evans, J., 2006. Ice shelf history from petrographic and foraminiferal evidence, Northeast Antarctic Peninsula. Quaternary Science Reviews, 25, 2357-2379.

Pugh, R.S., McCave, I.N., Hillenbrand, C.-D., Kuhn, G., 2009. Circum-Antarctic age modeling of Quaternary marine cores under the Antarctic Circumpolar Current: Ice-core dust-magnetic correlation. Earth and Planetary Science Letters, 284, 113-123.

Putnam, A.E., Denton, G.H., Schaefer, J.M., Barrell, D.J.A., Andersen, B.G., Finkel, R.C., Schwartz, R., Doughty, A.M., Kaplan, M.R., Schlüchter, C., 2010. Glacier advance in southern middle-latitudes during the Antarctic Cold Reversal. Nature Geoscience, 3, 700-704.

Rahmstorf, S., 2002. Ocean circulation and climate during the past 120,000 years. Nature, 419, 207-214.

Raisbeck, G.M., Yiou, F., Jouzel, J., Stocker, T.F., 2007. Direct north-south synchronization of abrupt climate change record in ice cores using Beryllium 10. Climate of the Past, 3, 541-547.

Reid, J.L., 1986. On the toal geostrophic circulation of the South Pacific Ocean: Flow patterns, tracers and transports. Progress in Oceanography, 16, 1-61.

Reid, J.L., 1989. On the total geostrophic circu1ation of the South Atlantic Ocean: Flow patterns, tracers, and transport. Progress in Oceanography, 23, 149-244.

Reimer, P.J., Baillie, M.G.L., Bard, E., Bayliss, A., Beck, J.W., Blackwell, P.G., Ramsey, C.B., Buck, C.E., Burr, G.S., Edwards, R.L., Friedrich, M., Grootes, P.M., Guilderson, T.P., Hajdas, I., Heaton, T.J., Hogg, A.G., Hughen, K.A., Kaiser, K.F., Kromer, B., McCorcac, F.G., Manning, S.W., Reimer, R.W., Richards, D.A., Southon, J.R., Talamo, S., Turney, C.S.M., van der Plicht, J., Weyhenmeyer, C.E., 2009. INTCAL09 and MARINE09 radiocarbon age calibration curves, 0-50,000 years cal BP. Radiocarbon, 51, 1111-1150.

Renssen, H., Goosse, H., Fichefet, T., Masson-Delmotte, V., Koç, N., 2005. Holocene climate evolution in the high-latitude Southern Hemisphere simulated by a coupled atmospheric–sea-ice–ocean–vegetation model. The Holocene, 15, 7, 951–964.

Renssen, H., Goosse, H., Muscheler, R., 2006. Coupled climate model simulation of Holocene cooling events: oceanic feedback amplifies solar forcing. Climate of the Past, 2, 79-90.

Revel-Rolland, M., De Deckker, P., Delmonte, B., Hesse, P.P., Magee, J.W., Basile-Doelsch, I., Grousset, F., Bosch, D., 2006. Eastern Australia: A possible source of dust in East Antarctica interglacial ice. Earth and Planetary Science Letters, 249, 1-13.

Roberts, A.P., Winklhofer, M., 2004. Why are geomagnetic excursions not always recorded in sediments? Constraints from post-depositional remanent magnetization lock-in modelling. Earth and Planetary Science Letters, 227, 345-359.

Roberts, A.P., 2008. Geomagnetic excursions: Knowns and unknowns. Geophysical Research Letters, 35, L17307, doi:10.1029/2008GL034719.

Robinson, R., Sigman, D.M., 2008. Nitrogen isotopic evidence for a poleward decrease in surface nitrate within the ice age Antarctic. Quaternary Science Review, 27, 1076-1090.

Rodbell, D.T., Smith, J.A., Mark, B.G., 2009. Glaciation in the Andes during the Lateglacial and Holocene. Quaternary Science Reviews, 28, 2165-2212.

Rojas, M., Moreno, P., Kageyama, M., Crucifix, M., Hewitt, C., Abe-Ouchi, A., Ohgaito, R., Brady, E., Hope, P., 2009. The Southern Westerlies during the last glacial maximum in PMIP2 simulations. Climate Dynamics, 32, 525-548.

Round, F.E., Crawford, R.M., Mann, D.G., 1990. The Diatoms: Biology and Morphology of the Genera, Cambridge University Press, UK, 760 pp.

Röthlisberger, R., Crosta, X., Abram, N.J., Armand, L., Wolff, E.W., 2010. Potential and limitations of marine and ice core sea ice proxies: an example from the Indian Ocean sector. Quaternary Science Reviews 29, 296-302.

Ruth, U., Barnola, J.-M., Beer, J., Bigler, M., Blunier, T., Castellano, E., Fischer, H., Fundel, F., Huybrechts, P., Kaufmann, P., Kipfstuhl, S., Lambrecht, A., Morganti, A., Oerter, H., Parrenin,

F., Rybak, O., Severi, M., Udisti, R., Wilhelms, F., Wolff, E., 2007. "EDML1": a chronology for the EPICA deep ice core from Dronning Maud Land, Antarctica, over the last 150 000 years. Climate of the Past, 3, 475-484.

Sachs, J.P. and Anderson, R.F., 2003. Fidelity of alkenone paleotemperatures in southern Cape Basin sediment drifts. Paleoceanography, 18(4), 1082, doi: 10.1029/2002PA000862.

Sagnotti, L., Macri, P., Camerlenghi, A., Rebesco, M., 2001. Environmental magnetism of Antarctic Late Pleistocene sediments and interhemispheric correlation of climatic events. Earth and Planetary Science Letters, 192, 65-80.

Sambrotto, R.N., Matsuda, A., Vaillancourt, R., Brown, M., Langdon, C., Jacobs, S.S., Measures, C., 2003. Summer plankton production and nutrient consumption patterns in the Mertz Glacier Region of East Antarctica. Deep-Sea Research II, 50, 1393-1414.

Sarnthein, M., Grootes, P.M., Kennett, J.P., Nadeau, M.-J., 2007. ^{14}C reservoir ages show deglacial changes in ocean currents and carbon cycle. In: Ocean Circulation: Mechanisms and Impacts – Past and future changes of the meridional overturning. Geophysical Monograph Series 173, edited by: Schmittner, A., Chiang, J., and Hemming, S., American Geophysical Union, Washington, DC, 175-196.

Schaefer, J.M., Denton, G.H., Kaplan, M., Putnam, A., Finkel, R.C., Barrell, D.J.A., Andersen, B.G., Schwarty, R., Mackintosh, A., Chinn, T., Schlüchter, C., 2009. High-frequency Holocene glacier fluctuations in New Zealand differ from the northern signature. Science, 324, 622-625.

Scher, H.D. and Martin, E.E., 2006. Timing and climatic consequences of the opening of Drake Passage. Science, 312, 428-430.

Schilt, A., Baumgartner, M., Blunier, T., Schwander, J., Spahni, R., Fischer, H., Stocker, T.F., 2010. Glacial-interglacial and millenial-scale variations in the atmospheric nitrous oxide concentration during the last 800,000 years. Quaternary Science Reviews, 29, 182-192.

Schlosser, P., Kromer, B., Bayer, R., Münnich, K.O., 1989. ^{14}C profiles in the central Weddell Sea. Radiocarbon, 31, 544-556.

Schmieder, F., 2004. Magnetic signals in Plio-Pleistocene sediments of the South Atlantic: Chronostratigraphic usability and paleoceanographic implications; In: The South Atlantic in the late Quaternary: Reconstruction of material budgets and current systems (eds) Wefer, G., Mulitza, S. and Ratmeyer, V. (Springer-Verlag: Berlin), pp. 261–277.

Schrader, H.J. and Gersonde, R., 1978. Diatoms and silicoflagellates, in: Zachariasse (Ed.), Micropaleontological Method and Technique—An Exercise on an Eight Metres Section of the Lower Pliocene of Capo Rossello, Sicily, Micropaleontol. Bull., 17, 129-176.

Schröder, M. and Fahrbach, E., 1999. On the structure and transport of the eastern Weddell Gyre. Deep-Sea Research II, 46, 501-527.

Schulz, M. and Mudelsee, M., 2002. REDFIT: estimating red-noise spectra directly from unevenly spaced paleoclimatic time series. Computer & Geosciences, 28, 421-426.

Seidov, D. and Maslin, M., 2001. Atlantic Ocean heat piracy and the bipolar climate see-saw during Heinrich and Dansgaad-Oeschger events. Journal of Quaternary Science 16(4), 321-328.

Severi, M., Becagli, S., Castellano, E., Morganti, A., Traversi, R., Udisti, R., Ruth, U., Fischer, H., Huybrechts, P., Wolff, E., Parrenin, F., Kaufmann, P., Lambert, F., Steffensen, J.P., 2007. Synchronisation of the EDML and EDC ice cores for the last 52 kyr by vocanic signiture matching. Climate of the Past, 3, 367-374.

Shakun, J. and Carlson, A.E., 2010. A global perspective on Last Glacial Maximum to Holocene climate change. Quaternary Science Reviews 29, 1801-1816.

Shemesh, A., Hodell, D., Crosta, X., Kanfoush, S., Charles, C., Guilderson, T., 2002. Sequence of events during the last deglaciation in Southern Ocean sediments and Antarctic ice cores. Paleoceanography, 17(4), 1056, doi: 10.1029/2000PA000599.

Shevenell, A. E., Ingalls, A., Domack, E., 2011. Holocene Southern Ocean surface temperature variability west of the Antarctic Peninsula. Nature, 470, 250-254.

Shulmeister, J., Goodwin, I., Renwick, J., Harle, K., Armand, L., McGlone, M.S., Cook, E., Dodson, J., Hesse, P.P., Mayewski, P., Curran, M., 2004. The Southern Hemisphere westerlies in the Australasian sector over the last glacial cycle: a synthesis. Quaternary International, 118-119, 23-53.

Sieger, R., Gersonde, R., Zielinski, U., 1999. New software package available for quantitative paleoenvironmental reconstructions. EOS, 80, 223.

Sigman, D. and Boyle, E., 2000. Glacial/interglacial variations in atmospheric carbon dioxide. Nature, 407, 859-869.

Sigman, D.M., Jaccard, S.L., Haug, G.H., 2004. Polar ocean stratification in a cold climate. Nature, 428, 59-63.

Sigman, D.M., Hain, M.P., Haug, G.H., 2010. The polar ocean and glacial cycles in atmospheric CO_2 concentration. Nature, 466, 47-55.

Sikes, E. L., Samson, C. R., Guilderson, T. P., Howard, W. R., 2000. Old radiocarbon ages in the southwest Pacific Ocean during the last glacial period and deglaciation. Nature, 405, 555-559.

Skilbeck, C.G., Rolph, T.C., Hill, N., Woods, J., Wilkens, R.H., 2005. Holocene millennial/centennial-scale multiproxy cyclicity in temperate eastern Australian estuary sediments. Journal of Quaternary Science, 20(4), 327-347.

Skinner, L.C., Fallon, S., Waelbroeck, C., Michel, E., Barker, S., 2010. Ventilation of the deep Southern Ocean and deglacial CO_2 rise. Science, 328, 1147-1151.

Smellie, J.L., 1999. The upper Cenozoic tephra record in the south polar region: a review. Global and Planetary Change, 21, 51-70.

Smetacek, V., 1985. Role of sinking in diatom life-history cycles: ecological, evolutionary and geological significance. Marine Biology, 84, 239-251.

Socal, G., Noethig, E.M., Bianchi, F., et al., 1997. Phytoplankton and particulate matter at the Weddell/Scotia Confluence (47°W) in summer 1989, as a final step of a temporal succession (EPOS project). Polar Biology, 18, 1-9.

Sowers, T., 2010. Atmospheric methane isotope records covering the Holocene period. Quaternary Science Reviews, 29, 213-221.

Stanford, J.D., Rohling, E.J., Hunter, S.E., Roberts, A.P., Rasmussen, S.O., Bard, E., McManus, J., Fairbanks, R.G., 2006. Timing of meltwater pulse 1a and climate responses to meltwater injections. Paleoceanography, 21, PA4103, doi: 10.1029/2006PA001340.

Steig, E.J., Hart, C.P., White, J.W.C., Cunningham W.L., Davis, M.D., Saltzman, E.S., 1998. Changes in climate, ocean and ice-sheet conditions in the Ross embayment, Antarctica, at 6 ka. Annals of Glaciology, 27, 305-310.

Stenni, B., Masson-Delmotte, V., Selmo, E., Oerter, H., Meyer, H., Röthlisberger, R., Jouzel, J., Cattani, O., Falourd, S., Fischer, H., Hoffmann, G., Iacumin, P., Johnsen, S.J., Minster, B., Udisti, R., 2010. The deuterium excess records of EPICA Dome C and Dronning Maud Land ice cores (East Antarctica). Quaternary Science Reviews, 29, 146-159.

Stenni, B., Buiron, D., Frezzotti, M., Albani, S., Barbante, C., Bard, E., Barnola, J.M., Baroni, M., Baumgartner, M., Bonazza, M., Capron, E., Castellano, E., Chappellaz, J., Delmonte, B., Falourd, S., Genoni, L., Iacumin, P., Jouzel, J., Kipfstuhl, S., Landais, A., Lemieux-Dudon, B., Maggi, V., Masson-Delmotte, V., Mazzola, C., Minster, B., Montagnat, M., Mulvaney, R., Narcisi, B., Oerter, H., Parrenin, F., Petit, J.R., Ritz, C., Scarchilli, C., Schilt, A., Schüpbach, S., Schwander, J., Selmo, E., Severi, M., Stocker, T.F., Udisti, R., 2011. Expression of the bipolar see-saw in Antarctic climate records during the last deglaciation. Nature Geoscience, 4, 46-49.

Stephens, B.B. and Keeling, R.F., 2000. The influence of Antarctic sea ice on glacial-interglacial CO_2 variations. Nature, 404, 171-174.

Stickley, C.E., Pike, J., Leventer, A., Dunbar, Domack, E.W., Brachfeld, S., Manley, P., McClennan, C., 2005. Deglacial ocean and climate seasonality in laminated diatom sediments, Mac.Robertson Shelf, Antarctica. Palaeogeography, Palaeoclimatology, Palaeoecology, 227, 290-310.

Stocker, T.F., 2003. South dials North. Nature, 424, 496-499.

Stockwell, D.A., 1991. Distribution of Chaetoceros resting spores in the Quatemary sediments from Leg 119. Proceedings of the Ocean Drilling Program, 119, 599-610.

Stoner, J.S., Lay, C., Channell, J.E.T., Kissel, C., 2002. South Atlantic and North Atlantic geomagnetic paleointensity stacks (0-80 ka): implications for inter-hemispheric correlation. Quaternary Science Reviews, 21, 1141-1151.

Stoner, J.S., Channell, J.E.T., Hodell, D.A., Charles, C.D., 2003. A ~580 kyr paleomagnetic record from the sub-Antarctic South Atlantic (Ocean Drilling Programm Site 1089). Journal of Geophysical Research, 108 (B5), 2244, doi:10.1029/2001JB001390.

St-Onge, G., Stoner, J.S., Hillaire-Marcel, C., 2003. Holocene palaeomagnetic records from the St. Lawrence Estuary, eastern Canada: centennial- to millennial-scale geomagnetic modulation of cosmogenic isotopes. Earth and Planetary Science Letters, 209, 113-130.

Stott, L., Timmermann, A., Thunell, R., 2007. Southern Hemisphere and deep-sea warming led deglacial atmospheric CO_2 rise and tropical warming. Science, 318, 435-438.

Stuiver, M. and Östlund, H.G., 1980. GEOSECS Atlantic radiocarbon. Radiocarbon, 22, 1-24.

Stuiver, M. and Braziunas, T., 1993. Modeling atmospheric ^{14}C influence and ^{14}C ages of marine samples to 10,000 BC. Radiocarbon, 35(1), 137-189.

Stuiver, M. and Reimer, P.J., 1993. Extended ^{14}C database and revised CALIB radiocarbon calibration program. Radiocarbon 35, 215-230.

Stuut, J.-B.W., and Lamy, F., 2004. Climate variability at the southern boundaries of the Namib (southwestern Africa) and Atacama (northern Chile) coastal desert during the last 120,000 years, Quaternary Research, 62, 301-309.

Sugden, D.E., Bentley, M.J., Fogwill, C.J., Hulton, N.R.J., McCulloch, R.D., Purves, R.S., 2005. Late-glacial glacier events in southernmost South America: A blend of Northern and Southern hemispheric climatic signals? Geografiska Annaler, 87A(2), 273-288.

Sugden, D.E., Bentley, M.J., O'Cofaigh, C., 2006. Geological and geomorphological insights into Antarctic ice sheet evolution. Philosophical Transactions of the Royal Society A, 364, 1607-1625.

Svensson, A., Andersen, K.K., Bigler, M., Clausen, H.B., Dahl-Jensen, D., Davies, S.M., Johnsen, S.J., Muscheler, R., Parrenin, F., Rasmussen, S.O., Röthlisberger, R., Seierstad, I., Steffensen, J.P., Vinther, B.M., 2008. A 60 000 year Greenland stratigraphic ice core chronology. Climate of the Past, 4, 47-57.

Tauxe, L., 1993. Sedimentary Records of Relative Paleointensity of the Geomagnetic Field: Theory and Practice. Reviews of Geophysics, 31(3), 319-354.

Taylor, F. and Sjunneskog, C., 2002. Postglacial marine diatom record of the Palmer Deep, Antarctic Peninsula (ODP Leg 178, Site 1098) 2. Diatom assemblages. Paleoceanography, 17(3), doi: 10.1029/2000PA000564.

Thomas, D.N. and Dieckmann, G.S. (ed), 2010. Sea Ice (Second Edition). Wiley-Blackwell. 621p.

Thompson, L.G., Davis, M.E., Mosley-Thompson, E., Sowers, T.A., Henderson, K.A., Zagorodnov, V.S., Lin, P.-N., Mikhalenko, V.N., Campen, R.K., Bolzan, J.F., Cole-Dai, J., Froncou, B., 1998. A 25,000-year tropical climate history from Bolivian ice cores. Science, 282, 1858-1864.

Thompson, L.G., Mosley-Thompson, E., Henderson, K.A., 2000. Ice-core palaeoclimate records in tropical South America since the Last Glacial Maximum. Journal of Quaternary Science, 15(4), 377-394.

Timmermann, A., Timm, O., Stott, L., Menviel, L., 2009. The roles of CO_2 and orbital forcing in driving Southern Hemispheric temperature variations during the last 21 000 yr. Journal of Climate, 22, 1626-1640.

Toggweiler, J.R., Russell, J.L., Carson, S.R., 2006. Midlatitude westerlies, atmospheric CO2, and climate change during the ice ages. Paleoceanography, 21, PA2005, doi: 10.1029/2005PA001154.

Toggweiler, J.R. and Russell, J.L., 2008. Ocean circulation in a warming climate. Nature, 451, 286-288.

Toggweiler, J.R., 2009. Shifting Westerlies. Science, 323, 1434-1435.

Tréguer, P., Linder, L., van Bennekon, A.J., et al., 1991. Production of biogenic silica in the Weddell-Scotia Seas measured by using ^{32}Si. Limnology and Oceanography, 36, 1217-1227.

Tréguer, P., Nelson, D.M., Van Bennekom, A.J., DeMaster, D.J., Leynaert, A., Quéguiner, B., 1995. The silica balance in the world ocean: a reestimate. Science, 268, 375-379.

Trinchitella, M. and Dinkelman, M.G, 1980. Regional biostratigraphic correlations of Eltanin piston cores in the southeast Pacific, subantarctic and Antarctic. Antarctic Journal of the United States, 15, 124-127.

Trull, T., Rintoul, S.R., Hadfield, M., Abraham, E.R., 2001. Circulation and seasonal evolution of polar waters south of Australia: implications for iron fertilization of the Southern Ocean. Deep-Sea Research II, 48, 2439-2466.

United Nations Scientific Committee on the Effect of Atomic Radiation, 2000. UNSCEAR 2000 Report to the General Assembly, with scientific annexes. Sources and effects of ionizing radiation. Volume1: Sources. Annex C. New York. 329-350.

van Beek, P., Reyss, J-L., Paterne, M., Gersonde, R., van der Loeff, M.R., Kuhn, G., 2002. ^{226}Ra in barite: Absolute dating of Holocene Southern Ocean sediments and reconstruction of sea-surface reservoir ages. Geology, 30(8), 731–734.

Vallelonga, P., Gabrielli, P., Balliana, E., Wegner, A., Delmonte, B., Turetta, C., Burton, G., Vanhaecke, F., Rosman, K.J.R., Hong, S., Boutron, C.F., Cescon, P., Barbante, C., 2010. Lead isotopic compositions in the EPICA Dome C ice core and Southern Hemisphere potential source areas. Quaternary Science Reviews, 29, 247-255.

Verosub, K.L. and Roberts, A.P., 1995. Environmental magnetism: Past, present and future, J. Geophys. Res., 100, 2175–2192.

Vonmoos, M., Beer, J., Muscheler, R., 2006. Large variations in Holocene solar activity: Constraints from ^{10}Be in the Greenland Ice Core Project ice core. Journal of Geophysical Research, 111, A10105, doi: 10.1029/2005JA011500.

Waelbroeck, C., Duplessy, J.-C., Michel, E., Labeyrie, L., Paillard, D., Duprat, J., 2001. The timing of the last deglaciation in North Atlantic climate records. Nature, 412, 724-727.

Wagner, B., Cremer, H., Hultzsch, N., Gore, D.B., Melles, M., 2004. Late Pleistocene and Holocene history of Lake Terrasovoje, Amery Oasis, East Antarctica, and its climatic and environmental implications. Journal of Paleolimnology, 32, 321-339.

Wagner, B. and Melles, M., 2007. The heterogeneity of Holocene climate and environmental history along the East Antarctic coastal regions. In Antarctica: A Keystone in a Changing World – Online Proceedings of the 10th ISAES, edited by A.K. Cooper and C.R. Raymond et al., USGS Open-File Report 2007-1047, Extended Abstract 161, 4 p.

Warner, N.R. and Domack, E.W., 2002. Millenial- to decadal-scale paleoenvironmental change during the Holocene in the Palmer Deep, Antarctica, as recorded by particle size analysis, Paleoceanography, 17(3), 8004, doi:10.1029/2000PA000602.

Watson, A.J., Bakker, D.C.E., Ridgwell, A.J., Boyd, P.W., Law, C.S., 2000. Effect of iron supply on Southern Ocean CO_2 uptake and implications for glacial atmospheric CO_2. Nature, 407, 730-733.

Watson, A. and Naveira Garabato, A., 2006. The role of Southern Ocean mixing and upwelling in glacial-interglacial atmpshreric CO_2 change. Tellus, 58B, 73-87.

Weaver, A.J., Saenko, O.A., Clark, P.U., Mitrovica, J.X., 2003. Meltwater Pulse 1A from Antarctica as a Trigger of the Bolling-Allerod Warm Interval. Science, 299, 1709-1713.

Weiss, R.F., Östlund, H.G., Craig, H., 1979. Geochemical studies of the Weddell Sea. Deep-Sea Research, 26, 1093-1120.

Whitworth III, T. and Peterson, R.G., 1985. Volume transport of the Antarctic Circumpolar Current from bottom pressure measurements. Journal of Physical Oceanography, 15, 810–816.

Williams, G.P. and Bryan, K., 2006. Ice age winds: An aquaplanet model. Journal of Climate, 19, 1706-1715.

Willmott, V., Domack, E.W., Canals, M., Brachfeld, S., 2006. A high resolution relative paleointensity record from the Gerlache-Boyd paleo-ice stream region, northern Antarctic Peninsula. Quaternary Research, 66, 1-11.

Wolff, E.W., Rankin, A.M., Röthlisberger, R., 2003. An ice core indicator of Antarctic sea ice production? Geophysical Research Letters, 30(22), 2158, doi: 10.1029/2003GL018454.

Wolff, E.W., Fischer, H., Fundel, F., Ruth, U., Twarloh, B., Littot, G.C., Mulvaney, R., Röthlisberger, R., de Angelis, M., Boutron, C.F., Hansson, M., Jonsell, U., Hutterli, M.A., Lambert, F., Kaufmann, P., Stauffer, B., Stocker, T.F., Steffensen, J.P., Bigler, M., Siggaard-Andersen, M.L., Udisti, R., Becagli, S., Castellano, E.,

Severi, M., Wagenbach, D., Barbante, C., Gabrielli, P., Gaspari, V., 2006. Southern Ocean sea-ice extent, productivity and iron flux over the past eight glacial cycles. Nature, 440, 491-496.

Wolff, E.W., Fischer, H., Röthlisberger, R., 2009. Glacial terminations as southern warmings without northern control. Nature Geoscience, 2, 206-209.

Wolff, E.W., Barbante, C., Becagli, S., Bigler, M., Boutron, C.F., Castellano, E., de Angelis, M., Federer, U., Fischer, H., Fundel, F., Hansson, M., Hutterli, M., Jonsell, U., Karlin, T., Kaufmann, P., Lambert, F., Littot, G.C., Mulvaney, R., Röthlisberger, R., Ruth, U., Severi, M., Siggaard-Andersen, M.L., Sime, L.C., Steffensen, J.P., Stocker, T.F., Traversi, R., Twarloh, B., Udisti, R., Wagenbach, D., Wegner, A., 2010. Changes in environment over the last 800,000 years from chemical analysis of the EPICA Dome C ice core. Quaternary Science Reviews, 29, 285-295.

Wunsch, C., 2006. Abrupt climate change: An alternative view. Quaternary Research, 65, 191-203.

Yamazaki, T., Kanamatsu, T., Mizuno, S., et al., 2008. Geomagnetic field variations during the last 400 kyr in the western equatorial Pacific: Paleointensity-inclination correlation revisited. Geophysical Research Letters, 35, doi:10.1029/2008GL035373.

Yiou, P., Fuhrer, K., Meeker, L.D., Jouzel, J., Johnsen, S., Mayewski, P.A., 1997. Paleoclimatic variability inferred from the spectral analysis of Greenland and Antarctic ice-core data. Journal of Geophysical Research, 102(C12), 26441-26454.

Yokoyama, Y., Lambeck, K., de Dekker, P., Johnston, P., Fifield, K., 2000. Timing for the maximum of the Last Glacial constrained by lowest sea-level observations. Nature 406, 713-716.

Yoon, H.I., Khim, B.K., Yoo, K.-C., Bak, Y.S., Lee, J.I., 2007. Late glacial to Holocene climatic and oceanographic record of sediment facies from the South Scotia Sea off the northern Antarctic Peninsula. Deep-Sea Research. II, 54,2367-2387.

Zachos, J., Pagani, M., Sloan, L., et al., 2001.Trends, rhythms, and aberrations in global climate 65 Ma to Present. Science, 292, 686-693.

Zheng, Y., Anderson, R.F., Froelich, P.N., Beck, W., McNichol, A.P., Guilderson, T., 2002. Challenges in radiocarbon dating organic carbon in opal-rich marine sediments. Radiocarbon, 44, 123-136.

Zielinski, U., 1993. Quantitative estimation of palaeoenvironmental parameters of the Antarctic Surface Water in the Late Quaternary using transfer functions with diatoms. Berichte zur Polarforschung, 126, ISSN: 0176-5027.

Zielinski, U. and Gersonde, 1997. Diatom distribution in Southern Ocean surface sediments (Atlantic sector): implications for paleoenvironmental reconstructions. Palaeogeography, Palaeoclimatology, Palaeoecology, 129, 213-250.

Zielinski, U., Gersonde, R., Sieger, R., Fuetterer, D., 1998. Quaternary surface water temperature estimations: Calibration of a diatom transfer function for the Southern Ocean. Paleoceanography, 13, 365-383.

Zielinski, U., Bianchi, C., Gersonde, R., Kunz-Pirrung, M., 2002. Last occurrence datums of the diatoms *Rouxia leventerae* and *Rouxia constricta*: indicators for marine isotope stages 6 and 8 in Southern Ocean sediments. Marine Micropaleontology, 46, 127-137.

Zielinski, U. and Gersonde, R., 2002. Plio-Pleistocene diatom biostratigraphy from ODP Leg 177, Atlantic sector of the Southern Ocean. Marine Micropaleontology, 45, 225-268.

Zwally, H.J., Parkinson, C.L., Comiso, J.C., 1983. Variability of Antarctic sea ice and changes in carbon dioxide. Science 220, 1005-1012.